Epigenetic regulation of germline stem cell fate by Centromere Protein C

Ben L. Carty

Supervisor: Dr Elaine Dunleavy

A thesis submitted to the National University of Ireland, Galway
for the degree of Doctor of Philosophy

October 2020

Centre for Chromosome Biology,
School of Natural Sciences,
National University of Ireland, Galway

Table of Contents

Acknowledgements ..... *iv*

Thesis Declaration ..... *v*

List of Abbreviations ..... *vi*

Thesis Abstract ..... *x*

1. Introduction *1*

1.1 Asymmetric Cell Division in Stem Cells **2**
1.1.1 Cells, Cell Division and the Cell Cycle – An Overview 2
1.1.2 Stem Cells and the Maintenance of Specialised Cell Lineages 6
1.1.3 Asymmetric Cell Division in Specialised Tissues 8

1.2 The Control of Asymmetric Cell Division in Stem Cells **11**
1.2.1 Extrinsic versus Intrinsic Control of Adult Stem Cells 11
1.2.2 Non-Random Segregation of Sister Chromatids 12
1.2.3 Non-Random Chromosome Segregation and the Immortal Strand Hypothesis 14
1.2.4 An Alternative Explanation: the Silent Sister Hypothesis 16

1.3 A Paradigm of Epigenetic Maintenance: Centromeric Chromatin **21**
1.3.1 The Centromeric Locus and Centromere Protein-A (CENP-A) 21
1.3.2 Nucleosome Structure and the Packaging of Chromatin 25
1.3.3 The Unique Structure of CENP-A Nucleosomes 25
1.3.4 Building a Stable Centromere: The Constitutive Centromere Associated Network 29
1.3.5 The Characteristics of CENP-C and its Role in CENP-A Nucleosome Stability 31
1.3.6 The *Drosophila* Centromere: A Simplification of an Epigenetic Inheritance Loop 34
1.3.7 The Structural Basis of *Drosophila* Centromere Maintenance 40

1.4 Centromere Asymmetry and Non Random Sister Chromatid Segregation **44**
1.4.1 Asymmetric Inheritance of Canonical and Centromeric Histones 44
1.4.2 Centromere Asymmetry 46
1.4.3 CENP-A Assembly and Sister Centromere Asymmetry 48
1.4.4 A Role for CENP-C in CENP-A Asymmetry 51
1.4.5 Centromeric Regulation of Stem Cell Fate 53

1.5 *Drosophila melanogaster* and the Germline Stem Cell Niche **55**
1.5.1 Arthropods, Insects and the Order Diptera 55
1.5.2 The Model Organism: *Drosophila melanogaster* 57
1.5.3 Oogenesis and the Female Germline Stem Cell Niche 59
1.5.4 The Spectrosome, Fusome, and the Control of Cell Synchrony in Gametogenesis 61

1.6 Project Hypothesis and Objectives **65**

2. Materials and Methods *67*

2.1 Chemical Reagents and Experimental Kits **68**

2.2 *Drosophila* Husbandry, Genetics and Techniques **68**
2.2.1 Fly Stocks and Husbandry 68
2.2.2 Targeted Genetic Manipulation: GAL4-UAS System 68

2.3 Cell Biology Techniques **73**

2.3.1 Preparation of Ovaries for Immunostaining ... 73
2.3.2 5-ethynyl-2'-deoxyuridine (EdU) Incorporation and Detection ... 74
2.3.3 Microscopy and Image Processing ... 74
2.3.4 Centromere Fluorescence Intensity Quantification ... 75
2.3.5 Assay of GSC Self-Renewal: Sex-Lethal and pMad Quantitation ... 75

2.4 Molecular Biology Techniques ... **77**
2.4.1 Single-fly genomic DNA preparation ... 77
2.4.2 Single-fly Polymerase Chain Reaction (PCR) ... 77

3. Understanding CENP-C's role in centromere assembly and centromere asymmetry in female germline stem cells ... ***78***

3.1 Chapter Introduction ... **79**

3.2 CENP-C is assembled from G_2 phase – prophase in female GSCs ... **81**

3.3 Characterising the role of CENP-C in CENP-A assembly in GSCs. ... **83**

3.4 CENP-C is asymmetrically distributed between stem and daughter cells ... **95**

3.5 CENP-C maintains an asymmetric distribution of CID in GSCs ... **98**

3.6 Chapter Summary and Discussion ... **104**
3.6.1 CENP-C assembles in G_2/prophase and is required for CID assembly at the same cell cycle time. ... 104
3.6.2 CENP-C maintains an asymmetric distribution of CID between stem and daughter cells ... 105

4. Understanding the role of the centromere in GSC maintenance and differentiation ... ***107***

4.1 Chapter Introduction ... **108**

4.2 CENP-C regulates GSC proliferation and long term GSC maintenance. ... **109**

4.3 CID level reduces in GSCs with age, and CENP-C depletion accelerates its loss ... **112**

4.4 CENP-C-depleted germ cells accumulate in S-phase, but not in mitosis. ... **116**

4.5 CENP-C function in CID assembly/asymmetry in GSCs is distinct from its requirement outside of the niche ... **119**

4.6 CID assembly dynamics differ between GSCs and cysts ... **122**

4.7 Chapter Summary and Discussion ... **124**
4.7.1 CENP-C is required for long term GSC maintenance. ... 124
4.7.2 CID levels in GSCs decrease with age, and CENP-C accelerates this loss. ... 126
4.7.3 CID inheritance changes from GSCs to germ cell cysts. ... 126

5. Investigating the role of the centromere in cell fate in an asymmetrically-dividing system ... ***128***

5.1 Chapter Introduction ... **129**

5.2 Establishing an assay to measure female *Drosophila* GSC self-renewal ... **130**

5.3 Disruption to the centromeric core increases GSC self-renewal ... **133**

5.4 Chapter Summary and Discussion ... **138**
5.4.1 GSC self-renewal can be reliably assayed using a ratio of SXL/pMad. ... 138
5.4.2 Disruption to the centromeric core promotes GSC self-renewal ... 140

6. Discussion ... ***142***

6.1 Stem cells epigenetically distinguish sister chromatids at the centromere ... 143

6.2 CENP-C contributes towards mitotic drive by facilitating CID assembly, maintaining CID asymmetry and assembling a strong 'GSC-side' kinetochore. ... 144

6.3 Making sense of parental histones: how might parental CID be maintained? ... 146

6.3 The centromere as a driver of asymmetric division in stem cells ... 148

6.4 The Model of Centromere Assembly in Asymmetric Cell Division ... 150

6.5 Adult stem cell age epigenetically at the centromere ... 151

6.6 Centromeres epigenetically regulate stem cell fate ... 153

6.7 Concluding Remarks and Outstanding Questions ... 155

7. Bibliography ... 157

8. Appendices ... 175

8.1 Chemical Reagents and Common Buffers ... 176

8.2 Fly Stocks used during this study ... 178

8.3 List of Primary Antibodies ... 180

8.4 List of Secondary Antibodies ... 181

8.5 Ben L. Carty and Elaine M. Dunleavy, 2020 ... 182

8.6 Anna Ada Dattoli, Ben L. Carty, Antje M. Kochendoerfer, Conall Morgan, Annie E. Walshe, Elaine M. Dunleavy, 2020. ... 183

Acknowledgements

Firstly, the biggest thank you goes to my supervisor Elaine for everything over the last 5 years. I was very lucky to find myself allocated to your lab as a final year undergrad – and developing that undergrad project into a full PhD is something I never would have thought I would have the opportunity to do! You've always had an open door for advice and encouragement over the years, given me opportunities to travel and always allowed me to develop my own research interests. I will always be very grateful!

I also want to thank all the members of the Dunleavy lab both past and present. To Ada, you are the most motivated scientist I know and an outstanding mentor, particularly my earlier days when I was finding my feet. To Caitriona, thank you for all the advice, support and craic that kept me sane over the last 4+ years – it wouldn't have been the same experience without you! Thanks to Antje, and recently Federica for making the lab a great place to work. Also can't forget Annie, and Conall – a great man for the tae over the years.

I have to thank all my family, especially my parents for their belief and constant support. You've invested a lot in me, helped me out when I needed it and never doubted my abilities. I hope this has been able to pay it back somewhat! Nan and Grandad, I know you are looking down. My brother Colin, hopefully I wasn't too moody over the last year trying to get this over the line! Last but not least to Emma, thank you for sticking by me in what was a rollercoaster few years. You are the best!

Oh, and coronavirus..absolutely no thanks to you!!

Thesis Declaration

I declare that I have not obtained any previous qualifications from NUI Galway or elsewhere based on any of the work obtained in this thesis.

I conducted all experiments and wrote this thesis under the supervision of Dr Elaine Dunleavy

List of Abbreviations

8cc	8 cell cyst
Ago1	Argonaute-1
ANOVA	Analysis of Variance
AT-Hook	Adenine Thymine Hook
bam	bag of marbles
BDSC	Bloomington Drosophila Stock Centre
Bgcn	Benign gonial cell neoplasm protein
BMP	Bone Morphogenic Protein
Brat	Brain tumour protein
BrdU	5-bromo-2'-deoxyuridine
BSA	Bovine Serum Albumin
MTOC	Microtubule Organising Centre
CAL1	Chromosome Alignment 1
CATD	CENP-A Targeting Domain
CB	Cystoblast
CCAN	Constitutive Centromere-Associated Network
CENP-A	Centromere Protein A
CENP-B	Centromere Protein B
CENP-C	Centromere Protein C
CENP-C^{CD}	CENP-C Central Domain
CENP-C^{CM}	CENP-C Motif
CENP-H	Centromere Protein H
CENP-I	Centromere Protein I
CENP-N	Centromere Protein N
ChIP	Chromatin Immunopercipitation
CID	Centromere Identifier
CO-FISH	Chromosome-orientation Fluorescence *in situ* Hybridisation
CREST	Calcinosis, Raynaud phenomenon, Esophageal hypomotility, Sclerodactyly, and Telangiectasia**.**
CyO	CurlyO

DAPI	4′,6-diamidino-2-phenylindole
Dcr-2	Dicer-2
DNA	Deoxyribonucleic Acid
Dnmt	DNA methyltransferase
Dpp	Decapentaplegic
Dr	Drop
DSas-4	*Drosophila* Spindle assembly abnormal – 4
dsRNA	double stranded RNA
EB	Enteroblast
EdU	5-Ethynyl-2′-deoxyuridine
EE	Enteroendocrine cells
ER	Endoplasmic Reticulum
ESC	Embryonic Stem Cell
ESC	Escort Stem Cell
Flp-FRT	Flippase - flippase recognition target
FRAP	Fluorescence Recovery after Photobleaching
G_1 phase	Gap phase 1
G_2 phase	Gap phase 2
GAL4	Galactose 4
GB	Gonialblast
GFP	Green Fluorescent Protein
GSC	Germline Stem Cell
H3S10P	Histone H3 phosphorylated at Serine 10
H3T3P	Histone H3 phosphorylated at Threonine 3
HA	haemagglutinin
HFD	Histone Fold Domain
HJURP	Holliday Junction Recognition Protein
IF	Immunofluorescence
IgG	Immunoglobulin G
iPSC	induced Pluripotent Stem Cell
ISC	Intestinal Stem Cell
JAK-STAT	Janus Kinase/Signal Transducer and Activator of Transcription
Knf4	Krüppel-like factor 4

L1/L2	Loop 1/2
LINE	Long interspersed nuclear elements
LTR	Long Terminal Repeat
M-phase	Mitosis - Phase
MCM	mini-chromosome maintenance
Mei-P26	Meiosis Protein 26
mRNA	messenger RNA
NA	Numerical Aperture
NC	Nurse Cell
Ns	Non-significant
Oct 3/4	Octamer-binding transcription factor 3/4
PBST	Phosphate-Buffered Saline with Triton-X
PCR	Polymerase Chain Reaction
PFA	Paraformaldehyde
pMad	phosphorylated Mothers Against Decapentaplegic
RNA	Ribonucleic Acid
RNAi	RNA interference
RT	Room Temperature
S-phase	Synthesis Phase
SAC	Spindle Assembly Checkpoint
SB	Squishing Buffer
SCD	Symmetric Cell Division
SEM	Standard Error of the Mean
SIM	Structured Illumination Microscopy
siRNA	small interfering RNA
SM6, Cy	Second Multiple 6, Curly
Sox 2	(sex determining region Y)-box 2
SSC	Somatic Stem Cells
Sxl	Sex-lethal
TF	Terminal Filament
TM3, Sb	Third Multiple 3, Stubble
TRiP	Transgenic RNAi Project
UAS	Upstream Activating Sequence
UTR	Untranslated Region

Wg (Sp-1)	Sternopleural
YFP	Yellow Fluorescent Protein
*	$p<0.05$
**	$p<0.01$
***	$p<0.001$
****	$p<0.0001$

Thesis Abstract

Germline stem cells (GSCs) divide asymmetrically to produce one new daughter stem cell and one daughter cell that will subsequently undergo meiosis and differentiate to generate the mature gamete. The 'silent sister hypothesis' proposes that in asymmetric divisions, the selective inheritance of sister chromatids carrying specific epigenetic marks between stem and daughter cells impacts cell fate. To facilitate selective sister chromatid segregation in stem cells, this hypothesis specifically proposes that the centromeric region of each sister chromatid is distinct. In *Drosophila* GSCs, it has recently been shown that the centromeric histone CENP-A - the epigenetic determinant of centromere identity - is asymmetrically distributed on sister chromatids. In these cells, CENP-A deposition occurs in G_2 phase such that sister chromatids destined to end up in the stem cell harbour more CENP-A, assemble more kinetochore proteins and capture more spindle microtubules. These results suggest a potential mechanism of 'mitotic drive' that might bias chromosome segregation.

In this thesis, we report that the inner kinetochore protein CENP-C, which binds to centromeric chromatin, is required for the assembly of CENP-A in G_2 phase in GSCs. Moreover, CENP-C is required to maintain a normal asymmetric distribution of CENP-A between stem and daughter cells. In addition, we show that CENP-A is gradually lost at the centromere of GSCs over time, with depletion of CENP-C accelerating this loss of CENP-A. Finally, we show that disruption to the centromeric core in GSCs disrupts the balance of stem and daughter cells in the ovary, shifting GSCs toward a self-renewal tendency. Ultimately, we provide evidence that centromere assembly and maintenance via CENP-C is required for efficient asymmetric division in female *Drosophila* GSCs.

1. Introduction

1.1 Asymmetric Cell Division in Stem Cells

1.1.1 Cells, Cell Division and the Cell Cycle – An Overview

The most basic unit of life is a cell, first observed and published in the book *Micrographia* by Robert Hooke in 1665. Cells provide the most fundamental structural and functional building block of an organism – assembling from cells, to tissues and beyond into a fully functioning organism. Moreover, cells are generally specialised for function. For example, epithelial cells lining the surface of the body including skin, internal organs and blood vessels. Similarly, germ cells give rise to gametes (sperm and egg). Importantly, these cells are required to proliferate to build their specialised tissues (Alberts et al., 2014). Cell proliferation is the process by which a cell increases the population of cells by way of cell division. Cell division involves a mother cell dividing to give rise to two new (usually identical) daughter cells. In order to grow and increase tissue size, cells need duplicate their genetic material and to divide it equally between its two new daughter cells. The process of cell division was first described by Walther Flemming in 1882 (Flemming, 1882).

A cell's genetic material is referred to as it genome, and provides the instructions for the cell to grow, adapt, respond to its environment and carry out its function (Alberts et al., 2014). Deoxyribonucleic acid (DNA) is the basic genetic material of most organisms, and is maintained primarily in the nucleus of a cell and packaged into chromosomes (discussed later). Each species has a specified number of chromosomes. For example, *Homo sapiens* (humans) contain 46 chromosomes. Here, human (and most organisms) cells are diploid ($2n$), meaning they contain 23 homologous chromosome pairs ($2n = 46$; with the exception of X/Y chromosomes in the case of males). *Drosophila melanogaster* (fruit fly) on the other hand contain 8 chromosomes, also organised into 4 homologues ($2n = 8$). In contrast, sperm and egg cells contain only one copy of each chromosome (haploid, $1n$). When a sperm and egg fuse, these two haploid cells combine their genetic material to form a complete diploid cell (and effectively new organism). Furthermore, each chromosome contains an exact 'sister' copy of its genetic material known as a sister

chromatid, produced by DNA replication. A cell segregates these sister chromatids equally and randomly into two daughter cells by means of a process called mitosis. To allow access to the DNA for replication (discussed below) and gene expression, DNA is decondensed and loosely packed into chromatin structures. Upon entering into mitosis, these chromatin structures are condensed into the classical chromosome structure to allow efficient segregation of the sister chromatids (Alberts et al., 2014). Each chromosome consists of a central constriction site, the centromere, which separate the short ('petit' or 'p') to longer ('q') chromosome arms (Figure 1.1).

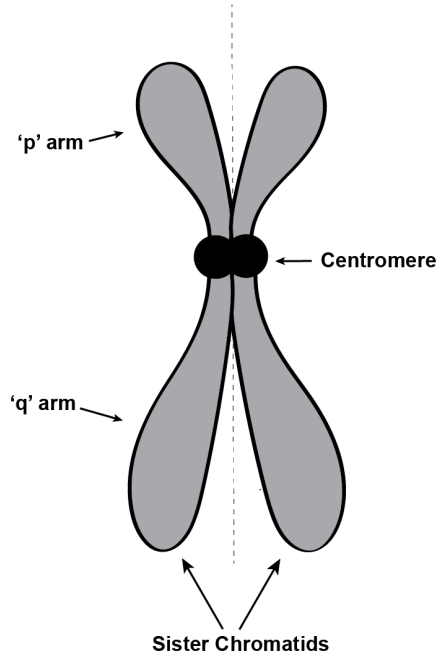

Figure 1.1: The basic structure of the mitotic chromosome. DNA condenses into mitotic chromosomes before segregation into daughter nuclei. The basic structure of a chromosome contains shorter 'p' arms (top, grey) and longer 'q' arms (bottom, grey) separated by a primary constriction site (the centromere, black). DNA is duplicated during the Synthesis 'S' phase in order to allow equal inheritance of genetic material between daughter nuclei during mitosis. A genetically identical copy of a chromosome, called a sister chromatid, is generated in S phase. One sister chromatid is segregated into each daughter cell upon mitosis.

Cells undergo a cell cycle in preparation for the next cell division. After a cell divides, each chromosome consists of only one copy of its genetic material. In order to divide again, this genetic material needs to be copied for each chromosome to re-establish the sister chromatids of each individual chromosome. The cell cycle is thus series of events (beginning after mitosis) the cell goes through to prepare for the mitosis. It consists of an interphase and mitosis (M-Phase). Interphase is subdivided into three phases: G_1 phase, S-phase, and G_2 phase. G_1 phase represents the first 'gap' phase and its primary function growth and replenishment of organelles and proteins for the upcoming cell cycle. The duration of G_1 phase is highly variable depending on cell type (discussed later). Progression through this stage is governed by G_1/S cyclin proteins at the G_1/S transition (restriction point). S-phase (S for 'Synthesis') represents the stage of the cell cycle where DNA is duplicated from a parental strand, providing the genetic material to be sufficient for two new daughter cells. It is a highly complex process whereby the DNA replication machinery synthesises an extra copy of the same DNA strand, whilst retaining the correct chromosome number or 'ploidy'. Upon completion, each chromosome will be represented by two identical sister chromatids (parent and newly-synthesised) separated by a central constriction point (the centromere) to be segregated later during mitosis. Lastly, a second gap phase (G_2-phase) follows S-phase and is the final preparation before mitosis. It represents a phase of significant protein synthesis and cell growth before mitosis. Here, microtubules begin to organise to form the mitotic spindle and the G_2/M-checkpoint reviews the cell for DNA damage. The G_2/M checkpoint cyclins allow progression to mitosis once these 'checks' are complete.

Mitosis represents the most common form of nuclear division within a cell division. It is a highly organised event whereby the chromosomes organise, align and segregate their sister chromatids into two daughter nuclei, followed by physical cell division via cytokinesis. M-phase can also be subdivided into distinct stages: prophase, prometaphase, metaphase, anaphase, telophase, followed by cytokinesis. Briefly, these stages are summarised below:

- Prophase: During prophase, the loosely packed chromatin condenses into its individual tightly-packed chromosomes. Transcription/gene expression largely ceases and the nucleolus disintegrates. Centrosomes,

the primary microtubule organising centre (MTOC), emanate microtubules (mitotic spindle) from centrosomes at both cellular poles.

- Prometaphase: The nuclear envelope is broken down and the polymerised microtubules invade the nucleus to attach to chromosomes via kinetochores. Kinetochores are proteinaceous structures which form at chromosome centromeres, to which the mitotic spindle attaches (or biorientes). At prometaphase, chromosomes are beginning to align themselves at the metaphase plate.
- Metaphase: The microtubules are now attached to the kinetochores of each sister chromatid, and the centrosome now begins to pull kinetochores towards their respective poles, with bivalent sister chromatids remaining attached to each other. This pull creates a tension which aligns the chromosomes centrally at the metaphase plate. The spindle assembly checkpoint (SAC) ensures each kinetochore has a spindle attached and that each daughter cell receives one sister chromatid.
- Anaphase: The mitotic spindle is contracted and the sister chromatids are pulled apart towards their opposite poles. The cell elongates to ease the final cleavage.
- Telophase: Each daughter nucleus now contains an identical chromosome set. The nuclear envelope reforms around each daughter nucleus and the chromosomes begin to decondense into their chromatin state.
- Cytokinesis: Cytokinesis is not a stage of mitosis but is the penultimate stage cell division. In animal cells, the cytoplasm pinches inwards (cleavage furrow) to form the two new daughter cells.
- Abscission: Cell division concludes with the breaking of the microtubule and membrane bridge that intercellularly connects the two daughter cells.

In the case of regular, mitotically-dividing cells, equal inheritance of sister chromatids (and in turn chromosome number) is paramount to maintaining the cell's ploidy. Moreover, the segregation of sister chromatids is random, depending

on the orientation of the chromosome and the spindle biorientation. Hence, the sister chromatids of each chromosome (parental or newly-synthesised) have equal chance of inheritance to either daughter cell. However, exceptions to this rule of equal and random inheritance must exist in nature in order for purposely unspecialised cells to develop and maintain tissue homeostasis. This thesis will bring into focus the non-random nature of chromosome segregation in stem cell divisions, and the adaptions of sister chromatids to facilitate a non-random segregation in the context of adult germline stem cells (GSCs).

1.1.2 Stem Cells and the Maintenance of Specialised Cell Lineages

Complex multicellular organisms display a diverse range tissues working in tandem to facilitate the optimum functioning of the living-being. Each tissue is composed of a specialised set of cells with a defined function within the organism, e.g. blood, skin, muscle, germline tissues. These tissues will be required to grow and develop from the embryo through to adult-life. Moreover, adult tissues (and earlier tissues) will require substantial maintenance, continuously repairing and replacing dead, damaged or old cells within the specialised tissue. In the case of the germline, the production of gametes is also a continuous process, requiring a constant supply of new germ cells to produce sperm/eggs on demand. Cellular differentiation is the process whereby specialised cell types arise from unspecialised (undifferentiated) cells in development. Thus, the development of an embryo and maintenance of adult tissues require the process of cellular differentiation in order to grow and survive in its environment.

Stem cells are unspecialised cells of multicellular organisms that can differentiate into a broad spectrum of cell types. They are found through embryonic development and in adult tissues. Unlike regular mitotic cells, stem cells divide to produce two daughter cells of differing cell fate: 1) a differentiating daughter cell, and 2) a self-renewing stem cell. As a result, the stem cell population is maintained by stem cell self-renewal whilst allowing cellular differentiation for the development of, or maintenance of the organism. Thus, a stem cell will remain the earliest cell within a cell lineage/tissue.

Stem cells maintain lineages by ensuring self-renewal (Morrison and Kimble, 2006). They achieve this through two types of cell division: symmetric and asymmetric cell divisions. A symmetric cell division (SCD; analogous to a canonical mitotically-dividing cell) gives rise to two daughter cells of cell fate. SCD can thus increase or decrease stem cell population by producing two 'stem' (thus doubling the stem cell population) or two 'differentiating' daughter cells (thus reducing the stem cell number) In contrast, asymmetric cell division (ACD) results in daughter cells of unequal cell fate: producing a self-renewing stem cell to maintain the stem cell population, and a daughter (progenitor) cell committing to differentiation into a defined cell type (Horvitz and Herskowitz, 1992; Knoblich, 2008; Morrison and Kimble, 2006). Therefore, ACD is required in all stem cells (totipotent to unipotent) in order to generate and retain organism complexity from the developing embryo through adult life

There are two general stem cell types: embryonic and adult stem cells (Fuchs and Segre, 2000):

Embryonic stem cells (ESCs) are one of the earliest stem cells in an organism. Totipotent (embryonic) stem cells, derived in the first few divisions after fertilisation (0-4 days) are the only stem cells in an organism capable of differentiating into all cells of the human body (i.e. all three germ layers and the extra-embryonic tissue). However, these cells lose their totipotency after 4 days. Thus, they are naturally very ethically challenging and difficult to isolate (Rathjen and Rathjen, 2013). Instead, later-stage ESCs are generally used in research, derived from the inner cell mass of the blastocyst stage (~5 days post fertilisation) during embryonic development (Shamblott et al., 1998; Thomson, 1998). These cells are pluripotent, meaning they have the capacity to differentiate into almost every cell type in the body (in excess of 200 cell types), minus the extra-embryonic tissue (e.g. placenta). ESC differentiation begins with differentiation into the three germ layers at the gastrulation stage of development: the ectoderm, mesoderm and endoderm (Rathjen and Rathjen, 2013). Thus, these cells are highly valuable in terms of regenerative medicine.

Adult (somatic) stem cells are distinguished from ESCs in that they are found in select stem cell microenvironments (also termed 'niche') (e.g. germline, bone marrow, adipose) (Fuchs et al., 2004). Their primary role is the replenishment and replacement of cells within a select tissue. Hence, in contrast to ESCs they are either multipotent or unipotent, meaning they can only differentiate into a few/one cell type(s). Examples of such adult stem cells include hematopoietic stem cells (blood and immune cells; multipotent), mesenchymal stem cells (muscle, adipose, bone and cartilage; multipotent) and germline stem cells (gametes; unipotent). Thus, within their lineage/tissue, adult stem cells are vastly outnumbered by progenitor (cells that are pushed towards differentiating into a specific cell type) and terminally-differentiated cells. Unlike ESCs, adult stem cells lack the ability to differentiate into the three germ layers. However, adult epithelial cells can be reprogrammed into (induced) pluripotent stem cells (iPSCs). Yamanaka famously first demonstrated this using transcription factors (Octamer-binding transcription factor 3/4 (Oct3/4); Sex determining region Y-box 2 (Sox2); Myc; Krüppel-like factor 4 (Klf4)) resulting in the reprogramming of mouse fibroblast cells into a pluripotent state (Takahashi and Yamanaka, 2006).

1.1.3 Asymmetric Cell Division in Specialised Tissues

To generate differing cell types and organism complexity, subsets of cells within a living organism maintain an ability to divide asymmetrically (Horvitz and Herskowitz, 1992; Knoblich, 2008; Morrison and Kimble, 2006) Here, ACD produces daughter cells of differing cell fates (discussed above). Notably, all stem cells can divide asymmetrically to produce 1) a daughter cell that self-renews and maintains stem-like properties, and 2) a daughter cell committed to differentiation (Figure 1.2). For example, adult neural and germline stem cells are the foundation to the processes of neurogenesis (Zhao and Moore, 2018) and gametogenesis (Lehmann, 2012; Spradling et al., 2011) – the development of neurons and gametes. Hence, the asymmetry of a stem cell division allows for the generation and maintenance of diverse cellular complexity, from development of the three germ layers to the maintenance of adult lineages.

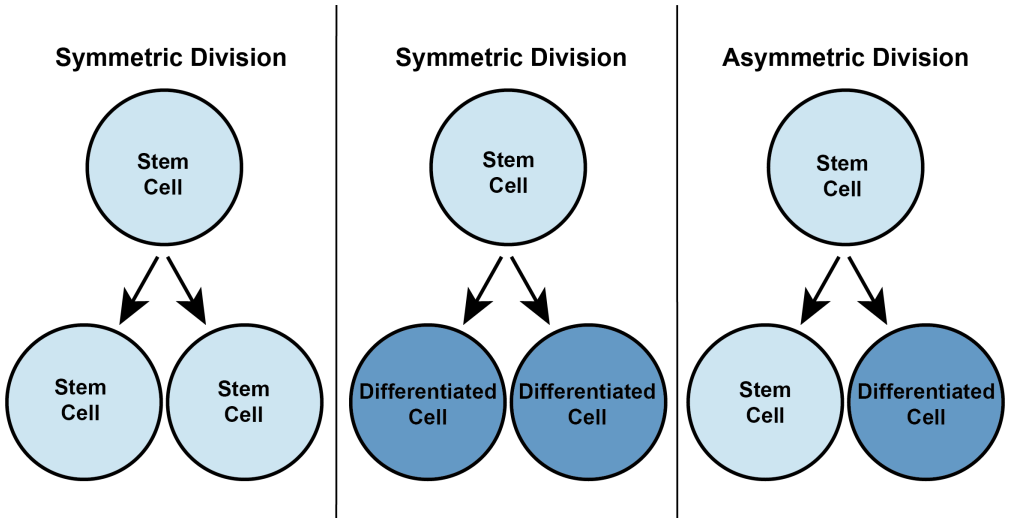

Figure 1.2: Schematic of symmetric and asymmetric divisions of a stem cell. Analogous to a canonical mitotically-dividing cell (e.g. HeLa cell), stem cells can divide symmetrically to produce daughter cells of equal cell fate, such as that of stem cell self-renewal (left) or stem cell loss (middle). To maintain a the stem cell population, stem cells must divide asymmetrically to produce daughter cells of unequal cell fate; a self-renewing stem cell and a differentiating daughter cell (right). The molecular control of these cell fate decisions are fundamental to stem cell biology.

Measuring the frequency of ACD versus SCD in a multicellular organism presents its own challenges due to dissection and fixation at specific timepoints. Moreover, long-term live imaging *ex vivo* also presents issues with tissue viability. Hence, to date, the frequency has been estimated best through lineage tracing methods whereby fluorescent tags (e.g. Green Fluorescent Protein, GFP) or nucleotide analog (e.g. 5-Ethynyl-2′-deoxyuridine, EdU) can be used to track stem cells dividing symmetrical versus asymmetric. Hence, stem cells undergoing SCD will express GFP (or alternative) in both daughter cells, whereas asymmetric stem cells will not. For example, the frequency of ACD versus SCD was measured for *Drosophila* male germline stem cells (GSCs). Here, SCD is limited to 1-2 % of all GSC divisions (Salzmann et al., 2013). In contrast, Sheng and Matunis reported much higher frequencies of symmetric self-renewal (7 %) versus symmetric

differentiation/GSC loss (13 %) using live analysis (Rebecca Sheng and Matunis, 2011). Thus, an exact measurement on ACD versus SCD frequencies in any tissue proves difficult. Nonetheless, ACD and SCD exist *in vivo* and function to maintain (ACD) and increase/decrease (SCD) stem cell number respectively.

Ultimately, the control ACD poses a unique biological question, as unlawful disturbance to asymmetry (stem cell self-renewal versus differentiation) will have profound implications on normal tissue homeostasis. This may potentially drive the development of diseases such as cancer and infertility due to aberrant proliferation of differentiated versus undifferentiated cell states (Clevers, 2005; Knoblich, 2010; Morrison and Kimble, 2006).

1.2 The Control of Asymmetric Cell Division in Stem Cells

1.2.1 Extrinsic versus Intrinsic Control of Adult Stem Cells

Stem cells regulate their proliferation and cell fate decisions through a multifaceted combination of extrinsic and intrinsic cues (Knoblich, 2008). The stem cell microenvironment (or niche), defined as a region of tissue where the stem cell resides and interacts with that region, plays a pivotal intercellular role in the regulation of the extrinsic factors that control the adult stem cell fate decisions. That is, to self-renew or differentiate (Losick et al., 2011; Morrison and Spradling, 2008; Resende and Jones, 2012). Here, the activation or suppression of signalling ligands from the niche act to regulate stem cell proliferation in space and time. For example, Janus Kinase Signal Transducers and Activators of Transcription (JAK-STAT) and Bone Morphogenic Protein (BMP) are well conserved signalling and are known to influence spatiotemporal cell division within stem cell niches (Herrera and Bach, 2019; Issigonis et al., 2009; Stine and Matunis, 2013; Zhang and Li, 2005). In *Drosophila* stem cell niches, these signalling pathways have been extensively studied and are reasonably well understood. This signal transduction from the stem cell niche provides the self-renewal or differentiation cues to maintain or differentiate away from the niche.

Intrinsic factors have also been extensively studied, particularly in relation to cell polarity and protein/RNA localisation (Ryder and Lerit, 2018; Shlyakhtina et al., 2019; Venkei and Yamashita, 2018). Stem cells must be polarised (meaning they possess directionality) relative to their microenvironment to facilitate an ACD, meaning the cellular architecture and its surroundings is asymmetrically orientated to divide away from the niche (Knoblich, 2008). Here, ACD versus SCD depends on spindle (and centrosome) orientation within the cell (Morin and Bellaïche, 2011). ACD in adult stem cells require a mitotic spindle orientated perpendicular to the apical stem cell niche, as opposed to spindle orientation ‘in parallel’ to the stem cell niche. Thus, microtubules and their organising centres respond to self-renewal and differentiation cues accordingly (Morin and Bellaïche, 2011). Ultimately, regardless of the type of ACD (stem or meiotic), intrinsic factors work

on multiple levels to coordinate polarity and ultimately suppression or activation of gene expression within the cell.

1.2.2 Non-Random Segregation of Sister Chromatids

Before a cell divides, its genetic material needs to be replicated, condensed and segregated between daughter cells (Section 1.1.1). Here, the parent cell segregates its chromosomes equally between daughter cells to avoid chromosome gain/loss (aneuploidy). Moreover, each sister chromatid segregation for each chromosome is random and therefore non-selective. However, a small subset of cells maintain an ability to segregate their chromosomes non-randomly, and this selective partitioning for sister chromatids could ultimately impact the cell fate or future identity of the daughter cell. Non-random sister chromatid segregation is the phenomenon by which two, supposedly, identical sister chromatids can be recognised and selectively segregated towards a specific daughter cell (Figure 1.3; Schematic of Non-random Chromosome Segregation). Non-random segregation of these DNA strands have been observed in numerous stem cell populations (Conboy et al., 2007; Fei and Huttner, 2009; Rocheteau et al., 2012). Here, the information stored between sister chromatids (i.e. epigenetic marks and/or DNA strand inheritance *per se*) would influence its segregation to stem or daughter cell. However, the exact 'randomness' of the DNA strand inheritance itself between daughter cells in a stem cell division rema ins highly debatable. In order to explain non-random sister chromatid segregation and its impact on cell fate in an asymmetric (stem) cell division, two primary (opposing) hypotheses have been proposed: the 'Immortal Strand' hypothesis and the 'Silent Sister' hypothesis.

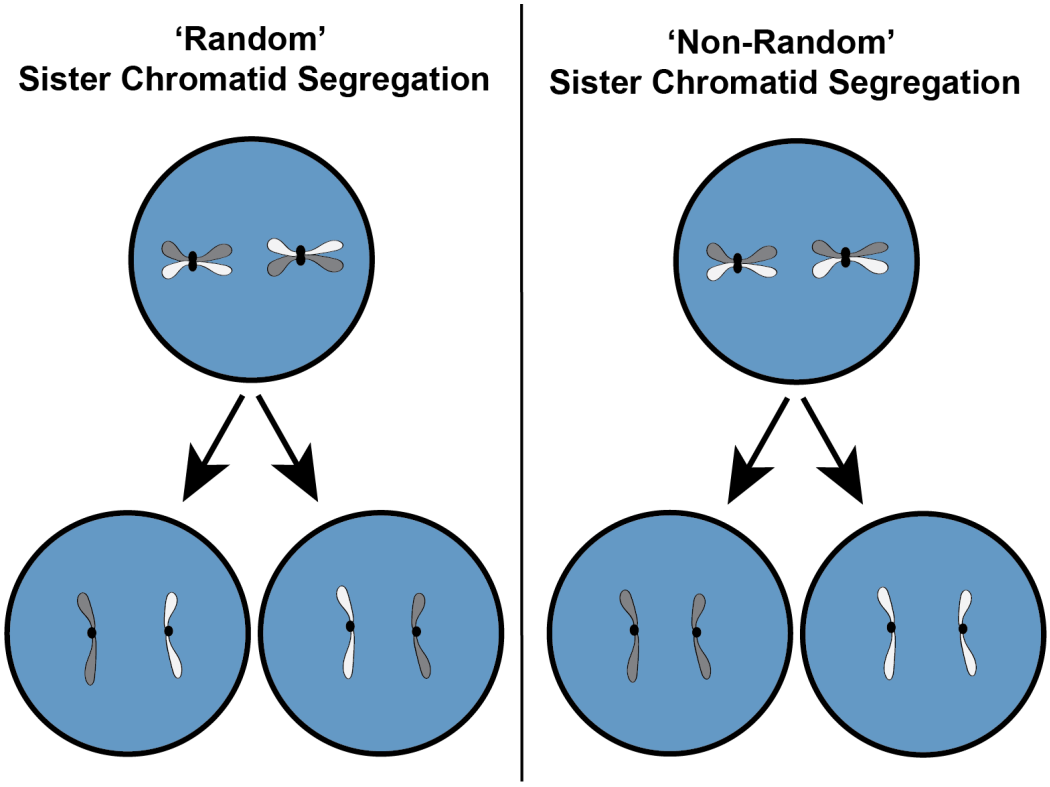

Figure 1.3: Schematic of Non-random Sister Chromatid Segregation. Sister chromatids in a canonical symmetrically-dividing mitotic cell divide randomly (left). Sister strands condense into mitotic chromosomes and orientate themselves randomly at the metaphase plate. Completion of mitosis segregates each sister chromatid randomly into each daughter cell. Some cells (e.g. stem cells) segregate their chromosomes non-randomly (right). Asymmetrically-dividing mitotic cells align their chromosomes in a specific orientation at the metaphase plate to favour segregation into a specific daughter cell.

1.2.3 Non-Random Chromosome Segregation and the Immortal Strand Hypothesis

In 1975, Cairns proposed the 'immortal stand' hypothesis in order to explain the non-random segregation observed in stem cell populations (Cairns, 1975). This hypothesis proposes that stem cells divide predominantly asymmetrically, but these adult stem cells retain the older, parental DNA template. In retaining the parental DNA strand, the hypothesis assumes the parental stand is protected from aberrant mutations resulting from erroneous DNA replication ('immortal'). Hence, the accumulation of errors within the stem cell pool is vastly decreased and protected from genetic instability (Cairns, 1975).

Until recently, the immortal strand hypothesis has proved quite resistant to challenge, given the limitations in methodology to robustly test its claim. However, no clear molecular mechanism has been proposed and numerous pieces of evidence now strongly oppose this hypothesis (reviewed by Lansdorp, 2007; briefly summarised below):

- The DNA in each cell is subject to thousands of chemical modifications and lesions each day, independent of replication error. These mutations occur on both DNA strands an are efficiently repaired by the DNA repair machinery.
- Both strands of DNA in a cell encode genes, with some genes even overlapping on opposing strands. Hence, the idea of some genes being better protected than others appears unlikely.
- Some DNA repair pathways are known to require exchange between sister chromatids. Sister chromatid exchange (an active process in some DNA repair pathways) would interfere with the maintenance of the parental strand. Cairns proposed that would stem cells combat this by 'altruistic suicide' upon DNA damage. This requires a DNA damage response that neither exists in precursors of, or progeny of stem cells.
- It has been suggested that telomere shortening is prevented in stem cells that retain immortal strands. However, only the 3' end of a parental stand could be prevented from telomere shortening. This is due to the requirement

of the 5' end to be processed after replication, creating a single strand 3' overhang essential for telomere function. Hence, telomere shortening is predicted to occur in stem cells, regardless of which strand is retained. Indeed, it has recently been shown that human ESCs regulate their telomere length between two extremes through elongation and trimming processes (Rivera et al., 2017).

- The coding sequence of a genome is not the only determining factor behind normal development and the aetiology of disease. Nuclear transplantation experiments have shown that the transfer of nuclei from a differentiated somatic cell, or even a tumour cell, can produce a mammalian offspring. Hence, these experiments show that the epigenetics behind both normal development and oncogenesis are vastly underpinned in the context of reprogramming.

Studies from the Yamashita lab in the well-characterised *Drosophila melanogaster* male germline stem cell (GSC) niche unambiguously oppose this hypothesis, concluding that immortal strands do not exist in this system (Sherley, 2011; Yadlapalli et al., 2011a, 2011b). Firstly, they used 5'-bromo-2'-deoxyuridine (BrdU) labelling combined with direct visualisation of GSC-Gonialblast (stem-daughter) 'pairs' to score chromosome strand segregation (Yadlapalli et al., 2011a). Moreover, the authors revisited this topic whist developing the chromosome orientation fluorescence in situ hybridization (CO-FISH) technique with single strand resolution for use in tissue (Yadlapalli and Yamashita, 2013). Surprisingly, they show that sister chromatids of X and Y chromosomes, but not autosomes, are selectively segregated between stem and daughter cell. However, these parental strands of both X and Y chromosomes are not immortal, switching template strands approximately 1/7 GSC divisions (Yadlapalli and Yamashita, 2013). Significantly, when analysing *DNA methyltransferase-2* (*dmnt2*) mutants, this selective segregation of sex chromosomes was randomised (Yadlapalli and Yamashita, 2013). Although the exact function of DNA methylation and Dnmt2 in *Drosophila melanogaster* remains elusive and controversial (Kunert et al., 2003; Takayama et al., 2014; Zemach et al., 2010), these results clearly show an epigenetic component in controlling and maintaining a model of non-random segregation. The requirement of DNA methyltransferase activity to the fidelity of

non-random segregation was further backed up in asymmetrically-dividing, differentiating embryonic stem cells (human and mouse), when Elabd *et al* clearly demonstrated the involvement Dnmt3 in this process. Here, the authors show non-random chromosome segregation is associated with asymmetric cell fate, and used Dnmt inhibitors and (separately) Dnmt3 null mutants to confirm a role for the methyltransferase in this process (Elabd et al., 2013). Thus, it is clear that the concept of 'immortal' template strands is not sufficient to explain a molecular mechanism of non-random segregation in asymmetrically-dividing stem cells.

1.2.4 An Alternative Explanation: the Silent Sister Hypothesis

Many lines of evidence (described above) conclude that the fundamental principles behind immortal strand hypothesis are an inadequate explanation of non-random chromosome segregation. The 'silent sister' hypothesis, proposed by Lansdorp, may help better explain this phenomenon (Lansdorp, 2007). This hypothesis states that rather than immortal strands, ACD (and the subsequent cell fate decisions arising from an ACD) are orchestrated by epigenetic differences between sister chromatids. Here, Lansdorp proposes that following DNA replication, tissue-specific stem cells or progenitor cells maintain differential epigenetic marks between sister chromatids at centromeric DNA and specific genomic loci (Figure 1.4).

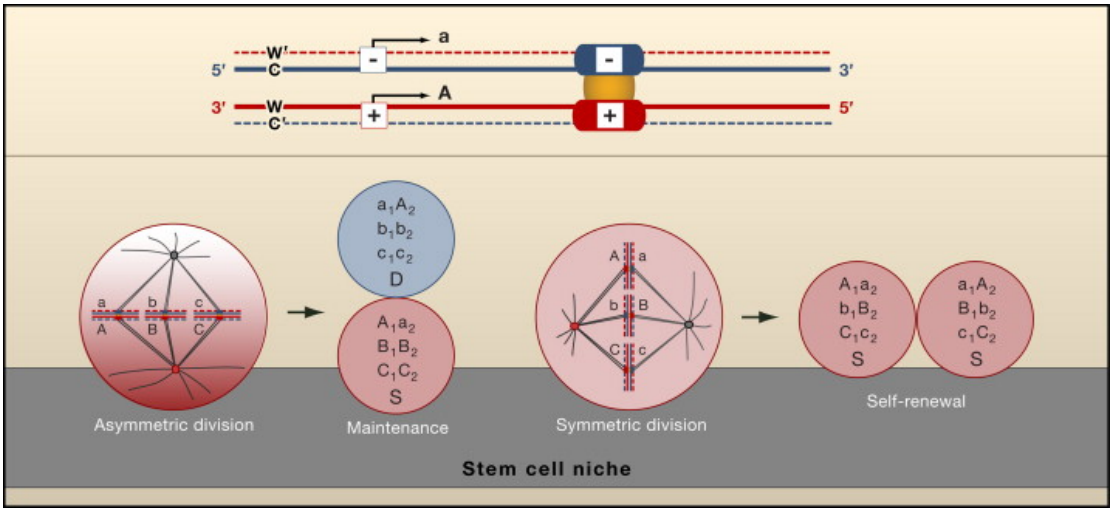

Figure 1.4: The 'Silent Sister' Chromatid Hypothesis as illustrated by Lansdorp, 2007. (Top Panel) At metaphase, differential epigenetic marks at the centromere and other stem cell gene locations (indicated by +/-) distinguish sister chromatids to be inherited by stem and daughter cells. This epigenetic distinction at centromeres enables recognition and distinction of sister chromatids for segregation. This non-random sister chromatid segregation is proposed to regulate the activation/silencing (A, expressed; a, silent) of genes in the differentiating cell. (Watson 5'strand, W; Crick 3' strand, C).

(Bottom Panel, left, Asymmetric Division) Adult stem cells divide asymmetrically away from the stem cell niche creating polarity in its division. Here, a polar asymmetric stem cell division shows a selective attachment of microtubules emanating from asymmetric centrosome inheritance, perpendicular to the stem cell niche. Selective partitioning of sister chromatids results in higher maintenance of active copies of stem cell genes (numbered; A_1/A_2, B_1/B_2, C_1/C_2) in the stem cell (red) compared to silent copies of the same stem cell genes (lower case; a, b, c) in the differentiating cell (blue). Disruption to the epigenetic maintenance of stem gene expression (possibly in combination with inadequate tumour suppression functions may result in defective cell proliferation. These defects may arise due to disrupted cell polarity, sister-chromatid exchange, centromere mispropogation or other pathways proposed to be involved in selective strand segregation.

(Bottom panel, right, Symmetric Division) Adult stem cells can also divide symmetrically, maintaining daughter cell attachment to the stem cell niche in a non-polar manner through the parallel alignment of the centrosome. A non-polar

sister chromatid segregation results in the randomised distribution of active and silent stem genes between daughter cells. This results in the self-renewal of stem cells, maintaining the stem cell's attachment to the stem cell niche. The epigenetic differences between sister chromatids is then restored in the following DNA replication after this symmetric cell division.

Epigenetics is the study of the chemical changes to DNA and its associated proteins that alter the gene expression of an cell, without altering the original genetic code. Hence, the original DNA sequence is not inherited alone. In order to pass this 'epigenetic memory' through a (symmetrical) cell division, parental chromatin itself needs to be inherited along with the replicated DNA sequence. Chromatin consists of a complex organisation of DNA and proteins (primarily histone proteins), functioning to package the long complex chains of DNA into compact, heritable structures [discussed in detail in Section 1.2.2] (Alberts et al., 2014). Hence, given this inheritance of a cell's epigenetic signature, the transcriptional status of the daughter cell in a canonical cell division is informed.

Specifically, Lansdorp proposes that epigenetic differences between sister centromeres is required to direct non-random sister chromatid segregation during mitosis. Furthermore, differential epigenetics at certain genetic loci could positively/negatively regulate expression of 'stem'-specific genes post-mitotically between stem and daughter cells. Apart from at these specific sites, the cellular asymmetries predicted (and since proven) would be otherwise limited to cell polarity and mitotic spindle orientation (or timing). Briefly, the centrosome (the main microtubule organising centre) has been shown to be preferentially orientated in multiple systems, and so influencing ACD through intrinsic cellular orientation. To facilitate ACD versus SCD within a stem cell niche, the centrosome polarises itself perpendicular to (ACD) or parallel to (SCD) to the niche in order to organise the microtubules in such a way as to maintain or increase stem cell number (Figure 1.4). Moreover, mother/daughter centrosome inheritance between stem and daughter cell in different adult stem cell populations varies in its directionality (discussed later). Seemingly, a coordinated effort between the microtubule organising centre(s) and the epigenetic landscape of each sister chromatid (particularly at the centromere/kinetochore) would be important for the intrinsic control of ACD in adult stem cells. Importantly, regardless of whether 'immortal strand' or 'silent sister' hypotheses are preferred, both ideologies still require distinction of sister chromatids at kinetochores to facilitate non-random segregation (Lansdorp et al., 2012; Tran et al., 2013). The nature of these epigenetic asymmetries between sister centromere/kinetochores (Dattoli et al., 2020; Ranjan et al., 2019), as well as on chromatin (Tran et al., 2012; Wooten et

al., 2019b; Xie et al., 2015), are now beginning to emerge. These will be discussed in detail throughout. In the context of an ACD, any alteration to this transgenerational heritability of parental chromatin between parent and daughter cell could allow for changes to the inherent 'asymmetry' of the division and subsequently impact cell fate decisions (Lansdorp et al., 2012; Tran et al., 2013).

1.3 A Paradigm of Epigenetic Maintenance: Centromeric Chromatin

1.3.1 The Centromeric Locus and Centromere Protein-A (CENP-A)

The centromere is a chromosomal locus, first identified as the primary constriction site of a condensed mitotic chromosome (Flemming, 1882). It represents a key focal point in the segregation of sister chromatids. It provides the foundation to which the kinetochore is assembled – a large multi-protein complex that provides the link from the centromere to the mitotic spindle. Hence, the centromere and kinetochore are essential to the integrity of chromosome segregation in mitosis and meiosis (Allshire and Karpen, 2008; Barra and Fachinetti, 2018; Black and Cleveland, 2011; McKinley and Cheeseman, 2016; Musacchio and Desai, 2017; Verdaasdonk and Bloom, 2011; Westhorpe and Straight, 2013). Most eukaryotic chromosomes contain only one stable centromere (monocentric) to ensure faithful segregation of genetic material. Hence, dicentric chromosomes are largely unstable and subject to detrimental chromosomal fragmentation, and are a common feature of cancer cells. Stable dicentrics have been observed in both maize and wheat (Han et al., 2006; Zhang et al., 2010), but these plants overcome this problem by centromere inactivation, effectively functioning as a monocentric chromosome. Moreover, loss of centromeric integrity and function will lead to a mis-segregation, aneuploidy and subsequent cell death (Barra and Fachinetti, 2018; McKinley and Cheeseman, 2016).

The molecular composition of the centromere can differ greatly between species (Black, 2017). However, the overall function of the eukaryotic centromere remains highly conserved through evolution. Although centromeric size, complexity, specification and underlying DNA sequences are varied, centromeres can be characterised as point or regional centromeres based on their chromatin composition and their centromeric DNA. The basic point centromere of *Saccharomyces cerevisiae* (budding yeast) is specified genetically by the recruitment of centromeric proteins to a 125 bp consensus site (Furuyama and Biggins, 2007). However, most eukaryotic centromeres/kinetochores are generally associated to these complex arrays of repetitive centromeric DNA sequences.

These regional centromeres of higher eukaryotes (e.g. mammals, plants, flies) are more complex and the underlying DNA alone is not sufficient to define the centromere (Verdaasdonk and Bloom, 2011). Centromeres are thus defined epigenetically by the presence of the histone H3 variant Centromere Protein-A (CENP-A) (McKinley and Cheeseman, 2016).

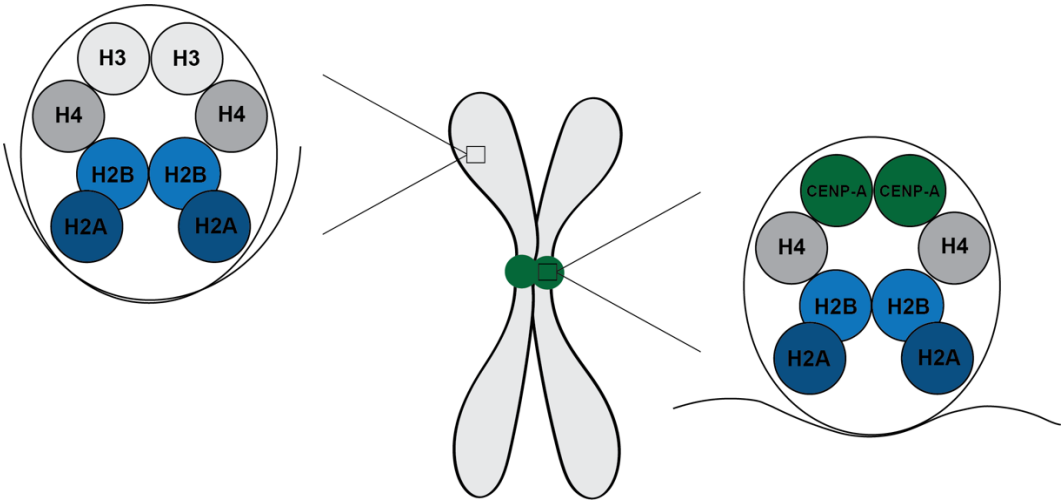

Figure 1.5: The centromere locus and CENP-A nucleosomes. The centromere is located at the primary constriction site of a mitotic chromosome (middle). Canonical nucleosomes containing histone H3 (light grey) on chromosome arms versus CENP-A nucleosomes containing the H3-variant CENP-A (green) at the centromere.

Centromere Proteins -A, -B and -C (CENP-A, CENP-B and CENP-C) were first identified in patients of Calcinosis Raynaud's Esophageal dismotility Sclerodactyly and Telangiectasia (CREST) syndrome, where blotting serum from these patients were found to recognise the centromere locus (Earnshaw et al., 1986; Earnshaw and Rothfield, 1985; Valdivia and Brinkley, 1985). Later, the biochemical composition of CENP-A was determined to be histone-like (Palmer et al., 1991, 1987), with 60% homology to histone H3 and an ability to replace H3 at centromeric nucleosomes (Sullivan et al., 1994; Yoda et al., 2000). At the centromere, CENP-A replaces canonical histone H3 in the central nucleosomal hetero-tetramer (Sekulic et al., 2010; Tachiwana et al., 2011), and is essential for centromeric protein recruitment (Allshire and Karpen, 2008; McKinley and Cheeseman, 2016). Here, centromeric chromatin contains an interspersed arrangement of histone H3 and CENP-A nucleosomes, organised three-dimensionally to orient the CENP-A nucleosomes outwards and the bulk histone H3 towards the inner chromosome (Blower et al., 2002). Moreover, the amount of CENP-A recruited has direct implications on the centromeric architecture and its epigenetic inheritance. It has been determined that the human centromere contains approximately 400 molecules of CENP-A (Bodor et al., 2014). Although this represents a small fraction of the total CENP-A availability, centromeres contain a 50-fold enrichment of CENP-A at the centromere compared to chromosome arms and are dispersed at a ratio of approximately 1:25 with histone H3 (versus 1:200 at other genomic regions) (Bodor et al., 2014). Hence, the centromere organisation is highly complex, requiring a robust mechanism of epigenetic inheritance and maintenance.

Centromeric sequences are amongst the most rapidly evolving genomic regions (Henikoff et al., 2001; Malik and Henikoff, 2009). The repetitive nature of these sequences is highly conserved, but the conservation of the exact sequences themselves are poor. This lends the genetic component of the centromeric region to be largely neither necessary nor sufficient for centromere specification. Centromere size and composition also varies greatly between both individual chromosomes and species. Human centromeres range from 0.5 - 1.5 Mb and consists of 171 bp repeats of α-satellite DNA (Jain et al., 2018; Manuelidis, 1978; Musich et al., 1980; Nechemia-Arbely et al., 2019). The exact role of these

sequences in centromere function is controversial and still under investigation. In some cases, these α-satellites are shown to confer centromere function (Harrington et al., 1997; Ikeno et al., 1998); but data also suggests that they are neither necessary nor sufficient for centromere function (Earnshaw et al., 1986; Warburton et al., 1997). Most compelling however, is the formation of neo-centromeres in the absence of α-satellite DNA (Lam *et al.*, 2006; reviewed by Rocchi *et al.*, 2012) and (α-satellite) centromere inactivation in pseudo-dicentric chromosomes (Rivera et al., 1989), strongly suggesting that these repetitive sequences are not required for centromere function.

In contrast to the rapidly evolving centromeric sequences, the presence of CENP-A on centromeric chromatin is highly conserved and both necessary and sufficient for centromere function. Furthermore, the requirement of CENP-A as the epigenetic mark for centromere specification and function is compelling. Neocentromeres provided the first pieces of evidence for CENP-A as the epigenetically-defining mark – forming centromeres at ectopic sites on chromosome arms (Lam et al., 2006). These rare events have been observed in humans (Voullaire et al., 2001), as well as other species (Rocchi et al., 2012). Specifically, CENP-A is recruited to these neo-centromere sites, yet these sites are absent of α-satellite DNA (and also CENP-B) (Amor and Andy Choo, 2002; Voullaire et al., 2001). These events represent a novel epigenetic event by which the centromere can: 1) be specified by CENP-A alone, 2) be maintained through chromosome segregation, and 3) be trangenerationally inherited (if present in the germline). Similarly, overexpression of CENP-A can result in functional ectopic centromeres (Gonzalez et al., 2014; Heun et al., 2006). Using the *LacO/LacI* system for chromatin labelling, Mendiburo *et al* provided the key data to show CENP-A is sufficient for centromere specification and its epigenetic inheritance (Mendiburo et al., 2011). Palladino *et al* used the same system recently to show de novo centromere formation can be targeted to some specific euchromatic and heterochromatic loci, and maintained through mitotic tissues (Palladino et al., 2020). Ultimately, stable incorporation of CENP-A into chromatin is the foundation to inner kinetochore assembly (primarily CENP-C and CENP-N, discussed later) (Kixmoeller et al., 2020). The epigenetic inheritance of CENP-A is thus key to mitotic potential. Understanding the principles of centromere

inheritance in the context a symmetrical cell division, and how the inheritance of centromeres differs in asymmetric cell divisions will provide the community with intimate detail as to what definitively established, assembles and maintains the centromere, regardless of the (a)symmetry or division.

1.3.2 Nucleosome Structure and the Packaging of Chromatin

The diploid human genome (23 pairs of chromosomes) contains approximately 6 x 10^9 base pairs ("Whole genome - Homo sapiens - Ensembl genome browser 99," 2019) and approximately 2 metres of DNA per cell. Hence, to inherited genetic information between daughter cells in a cell division, the genetic material in a cell needs to be efficiently organised and wrapped into chromatin, and condensed into chromosome structures. This packaging is facilitated by highly basic proteins called histones. A specific arrangement of histone make up the basic DNA packaging unit, the nucleosome – the basic unit of chromatin. Canonical nucleosomes are composed of histones H2A, H2B, H3 and H4, arranging a central $(H3\text{-}H4)_2$ hetero-tetramer around two H2A-H2B dimers (Luger et al., 1997). The nucleosome wraps 146 bp of genetic material in a 1.67 super-helical left handed turn. This left-handed chirality is a consequence is DNA chirality, and is important for allowing the removal of nucleosome and access to particular sequences, e.g. promotors. Each nucleosome is interconnected by a short stretch of linker DNA, of varying length depending on the species and/or tissue-type (Luger et al., 1997). Together, this classical 'beads on a string' model of nucleosomes and chromatin structure (although more heterogenous than originally proposed; (Baldi et al., 2020)) forms the basic structure of chromatin

1.3.3 The Unique Structure of CENP-A Nucleosomes

As previously mentioned, centromeric chromatin comprises of a more concentrated ratio of CENP-A:H3-containing nucleosomes versus other genomic regions (1:25 versus 1:200) (Bodor et al., 2014). Hence, CENP-A replaces histone H3 in some, but not all, nucleosomes at the centromere. The histone-fold domain (HFD) mediates the interactions between histones. The HFD contains three alpha

helices (α1-3) interspersed between two loops (L1 and L2). Canonical histones contain a highly conserved HFD. However, CENP-A is an exception, being relatively poorly conserved (~60 % homology with H3) (Sullivan et al., 1994).

CENP-A contains some unique features allowing it to be distinguished from histone H3 and other H3 variants (Figure 1.6). In general, the histone core of CENP-A is more hydrophobic, but the overall structure of the CENP-A nucleosome largely resembles a canonical H3 nucleosome (Sekulic et al., 2010; Tachiwana et al., 2011). However, some key differences have been observed in Sekulic et al and Tachiwana et al, when reconstituting and crystalizing the (CENP-A–H4)$_2$ heterotetramer and human-CENP-A nucleosomes respectively.

- Firstly, Sekulic et al observed that overlaying a CENP-A molecule with histone H3 reveals a distortion in the CENP-A-H4 heterotetramer by between 9-14° between the CENP-A-H4 and H3-H3 dimer pairs (Figure 1.6). This rotation is primarily caused by 2 non-conserved residues specific to the CENP-A-CENP-A interface on the α2 helix (H104, L112) (Sekulic et al., 2010).
- Secondly, when superimposing H3 with CENP-A, a clear difference can be seen at the L1 region (Phe 78 – Phe 84) of CENP-A (Sekulic et al., 2010; Tachiwana et al., 2011). The L1 loop of CENP-A bulges out of the CENP-A nucleosome, with two additional residues (Arg 80 and Gly 82) at the tip of the L1 loop (Sekulic et al., 2010; Tachiwana et al., 2011). Moreover, these additional residues are not required from CENP-A recruitment to centromeres, but are required for the long term stability of CENP-A at the centromere (Tachiwana et al., 2011). The L1/α2 interface of the CENP-A histone core constitutes the CENP-A targeting domain (CATD). This region had previously been shown to be both necessary and sufficient for the recruitment of CENP-A to human and *Drosophila* centromeres (Black et al., 2007, 2004; Vermaak et al., 2002). Moreover, Fachinetti et al demonstrated the importance of the CATD to maintaining centromere positioning (Fachinetti et al., 2013). It has been proposed that this protruding CATD could be responsible for the recruitment of the

constitutive centromere associated network (CCAN), allowing the recognition of the centromere site and building of the kinetochore (Stellfox et al., 2013). Indeed, both human CENP-C and CENP-N interact with the CATD of CENP-A, forming the basis of the constitutive centromere associated network (CCAN, discussed in section 1.2.4). Holliday Junction Recognition Protein (HJURP), the molecular chaperone of CENP-A (Dunleavy et al., 2009; Foltz et al., 2009), also recognises CENP-A via the CATD, and is sufficient for CENP-A assembly (Bassett et al., 2012; Foltz et al., 2009).

- It was also reported the 13 bp of DNA at the entrance and exit regions of the CENP-A nucleosome were disordered, with only the central 121 bp α-satellite DNA visible (Tachiwana et al., 2011). The differences of these 'DNA-end' structures could be explained by structural differences between CENP-A and H3, particularly at the amino-terminal. Most likely, these regions facilitate the adaption of the nucleosome into tightly-packed, heterochromatic regions.

In conclusion, the CENP-A nucleosome is highly adapted for function in centromeric chromatin. Particularly, the CATD region of CENP-A bulges outward and is the focal point for connecting the CENP-A nucleosome to the kinetochore (CENP-C, CENP-N and also HJURP). Ultimately, this CATD is critical for maintenance (next section) and assembly (Section 1.3) of CENP-A in the cell cycle. In the context of ACD, any epigenetic differences at the centromere (proposed by the silent sister chromatid hypothesis) will require the cooperation between the maintenance and assembly of CENP-A between sister centromeres, and a detailed understanding of the self-propagation of the centromere throughout the cell cycle.

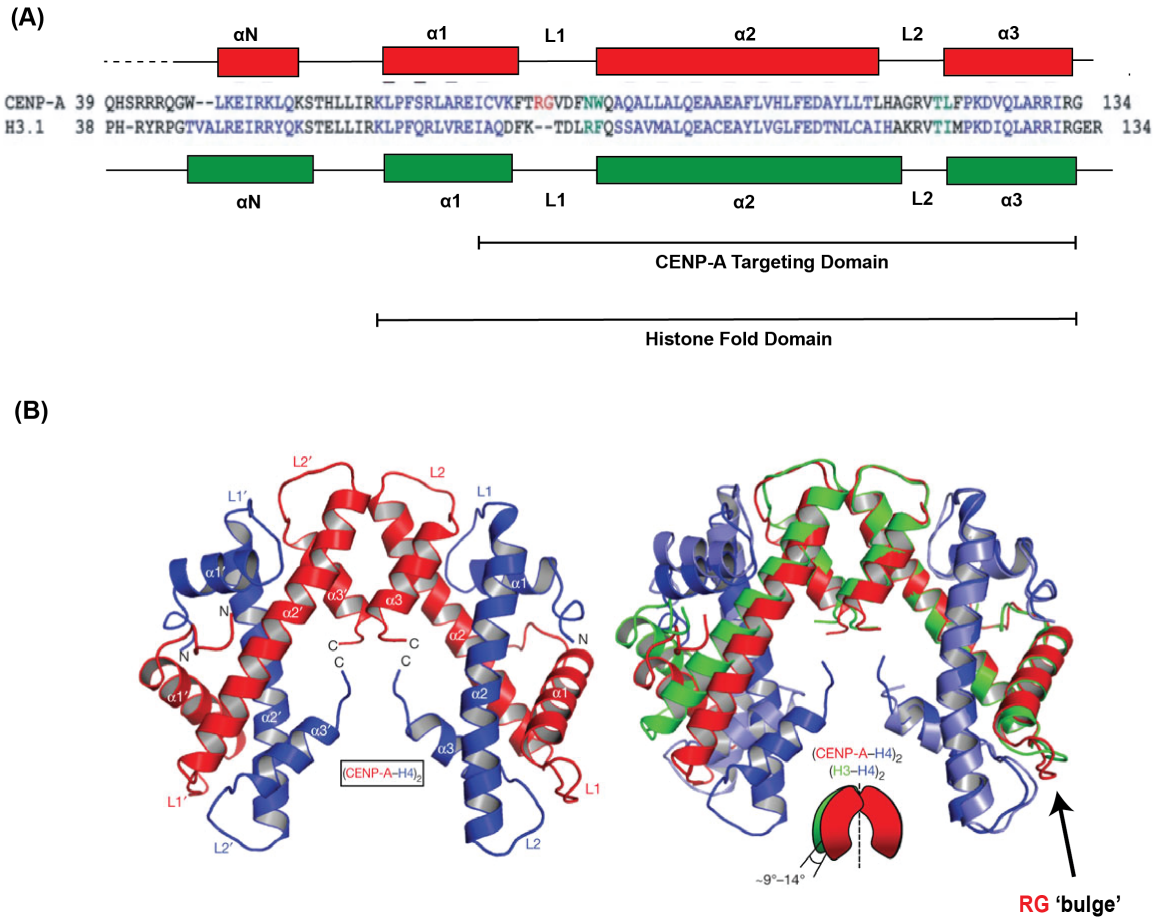

Figure 1.6: Overlay of human Histone H3 and CENP-A. (A) Comparison of the amino acid differences between CENP-A (red) and H3.1 (green). Note the Arg-Gly insertions (red) in the L1 loop. Adapted from Tachiwana et al, 2011. (B) Crystal structure of the CENP-A-H4 heterotetramer (left) and an overlay of $(CENP\text{-}A\text{-}H4)_2$ with $(H3\text{-}H4)_2$ (right). Note: (1) the rotation of the CENP-A relative to H3 and (2) the L1 bulge caused by the Arg-Gly (RG 'bulge') insertion. Adapted from Sekulic et al, 2010.

1.3.4 Building a Stable Centromere: The Constitutive Centromere Associated Network

Faithful segregation of the duplicated genetic material is achieved through the tightly regulated alignment of chromosomes at the metaphase plate, and the bridging of mitotic spindle to the sister centromere via the kinetochore. Here, most eukaryotic kinetochores harbour bundles of microtubules (called k-fibres) that create a tensile force to allow chromosome segregation to occur. However, the underlying centromere needs to be propagated and maintained in an epigenetic loop throughout the cell division and cell cycle to prevent the loss of centromere identity. Alone, CENP-A is unstable through the cell cycle (particularly through S-phase) (Nechemia-Arbely et al., 2019). The Constitutive Centromere Associated Network (CCAN) is a complex of proteins associated with centromeric chromatin whose roles are to maintain the centromere identity through the cell cycle, and form the inner kinetochore interface to assemble the microtubule binding complex (Figure 1.7).

Originally named the CENP-A NAC/CAD (CENP-A Nucleosome Associated Complex/CENP-A Distal) complex and the CENP-H/I kinetochore complex, the CCAN was first identified as a set of proteins that could be affinity purified with CENP-A nucleosomes (Foltz et al., 2006; Okada et al., 2006). These same proteins were identified also in an interphase centromeric complex (Izuta et al., 2006), suggesting that these proteins could be ‘constitutive’ at the centromere throughout the cell cycle. Thus, in addition to CENP-A, a group of 16 other CENP’s associate proximally with centromeric chromatin (CENP-C/-H/-I/-K/-L/-M/-N/-O/-P/-Q/-R/-U/-S/-T/-W/-X). These proteins were analysed bioinformatically and identified as orthologues of the *Schizosaccharomyces pombe* Sim4 complex of kinetochore proteins (Liu et al., 2005; Meraldi et al., 2006; Pidoux et al., 2003), suggesting that these proteins are conserved. Importantly, some these of these protein complexes are directly involved in stabilising CENP-A at centromeric chromatin. Two (inner kinetochore) proteins in particular bind directly to CENP-A and confer this strong stability (in humans): CENP-N and CENP-C (Guo et al., 2017). These proteins form the foundation of the Constitutive Centromere Associated Network (CCAN), participating in centromere maintenance and forming the basis of the connections

between centromeric DNA/chromatin and incoming microtubules. This study uses *Drosophila melanogaster* as a model system, which does not contain a known CENP-N homologue (discussed later in 1.2.6). Hence, this thesis gives particular focus to CENP-C's involvement in the maintenance and assembly of CENP-A.

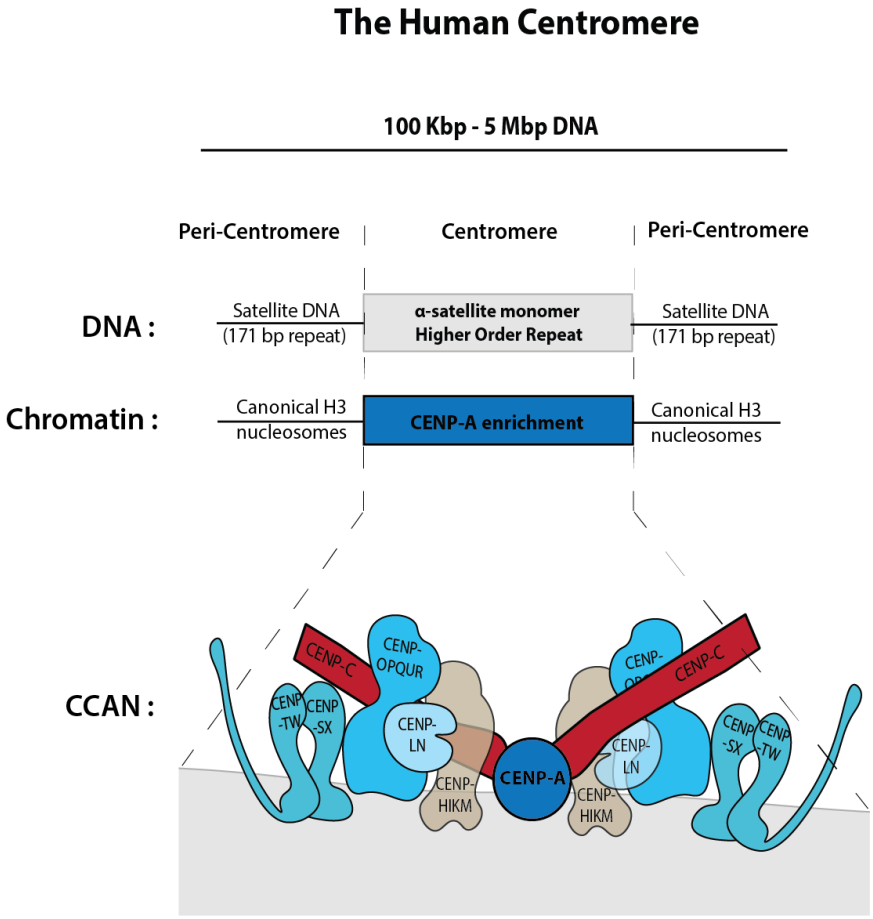

Figure 1.7: Schematic of the mammalian centromere and CCAN. The human centromere spans 100 Kbp to 5 Mbp of DNA sequence. The underlying sequence of human DNA consists of a 171bp alpha-satellite monomer tandemly repeated into a higher order repeat (HOR). Centromeric chromatin consists of an enrichment of CENP-A-containing nucleosomes. The Constitutive Centromere Associated Network (CCAN) is a complex multi-protein arrangement of CENP's that form the foundation of the inner kinetochore link between the centromeric locus and the mitotic machinery. The CCAN can is arranged into a number of sub-complexes including: CENP-C, CENP-L/N, CENP-O/P/Q/U/R, CENP-T/W/S/X (Figure by Dr Caitriona Collins).

1.3.5 The Characteristics of CENP-C and its Role in CENP-A Nucleosome Stability

CENP-C was among the first centromere proteins to be identified along with CENP-A and CENP-B in serum of CREST syndrome patients (Earnshaw and Rothfield, 1985; Saitoh et al., 1992). It is an essential and constitutive centromere protein that forms the platform to which the kinetochore can assemble in many systems (Klare et al., 2015; Przewloka et al., 2011) (Figure 1.8). When depleted, centromere and kinetochore formation are drastically compromised, abolishing CCAN localisation to the kinetochore (Klare et al., 2015; Orr and Sunkel, 2011; Przewloka et al., 2011). Specifically, the N-terminal PEST-region of CENP-C is responsible for the recruitment of the CCAN and the principle connection between centromere and kinetochore (Cohen et al., 2008; Klare et al., 2015). However, along with its role in kinetochore formation, it has also been shown to be intimately involved in the maintenance of CENP-A at the centromere via its central or C-terminus domain (depending on the system) (Cohen et al., 2008; Falk et al., 2016, 2015; Heeger et al., 2005; Roure et al., 2019). The C-terminus also mediates dimerisation of CENP-C (Medina-Pritchard et al., 2020; Roure et al., 2019; Trazzi et al., 2009; Xiao et al., 2017) in addition to interacting with the CENP-A assembly machinery (see later sections). Although numerous studies had shown that CENP-C is essential for maintaining centromere identity, structural data for how (human) CENP-C maintains CENP-A at the centromere remained elusive until recently.

Initially, crystal structures of (CENP-A-H4)$_2$ revealed a unique conformation; in which the CENP-A-CENP-A interface is significantly rotated in comparison to the H3-H3 interface of canonical nucleosomes (Sekulic et al., 2010). To avoid steric clashing, this rotation requires a ‘stretching’ of H2A-H2B dimers. In 2015, the Black laboratory biochemically reconstituted the human CENP-A nucleosomes with and without its binding partner CENP-C, unveiling some interesting details about the relationship between CENP-A/CENP-C’s interaction (Falk et al., 2015) (Figure 1.8). In humans, CENP-C recognises CENP-A via its central domain (CD; aa426-537) (Carroll et al., 2010; Kato et al., 2013). Measuring FRET efficiency between two fluorophores on histone H2B subunits, Falk *et al* first determined that H2B distances for CENP-A nucleosomes are further apart (~ 5 Å) in the absence

of CENP-C^{CD} and gets closed when bound to CENP-C^{CD} (Falk et al., 2015). Thus, only upon CENP-C binding is the CENP-A nucleosome reshaped into a functional conformation resembling a canonical H3 nucleosome.

In the same study, Falk *et al* confirmed that this reshaping and 'protection' of CENP-A nucleosomes occurs both at the surface and internally in the nucleosome. Internally, CENP-A nucleosomes lacking CENP-C^{CD} primarily weaken the physical connection between H2A and H4 via an intermolecular β-sheet (Falk et al., 2015). Externally, CENP-C^{CD} was predicted and proven to bind a region spanning the α3 helix and C-terminal residues of CENP-A, as well as discrete regions of histones H2A and H4 (Falk et al., 2015). Hence, CENP-C binding is not limited to the CENP-A histone, but encompasses the entire CENP-A nucleosome to make this rotation and lock CENP-A in place. Significantly, when CENP-C^{CD} binds, the DNA wrapping reverts to that similar to H3 nucleosomes (Falk et al., 2016).

Finally, CENP-C is also DNA binding (Politi et al., 2002; Sugimoto et al., 1994; Xiao et al., 2017). Indeed, the CENP-C^{CD} facilitates this binding in humans (Kato et al., 2013; Trazzi et al., 2009). Moreover, although the budding yeast CENP-C homologue Mif2 does not contain a vertebrate DNA-binding domain, it does contain a CENP-C^{CM} and an AT-hook, already shown to have a role in CENP-A/Cse4 recruitment *in vivo* (Brown, 1995; Cohen et al., 2008; Lanini and McKeon, 2017; Meluh and Koshland, 2017). Xiao *et al* showed that the AT-rich centromeric sequences have an important role in CENP-C recruitment (Xiao et al., 2017). Similarly, *Drosophila* CENP-C contains two AT-hooks that most likely imparts a similar function. Our current picture of centromeric chromatin is largely epigenetic, though other factors (such as sequence) are probably vital to the preferences for centromere identity and function. Although beyond the scope of

this thesis, CENP-C is clearly also occupying crucial real estate for potentially carrying out these functions.

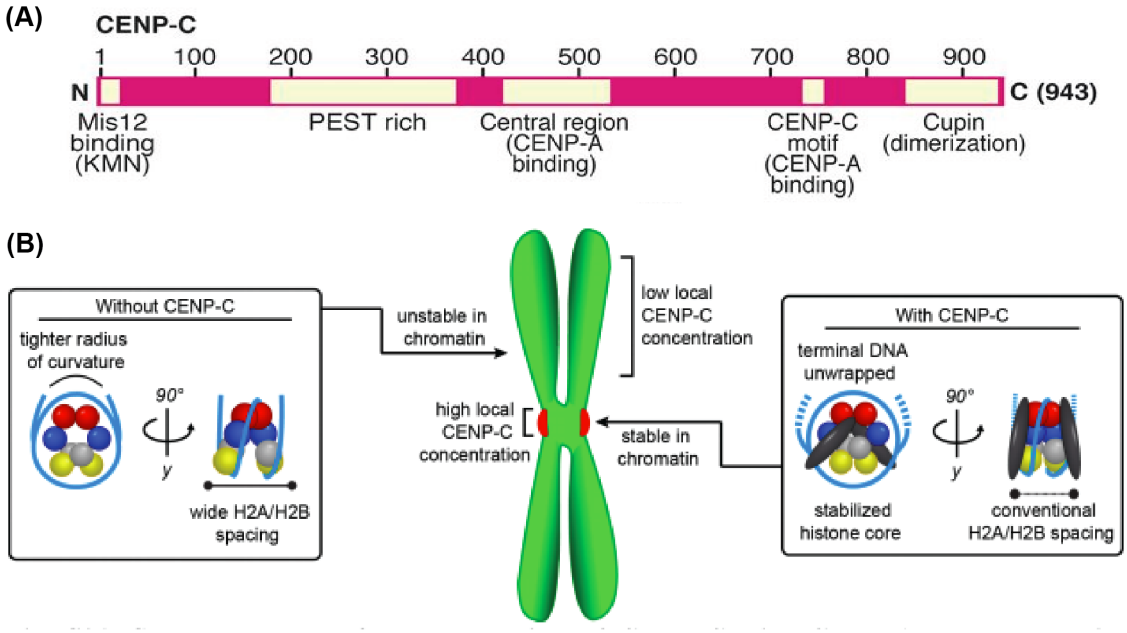

Figure 1.8: CENP-C reshapes the CENP-A nucleosome into its functional conformation. (A) Schematic of human CENP-C (Klare et al, 2015) including: N-terminal Mis12 binding domain, PEST region (CENP-HIKM interactions), Central region (CENP-A binding), CENP-C motif (CENP-A binding), and Cupin domain (CENP-C dimerisation). (B) Illustration of CENP-C-mediated stabilisation of CENP-A nucleosomes at the centromere. Without CENP-C binding, the CENP-A nucleosome adopts a wider spacing, measured by the distance between histones H2A/H2B from the side-on view (left). With CENP-C binding (black oblong), there is a tightening and stabilisation of the CENP-A nucleosome. The spacing between histones H2A/H2B now adopts a conventional H2A/H2B spacing.

To conclude, there is strong structural data for the interactions between CENP-A nucleosomes and CENP-C. CENP-A/CENP-C bind in a manner analogous to an allosteric enzyme reaction or "lock and key" mechanism, whereby CENP-C reshapes and stabilises the CENP-A nucleosome and nucleosomal DNA into its functional conformation (Falk et al., 2016, 2015). In a situation where an ACD requires an asymmetric distribution of CENP-A (discussed in detail in Section 1.3), CENP-C can be predicted to play an important role to maintain (or establish) asymmetry of CENP-A between sister centromeres. By understanding its epigenetic inheritance in context of asymmetric chromosome segregation, one can appreciate the driving factors towards establishing and maintaining a centromere in symmetrically segregating systems.

1.3.6 The *Drosophila* Centromere: A Simplification of an Epigenetic Inheritance Loop

The model organism utilised in this study, *Drosophila melanogaster*, contains a uniquely simple centromere, void of homologs of many of the CCAN components present in mammalian systems (Figure 1.9). Here, in addition to CENP-A (CID in *Drosophila*; hereafter $CID^{CENP\text{-}A}$ (Blower et al., 2002)), only two other centromere proteins have been identified to date: the CENP-A-specific chaperone Chromosome Alignment 1 (CAL1; functional homolog of mammalian HJURP) (Chen et al., 2014; Erhardt et al., 2008; Goshima et al., 2007) and CENP-C (Heeger et al., 2005). Importantly, the CENP-A targeting domain (CATD) of *Drosophila* CENP-A is overall structurally similar to its human counterparts yet contains some distinctions (Vermaak et al., 2002), comprising of aa161-222 (Roure et al., 2019). Particularly, the *Drosophila* CATD is larger than the human CATD, stretching into α3 helix (Roure et al., 2019). Similarly, CENP-A's CATD is akin to the domain recognised by CAL1 (Medina-Pritchard et al., 2020; Rosin and Mellone, 2016). This hints towards similar but simplified epigenetic loop of self-maintenance and propagation compared to the human centromere.

As previously alluded to, centromere specification is epigenetically defined by CENP-A, but sequence does appear to play its role. Recently, the Mellone and

Larracuente labs revisited the *Drosophila* centromeric sequences, deconstructing and elucidating their organisation in detail by combining Chromatin Immunopercipitation (ChIP) with long read sequencing and chromatin fibre immunofluorescence (Chang et al., 2019). In contrast to the previous model where satellite repeats were the thought to be the major functional components, Chang *et al* discovered that a specific retroelement, G2/Jockey-3, was the major component of *Drosophila* centromeric DNA shared across all centromeres. These 'islands' of DNA are enriched in non-Long Terminal Repeat (non-LTR) retroelements buried within a tandem array of repeat sequences (Chang et al., 2019). Retroelements are also not uncommon to centromere sequences, with retroelements being found in humans (Miga et al., 2014), fungi (Yadav et al., 2018), bats (de Sotero-Caio et al., 2017), marsupials (Waugh O'Neill et al., 1998) and gibbons (Carbone et al., 2012). Moreover, donkey centromeres provide a model of evolutionary new centromeres, which are also Long Interspersed Nuclear Elements (LINE)-rich regions (a subgroup of non-LTR retrotransposons) (Nergadze et al., 2018). Significantly, these LINE-rich sequences are also known preferential components of human neo-centromeres (Chueh et al., 2009, 2005), suggesting that CENP-A could in fact be binding preferentially to these retroelement-associated genomic regions (Klein and O'Neill, 2018). Overall, the genetic component behind CENP-A binding and centromere specification is complex and current understanding of such is insufficient to rule out its involvement in centromere function. Hence, centromere sequences do also require some consideration in any study involving the epigenetic specification and inheritance of the centromere, even in future studies involving the centromere and ACD.

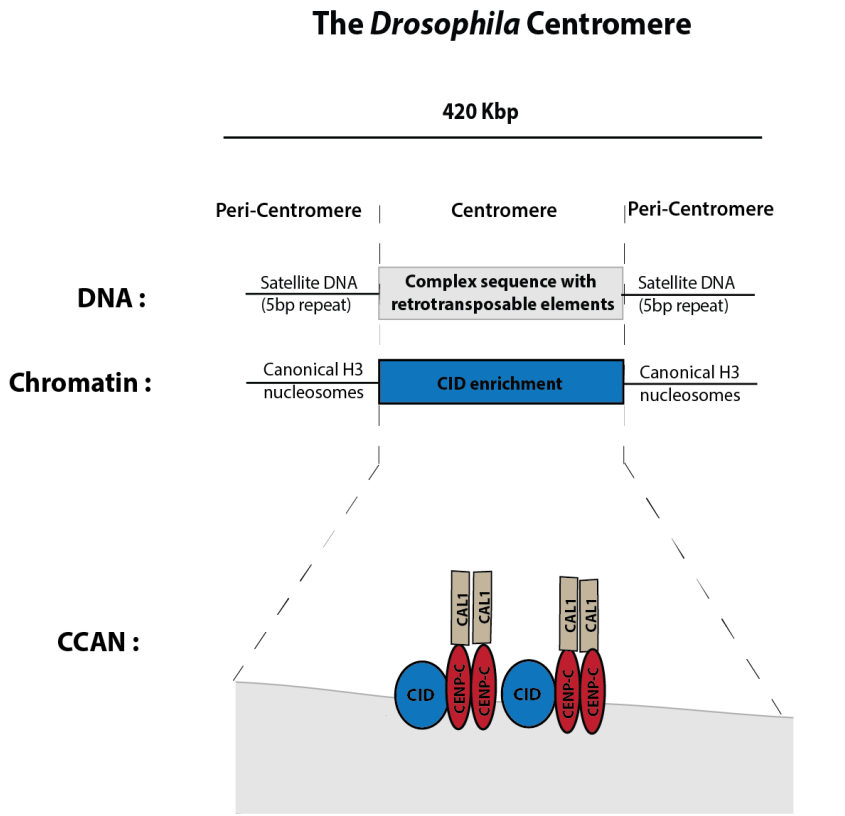
The Drosophila Centromere
420 Kbp
Peri-Centromere
Centromere
Peri-Centromere
DNA :
Satellite DNA
(5bp repeat)
Complex sequence with
retrotransposable elements
Satellite DNA
(5bp repeat)
Chromatin :
Canonical H3
nucleosomes
CID enrichment
Canonical H3
nucleosomes
CCAN :
CAL1
CAL1
CAL1
CAL1
CENP-C
CENP-C
CENP-C
CENP-C
CID
CID

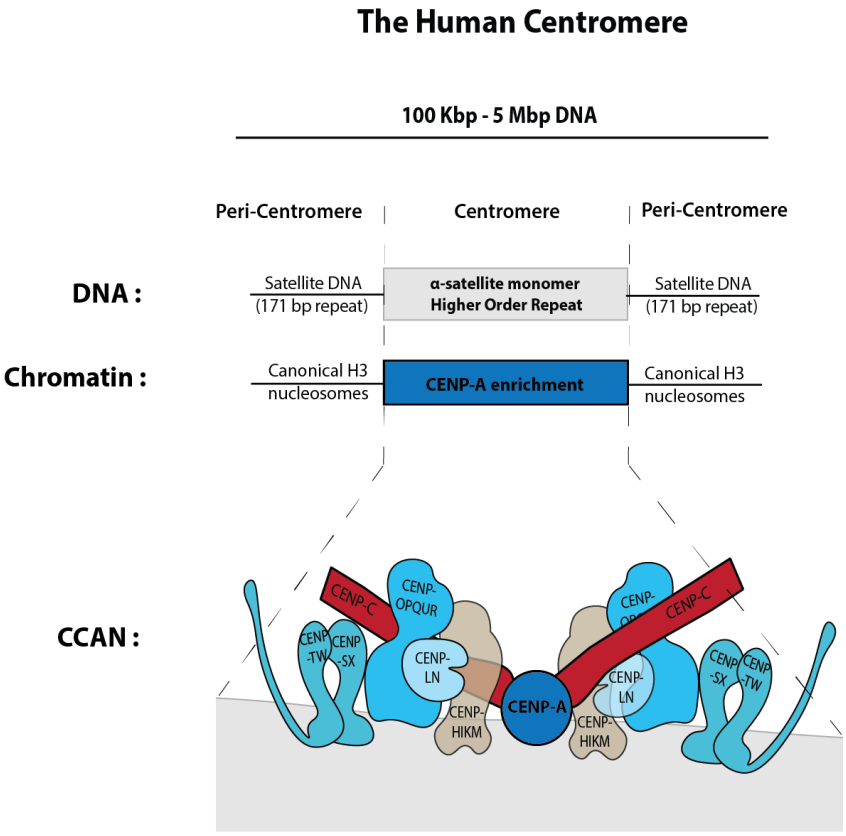
The Human Centromere
100 Kbp - 5 Mbp DNA
Peri-Centromere
Centromere
Peri-Centromere
DNA :
Satellite DNA
(171 bp repeat)
α-satellite monomer
Higher Order Repeat
Satellite DNA
(171 bp repeat)
Chromatin :
Canonical H3
nucleosomes
CENP-A enrichment
Canonical H3
nucleosomes
CCAN :
CENP-C
CENP-OPQUR
CENP-TW
CENP-SX
CENP-LN
CENP-HIKM
CENP-A
CENP-C
CENP-LN
CENP-HIKM
CENP-SX
CENP-TW

Figure 1.9: Comparison of the *Drosophila melanogaster* (top) and human (bottom) centromere and CCAN. The *Drosophila* centromere contains a more simplified CCAN compared to humans. Underlying centromeric DNA in *Drosophila* is a complex retroelement sequence (G2/Jockey-3; (Chang et al., 2019) versus 171 bp alpha-satellite tandem repeats at human centromeres. The *Drosophila* centromere consists of CENP-A, CAL1 and CENP-C, whereas the mammalian CCAN is larger and organised into arrangements of CENP subcomplexes (Figure by Dr Caitriona Collins).

Nonetheless, given the simplicity of the centromere in *Drosophila*, these proteins are reliant on each other for faithful centromere specification and function (Erhardt et al., 2008; Schittenhelm et al., 2010). CAL1 has been shown to bind CENP-A via its N-terminus and CENP-C via its C-terminus (Chen et al., 2014). Moreover, yeast two-hybrid screenings suggest that the interaction between CENP-A and CENP-C may be indirect in *Drosophila*, dependent on CAL1 (Schittenhelm et al., 2010), contrasting their interaction in mammalian systems (discussed in 1.2.5). The interdependence of CENP-A/CAL1/CENP-C in turn had led to difficulties in teasing out the individual roles of CAL1 and CENP-C in a homologous *Drosophila* system. Until recently, exactly how *Drosophila* CENP-C interacts with the centromere was not understood, leaving questions as to how the epigenetic loop of centromere self-propagation is closed in *Drosophila*. In 2019, Roure *et al* used a human U2OS cell heterologous system to express and probe the role of each *Drosophila* centromere protein, where viability of the system is uncompromised upon disruption of each *Drosophila* centromere protein (Roure et al., 2019). Here, a number of key points were made in terms of elucidating the step-by-step mechanism of how the *Drosophila* centromere self-propagates, putting CENP-C in its place (summarised below) (Figure 1.10):

- CENP-C is the recruitment factor for CAL1/CENP-A-H4 complexes through its interaction with CAL1.
- Dimerisation of CAL1 is not required for interaction with CENP-A-H4, but is required for deposition of CENP-A-H4 to chromatin. Moreover, CAL1 dimerisation is also not required for its association with CENP-C.

- CENP-C has an affinity for CENP-A nucleosomes, albeit a weak direct interaction. CAL1 and CENP-A collaboration is required for initial loading of CENP-C to the newly assembled CENP-A nucleosome. However, only nucleosomal CENP-A (as opposed to CAL1) is important for CENP-C's chromatin binding. Therefore, these interactions most likely occur most prominently on assembled centromeric chromatin – an observation most likely missed by a yeast two-hybrid assay (Schittenhelm et al., 2010). This stable chromatin binding by CENP-C most likely involves DNA binding properties observed in mammalian and yeast CENP-C (Cohen et al., 2008; Politi et al., 2002; Sugimoto et al., 1994). The AT-hook in CENP-C likely could be important for carrying out this role in *Drosophila*.
- CENP-C dimerisation is required for its association with CAL1.
- Importantly, CENP-A, CAL1 and CENP-C alone are sufficient for *Drosophila* centromere self-propagation in a heterologous system.

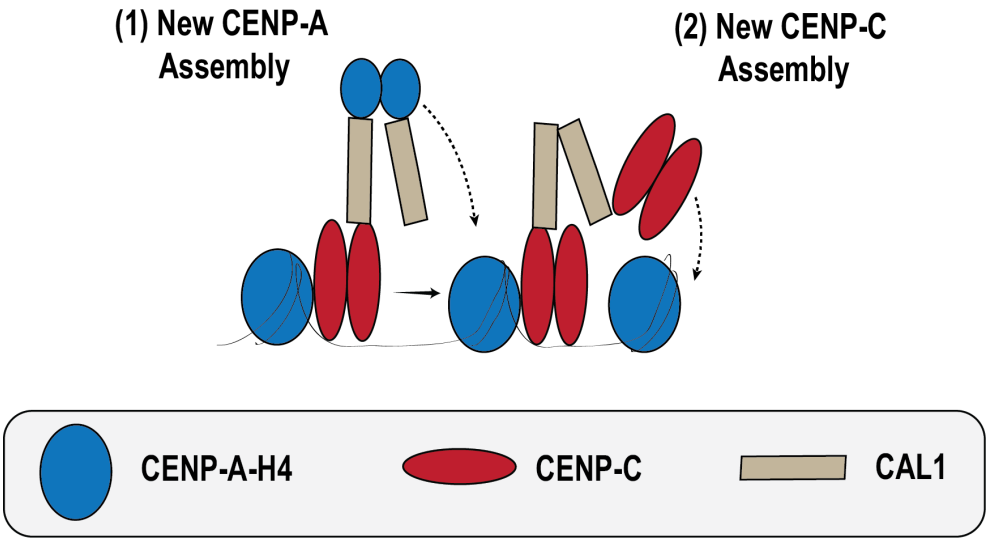

Figure 1.10: Schematic of the self-propagating *Drosophila* Centromere. (1) CAL1 recognises centromeric CENP-C in order to assemble new CID^{CENP-A}-H4 heterotetramers at the centromere. (2) Newly assembled CENP-A nucleosomes now are stabilised via loading of CENP-C. CAL1 recognises dimerised CENP-C, recruiting new CENP-C to the centromere to become the platform for kinetochore assembly.

1.3.7 The Structural Basis of *Drosophila* Centromere Maintenance

For many years, the *Drosophila* centromere community had been largely limited in progress due to many questions surrounding the structural mechanism for centromere maintenance between CID^{CENP-A}, CAL1 and CENP-C. Recently, using X-ray crystallography, Medina-Pritchard *et al* provided some key insights to this process, elucidating the structural recognition of CID^{CENP-A}/H4 and CENP-C by CAL1 (Medina-Pritchard et al., 2020) (Figure 1.11).

Overall, the structure of CID^{CENP-A}/H4 largely resembles that of its human CENP-A/H4 counterparts. The N-terminus of CAL1 forms a 1:1:1 heterotrimeric complex with the HFD of CID^{CENP-A} and histone H4. Furthermore, CAL1 recognises the amino acid variation specific to CID^{CENP-A} (compared to histone H3), and chaperones CID^{CENP-A}/H4 by shielding the DNA binding domains that are critical for nucleosome assembly. Comparing HJURP and CAL1 interactions with CID^{CENP-A}/H4, there is a noticeable conformation change at the L1 loop. Most likely, these differences would represent the amino acid variation between the human and *Drosophila* assembly chaperones. Moreover, hydrophobic interactions at W22 and F29 on CAL1 appear critical for its CID^{CENP-A}/H4 binding *in vitro*; with *in vivo* confirmation of a strong reduction in CID^{CENP-A}-GFP-LacI recruitment (particularly in the $CAL1_{W22/F29A}$ and $CAL1_{W22/F29R}$ double mutants). Ultimately, in comparison with both HJURP (human) and Scm3 (*Kluyveromyces lactis*), the structural recognition of CID^{CENP-A}/H4 by CAL1 is similar, yet adapts some intermolecular interactions (specifically at the L1 loop) (Medina-Pritchard et al., 2020).

As previously discussed (Section 1.2.6), Roure *et al* showed CENP-C as a recruitment factor for pre-nucleosomal CAL1/CID^{CENP-A}/H4. Hence, in addition to CAL1 recognition of CID^{CENP-A}/H4, the authors also elucidated CENP-C's binding to CAL1. Previously, Schittenhelm *et al* showed a direct interaction between CAL1 and CENP-C's respective C-termini ($CAL1_{699-979}$; $CENP\text{-}C_{1009-1411}$) (Schittenhelm et al., 2010). Medina-Pritchard *et al* now have clearly demonstrated that CENP-C recognises CAL1 via its C-terminal cupin domain ($CENP\text{-}C_{1264-1411}$) (Medina-Pritchard et al., 2020). Structurally, the cupin domain is a highly

conserved domain among CENP-C counterparts in other species (e.g. human CENP-C, yeast Mif2p). However, this domain contains significant variation in sequence (18% and 11% homology with human and yeast cupin sequences respectively). The cupin fold is made up almost exclusively of β-strands, forming a β-barrel. The β strands are arranged into two β sheets: β1-β2-β3-β10-β5-β8 (preceded by an α1 helix with a large loop containing two short α helices) and β4-β9-β6-β7. Importantly, CENP-C dimerisation is facilitated by back-to-back arrangement of the above six-stranded β-sheet. Overall, the *Drosophila* CENP-C cupin domain fold structure (the β-barrel) is conserved, yet contains some significant conformational differences at two loops (CENP-C 1324-1333 and 1368-1376) when compared to the Mif2p cupin domain (Cohen et al., 2008; Medina-Pritchard et al., 2020).

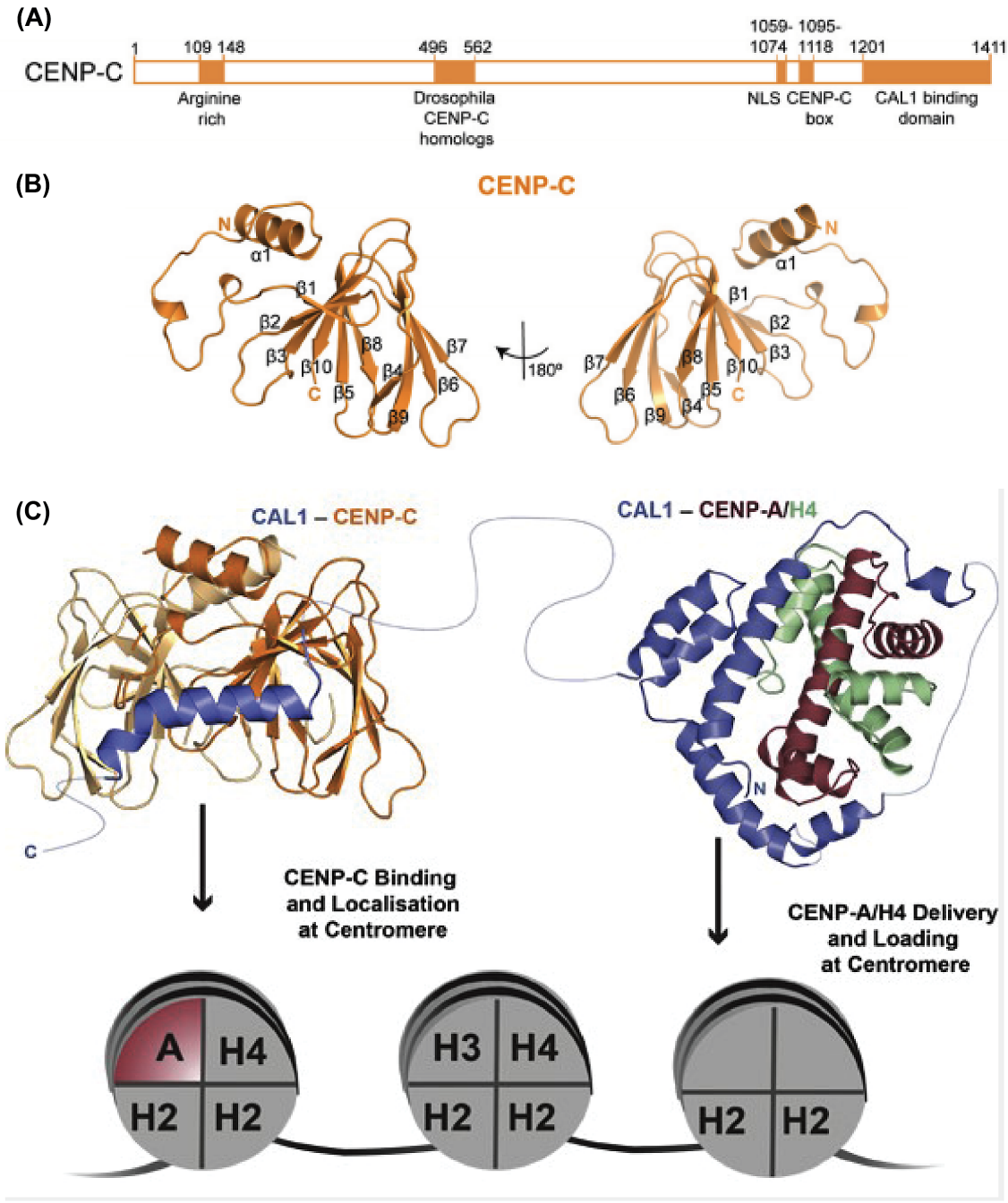

Figure 1.11: Drosophila CENP-C and the CENP-C Cupin Domain (adapted from Medina-Pritchard et al, 2020). *(A) Schematic of* Drosophila CENP-C with all its domains, including the CAL1 bi*nding domain (aa1201-1411) which contains the well conserved cupin domain (aa1264-1411). (B) The crystal structure of the CENP-C cupin domain at a resolution of 1.7 Å. (C) Crystal structure and summary of (1) CAL1-CENP-C binding (left) required for CENP-C localisation at the centromere (2) CAL1-CENP-A/H4 binding (right) required for CENP-A/H4 delivery and loading at the centromere.*

But how does CAL1 recognise CENP-C? CENP-C binds a single molecule of CAL1 proximal to the cupin dimerisation site at Loop L1 and β1, β2 and β3. $CAL1_{890\text{-}893}$ forms a β-strand interact with β1 in the CENP-C cupin domain

(Medina-Pritchard et al., 2020). Moreover, mutating CENP-C$_{1264\text{-}1411\ L1357E/M1404E}$, which is incapable of forming a cupin dimer, prevents interaction with CAL1 *in vitro* and CAL1 recruitment to GFP-CENP-C-LacI *in vivo* (Medina-Pritchard et al., 2020). Hence, CAL1 directly interacts with the evolutionary conserved cupin domain and this stabilises the CAL1 binding site. Furthermore, binding of CAL1-CENP-A/H4 and CAL1-CENP-C can happen simultaneously, further supporting the evidence supporting the model of epigenetic inheritance previously put forward by Roure *et al*.

The model of *Drosophila* epigenetic inheritance may still have some outstanding questions, particularly related to CENP-C's centromeric binding. Firstly, CENP-C contains two CAL1 binding sites, yet can only bind one at a time due to steric hindrance (Medina-Pritchard et al., 2020). Moreover, CAL1 is capable of oligomerising via its N-terminus (Roure et al., 2019). Thus, this creates a situation whereby CENP-C (already bound to CAL1) could in fact interact with a second CAL1, and bring another CID$^{CENP\text{-}A}$/H4 dimer, assembling another CENP-C (discussed by Medina-Pritchard *et al*., 2020). This hypothesis would be in line with previous studies that CENP-C requires both CID$^{CENP\text{-}A}$ and CAL1 for centromere localisation (Erhardt et al., 2008; Goshima et al., 2007; Roure et al., 2019; Schittenhelm et al., 2010) Secondly, in humans, CENP-C contains two nucleosome binding sites: the central domain (CD; discussed in Section 1.2.5) and the CENP-C motif (CENP-C^{CM}; the most conserved domain) (Carroll et al., 2010; Musacchio and Desai, 2017). Surprisingly, the CENP-C^{CM} is dispensable to CENP-A stability in humans (Guo et al., 2017). The binding specificity of these domains is also varied: CENP-C^{CM} can bind both CENP-A and canonical H3 nucleosomes, whereas CENP-C^{CD} only retains a high affinity for CENP-A nucleosomes (Carroll et al., 2010; Musacchio and Desai, 2017). Hence, this harbours a model (yet to be tested) whereby one CENP-C molecule could bind across the adjacent CENP-A or H3 nucleosome (through the CD and CM) domains to further confer stability (Fang et al., 2015). Whether such possibility exists in *Drosophila* CENP-C remains vacant and equally interesting given the simpler, more fundamental system.

1.4 Centromere Asymmetry and Non Random Sister Chromatid Segregation

1.4.1 Asymmetric Inheritance of Canonical and Centromeric Histones

The silent sister chromatid hypothesis represents a more accepted representation of the coordination of non-random sister chromatid segregation in stem cells

(Lansdorp, 2007). Evidence for epigenetically distinct sister chromatids have been emerging in the literature, particularly in *Drosophila melanogaster* stem cell models. Tran *et al* displayed the first clear evidence of asymmetric histone distribution in male *Drosophila* germline stem cells (GSCs) (Tran et al., 2012). Using a dual colour histone labelling system in combination with FLP-FRT recombination, the authors monitored the inheritance of old versus newly synthesised histone H3. Pre-existing 'old' histone H3 was selectively retained by the GSC whereas newly synthesised histone H3 was segregated to the gonialblast (GB) daughter cell (Tran et al., 2012). This data has recently been elaborated on to show both histones H3 and H4 are selectively retained by the GSC, but histones H2A and H2B are symmetrically distributed between stem and daughter cells (Wooten et al., 2019b). Moreover, phosphorylation at threonine 3 of histone 3 (H3T3P; by HASPIN kinase) is asymmetrically distributed in male GSCs (Xie et al., 2015). Hence, evidence suggests a highly ordered epigenetic regulation of chromatin in asymmetrically dividing stem cells.

What about the inheritance of centromeric chromatin in ACD? It has also been recently reported that parental 'old' CID^{CENP-A} is retained in intestinal stem cells (ISCs) and male GSCs (García del Arco et al., 2018; Ranjan et al., 2019). The latter, shown using a CID^{CENP-A} -dendra2 knock-in to monitor the old versus newly synthesised pools. Moreover, both Chen (male GSCs) and Dunleavy (female GSCs) labs have now implicated the centromere in the control of non-random sister chromatid segregation (Dattoli et al., 2020; Ranjan et al., 2019). Specifically, both studies show CID^{CENP-A} is asymmetrically assembled between sister centromeres. Upon division, more CID^{CENP-A} is retained by the self-renewed GSC. In addition to CENP-A, kinetochore proteins and microtubules are also asymmetrically distributed in a similar manner (Dattoli et al., 2020; Ranjan et al., 2019) (Figure 1.12). These asymmetries might ultimately orient the stem cell to bias chromosome segregation - proposed by the silent sister chromatid hypothesis.

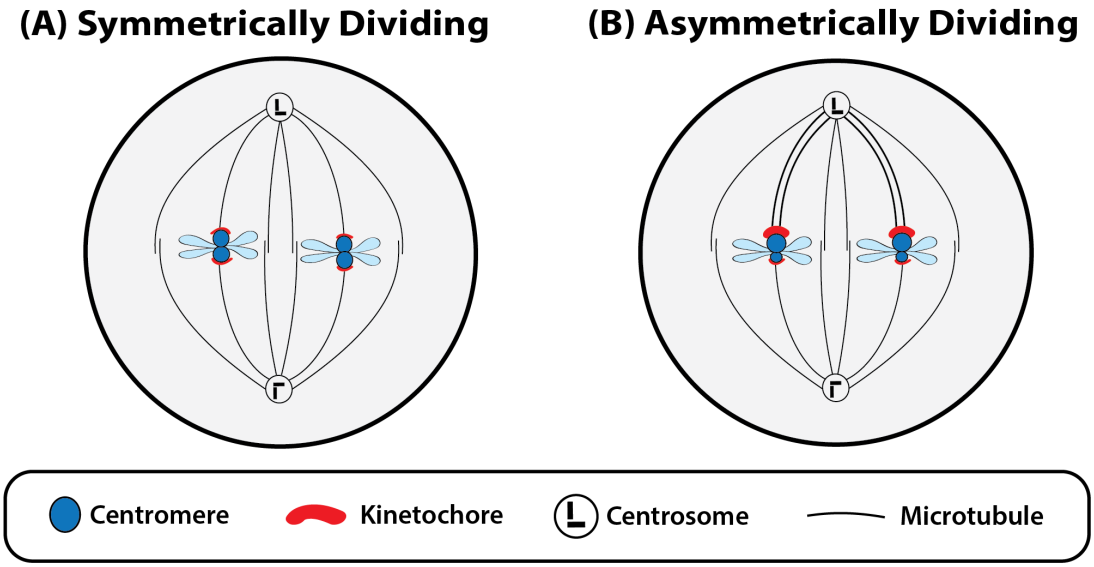

Figure 1.12: Centromere, kinetochore and spindle configurations in symmetric versus asymmetric mitotic divisions. (A) Metaphase of a canonical symmetrically dividing mitotic cell (e.g. RPE-1 or HeLa cell). The centromere (blue) is assembled equally between both sister centromeres. Subsequently, the kinetochores (red) assemble equally and captures mitotic spindle of equal strength. (B) Metaphase of an asymmetrically-dividing mitotic cell (e.g. *Drosophila* GSC). The centromere and kinetochore assemble asymmetrically and stronger on the sister chromatids to be retained by the stem cell. These stronger centromeres/kinetochores capture more microtubule fibres which result in a non-random chromosome segregation (Carty and Dunleavy, 2020).

1.4.2 Centromere Asymmetry

ACD is also not limited to stem cell populations (Brunet and Verlhac, 2011; Fabritius et al., 2011). Meiosis is the nuclear division counterpart to mitosis that gives rise to gametes. Because gametes are haploid (one copy of each chromosome), meiosis requires two rounds of division; the separation of homologous dichromatid chromosomes (Meiosis I) followed by the segregation of

sister chromatids (Meiosis II). Male meiosis follows a symmetric pattern of cell division. However, female meiosis is an innately asymmetric process, producing both an oocyte and polar bodies (Brunet and Verlhac, 2011; Fabritius et al., 2011). This division is controlled by an asymmetric meiotic spindle. Here, a G_2-phase primary oocyte (containing 4 genomic copies) will enter meiosis I and divide asymmetrically to produce the secondary oocyte and the first polar body (this polar body will divide in tandem with meiosis II). Meiosis II follows (absent of DNA replication) where the secondary oocyte segregates its sister chromatids into the ovum (unfertilised mature egg) and another polar body. Thus, the final result of asymmetric female meiosis is one mature egg and three polar bodies.

The centromere is fundamental to a faithful cell division (Section 1.3). In order for non-random chromosome segregation to occur, a mechanism of recognising centromeres and selectively segregating chromosomes to defined daughter lineages must exist (Lansdorp, 2007; Lansdorp et al., 2012). As previously described (Section 1.1), stem cell divisions are asymmetric and are oriented by means of cell and spindle polarities. Likewise, oocytes also display similar cell and spindle asymmetries (Akera et al., 2017). Moreover, oocytes harbour centromere 'strength' asymmetries that play a key role in biasing homologous chromosome segregation in meiosis (Chmátal et al., 2014; Iwata-Otsubo et al., 2017), a concept referred to as centromere drive (Chmátal et al., 2014; Lampson and Black, 2017; Malik, 2009). In this way, the asymmetric meiosis I division (where genetic elements are segregated to oocyte or polar bodies) provides a window of opportunity whereby genetic elements could 'cheat' and disproportionately segregate homologous chromosomes into the oocyte, eliminating competing gametes (Malik, 2009). The centromere, as the locus that directs chromosome segregation, could be acting as a 'selfish' element to direct its own transmission through meiosis at the expense of the homologues. The 'centromere drive' hypothesis was originally proposed to explain the paradox between the necessity of the centromere to cell division with the rapidly evolving centromeric DNA and its binding proteins (Malik, 2009). In a similar manner to centromere drive, mitotically dividing stem cells could also use differences in centromere strength between individual sister centromeres that could direct non-random sister chromatid segregation and ultimately drive stem cell identity. The concept of

'mitotic drive' was proposed to explain these asymmetries in stem cell populations (Wooten et al., 2019a).

Kinetochore proteins were first shown to be asymmetrically distributed in post-meiotic lineages of budding yeast (Thorpe et al., 2009). In the past year, Ranjan *et al* and Dattoli *et al* (and this thesis) have demonstrated that male and female GSCs have 'stronger' centromeres compared to daughter cells. These GSCs retain 1.2-1.4-fold more CENP-A and build stronger kinetochores (measured for CENP-C, NDC80) (Dattoli et al., 2020; Ranjan et al., 2019). Moreover, this asymmetry in centromere/kinetochore strength in favour of the GSC correlates with the emanation of more microtubules (measured by tubulin staining) from the stem pole (Dattoli et al., 2020; Ranjan et al., 2019) (Figure 1.12). These differential spindle activities also appear to be coordinated with the timing of nuclear envelope breakdown. At least in males, the nuclear envelope breaks down earlier on the stem cell side in G_2 phase (Ranjan et al., 2019).

How these asymmetries are ultimately directed and determined remains an open and relevant question. Models of ACD (particularly in adult stem cells e.g. *Drosophila*) are currently undervalued in terms of dissecting the epigenetic loop of centromere specification and maintenance. By understanding asymmetric modes of cellular division and chromosome segregation, one can begin to appreciate the specific roles for each component involved in the division. This is certainly true for understanding CENP-C's function in ACD, put forward in this study (discussed below).

1.4.3 CENP-A Assembly and Sister Centromere Asymmetry

Upon (symmetrical) mitotic division, the total CENP-A available is divided equally between the two daughter cells. To prevent dilution of the CENP-A pool and loss of centromere identity over time, CENP-A must be synthesised and deposited during the next cell cycle in order to replenish this loss of CENP-A across cell division back to 100%. This is measured by the increase or recovery of CENP-A over time (Jansen et al., 2007; Schuh et al., 2007). In general, centromere

assembly occurs at early G_1 phase (after mitosis, before S-phase) for symmetrically-dividing cells (Glynn et al., 2010). This allows for the redistribution of CENP-A during S-phase between sister centromeres. However, centromere assembly is not exclusive to G_1-phase in every organism/cell type, with other assembly timings having been reported in literature (Ahmad and Henikoff, 2001; Dunleavy et al., 2012; Mellone et al., 2011; Raychaudhuri et al., 2012; Swartz et al., 2019). Strikingly, cell types with unique assembly timings often portray specialised functions *in vivo*. For example, gametes assemble CENP-A before meiosis (after S-phase). This has been shown for *Drosophila* spermatocytes (Dunleavy et al., 2012; Raychaudhuri et al., 2012), as well as starfish oocytes (Swartz et al., 2019), which assembly CENP-A in meiotic prophase I. This unique timing too can be seen for asymmetrically-dividing stem cells in *Drosophila*, where male and female GSCs as well as neuroblasts, assemble CID^{CENP-A} in G_2 phase (up to prophase) (Dattoli et al., 2020; Ranjan et al., 2019).

As mentioned, centromeric chromatin is comprised of an interspersed array of CENP-A:H3 nucleosomes (Sullivan and Karpen, 2004), at an approximately 25:1 ratio (Bodor et al., 2014). This allows for a flexibility to vary the number of CENP-A nucleosomes assembled. Indeed, there are exceptions too in the amount of CENP-A assembled at centromeres, in addition to the cell cycle timing. Moreover, differences in CENP-A levels and cell cycle timing are often not mutually exclusive. This can be observed most strikingly in *Drosophila* spermatocytes, assembling more than a two-fold increase in CID^{CENP-A} (Dunleavy et al., 2012). This two-fold increase in CID^{CENP-A} compensates for two consecutive meiotic divisions in the absence of new CID^{CENP-A} loading in between. In *Drosophila* stem cells, centromere assembly appears to be gradual from prolonged G_2 phase up to prophase (Dattoli et al., 2020). Similarities can be drawn here to spermatocyte meiotic prophase I loading, starfish oocytes, as well as quiescent human cells (Dunleavy et al., 2012; Raychaudhuri et al., 2012; Swartz et al., 2019). Here, active CENP-A assembly potentially marks and maintains future proliferative potential. Moreover, CID^{CENP-A} increases by approximately 30% on average in female GSCs (Dattoli et al., 2020), hinting towards a potentially asymmetric loading of CID^{CENP-A} relative to the complete and equal 50% replenishment of CENP-A in symmetrical

systems. Hence, one can argue that CENP-A assembly is fluid, adapting is assembly timing and amount relative to function in the future daughter cell.

Many adult stem cell populations have characterised short G_1 phases (Fox et al., 2011; Hsu et al., 2008; Lange and Calegari, 2010; Orford and Scadden, 2008; Singh and Dalton, 2009). It has been proposed that these short G_1 phases limit the stem cell's sensitivity towards differentiation cues (Lange and Calegari, 2010; Orford and Scadden, 2008; Singh and Dalton, 2009). Significantly, new evidence has shown that cultured iPSCs (which contain longer G_1 phases) assemble CENP-A in G_1 phase (Milagre et al., 2020). Therefore, the assembly phase for CENP-A might reflect its pluripotent state, or perhaps self-renewal versus differentiating (symmetric versus asymmetric) cell divisions. In any case, centromere assembly in adult *Drosophila* stem cells could occur after DNA replication in these cells (given a lack of a robust G_1 phase). An alternative explanation for this could be the need first establish epigenetic (histone) asymmetry across the replication fork before assembling the newly-synthesised CENP-A. This hypothesis is supported by work from the Chen lab, where using testes-derived DNA and chromatin fibres, they observe a high frequency of biased, unidirectional replication fork movement (Wooten et al., 2019b). This highlights the probability of replication mechanisms establishing the histone asymmetry observed in male and female GSCs. Moreover, GSC centromeres/pericentromeres appear to replicate very early in S-phase (Dattoli et al., 2020), observed through the incorporation of DNA replication analog 5-Ethynul-2'-deoxyuridine (EdU). Most likely, due to the asymmetry in daughter cell fate, stem cells are required to organise their epigenetic pattern as early as possibly in the stem cell cycle. Ultimately in stem cells, this asymmetry of CENP-A between sister centromeres could be established two ways: 1) through a selective retention of parental ('old') CENP-A during across the replication fork (Figure 1.13, Hypothesis A), or 2) through an asymmetric assembly of 'new' CENP-A during G_2 phase (Figure 1.13, Hypothesis B), or 3) a combination of both.

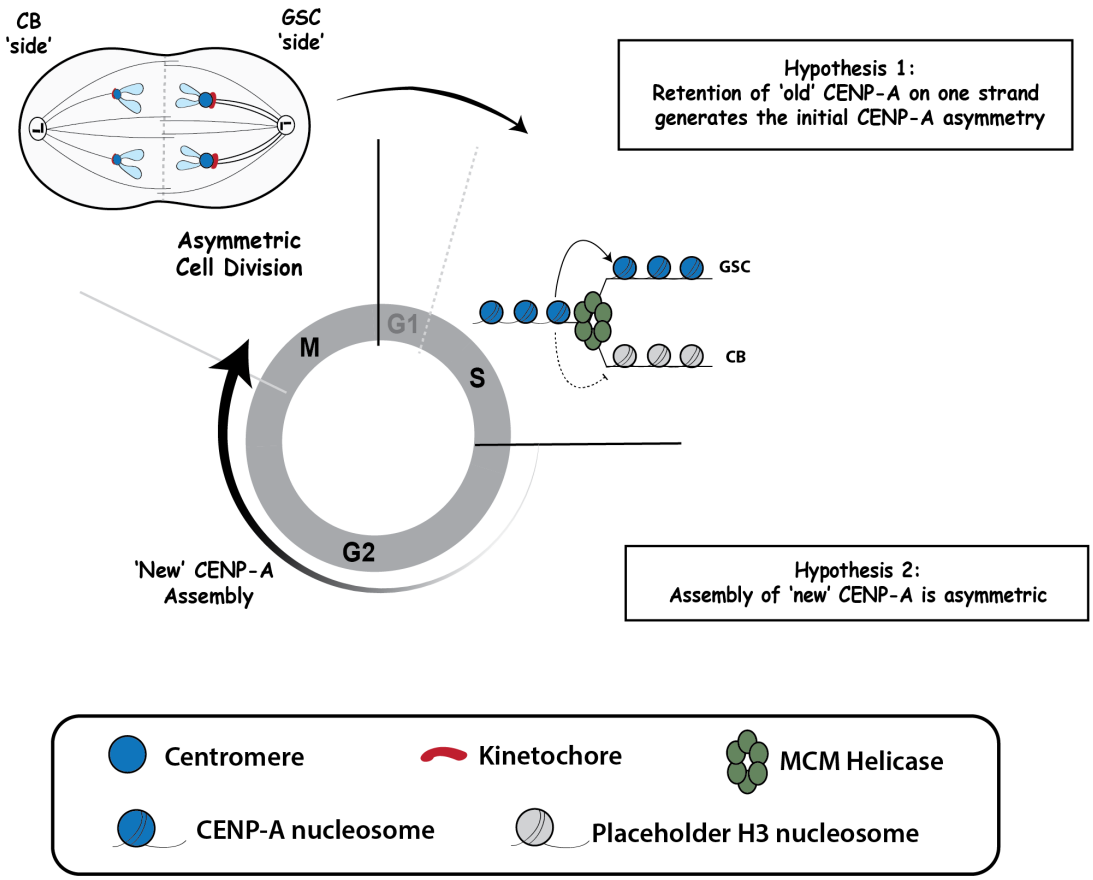

Figure 1.13: The Hypothesis on the Establishment of CENP-A Asymmetry in GSCs through the Cell Cycle. After (asymmetric) cell division, the recently divided GSC has a short G_1-phase, entering quickly into S-phase. Similar to H3-H4, a unidirectional replication fork could allow parental CENP-A-H4 to be asymmetrically retained between leading and lagging strands. H3 is deposited as a placeholder, preceding new CENP-A assembly in G_2-phase. Selective retention of old versus new CENP-A may establish the initial asymmetry between sister centromeres (Hypothesis 1). CENP-A assembly occurs from G_2/prophase. This assembly of CENP-A may occur in an asymmetric manner. (Hypothesis 2). Ultimately, the product of this mechanism is an asymmetric distribution of CENP-A to 'mitotically drive' stem cell division.

1.4.4 A Role for CENP-C in CENP-A Asymmetry

Understanding how a stem cell can distinguish sister chromatids through centromere asymmetry must rely on adapted CENP-A assembly and maintenance mechanisms. This roadmap can be prised from the already detailed understanding of the CCAN and its role in assembly and maintenance in symmetrical mitotic divisions (Section 1.2). Moreover, detailed knowledge of the epigenetic loop which prevents loss of centromere identity across a cell cycle is imperative (discussed in 1.2.6). The most basic system to study these mechanisms is in *Drosophila*, where the CCAN (comprising of CID^{CENP-A}, CENP-C and CAL1) is simple and the stem cell niches are well-characterised. As mentioned, ectopic targeting of *Drosophila* CID^{CENP-A}, CENP-C and CAL1 to human LacO arrays, the Heun lab probed the step-by-step epigenetic loop of centromere assembly and maintenance (Roure et al., 2019). In this model (Figure 1.10), CENP-C occupies crucial real estate for directing an asymmetric distribution of CID^{CENP-A}. In the context of the stem cell cycle, this may indeed occur during 'distributing' S-phase or the 'loading' G_2 phase. Significantly, CENP-C was a hit in numerous large-scale RNAi screens carried out in *Drosophila* stem cell niches (male/female GSCs, neuroblasts) (Liu et al., 2016; Neumüller et al., 2011; Yan et al., 2014). At initial glance, this observation may be unsurprising due to the essential nature of CENP-C to mitotic division. However, in addition to CID^{CENP-A}, CENP-C is also asymmetrically distributed between sister centromeres in GSCs (this thesis, Dattoli *et al*., 2020) and intestinal stem cells (ISCs) (García del Arco et al., 2018). Furthermore, it is directly involved in CENP-A maintenance and assembly (Erhardt et al., 2008; Falk et al., 2016, 2015; Roure et al., 2019).

These large-scale RNAi screens have been carried out in four different niches (male/female GSC, neuroblasts and intestinal stem cells). However, CENP-C was a negative hit in the ISC screen (Zeng et al., 2015). Although, there are fundamental differences between GSCs and ISCs related to CENP-C in this context, related to their future proliferative potential. In the female GSC niche, GSCs retain approximately 1.2-fold more CENP-C versus their cystoblast (CB) daughter cell (Dattoli et al., 2020). Importantly, this CB also retains its proliferative capacity. In contrast, Del Arco *et al* could only detect CENP-C in the ISC, and not its daughter cell enterocyte (EB) (García del Arco et al., 2018). Here, the EB is endoreplicating and has lost its mitotic capacity (thus losing CENP-C), and further differentiates

without dividing into either an enterocyte (EC) or enteroendocrine (EE). Hence, although these systems display fundamental 'stem' differences, CENP-C favours the stem cell in both. This strongly implies a role for CENP-C in the maintenance of parental 'old' CENP-A, already shown to be retained by the stem cell in male GSCs and ISCs.

1.4.5 Centromeric Regulation of Stem Cell Fate

As introduced in Section 1.1, ACD is regulated at multiple levels both intrinsically and extrinsically. Stem cell biologist constantly strive to understand the levels at which stem cells can regulate the self-renewal versus differentiation processes. Moreover, the relationship between stem cell potency (Section 1.1.2) and the epigenetic landscape remains widely open.

In 2010, Ambartsumyan *et al* first related the CENP-A level to self-renewal (Ambartsumyan et al., 2010). Depleting iPSCs of CENP-A allowed for stem cell self-renewal. However, once induced to differentiate, these cells could no longer commit to their lineage, subsequently undergoing a p53-dependant apoptosis (Ambartsumyan et al., 2010). Hence, CENP-A level plays a key role in cell fate decisions, requiring a higher CENP-A threshold to induce differentiation. However, whether this CENP-A threshold *per se* affects gene expression and thus can truly be an epigenetic mechanism of directing cell fate remains to be seen. Indeed, new evidence from the Jansen lab has uncovered that reprogramming fibroblasts to pluripotency results in depletion of CENP-A, CENP-C and CENP-T from the centromere (Milagre et al., 2020). Exactly why this occurs remains an open question. Nevertheless, it is apparent that the centromere is highly active and responsive to stem cell states.

Given the essential role of the centromere, elucidating a role for the centromere maintenance/assembly machinery in a multicellular organism presents some challenges. This was first indicated in the *Drosophila* midgut epithelium, where ISCs lose their proliferation capacity (implied by loss of clonal size) upon depletion of $CID^{CENP\text{-}A}$, CAL1 and CENP-C (García del Arco et al., 2018). Unsurprisingly,

long-term depletion of CAL1 resulted in ISC loss (García del Arco et al., 2018). Similarly in male GSCs, CAL1 depletion also reduced stem cell number (Ranjan et al., 2019), while in females GSC proliferation was blocked due to lack of centromere specification (Dattoli et al., 2020). Therefore, at a gross level, CAL1 clearly is required for centromere identity and subsequently the maintenance of stem populations. However, perturbing centromere localisation by depleting CAL1 does not allow distinction of the essential canonical mitotic role of CID^{CENP-A} /CENP-C/CAL1 versus potential stem-specific roles. In this case, co-overexpression of CAL1/CENP-A proved a more effective method of probing these roles. Here, this co-overexpression shifted CID^{CENP-A}'s distribution between GSC and CB from asymmetric (1.2:1), to symmetric (1:1) (Dattoli et al., 2020). Importantly, these cells are shifted more towards self-renewal (Dattoli et al., 2020). CAL1 depletion in male GSCs resulted in a similar loss of asymmetry (Ranjan et al., 2019). Ultimately, evidence is clearly gathering that adult *Drosophila* stem cells require asymmetry at centromeres in order to control non-random, selective sister chromatid segregation; and perturbation to this maintenance of asymmetry can lead to aberrant cell fate decisions. This thesis will further shed light on this process.

1.5 *Drosophila melanogaster* and the Germline Stem Cell Niche

1.5.1 Arthropods, Insects and the Order Diptera

Arthropods, members of the phylum Arthropoda, represents the largest phylum in the kingdom Animalia (or Metazoa), representing at least 50% of all species diversity. They are invertebrate bilaterians, characterised by an exoskeleton, body segmentation and paired, jointed appendages (Halanych, 2004). Within the phylum Arthropoda lies the class Insecta, subdivided into thirty orders, based on their body shape, legs, mouthparts but primarily by their wings (the suffix 'ptera' refers to the Greek work for 'wing'). Approximately 80% of all insects however, can be covered by five main orders, including: Hemiptera (e.g. bed bugs, water bugs), Coleoptera (e.g. beetles), Hymenoptera (e.g. wasp, honeybee), Lepidoptera (e.g. butterflies, moths) and Diptera (e.g. flies). True flies thus belong to the order Diptera ('Di' – two, 'ptera' – wing) - the second largest order (approximately 20,000 species) behind Coleoptera. Within dipterans, there lies a pronounced evolutionary divergence (<250 million years) from lower Dipterans (Nematocera; e.g. mosquitoes) to higher 'classical' Dipterans (Brachycera (Neodiptera); e.g. fruit flies) (Wiegmann et al., 2011).

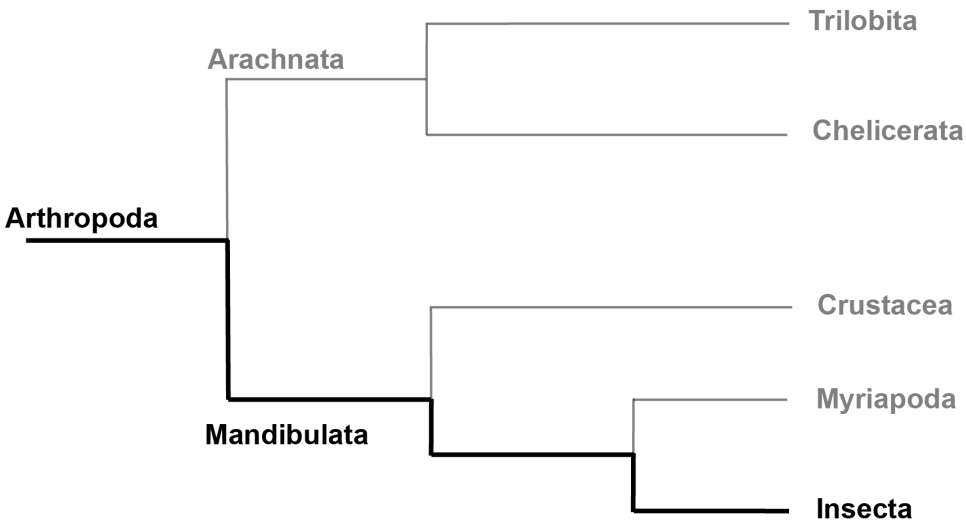

Figure 1.14: Phylogenetic tree of Arthropoda, including the class Insecta (highlighted). [Not to scale].

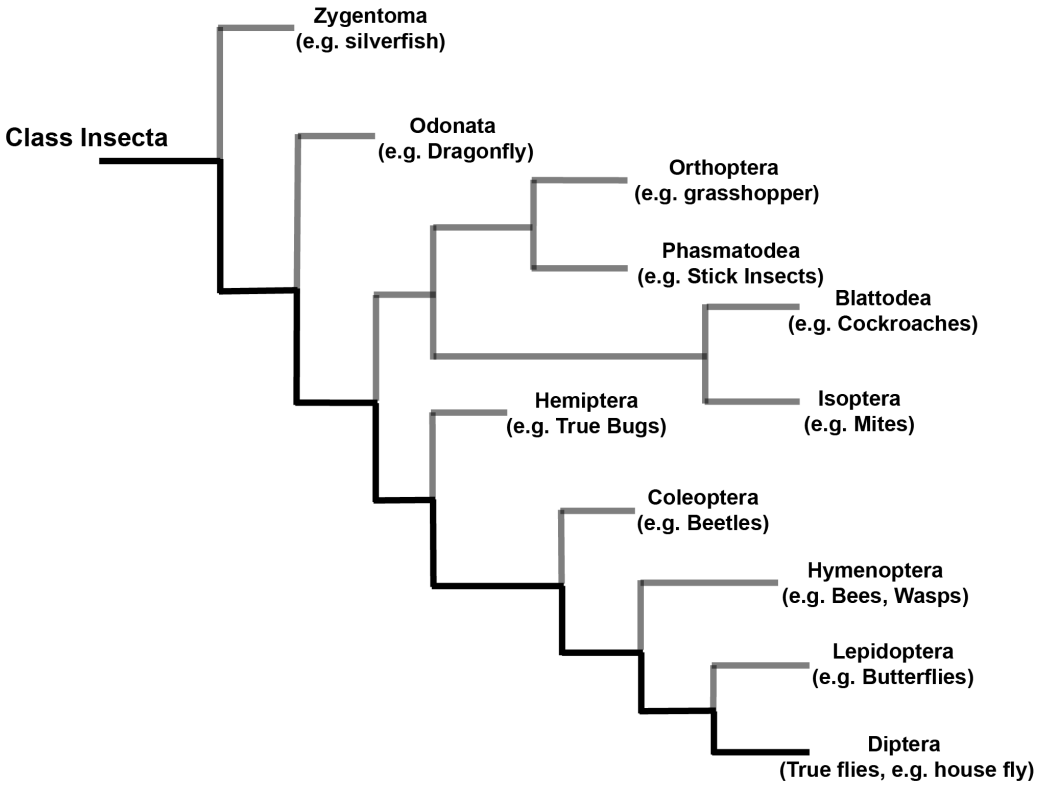

Figure 1.15: A non-extensive cladogram representing the class Insecta (not to scale). The order Diptera (highlighted in black) represents true flies.

1.5.2 The Model Organism: *Drosophila melanogaster*

The genus Drosophila is paraphyletic (composed of the last common ancestor and its descendants), and contains ≈1500 described species to-date. *Drosophila melanogaster* represents one of approximately 180 species recognised as being members of the *melanogaster* species group. Nine species belong to the *melanogaster* species subgroup, and are morphologically very similar to one another – most reliably identified from each other via their male genitals. These include the premiere model organism, *Drosophila melanogaster*, as well as *Drosophila simulans*, amongst others.

Drosophila melanogaster represents an excellent model organism for a number of reasons. They are very genetically tractable and easy to follow genetically through generations. Many genetic tools and mutant lines are readily available via different stock centres. Moreover, a large database of genomic data is available via the National Centre for Biotechnology (NCBI) and Flybase, the *Drosophila* community repository. They contain four (diploid) chromosomes ($2n$=8), making nuclear cell biology easy to analyse. Importantly, in terms of chromosome biology, processes such as chromosome segregation and cell cycle chromatin assembly remain largely conserved, often times to a more simpler degree (e.g. the centromere assembly process). For stem cell biologists, *Drosophila* contains numerous well-characterised and easily accessible stem cell niches and developmental pathways (e.g. male/female GSCs/germline, neuroblasts/thoracic ventral nerve chord, intestinal stem cells/midgut epithelium). Hence, this organism provides an excellent system to both characterise and manipulate adult stem cells within their stem cell niches.

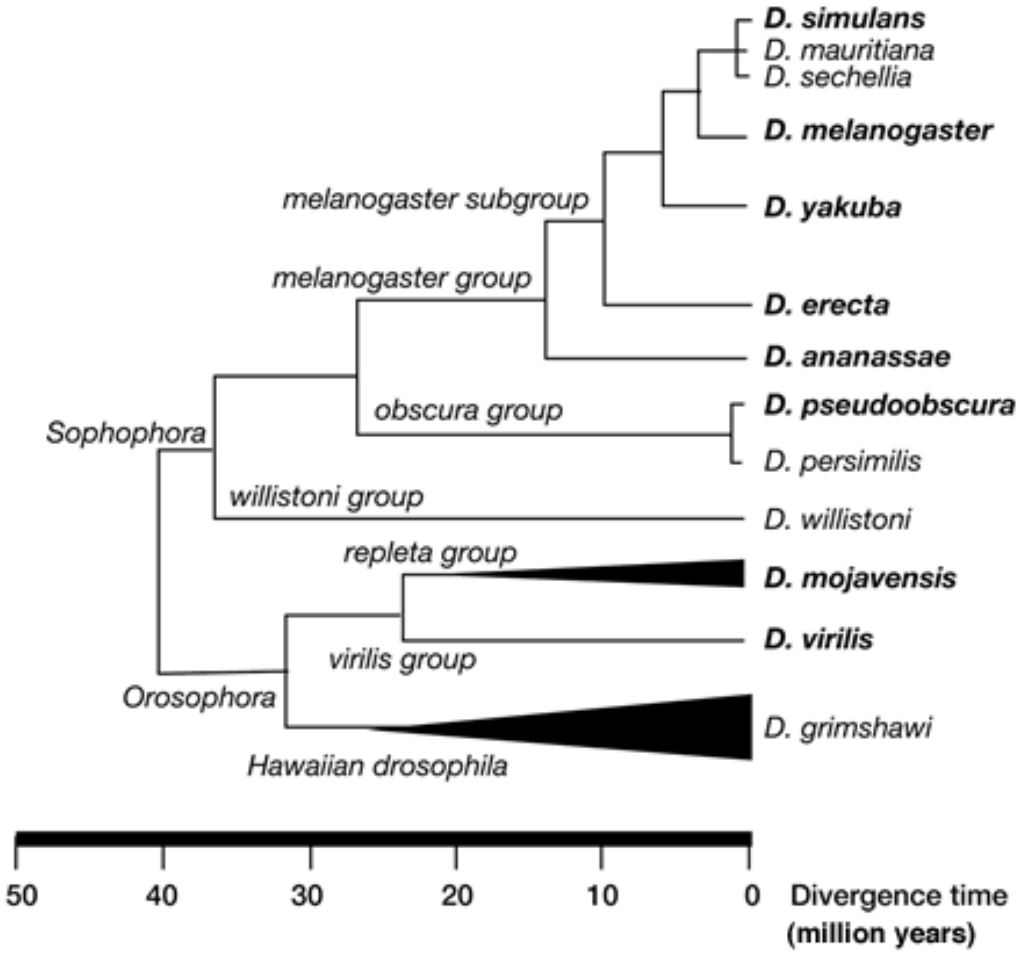

Figure 1.16: Phylogenetics of the suborder Sophophora within the genus Drosophila. The Sophophora suborder contains the *melanogaster* group and subgroup. The melanogaster subgroup contains the well-known model organism *Drosophila melanogaster*, and also *Drosophila simulans* (also used in research). Image taken from the 'Assembly/Alignment/Annotation of the 12 Drosophila Species' website.

1.5.3 Oogenesis and the Female Germline Stem Cell Niche

Due to a permanent stem cell population, the female *Drosophila* retains an ability to produce a vast number of eggs throughout its lifetime. Each female contains two ovaries, comprising of 12-16 individual ovarioles. Oogenesis can be organised into 14 distinct stages. Each ovariole is organised linearly into developmental chambers, beginning with the most apical chamber, the germarium (stage 1-3) (Spradling et al., 2011). The germarium is followed by the developing egg chambers (the vitellarium), up to the most distal fully developed egg chamber containing the mature oocyte (stage 14). At the anterior end of the germarium lies 8-10 terminal filament (TF) cells stacked linearly, where the most posterior TF cell makes contact with 5-7 cap cells (the stem cell niche). Anchored to the cap cells are two stem cell types: 2-3 germline stem cells (GSCs) and 4-6 escort stem cells (ESCs) (Huynh, 2007). Briefly, these ESCs also externally wrap the GSCs and their cellular extensions, and produce differentiated escort cells (ECs). In addition to the cap cells, these ECs also produce decapentaplegic (Dpp; *Drosophila* homolog of the vertebrate BMP signalling proteins) signalling ligand for full-strength BMP signalling, a requirement for GSC maintenance.

GSCs predominantly divide asymmetrically to produce a self-renewing GSC and differentiating cystoblast (CB), displacing the CB away from the GSC niche. This CB (encased by ECs) undergoes four rounds of mitotic divisions (with incomplete cytokinesis) to produce a 16-cell cyst, enclosed by somatic follicle cells (produced by somatic stem cells; SSCs) to bud away into the next developing egg chamber (Kirilly and Xie, 2007). These germ cell cysts (2-, 4-, 8-, 16-cell cysts; known as cystocytes) are interconnected via an endoplasmic reticulum (ER) – derived organelle called a fusome, originating from a singular spectrosome (a cytoplasmic spectrin organelle that anchors the GSC to the GSC niche) present in the GSC and CB (discussed below). Ultimately, the 16-cell cyst will be composed of one designated oocyte and fifteen metabolically active, polyploid nurse cells (NCs), linked via a intercellular fusome bridge derived from a single spectrosome in the GSC. These NCs are endocycling germ cells whose role is to synthesise and deposit proteins and RNAs into the oocyte. Thus, the germarium represents an easily

accessible and identifiable tissue in which to isolate and genetically manipulate germline and somatic stem cell populations, but most notably GSCs.

As introduced in Section 1.1, the niche controls stem cell maintenance by way of signalling factors. In female *Drosophila* germarium, the major signalling pathways are *Dpp* (GSC maintenance) and *bag of marbles* (*bam*; CB differentiation) (Dansereau and Lasko, 2008). Dpp is homologous to the human BMP2 signalling protein, and acts non-autonomously in the cap cells to repress the expression of *bam* in the GSC, and thus maintaining the GSC population (Chen and McKearin, 2003b; Song et al., 2004). On the other hand, earliest *bam* expression begins in the CB (up to 8-cell stage) and is essential of CB differentiation (McKearin and Ohlstein, 1995; Ohlstein and McKearin, 1997). Importantly, constitutive expression of *dpp* represses *bam* and CB differentiation, maintaining stemness of the daughter cell (Chen and McKearin, 2003a; Song et al., 2004). The Dpp transcriptional regulators, Mothers against Dpp (Mad) its binding partner Medea (Med), act directly on the *bam* promotor to silence *bam* expression in the GSC (Chen and McKearin, 2003a, 2003b; Song et al., 2004). Thus, BMP signalling can be measured using an antibody specific to the activated (phosphorylated) form of Mad (pMad).

Nanos (Nos) is a translational repressor that is essential for germline maintenance, and has been studied extensively in zebrafish, flies, *C. elegans* and mice (K. Subramaniam and G. Seydoux, 1999; Köprunner et al., 2001; Tsuda et al., 2003). In the *Drosophila* germline, Nos acts in conjunction with Pumilio (Pum), part of a large class of RNA binding proteins. At larval stage, Nos prevents premature differentiation of primordial germ cells (PGCs) and similarly maintains GSCs at adult stage (Tsuda et al., 2003; Wang and Lin, 2004). This translational regulation of Nos is still largely under investigation. However, recent evidence has shown proteins Ago1 (Argonaute 1) and Sxl (Sex Lethal; also known to mediate *nos* repression) bind via proximal miRNA binding sites and a distal Sxl binding sequence in the 3' Untranslated Region (3'UTR) of *nos* (Malik et al., 2020). Ago1 and Sxl most likely recruit Mei-P26 (meiotic-P26) and Brat (Brain tumour), followed by Bam and Bgcn (Benign gonial cell neoplasm) to *nos* mRNA to repress *nos* in the CB and allow differentiation to take over. (Malik et al., 2020). In the

context of this study, *nos* and *bam* are used as tissue-specific drivers of RNAi in the female germline, in the GSC/CB and 4/8-cell germ cysts respectively. On the other hand, Sxl is expressed in GSCs and CBs, and pMad is specific to GSCs. Using antibodies specific to these proteins, one can appreciate the GSC/CB composition in the female GSC niche.

1.5.4 The Spectrosome, Fusome, and the Control of Cell Synchrony in Gametogenesis

In the germarium, germ cell cysts are interconnected and share a common cytoplasm via a fusome organelle. In 1886, Platner first observed these fusome structures in several insect spermatocytes using light microscopy, referring to them as 'Verbindungsbrücken' (or 'bridging connections') (Huynh, 2007). Originally observed in and thought to be specific to the insect germline, a similar spectrin-containing structure has been (relatively) recently observed in *Xenopus laevis* germ cells (Kloc et al., 2004). Importantly though, stable intercellular bridges are a general feature of gametogenesis, having been observed in many mammalian species, including human (Greenbaum et al., 2011). Many of the key features of such bridges have been studied in *Drosophila*, although some distinguishing features between insect and mammalian bridges do exist (discussed by Greenbaum *et al,* 2011).

The spectrosome is a round spectrin-containing organelle in the cytoplasm of GSCs. The fusome, a membranous structure found in the developing germ cysts of many insect orders, develops from this spectrosome originating from the GSC. The spectrosome bridges off and expands through each mitotic division to link the oocyte to all germ cells within the cyst through ring canals. These bridges are derived via the midbody in an incomplete cytokinetic cleavage furrow. The spectrosome itself has been observed as early as the gastrulating embryo (Huynh, 2007). In the adult germline, this spectrosome is anchored to the apical end of the GSC making contact with the cap cells (thus maintaining the GSC in its niche). When the GSC divides, the spectrosome anchors the centrosome to the apical pole – orientating the axis of division away from the niche. Thus, the self-renewed GSC

maintains its location in the stem cell niche, and the differentiating CB moves away from the niche. During telophase, a transient ring canal forms between the GSC/CB and the new fusome material forms in the ring canal. The spectrosome elongates from the GSC anterior and fuses with the new fusome material in the cytoplasmic bridge, before being severed, releasing the new fusome into the CB (Huynh, 2007). The spectrosome then reorients itself back towards the apical GSC side. Hence, the morphology of the spectrosome can be characterised throughout the cell cycle (Kao et al., 2015) (using anti-Spectrin/Hts antibodies), making it a useful marker when analysing GSCs and germ cell cysts in fixed tissue samples (Figure 1.17 C).

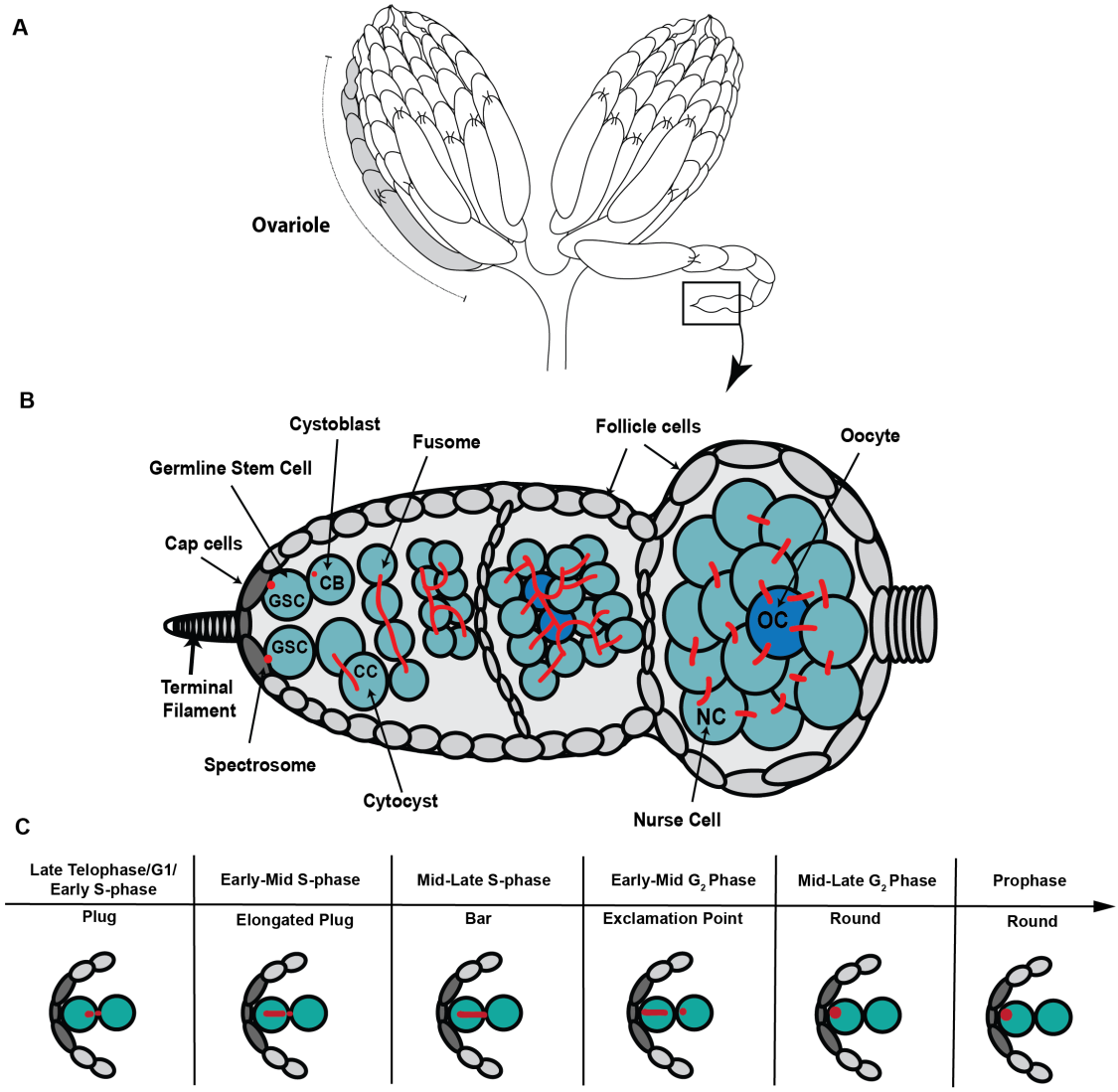

Figure 1.17: The *Drosophila* ovary and germarium/GSC niche. (A) Schematic of the female ovaries with individual ovariole (highlighted in grey), with developing egg chambers and germarium (boxed). (B) Schematic of germarium and GSC niche. The anterior tip of the germarium contains the GSC niche, with stacked terminal filament cells joined to the cap cells (dark grey). The germ cells (cyan), arise from a GSC that divides asymmetrically to produce a self-renewing GSC and daughter cell cystoblast (CB). The CB divides a further four times with incomplete cytokinesis into a 16-cell germ cyst. The spectrosome (red) elongates into a fusome and interconnects each germ cell within the cyst. The 16 cell cyst will contain one designated oocyte (OC, blue) and 15 nurse cells (NCs), which bud off into the next developing egg chamber to continue oogenesis. (C) Schematic of spectrosome morphology through the GSC cell cycle. After mitosis, the GSC has

a very short G_1-phase. In late telophase/G_1/early S-phase (left), the spectrosome displays a ‘plug’ morphology where the spectrosome has budded off into the ring canal. In S-phase, the GSC spectrosome elongates into a bar formation. In G_2-phase, the bar spectrosome moved back towards the anterior end of the GSC and the new fusome has formed in the CB, resembling an ‘exclamation point’ morphology. In mid-late G_2-phase, the spectrosome forms the classical round morphology anchored to the apical pole of the GSC, continuing into M-phase (Right, prophase)(Kao et al., 2015).

1.6 Project Hypothesis and Objectives

We hypothesise that CENP-C plays a key recruitment and maintenance role in regulating centromere asymmetry in ACD. Moreover, we hypothesise that disruption to the centromeric core, specifically relating to CENP-C, will ultimately influence GSC fate.

The rationale for these hypotheses lie in numerous pieces of evidence. Firstly, non-random sister chromatid segregation requires distinction at the centromere. Recent evidence has shown that CENP-A is asymmetrically distributed between stem and daughter cell within the *Drosophila* germline (Dattoli et al., 2020; Ranjan et al., 2019), and its disruption impacts cell fate, shifting the stem cell towards self-renewal (Dattoli et al., 2020). Secondly, in many *Drosophila* stem cell RNAi screens, CENP-C was noted as having influence on stem cell maintenance or differentiation (Liu et al., 2016; Neumüller et al., 2011; Yan et al., 2014). Thirdly, recent elucidation of the epigenetic loop surrounding *Drosophila* centromere propagation shows CENP-C as a recruitment factor in marking the centromere for new CENP-A assembly (Roure et al., 2019). Taken together, CENP-C fills in an important role in allowing centromere self-propagation in a symmetric system of epigenetic inheritance. In an asymmetric system, we hypothesise that adapting the canonical inheritance pathway, specifically the recruitment factor CENP-C, will allow coordination and distinction of stem versus daughter cell sister chromatids in accordance with the 'Silent Sister' hypothesis (Lansdorp, 2007; Lansdorp et al., 2012).

Using the female *Drosophila* GSC system, this project has three broad primary objectives:

1. To elucidate the role of CENP-C in the assembly and maintenance of CENP-A asymmetry in GSCs. We achieved this through tissue-specific RNAi and overexpression, combined with detailed immunofluorescence quantitation in GSC and CBs.
2. To determine the role of CENP-C-mediated centromere maintenance on stem cell fate and germline differentiation. We achieve this through

detailed phenotype characterisation and analysis of the GSC/CB balance in multiple genetic backgrounds.

3. To generate tools and methods required to further analyse the role of the centromere in ACD.

2. Materials and Methods

2.1 Chemical Reagents and Experimental Kits

Unless otherwise stated, chemical reagents and kits were obtained from Fisher Scientific, Invitrogen or Sigma-Aldrich. Specific reagents and/or kits are noted in the text. Common buffers and reagents are listed in Appendix 8.1.

2.2 *Drosophila* Husbandry, Genetics and Techniques

2.2.1 Fly Stocks and Husbandry

Stocks were cultured in 25 mm polystyrene vials on standard cornmeal medium (NUTRI-Fly^{TM}) preserved with 0.5 % propionic acid and 0.1 % Tegosept (APEX Bioresearch Products) at 20 ^{o}C under a 12 hours light-dark cycle. All fly stocks used were obtained from Bloomington Stock Centre (BDSC_#...) unless otherwise stated. The following fly stocks were used: *Oregon-R* (BDSC_25211), *wild type* RNAi isogenic control (BDSC_36303), *nanos-Gal4* (BDSC_25751), *bam-Gal4* (kind gift from Margaret T. Fuller), UAS-CENP-C RNAi (BDSC_38917), UASp-HA-CENP-C (kind gift from Kim S. McKim), HA-CENP-C; UAS-CENP-C-RNAi (this study), *Cenp-C^{IR35}* (Heeger et al., 2005), *Cal1^{2k32}* (Unhavaithaya and Orr-Weaver, 2013), Double Balancer: y[1] w[*]; wg[Sp-1]/CyO; Dr/TM3, Sb (#59967) (See Appendix 8.2 for full genotypes of fly stocks used)

2.2.2 Targeted Genetic Manipulation: GAL4-UAS System

To generate tissue-specific targeted manipulation of genes, we used the GAL4-UAS system available in flies (Duffy, 2002). This system, adapted from yeast, takes advantage of a GAL4 transcription factor binding to its enhancer upstream activating sequence (UAS) to promote transcription of the target gene. In *Drosophila*, it involves the crossing of a fly-line containing a GAL4 tethered to a tissue-specific promotor (Driver Line, e.g. *nanos-GAL4*) to a fly-line containing a gene or RNAi hairpin (Responder Line, e.g. UAS-CENP-C RNAi) (Fig 2.1). The resulting F_1 progeny contain both the GAL4 and the UAS sequence which can now bind, allowing for the manipulation of a gene of interest in a specified tissue (Fig 2.1).

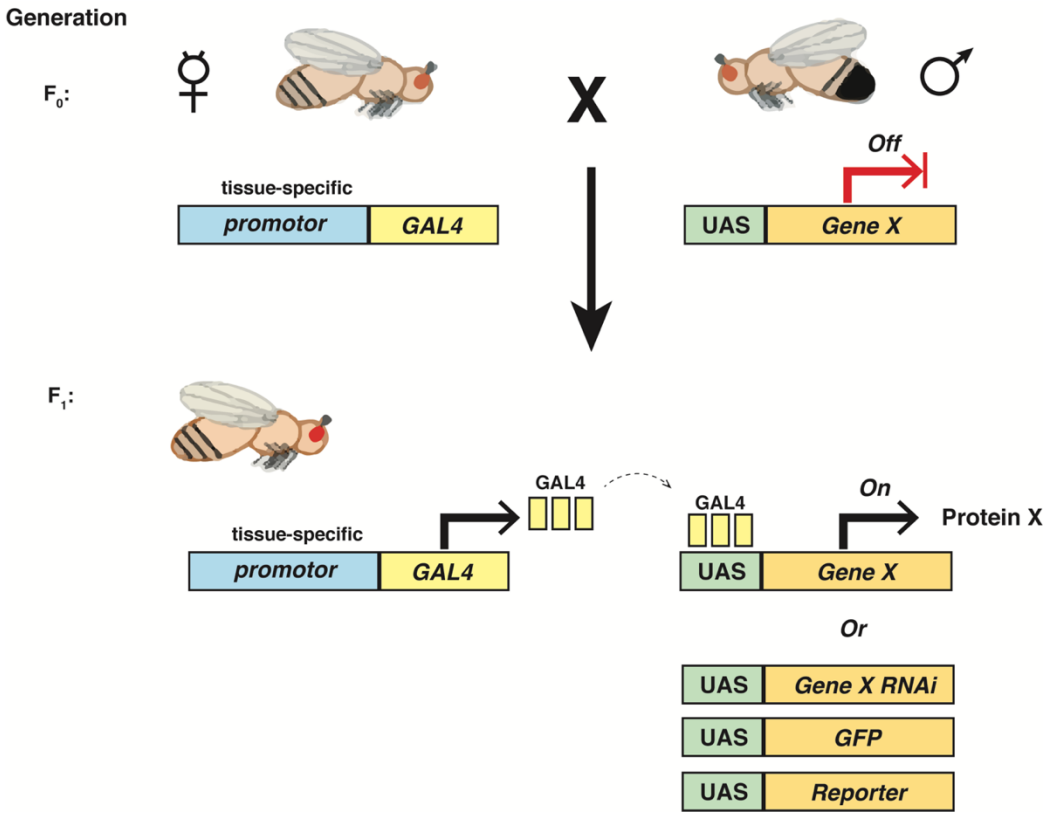

Figure 2.1: Schematic of the *Drosophila melanogaster* GAL4-UAS system. Female (virgin, unmated) driver GAL4 flies are crossed to male responder flies containing a Upstream Activating Sequence (UAS) adjacent to a Gene, RNAi, fluorescent tag or reporter. Transcription of the UAS-tethered gene is suppressed in the F_0 generation due to the absence of its GAL4 transcription factor. The F_1 progeny will express GAL4 in a tissue specific manner to the promotor (e.g. *nanos* in the early germline), allowing it to bind to the UAS sequence and initiate transcription of the target RNA (corresponding to a specific gene, RNAi, GFP or reporter).

The GAL4-UAS system is a temperature-dependant system – the efficiency of the binding of GAL4 to UAS increases with temperature. Crosses can be carried out at temperatures ranging from 18 °C to 29 °C, with main stocks maintained at 20 °C. RNAi and overexpression crosses were carried out at either 22 °C, 25 °C or 29 °C (specified below).

I. To determine the effect of depletion of CENP-C on the female GSCs, a transgenic line expressing UAS-CENP-C RNAi was crossed to *nanos-GAL4* (Fig 2.2 A). Given CENP-C is an essential gene, the cross was incubated at an intermediate temperature of 22 °C to allow the development of the phenotypes.
II. To determine the specificity of the effect of CENP-C to the GSC/CB, the UAS-CENP-C RNAi responder line was crossed to *bam-GAL4* (Fig 2.2 B). *bam-GAL4* drives expression of the RNA hairpin in the mid-germarium, where the *bag-of-marbles* gene is expressed, at the 4-8 cell cyst stage. This cross was carried out at 29 °C to maximise the knockdown efficiency.
III. To determine the effect of overexpression of CENP-C on female GSCs, a transgenic line expressing HA-CENP-C under control of UASp was crossed to *nanos-GAL4* (Fig 2.2 C). This cross was carried out at 25 °C.
IV. To rescue the CENP-C RNAi phenotype, the rescue responder line, UASp-HA-CENP-C; UAS-CENP-C RNAi, was crossed to *nanos-GAL4* at 22 °C (Fig 2.2 D). The generation of this transgenic fly line is schematised in Figure 2.3.

Note: The *nanos-GAL4* and *bam-GAL4* driver lines both have two copies of UAS-Dcr-2 on the X chromosome – this allows overexpression of the Dicer-2 gene (an RNase III family of double-stranded RNA-specific endonucleases). Expression of Dicer-2 under UAS control enhances the efficiency of the RNAi by processing long dsRNA into siRNAs and hairpin RNAs into endogenous siRNAs. When examining F_1 females, each progeny will contain one copy of the UAS-Dcr-2 to enhance RNAi efficiency (Fig 2.2).

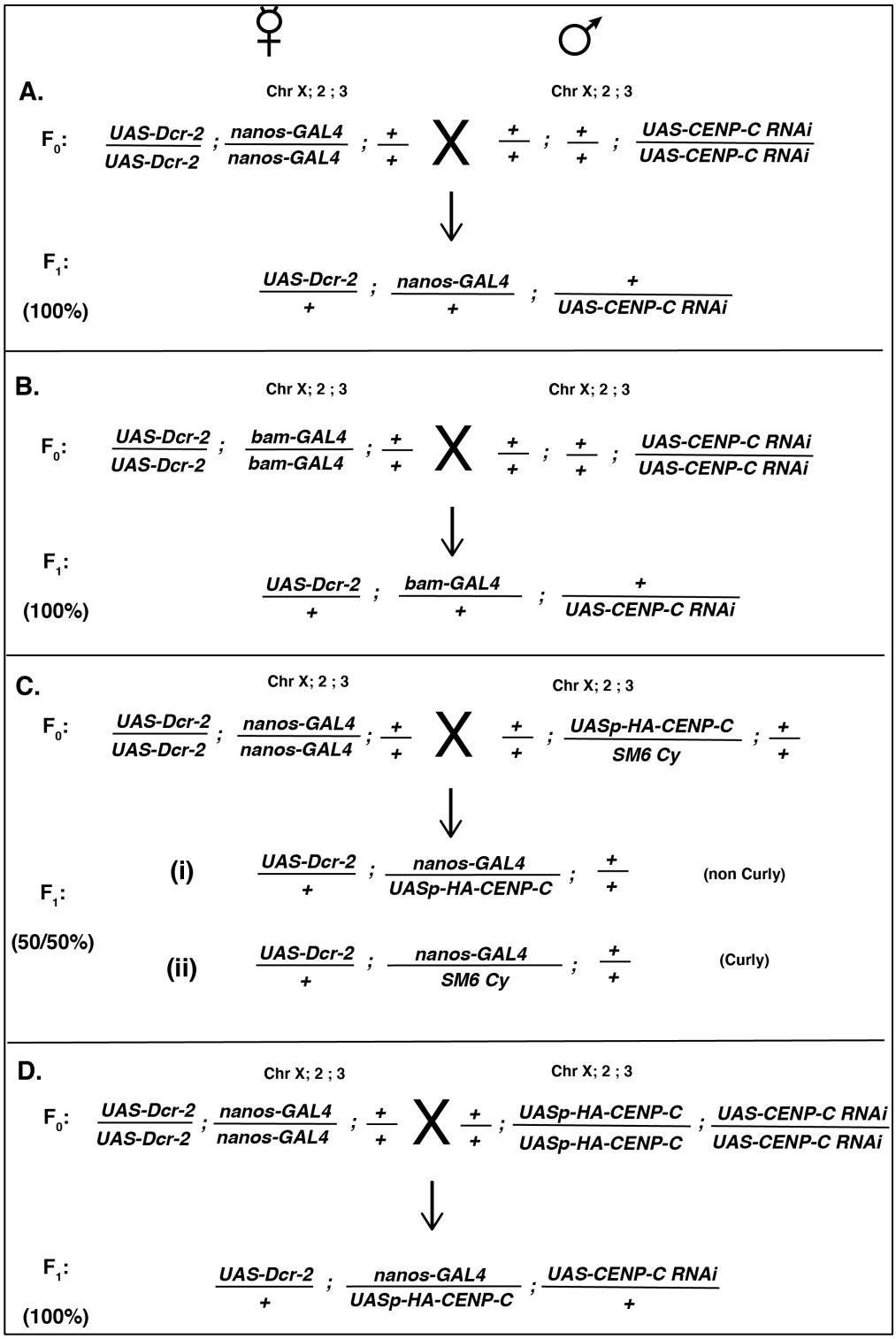

Figure 2.2: Schematic of GSC CENP-C RNAi (A), germ cell cyst CENP-C RNAi (B) and HA-CENP-C overexpression (C) and Rescue (D) fly crosses using the GAL4-UAS system. +/+ represents homozygous *wild type* alleles. UASp-HA-CENP-C is balanced with the balancer chromosome Second Multiple 6 (SM6) with marker Curly (Cy).

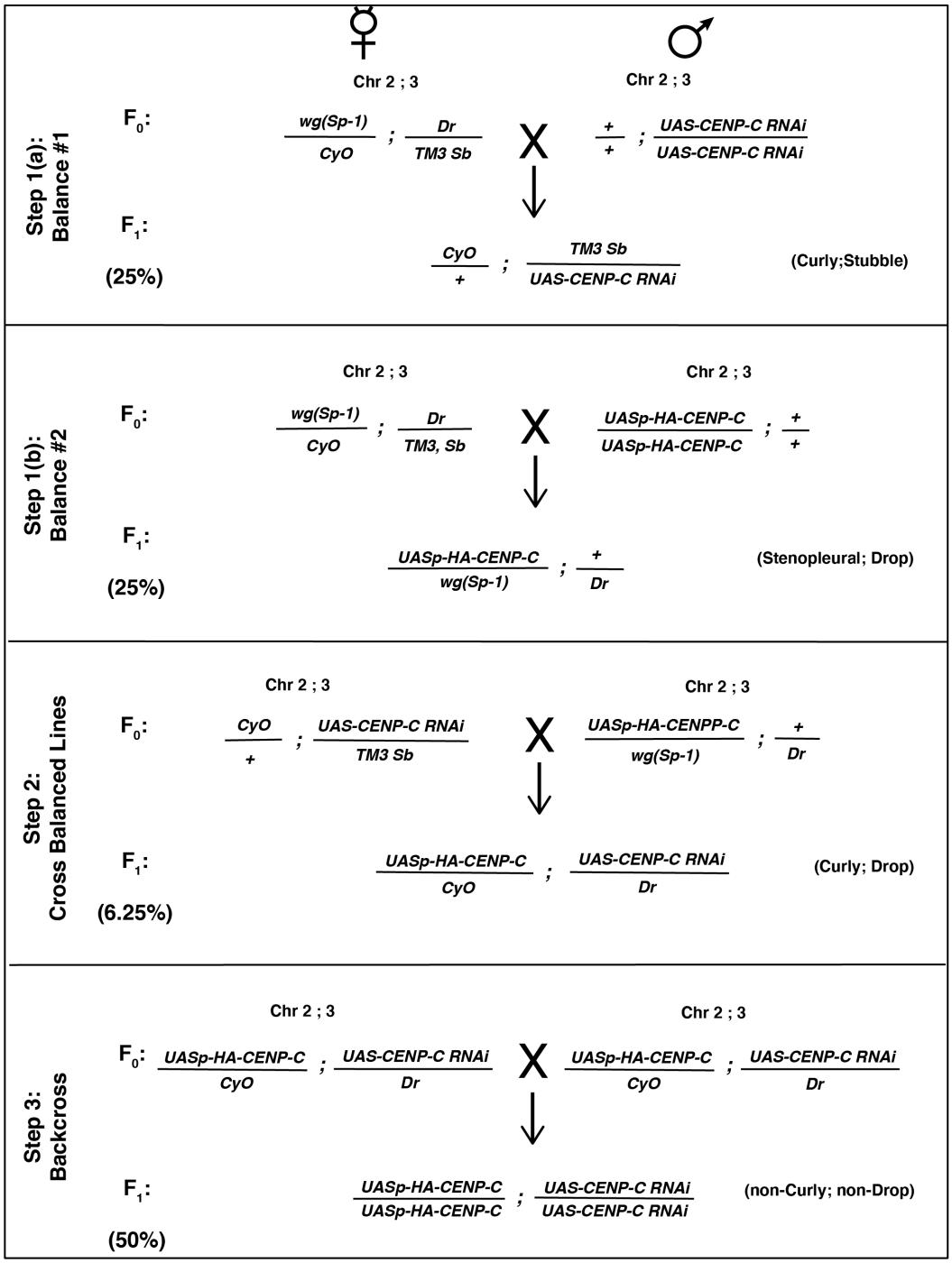

Figure 2.3: Schematic of the generation of HA-CENP-C; CENP-C RNAi rescue transgenic line. Step 1(a) and (b) requires the double balancing of *UAS CENP-C RNAi* and *UASp HA-CENP-C* fly lines. The 2nd and 3rd chromosome double balancer contains the markers Sternopleural ($wg^{Sp\text{-}1}$) and CurlyO (CyO) on chromosome 2; and Drop (Dr) and Third Multiple 3 (TM3) marked with Stubble (Sb) on chromosome 3. +/+ represents homozygous *wild type* alleles.

2.3 Cell Biology Techniques

2.3.1 Preparation of Ovaries for Immunostaining

For standard immunofluorescence (IF) staining of *Drosophila* ovaries, 10-15 flies of a specified age were dissected in 500 µL 1X PBS. Ovarioles were teased out using forceps to ensure efficient antibody penetration. Dissected ovaries were transferred to an 1.5 ml Eppendorf tube using a P1000 pipette, pre-wet in 1X PBS + 0.4 % Triton-X (0.4 % PBST). Samples were spun down in a centrifuge briefly at 12000 rpm and the supernatant removed. Samples were fixed in 4 % paraformaldehyde (PFA) in 1X PBS for between 5 and 30 mins (depending on antibody requirements), on a shaker. Note: all incubations/washes were agitated on a shaker or rotator. Once fixed, 4 % PFA was removed and samples were washed 3 times in 0.4 % PBST for 15 minutes. At this point, samples can be stored at 4 °C for future use if required.

Optionally, samples can be permeabilised with 1 % PBST before blocking. In most cases however, the continues washing with 0.4 % PBST appears sufficient. Samples were then blocked in 1ml of fresh 1-5 % bovine serum albumin (Fisher Scientific) in 0.4 % PBST. Samples were incubated at room temperature (RT) in blocking buffer for 2-4 hours. For primary antibody incubation, antibodies were diluted in fresh 1-5 % blocking buffer and incubated at 4 °C overnight on a rotator (See Appendix 8.3 for list of primary antibodies used). The following day, samples were again washed three times in 0.4 % PBST before detection of primary antibodies using fluorescently labelled secondary antibodies. Secondary antibodies were added also in blocking buffer at 1:500 concentration for 2 hours in the dark (covered in tin foil) (See Appendix 8.4 for list of secondary antibodies used. Samples are washed again in 0.4 % PBST three times before the detection of DNA. DNA was stained using 1 µg/ml solution of DAPI (diluted 1:1000 in 1X PBS) for 10 mins at RT. Samples were washed briefly in 0.4 % PBST and mounted in Slow-Fade Anti Fade Mounting Medium (Invitrogen) on Polysine slides (Fisher Brand). Coverslips (1.5; 22mmX22mm) were sealed with varnish.

2.3.2 5-ethynyl-2'-deoxyuridine (EdU) Incorporation and Detection

If the detection of DNA synthesis was required, EdU was incorporated before fixation. Ovaries from flies at a specified age were dissected and their ovarioles teased out as normal before transfer into a 1.5 ml tube in 1XPBS. These samples were spun down at 12000 rpm and supernatant removed. Samples were incubated with EdU (10 μM) in 1X PBS (EdU stock at 10 mM) for 45 mins. Samples were then washed briefly once for 20 mins in 0.4 % PBST. Fixation protocol then proceeded as normal. After washing of the fixative solution in 0.4 % PBST, EdU was then detected using a fluorescent azide. Samples were incubated for 30 minutes in the dark with 2 mM $CuSO_4$, 10 mM Na-L-Ascorbate (ascorbic acid) and 300 μM of 6-Carboxyfluorescein-TEG azide (Berry and Associates) (or alternative colour if required). Samples were then washed thoroughly in 0.4 % PBST (3 X 20 mins). Note: These washing steps were crucial to prevent interference of the copper sulphate with primary antibodies. After washing, samples can wither be stored at 4 °C or blocking buffer can be added as per the standard immunofluorescence protocol outlined in Section 2.4.1.

2.3.3 Microscopy and Image Processing

Fluorescence microscopy was largely carried out using a DeltaVision Elite widefield microscope system (Applied Precision) using a 100X oil immersion UPlanS-Apo objective (NA 1.4). All samples were mounted in SlowFade Gold antifade reagent (Invitrogen). Unless specifically indicated, images were acquired as z-stacks using a step size of 0.5μm, with sequential fluorescence passing through 435/48 nm; 525/48 nm; 597/45 nm; 632/34 nm band-pass filter for detection of DAPI, FITC (Alexa Fluor 488), TRITC and Cy5 (Alexa Fluor 647). Raw images were deconvolved using the deconvolution software available on SoftWorx, using 10 cycles of the 'conservative' iteration algorithm.

In specific circumstances for presentation of specific phenotypes, confocal microscopy was used. Images were taken using am inverted Olympus Fluoview (FV1000) laser scanning microscope with a 60X oil immersion UPlanS-Apo objective (NA 1.2). Z-stacks were acquired using a step-size of 0.5 μm. Samples

were excited using 404 nm, 473 nm, 559 nm, and 635 nm lasers for detection of DAPI, Alexa Fluor 488 (AF488), AF546 and AF647. D405/473/559/635 dichroic mirrors (Chroma) were used. Pinhole was set to 115 μm. Fluorescence was passed in sequentially through 430–455 nm, 490–540 nm, 575–620 nm, 655–755 nm bandpass filter to detect DAPI and AF488, AF546 and AF647.

Deconvolved or confocal Images were processed using FIJI (ImageJ) software.

2.3.4 Centromere Fluorescence Intensity Quantification

For each quantification one cell/germarium was considered. FIJI (Image J) software was used to measure fluorescent intensity of CID and CENP-C as follows: 8-bit images from a single cell (nucleus) were projected (max intensity) to capture all the centromeres present in the cell at a specific cell cycle phase. The background was subtracted from the projected image. Threshold was adjusted to only cover centromere signal. Following, the command "analyse particles" was used to select centromeres. Finally, integrated density (MGV*area) from each centromere foci were extracted and summed to measure the total amount of fluorescence per nucleus. All values measured are 'total centromere integrated density per nucleus'. Statistical analysis was performed using GraphPad Prism 8 software (La Jolla, USA). Data distribution was assumed to be normal, but this was not formally tested. P value in each graph showed was calculated with unpaired t test with Welch's correction. If there was a multiple comparison, a One-Way Analysis of Variance (ANOVA) with Tukey test was used to test P values.

2.3.5 Assay of GSC Self-Renewal: Sex-Lethal and pMad Quantitation

To assess the number of stem and daughter cells in an individual germarium, samples were stained with anti-SEX-LETHAL (SXL) and anti-SMAD3 (phospho S423 + S425) (pMad). [Note: pMad antibody works best with short (5-10 min fixation with 4 % PFA]. pMad is a classical stem cell marker in *Drosophila* (Chen and McKearin, 2003a). Only pMad positive cells that are specifically adjacent to the GSC niche were counted in each germarium. SXL is a key sex-determination protein that is involved in sex-specific splicing in *Drosophila* (Malik et al., 2020).

For our purposes, SXL is a cytoplasmic marker GSCs, CBs and 2-cell cyst stage germ cells in the female germline. Hence, SXL was used as an assessment of the immediate stem/daughter cell composition. To assay self-renewal, the number of pMad and SXL positive cells were counted through the z-stacks of each germarium and a ratio of SXL:pMad positive cells per germarium was then represented. Statistical analysis was carried out using One-Way Analysis of Variance (ANOVA) and Tukey test (if multiple comparisons) on GraphPad Prism 8 software (Dattoli et al., 2020).

2.4 Molecular Biology Techniques

2.4.1 Single-fly genomic DNA preparation

To confirm the presence of UASp-HA-CENP-C and UAS CENP-C RNAi transgenes in the generated rescue fly line (Fig 2.3), we performed single fly PCR on single fly genomic DNA preparations. Single flies were knocked out by placing the fly in an empty 1.5 ml Eppendorf tube on ice. Fresh Squishing Buffer (SB; Appendix 8.1) was made before each extraction (50 µl per fly). 50 µl of SB was then aspirated using a 200 µl pipette tip. Without expelling the SB in the pipette tip, the knocked-out fly was crushed using the pipette tip (some SB will leak out). The remaining liquid was then expelled and further mixed and crushed with the fly. Th mixture was then incubated for 30 mins at RT, followed by incubation at 95 °C for 5 mins. The sample was then put on ice for 5 mins before spinning down at 13000 rpm for 5 mins. The supernatant was then transferred into a fresh 1.5 ml tube and stored at 4 °C. These DNA preps can be stored at 4 °C for up to 2 months.

2.4.2 Single-fly Polymerase Chain Reaction (PCR)

For genotyping UASp-HA-CENP-C; UAS CENP-C RNAi rescue fly lines generated for this study, single fly PCR was performed with Q5 polymerase (New England Biolabs) according to manufacturer's protocols with the following primers:

Transgene (Vector)	**Primers Used**
HA-CENP-C (UASp)	Fw: 5' - CCAGATTACGCTGCTCATGGCGGA - 3' Rv: 5' - GGTAGTTTGGACTTGGGCTTAGCCTGAG - 3'
UAS CENP-C RNAi (VALIUM 22)	Fw: 5' - GGTGATAGAGCCTGAACCAG - 3' Rv: 5' - AATCGTGTGTGATGCCTACC - 3'

3. Understanding CENP-C's role in centromere assembly and centromere asymmetry in female germline stem cells

3.1 Chapter Introduction

The 'silent sister' hypothesis puts forward the idea that ACD requires epigenetic mechanisms to recognise sister chromatids for preferential segregation to stem and daughter cell (Lansdorp, 2007; Lansdorp et al., 2012). Importantly, this would require distinction of sister chromatids by the mitotic machinery, for example at the centromere. Recently, it has been shown that centromeres in male and female *Drosophila* GSCs display asymmetries in centromere strength (Dattoli et al., 2020; Ranjan et al., 2019). Moreover, parental versus newly synthesised CENP-A incorporation is asymmetric, with stem cells retaining parental CENP-A histones in a manner similar to histones H3-H4 (García del Arco et al., 2018; Ranjan et al., 2019). Until recently, the self-propagating epigenetic loop of centromere assembly in *Drosophila* remained elusive, making the study of these how this asymmetry is established speculative. Now, Roure *et al* and Medina-Pritchard *et al* have made substantial progress into understanding how the *Drosophila* centromere maintains its identity throughout the cell cycle and across a cell division (discussed in detail in sections 1.3.6 and 1.3.7). Briefly, CENP-C is the recruiting factor for CAL1-CENP-A-H4, with CAL1 recognising and binding directly to CENP-C via its cupin domain (Medina-Pritchard et al., 2020; Roure et al., 2019). Hence, CENP-C is ideally situated to direct an asymmetric centromere in asymmetrically dividing stem cell models.

We hypothesise that CENP-C plays a key role in recruiting CENP-A and maintaining centromere asymmetry in GSCs. This chapter investigates the mechanical role of CENP-C in the assembly and maintenance of CENP-A in female *Drosophila* GSCs. To do this, we use the GAL4-UAS system in *Drosophila* to induce tissue-specific RNAi and overexpression to probe the role of CENP-C in GSCs in a temperature sensitive manner. At a single cell level, we use detailed immunofluorescence quantitation to uncover the centromeric differences between stem and daughter cells. In doing so, this chapter uncovers some important findings:

1. Similar to CENP-A (Dattoli et al., 2020; Ranjan et al., 2019), CENP-C assembles in G_2/prophase.

2. CENP-C is asymmetrically distributed between GSC and CB (now published in Dattoli *et al.*, 2020).
3. Depletion of CENP-C in GSCs disrupts CENP-A assembly in G_2/prophase.
4. Absence of CENP-C leads to an increase in CENP-A asymmetry in favour of the GSC, whereas overexpression tends CENP-A to a more symmetric pattern.

3.2 CENP-C is assembled from G_2 phase – prophase in female GSCs

At the apical end of the *Drosophila* germarium (Fig. 3.1A), 2-3 GSCs are found attached to cap cells (Fig. 3.1B). Female GSCs divide asymmetrically to give differentiating daughter cell called a cystoblast (CB). To assess the cell cycle timing of CENP-C assembly in GSCs, we used a similar deduction method as Dattoli *et al* to identify GSCs at different cell cycle stages. Given GSCs have a very short to no G_1 phase, GSCs exit mitosis and are immediately incorporating EdU, eliminating the requirement to identify G_1 phase. EdU pulse (for 45 minutes) thus allows us to mark cells in and out of S-phase, and 1B1 to mark the spectrosome - the shape of which can be used to define the cell cycle stage (Ables and Drummond-Barbosa, 2013; Kao et al., 2015) (Fig 3.1 C, D). We focused on GSCs with a pan nuclear EdU staining pattern characteristic of mid to late S-phase, in which the spectrosome forms a bridge shape (Fig. 1C). GSCs that were EdU negative with a round spectrosome and with centromeres distributed throughout the nucleus, but without condensed chromosomes, were deemed to be in G_2 phase/prophase (Fig. 1D). We then quantified total CENP-C fluorescent intensity (integrated density) at centromeres at both stages (Fig. 1E). Dissecting 3-day old *wild type* (*OregonR*) ovaries, we found an increase in total CENP-C levels between cells in S-phase, compared to GSCs in G_2/prophase. Quantitation revealed an average of 38% increase in CENP-C, (S-phase=23.36±1.84, n=32 cells; G_2/prophase=32.14±1.611, n=34 cells). These results indicate that similar to CID, CENP-C is assembled at GSCs centromeres in G_2/prophase, and in a similar amount to CID.

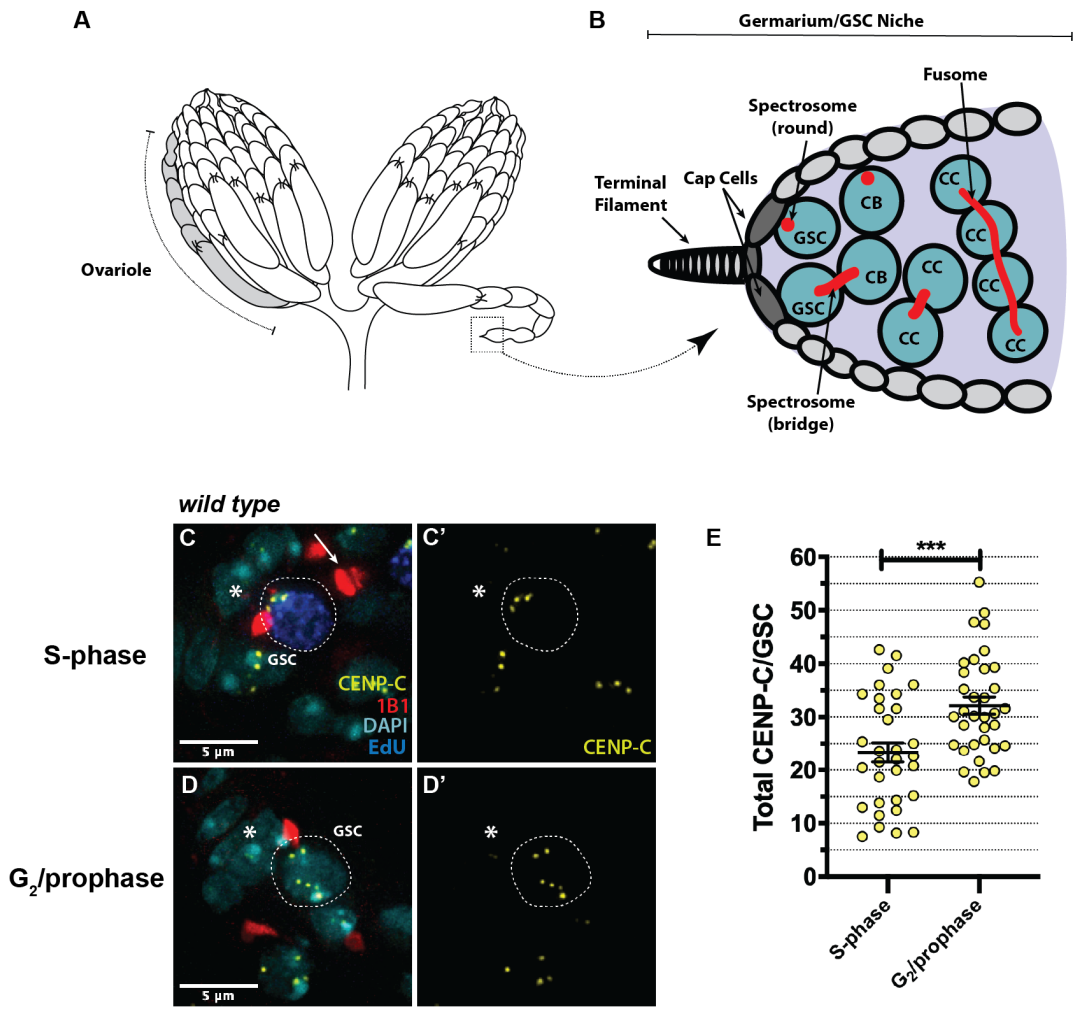

Figure 3.1: Quantitation of CENP-C assembly in *wild type* female GSCs. (A) Schematic of the *Drosophila* ovary, composed of 16 ovarioles (ovariole highlighted in grey) organised into developing egg chambers. The GSC niche is located in the anterior-most chamber of the ovariole, the germarium (boxed). (B) Schematic of the GSC niche and early stage germ cysts in the germarium (discussed in detail in section 1.5). G_2/prophase GSCs can be identified with a round spectrosome attached to the cap cells (GSC niche). (C-D) Immunofluorescence of *wild type* GSCs (circled) for S-phase (C, C') and G_2/prophase (D, D') stained with DAPI (cyan), EdU (blue), spectrosome (1B1, red) and CENP-C (yellow). * = cap cells. Arrows represent 'bridged' spectrosome associated with S-phase GSC. Scale bar = 5 µm. (E) Quantitation of total CENP-C fluorescent intensity (integrated density) in GSCs at S-phase versus G_2/prophase. ***$p<0.001$. Error bars = Standard Error of the Mean (SEM).

3.3 Characterising the role of CENP-C in CENP-A assembly in GSCs.

CENP-C was 1 of 42 hits common between male/female GSCs and neuroblast RNAi screens looking to identify genes involved in stem cell maintenance and/or differentiation (Liu et al., 2016; Neumüller et al., 2011; Yan et al., 2014). This suggested to us an unexpected role for CENP-C outside of its canonical role in kinetochore assembly. Thus, given the proposed silent sister hypothesis (Lansdorp, 2007; Lansdorp et al., 2012), that epigenetic differences may direct ACD in adult stem cells, we reasoned CENP-C to be an important candidate to investigate in this context.

To test this, we sought to investigate and characterise CENP-C-depleted GSCs as per Yan *et al* 2014 (female GSC screen), with a goal to understanding centromere dynamics with reduced CENP-C. We took advantage of the GAL4-UAS system available in flies to drive tissue specific RNAi-depletion of CENP-C using the germline specific driver *nanos-GAL4.* In the adult germline, *nanos-GAL4* will drive expression of the shRNA beginning in the GSCs. Given the temperature sensitive nature of the GAL4-UAS system, and thus the ability to manipulate efficiency of GAL4/UAS binding (and in turn knockdown strength) through temperature, we initially carried out the knockdown at 25 °C. However, given CENP-C is an essential protein, this unsurprisingly resulted in an agametic phenotype, void of any germ cells (data not shown). Therefore, we reduced the temperature gradient until we settled on a temperature (22 °C) that produced sufficient disruption whilst allowing germline development. To confirm CENP-C knockdown in GSCs, control *nanos-GAL4* and CENP-C RNAi ovaries were stained with antibodies against CENP-C (Fig 3.2 A-D). To ensure quantitation of a fully assembled centromere, total CENP-C fluorescence intensity was then quantified in GSCs with round spectrosome (indicative of G_2/prophase GSCs) (Fig 3.2E). Quantitation revealed an approximate 63% depletion of CENP-C in GSCs (*nanos-GAL4*=26.60±1.66, n=30 cells; CENP-C RNAi=9.79±1.76, n=27 germaria). Next, we labelled and quantified CID^{CENP-A} fluorescence intensity in CENP-C-depleted GSCs, measuring total CID^{CENP-A} at both S-phase and G_2/prophase (Fig. 3.3 A-D). In line with Dattoli *et al*, CID^{CENP-A} intensity increases between S-phase and G_2/prophase, by approximately 35% on average (S-

phase=15.82±0.73, n=40 cells; G_2/prophase=24.58±1.45, n=43 cells) (Fig. 3.3 E). However, this increase was not observed in CENP-C-depleted GSCs. Here, CID^{CENP-A} levels in G_2/prophase were comparable with that of S-phase (S-phase=17.46±1.06, n=36 cells; G_2/prophase=15.50±0.96, n=43 cells) (Fig 3.3 E). Thus, CID^{CENP-A} levels are reduced when CENP-C is depleted. Specifically, in line with previous findings in symmetrically dividing cells (Carroll et al., 2010; Erhardt et al., 2008; Roure et al., 2019; Shono et al., 2015), CENP-C is required for CID^{CENP-A} assembly in G_2/prophase in GSCs.

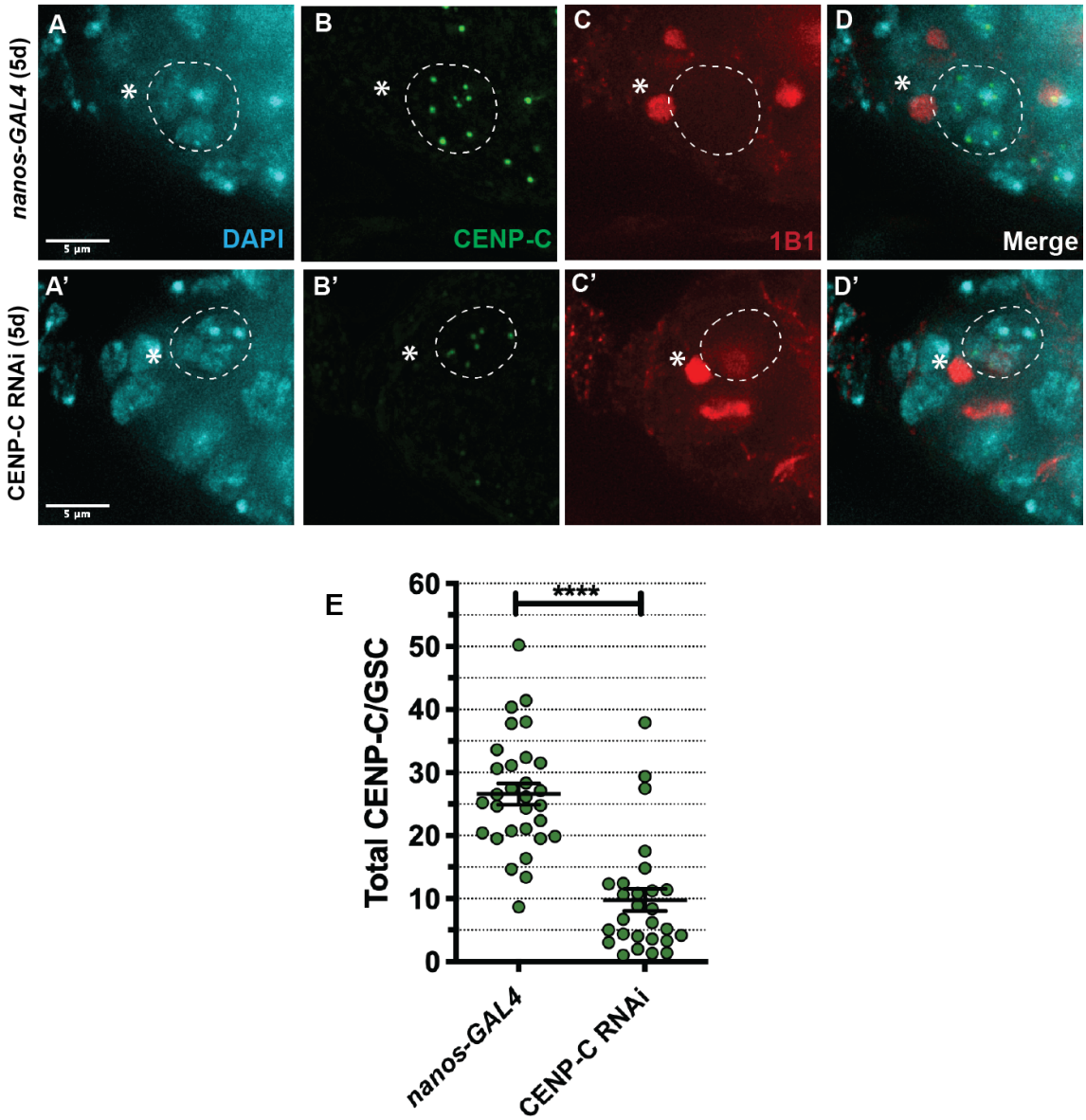

Figure 3.2: Quantitation of total CENP-C in *nanos-GAL4* versus CENP-C RNAi GSCs. (A-D') Immunofluorescence of G_2/prophase GSCs (circled) for *nanos-GAL4* (parent control, A-D) and CENP-C RNAi (A'-D') stained with DAPI (cyan), CENP-C (green) and 1B1 (red). (E) Quantitation of total CENP-C fluorescent intensity (integrated density) per GSC in *nanos-GAL4* versus CENP-C RNAi. ****p<0.0001. Scale bar = 10 µm. Error bars = SEM.

Given that CENP-C is required for CID^{CENP-A} assembly, we next investigated whether the localisation of the CID^{CENP-A} assembly chaperone CAL1 was affected by CENP-C knockdown. For this, we antibody-stained control and CENP-C knocked-down germaria for CAL1, co-stained with CENP-C in order to isolate centromeric CAL1 from nucleolar CAL1 (Fig. 3.4 A-H). Both centromeric and nucleolar CAL1 was visible in the *nanos-GAL4* and CENP-C RNAi. However, when we quantified total centromeric CAL1 in GSCs at G_2/prophase and found centromeric CAL1 to be reduced in the CENP-C RNAi compared to the *nanos-GAL4* control (*nanos-GAL4*=16.01±1.45, n=30 cells; CENP-C RNAi=9.44±0.85, n=29 germaria) (Fig. 3.4 E). This result is in line with the emerging structural and *de novo* evidence that CENP-C is the recruitment factor for CAL1- CID^{CENP-A}-H4 complexes, marking the centromere for new assembly (Medina-Pritchard et al., 2020; Roure et al., 2019).

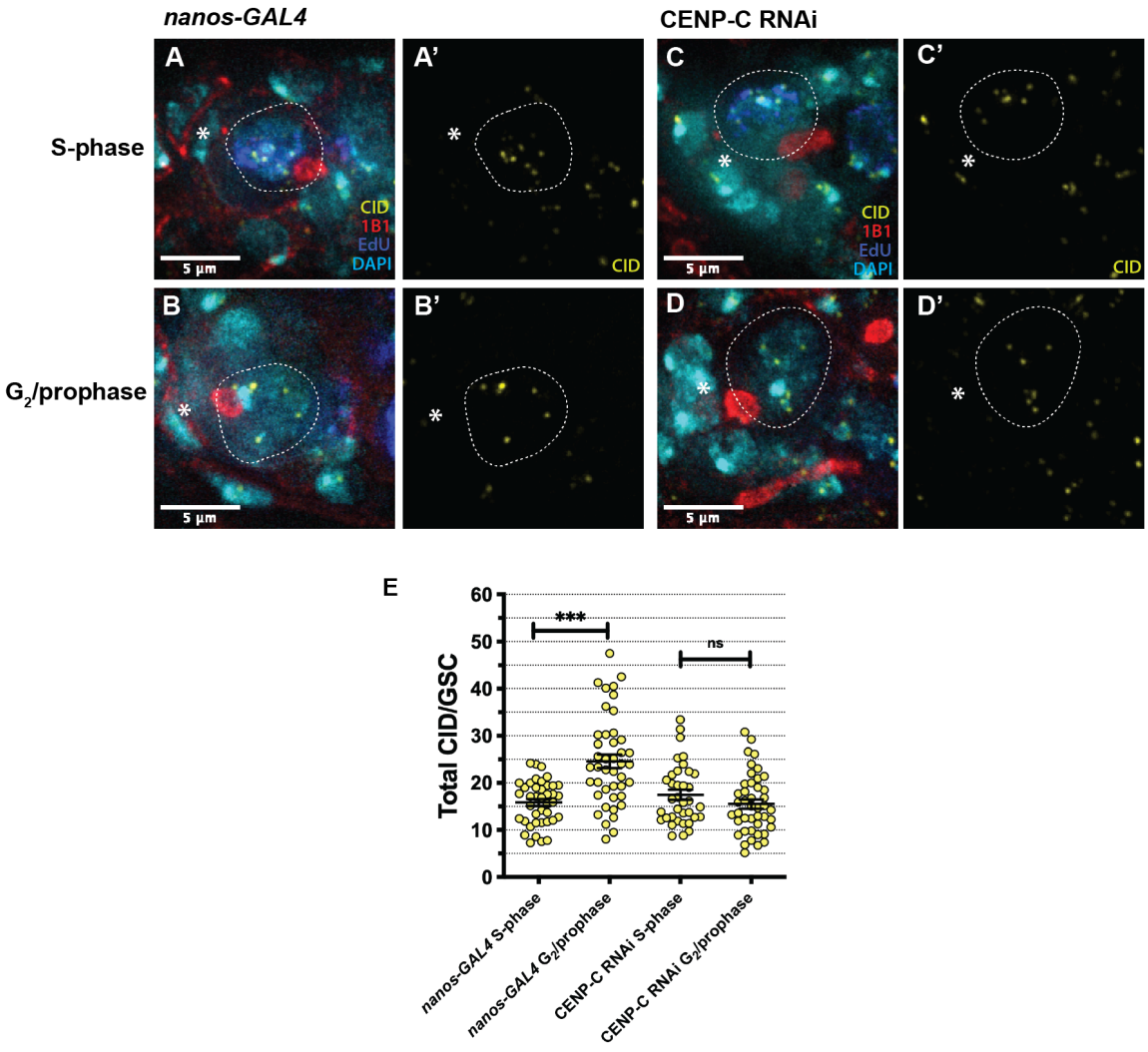

Figure 3.3: Quantitation of CID^{CENP-A} assembly in *nanos-GAL4* versus CENP-C RNAi. (A-D) *nanos-GAL4* and CENP-C RNAi stained with DAPI (cyan), EdU (blue), 1B1 (red) and CID^{CENP-A} (yellow, A'-D'). S-phase GSCs (A and C) are positive for EdU, contain a bridge spectrosome and clustered centromeres. G_2/prophase GSCs are EdU negative, contain a large round spectrosome and dispersed centromeres. GSCs are circled. * denotes cap cells/GSC niche. Scale bar = 5 µm. (E) Quantitation of total CID^{CENP-A} fluorescent intensity (integrated density) for S-phase and G_2/prophase *nanos-GAL4* and CENP-C RNAi GSCs. ***p<0.001. ns = non-significant. Error bars = SEM.

To further probe the effects of CENP-C on CID^{CENP-A} assembly, we monitored the effects of excess CENP-C on CID^{CENP-A} assembly. To do this, we used an inducible overexpression of an N-terminally haemagglutinin-tagged (HA-tagged) CENP-C coding sequence (HA-CENP-C). Again, we induced the HA-CENPC expression using the same *nanos-GAL4* driver. Firstly, we used an antibody against HA to characterise the expression pattern of HA-CENP-C (Fig 3.5 A-D). Next, we characterised CENP-C expression in G_2/prophase GSCs using the CENP-C antibody (Fig 3.6 A-H). Here, total CENP-C per GSC increased by approximately 45% (*nanos-GAL4* =39.82±3.45, n=11 cells; HA-CENP-C=57.77±5.38, n=11 cells). Following, we measured CID^{CENP-A} assembly between S-phase and G_2/prophase in the background of increased centromeric CENP-C (Fig 3.7 A and B). Unlike the results observed in the CENP-C RNAi, GSCs expressing HA-CENP-C displayed normal increase in CID^{CENP-A} levels from S-phase to G_2/prophase, in alignment with *nanos-GAL4* control samples (*nanos-GAL4*$_{Sphase}$=25.44±0.88, n=48 cells; *nanos-GAL4*$_{G2/prophase}$=36.77±2.01, n=45 cells; HA-CENP-C_{Sphase}=26.63±1.28, n=46 cells; HA-CENP-$C_{G2/prophase}$=37.99±2.20, n=41 cells) (Fig 3.7 E). Furthermore, CID^{CENP-A} levels between *nanos-GAL4* and HA-CENP-C are comparable, suggesting that increased CENP-C does not necessarily correlate with increased CID^{CENP-A}, at least in GSCs.

In order to determine whether these effects on assembly (and later, asymmetry) are a direct consequence of loss of CENP-C, we required a rescue line that contained an inducible non-degradable CENP-C to be expressed concurrently with the induction of the RNAi. For rescue experiments, we generated a transgenic fly line that contains both the UASp-HA-CENP-C expression transgene (on chromosome 2) and the UAS-CENP-C RNAi transgene (on chromosome 3). Given the shRNA against CENP-C targets the 5' Untranslated Region (5' UTR), the RNAi will not target HA-CENP-C induction. Thus, this allows the depletion of endogenous CENP-C and the overexpression of HA-CENP-C using the same *nanos-GAL4* driver and subsequent analysis of its effect on centromere dynamics. Firstly, we confirmed HA-CENP-C expression using antibodies against HA and endogenous CENP-C (Fig 3.5 E-H). We quantified total CENP-C levels, comparing the HA-CENP-C; CENP-C RNAi, to that of *nanos-GAL4* and CENP-C RNAi (Fig 3.5 I). Here, rescue GSCs displayed an 82% restoration of total CENP-C levels (*nanos-*

GAL4=35.84±2.11, n=30 cells; CENP-C RNAi=13.70±1.63, n=28 germaria; HA-CENP-C; CENP-C RNAi=29.49±2.09, n=28 germaria) (Fig 3.5 I). We measured CID assembly between S-phase and G_2/prophase in the background of HA-CENP-C; CENP-C RNAi background (Fig 3.7 C and D). In this case, CID assembly was partially rescued, displaying an increase in CID^{CENP-A} level from S-phase to G_2/prophase, although not quite to the CID^{CENP-A} level in the control (*nanos-GAL4*$_{Sphase}$=25.68±1.76, n=43 cells; *nanos-GAL4*$_{G2/prophase}$=37.24±1.98, n=44 cells; HA-CENP-C;CENP-C $RNAi_{Sphase}$=23.37±1.98, n=42 cells; HA-CENP-C;CENP-C $RNAi_{G2/prophase}$=32.51±2.47, n=41 cells) (Fig 3.7 F).

Lastly, we sought to determine whether *Cenp-C* and *cal1* C-terminal mutants could disrupt CID^{CENP-A} assembly (Fig 3.8). To do this, we obtained *Cenp-C* and *cal1* mutant alleles (*Cenp-C*^{IR35} and *cal1*^{2k32}) as previously published (Heeger et al., 2005; Unhavaithaya and Orr-Weaver, 2013), which result in C-terminal truncations of both proteins. In these mutants, the CENP-C/CAL1 binding domains are disrupted as a result and singularly, these alleles are homozygous lethal. Thus, we exploited transheterozygous c*al1*, *cenp-C*^{IR35}/*cenp-C*, *cal1*^{2k32} mutants (herein referred to as *cenp-C*^{IR35}/*cal1*^{2k32}) and analysed CENP-C assembly in these cases. Previously, this transheterozygote has been shown to at least have an impact on meiotic centromere clustering in the female germline (Unhavaithaya and Orr-Weaver, 2013). In our quantitation, we found that *Cenp-C*^{IR35}/*cal1*^{2k32} GSCs displayed a normal increase in CID^{CENP-A} level from S-phase to G_2/prophase, in alignment with *nanos-GAL4* control samples (*cenp-C*^{IR35}/*cal1*$^{2k32}{}_{Sphase}$=17.07±1.00, n=43 cells; *cenp-C*^{IR35}/*cal1*$^{2k32}{}_{G2/prophase}$=26.90±1.76, n=43 cells) (Fig 3.8 C). Given this transheterozygote contains one *wild type* copy each of *cenp-C* and *cal1*, this appears sufficient in this case to allow normal CID^{CENP-A} assembly in GSCs.

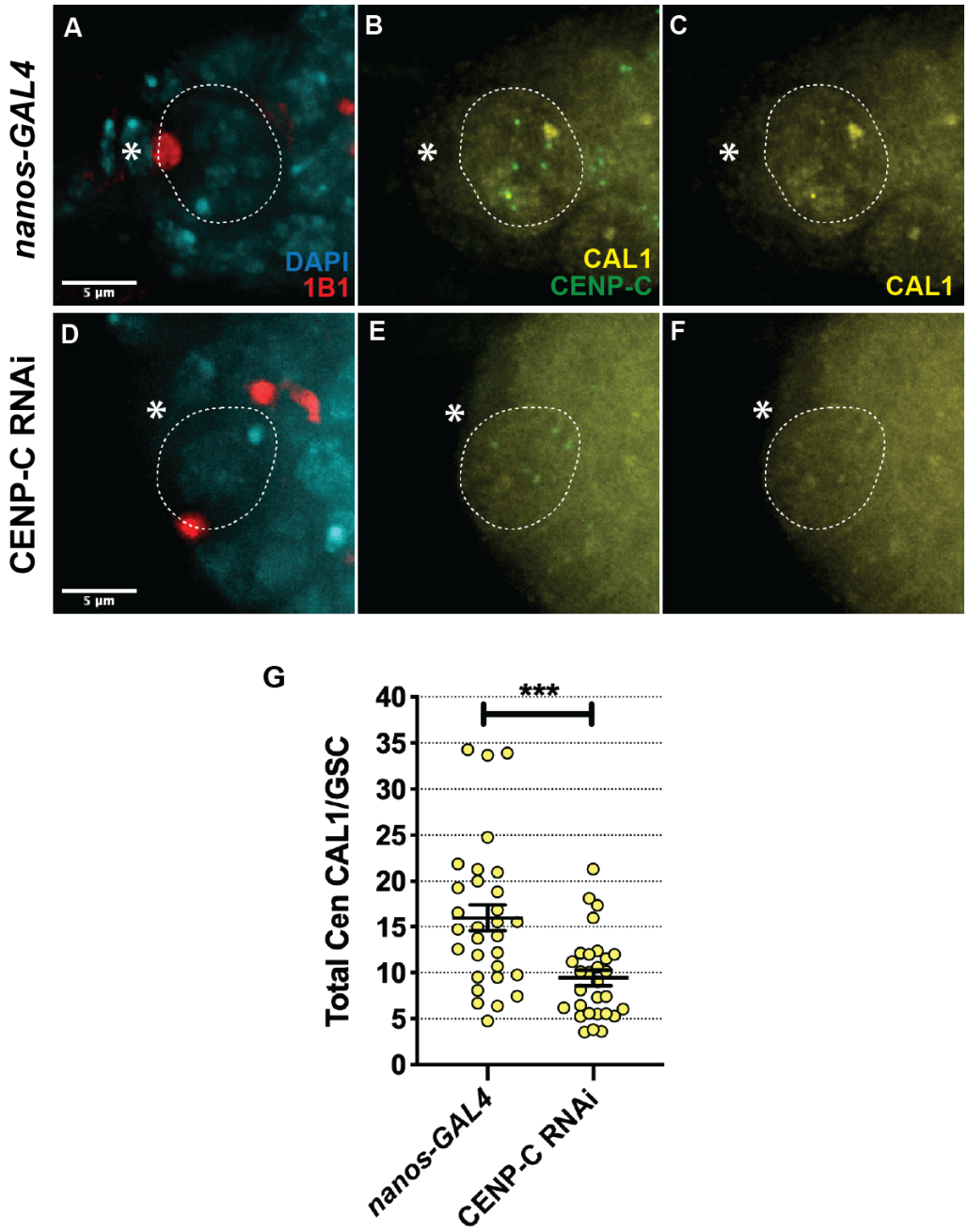

Figure 3.4: Quantitation of centromeric CAL1 in *nanos-GAL4* versus CENP-C RNAi. (A-F) *nanos-GAL4* and CENP-C RNAi stained for DAPI (cyan), 1B1 (red), CAL1 (yellow) and CENP-C (green). Centromeric CAL1 was identified as being colocalised with CENP-C. GSCs are circled. *denotes cap cells. Scale bar = 5 µm. (G) Quantitation of total centromeric CAL1 fluorescent intensity (integrated density) per GSC *nanos-GAL4* versus CENP-C RNAi. ***p<0.001. Error bars = SEM.

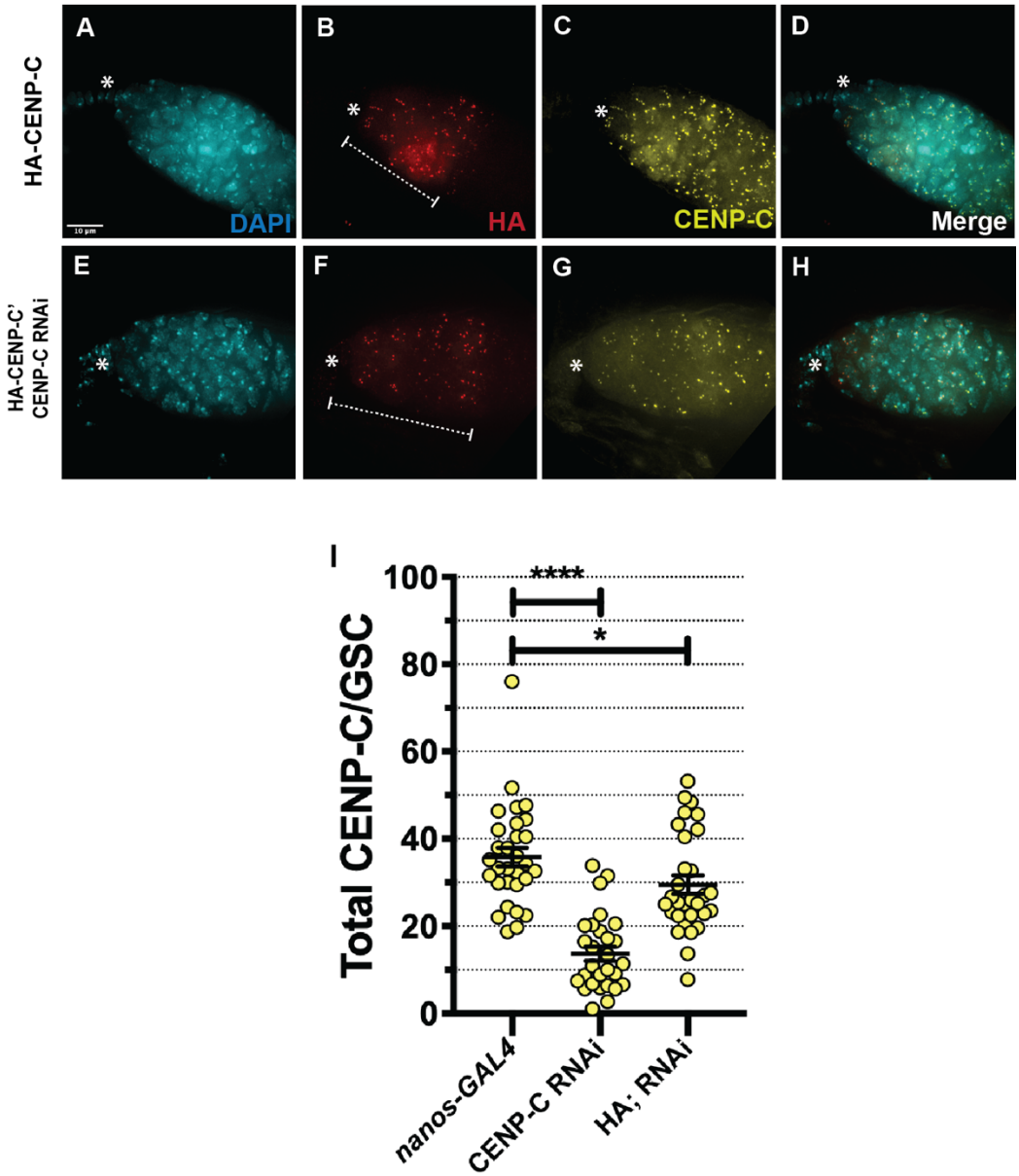

Figure 3.5: Characterisation of HA-CENPC and HA-CENP-C; CENP-C RNAi rescue lines. (A-D) Confirmation of induction of HA-CENP-C in the UASp HA-CENP-C overexpression line, stained with DAPI (cyan), HA (red) and CENP-C (yellow). (E-F) Confirmation of HA-CENP-C expression in the HA-CENP-C; CENP-C RNAi rescue line, stained with DAPI (cyan), HA (red) and CENP-C (yellow). Dashed line displays HA expression. *denotes cap cells. Scale bar = 10 μm. (I) Quantitation of total CENP-C antibody fluorescence intensity (integrated density) per GSC in *nanos-GAL4* versus CENP-C RNAi versus HA-CENP-C;CENP-C RNAi (rescue) GSCs. *$p<0.05$, ****$p<0.0001$. Error bars = SEM.

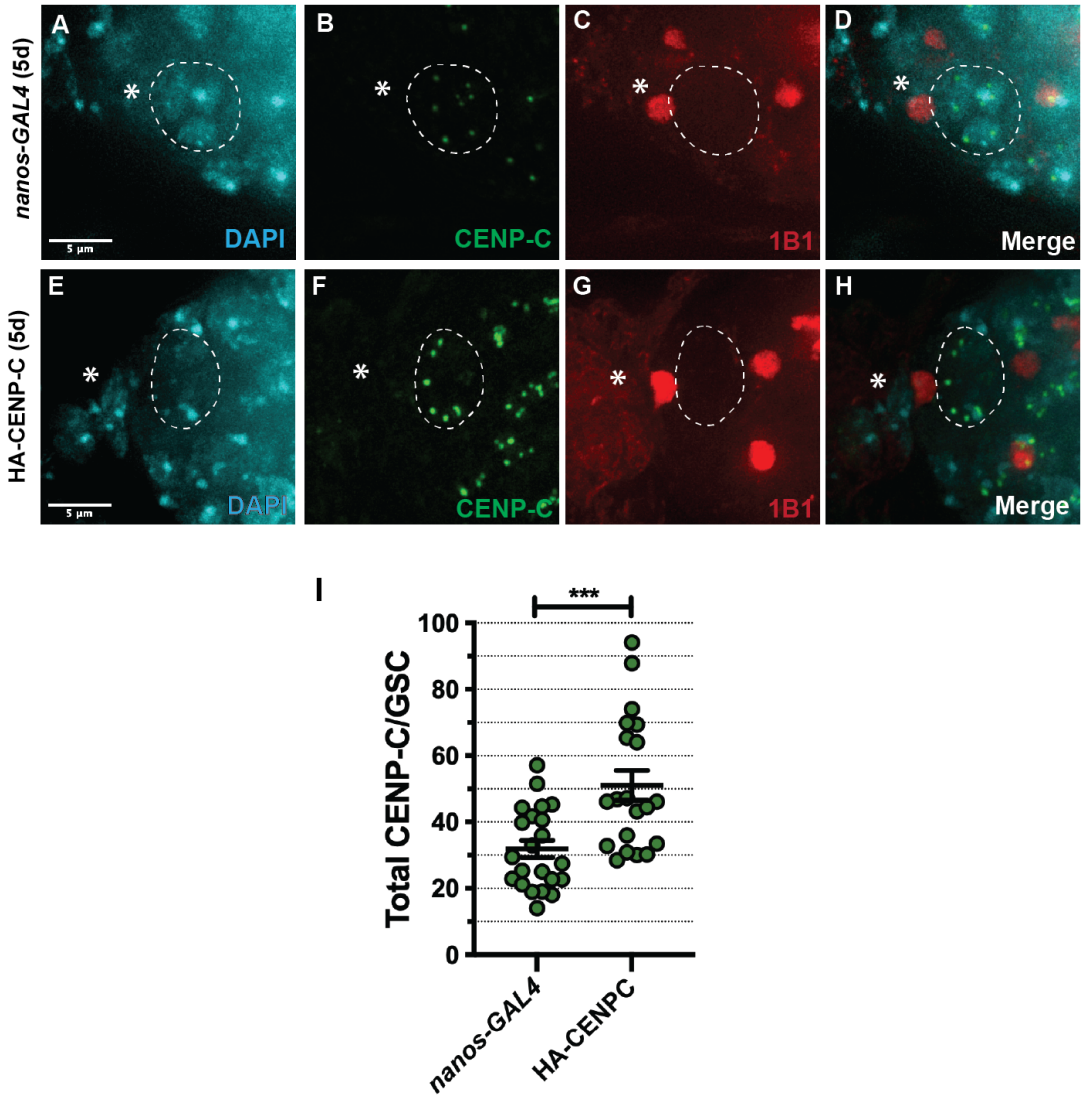

Figure 3.6: Quantitation of CENP-C level upon HA-CENP-C overexpression. (A-H) Immunofluorescence staining of *nanos-GAL4* and HA-CENP-C in G_2/prophase GSCs stained with DAPI (cyan), 1B1 (red) and CENP-C (green). * denotes cap cells. GSCs are circled. Scale bar = 10 μm. (I) Quantitation of total CENP-C fluorescent intensity (integrated density) per GSC in *nanos-GAL4* versus HA-CENP-C overexpression. *$p<0.05$. Error bars = SEM.

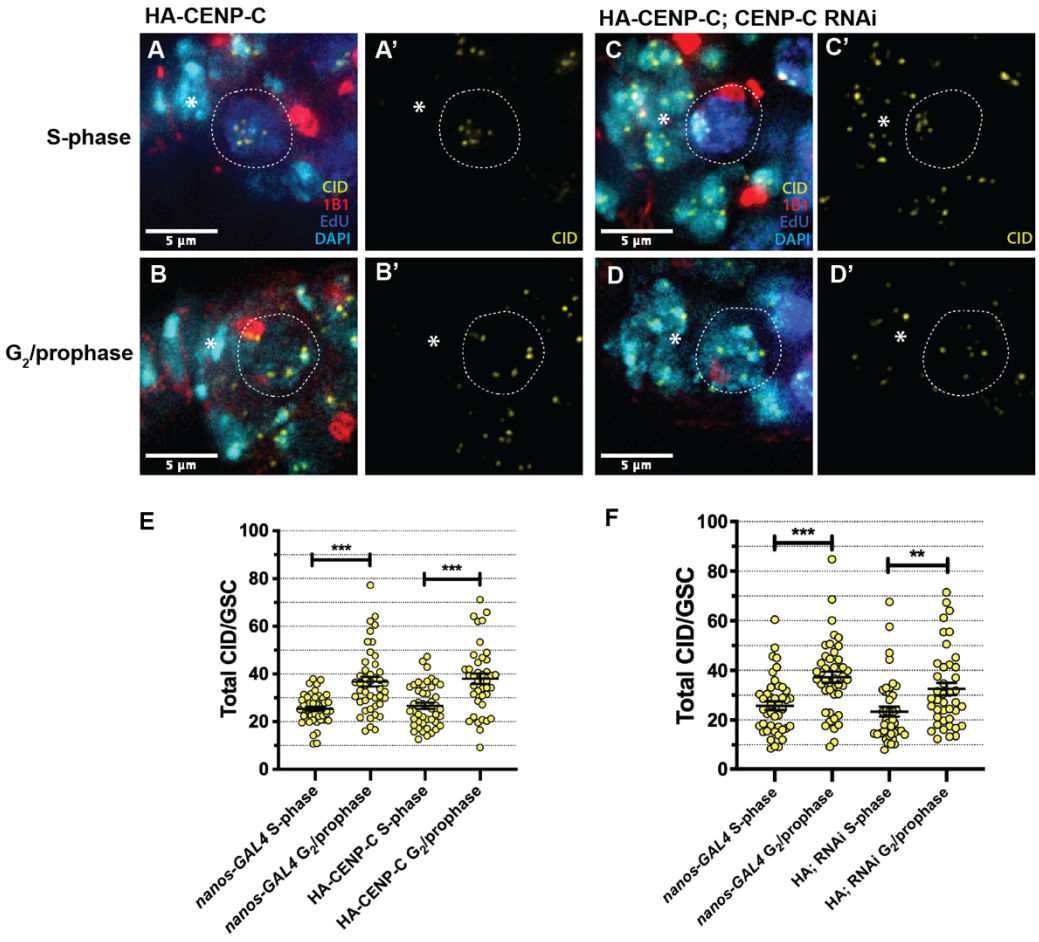

Figure 3.7: Quantitation of CID assembly in HA-CENP-C and HA-CENP-C; CENP-C RNAi GSCs. (A-D) HA-CENP-C and HA-CENP-C; CENP-C RNAi (rescue) stained with DAPI (cyan), EdU (blue), 1B1 (red) and CID^{CENP-A} (yellow, A'-D'). S-phase GSCs (A and C) are positive for EdU, contain a bridge spectrosome and clustered centromeres. G_2/prophase GSCs (B and D) are EdU negative, contain a large round spectrosome and dispersed centromeres. GSCs are circled. * denotes cap cells. Scale bar = 5 µm. (E) Quantitation of total CID^{CENP-A} fluorescent intensity (integrated density) per GSC for S-phase and G_2/prophase *nanos-GAL4* and HA-CENP-C (25 °C) GSCs. (F) Quantitation of total CID^{CENP-A} fluorescent intensity (integrated density) per GSC for S-phase and G_2/prophase *nanos-GAL4* and HA-CENP-C; CENP-C RNAi (22 °C). **p<0.01, ***p<0.001. Error bars = SEM.

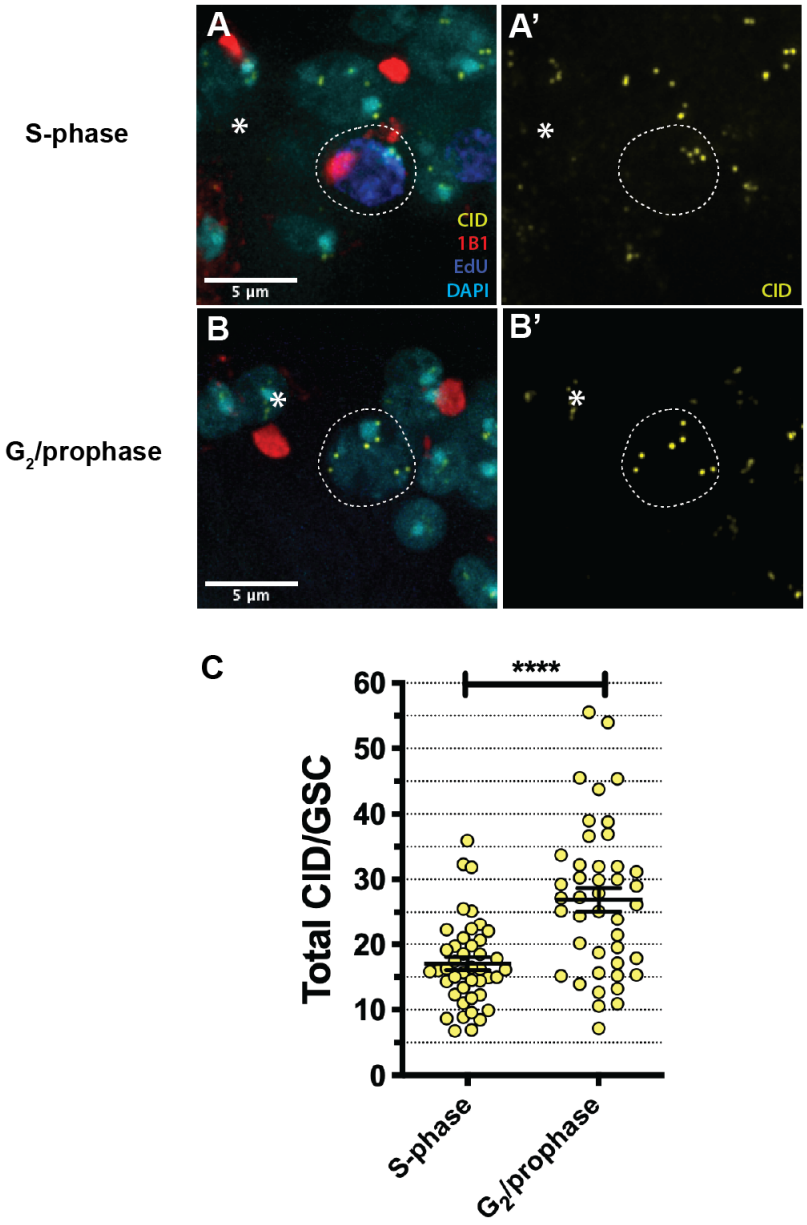

Figure 3.8: Quantitation of CID assembly in transheterozygous *cenp-C/cal1* mutant GSCs. (A and B) *cenp-C*^{IR35}/*cal1*^{2k32} stained with DAPI (cyan), EdU (blue), 1B1 (red) and CID^{CENP-A} (yellow, A'-D'). S-phase GSCs (A, A') are positive for EdU, contain a bridge spectrosome and clustered centromeres. G_2/prophase GSCs are EdU negative, contain a large round spectrosome and dispersed centromeres (B, B'). GSCs are circled. * denotes cap cells. Scale bar = 5 µm. (C) Quantitation of total CID^{CENP-A} fluorescent intensity (integrated density) per GSC for S-phase and G_2/prophase *cenp-C*^{IR35}/*cal1*^{2k32} GSCs. ****p<0.0001. Error bars = SEM.

3.4 CENP-C is asymmetrically distributed between stem and daughter cells

Ranjan *et al* and Dattoli *et al* recently elucidated that sister centromeres of male and female GSCs display an asymmetric distribution of CID between GSC and CB. There, sister centromeres to be inherited by the GSC display more CID^{CENP-A} compared to sister centromeres to be inherited by the CB daughter cell. In our hands, super resolution microscopy of prometaphase/metaphase female GSCs showed a 1.2 fold increase in 'GSC-side' CID^{CENP-A}. Thus, we observed a quantitative difference in the amount of CID^{CENP-A} assembled on each sister centromere in a mitotic system. Given this observation, we sought to further understand 1) the extent of this asymmetry to other centromere proteins (i.e. CENP-C), and 2) the effect of centromere disruption on this CID^{CENP-A} asymmetry. In turn, this would highlight the important aspects behind how this asymmetry is established and maintained across the cell cycle.

Firstly, we went about understanding to what extent the centromere builds its asymmetry. To do this, we took advantage of the short G_1 phase and cell cycle synchronicity of GSCs and their daughter CBs. Moreover, we know assembly of new centromere proteins does not occur until G_2/prophase (Dattoli et al., 2020; Ranjan et al., 2019). This allows us to isolate S-phase GSC and CB 'pairs' and quantitate and analyse centromere distributions post-mitotically, without the interference of centromere assembly. To prove this concept (now published in Dattoli *et al* 2020), we quantified total CID^{CENP-A} between GSC/CB S-phase 'pairs' and expressed the total CID^{CENP-A} in each cell as a ratio GSC:CB. Here, GSCs displayed an approximate 1.2-fold enrichment of CID^{CENP-A} compared to CBs, consistent with the ratio observed between sister centromeres at prometaphase/metaphase using Structured Illumination Microscopy (SIM). Following this, we next sought to determine whether CENP-C was also asymmetrically distributed between GSC and CB. To do this, EdU was incorporated for 45 mins to *wild type* (*OregonR*) ovaries and stained with DAPI, 1B1 and CENP-C. This allowed us to isolate S-phase GSC/CB pairs (Fig 3.9 A). We then quantified total CENP-C fluorescence intensity (integrated density) between respective S-phase GSC and CB pairs (Fig 3.9 B), and expressed each pair

as a ratio GSC:CB (Fig 3.9 C). Indeed, CENP-C was also asymmetrically distributed between GSC and CB (1.32:1 ± 0.07) [This data is now published in Dattoli et al, 2020 in Figure 3 O-P]. Therefore, GSCs lay a stronger centromere foundation and in turn build a stronger kinetochore. However, whether CENP-C is playing an active role in establishing and maintaining this asymmetry of CID^{CENP-A} remained unclear.

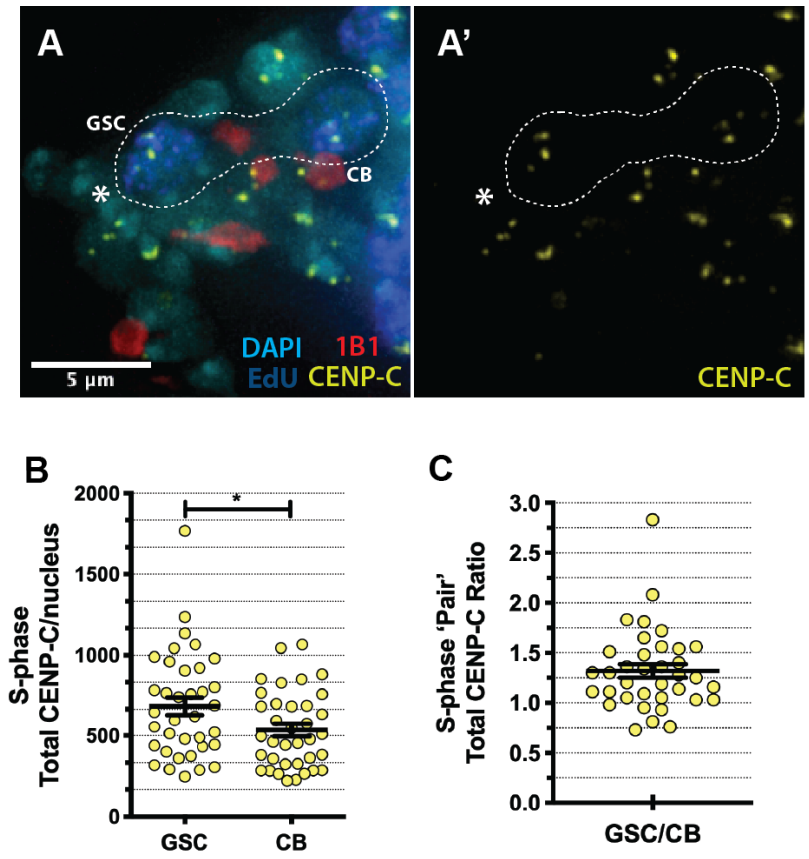

Figure 3.9: CENP-C is asymmetrically distributed between GSCs and CBs. (A) *Wild type* (*OregonR*) GSC/CB in S-phase, stained with DAPI (Cyan), EdU (blue), 1B1 (red) and CENP-C (yellow, A'). *denotes cap cells. Scale bar = 5 µm. (B) Quantitation of total CENP-C fluorescent intensity (integrated density) in S-phase GSCs and CBs in *wild type (OregonR)* germaria. Each point represents the total CENP-C integrated density per GSC/CB nucleus. (C) Quantitation of the ratio of total CENP-C fluorescent intensity (integrated density) between GSC/CB S-phase pairs. Each point represents the ratio of total CENP-C between GSC versus its corresponding CB. *$p<0.05$. Error bar = SEM. This data is published in Fig 3 (O-P) of Dattoli et al, 2020 (Dattoli et al., 2020).

3.5 CENP-C maintains an asymmetric distribution of CID in GSCs

Given that CENP-C is also asymmetrically distributed between GSC and CB, questions still remained regarding whether CENP-C is involved in the maintenance and establishment of asymmetric CID^{CENP-A}; or whether it was simply assembling a stronger kinetochore in response to more CID^{CENP-A}. CENP-C is clearly emerging in the literature as a recruitment factor for assembly of new CID by CAL1 (Medina-Pritchard et al., 2020; Roure et al., 2019). Hence, we hypothesised that CENP-C would be intrinsic to CID^{CENP-A} levels in an asymmetric model. To probe this idea, we quantified total CID^{CENP-A} in GSCs and their corresponding CB (Fig 3.10 C). We then analysed CID^{CENP-A} intensity in GSC/CB pairs in both *nanos-GAL4* and CENP-C RNAi (Fig 3.10 D). Quantitation revealed a significant increase in the GSC/CB ratio of CID^{CENP-A} intensity in the CENP-C RNAi compared to the expected average ratio of 1.2 in *nanos-GAL4* controls (*nanos-GAL4* $_{GSC/CB}$=1.19±0.06, n=40 cells; CENP-C $RNAi_{GSC/CB}$=1.44±0.08, n=36 cells (Fig. 3.10 D). This indicates that CENP-C functions not only in CID^{CENP-A} assembly between DNA replication and prophase, but also in the maintenance of CID^{CENP-A} asymmetry in S-phase. Given new CID^{CENP-A} assembly is likely deficient in the absence of CENP-C (Fig 3.3), GSCs are entering the upcoming division with largely parental, 'old' CID^{CENP-A}. This indicates a probable role for CENP-C in specifically maintaining the parental CID^{CENP-A} pool on GSC sister centromeres.

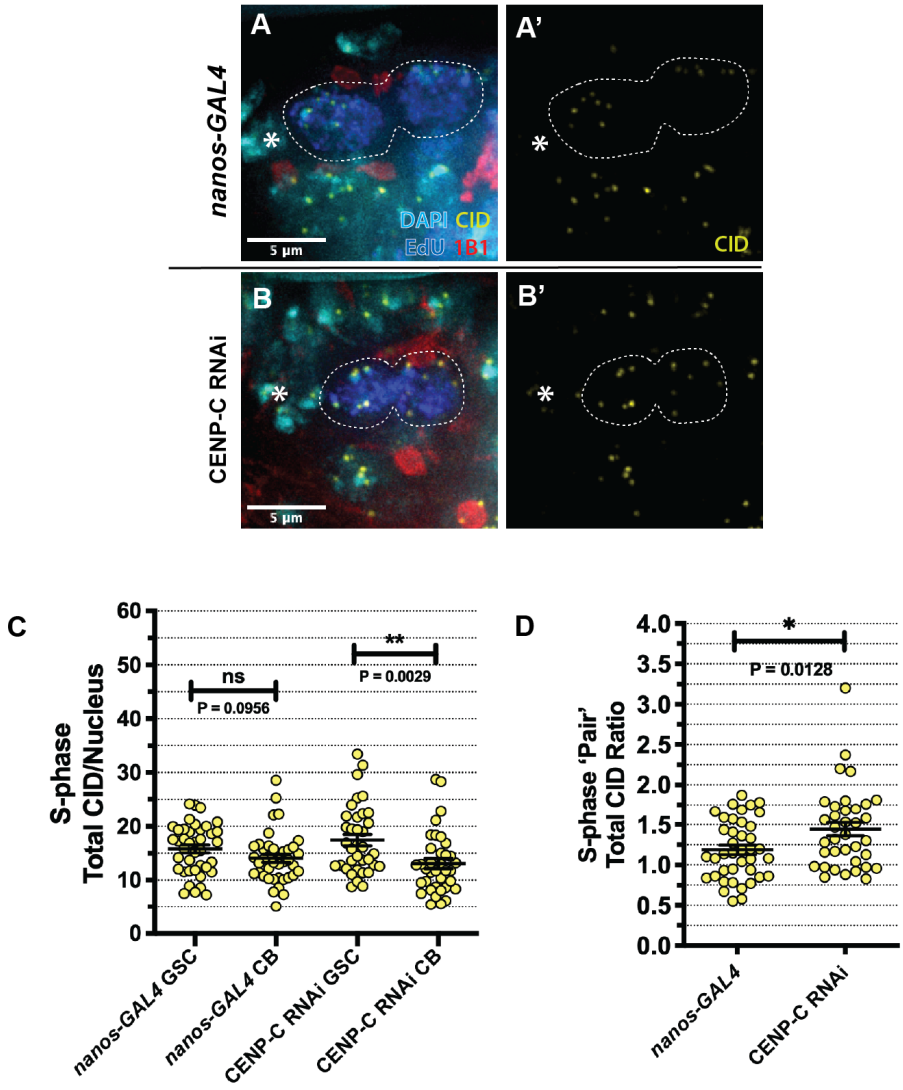

Figure 3.10: Quantitation of CID^{CENP-A} asymmetry between GSC and CB S-phase pairs in nanos-GAL4 versus CENP-C RNAi. (A-D) nanos-GAL4 and CENP-C RNAi stained with DAPI (cyan), EdU (blue), 1B1 (red) and CID^{CENP-A} (yellow, A', B'). S-phase GSCs and CBs (A and C) are positive for EdU, contain a bridge spectrosome and clustered centromeres. GSC/CB pairs are highlighted. * denotes cap cells. Scale bar = 5 µm. (C) Quantitation of total CID^{CENP-A} fluorescent intensity (integrated density) in S-phase GSCs and CBs in nanos-GAL4 versus CENP-C RNAi. Each point represents the total CID^{CENP-A} integrated density per GSC/CB nucleus. (D) Quantitation of the ratio of total CID^{CENP-A} fluorescent intensity (integrated density) between GSC/CB S-phase pairs in nanos-GAL4 versus CENP-C RNAi. Each point represents the ratio of total CID between GSC versus its corresponding CB. ns=non-significant. *p<0.05. **p<0.01. Error bars = SEM.

Next, we further investigated CENP-C-mediated CID^{CENP-A} maintenance by observing CID^{CENP-A} asymmetry upon overexpression of HA-CENP-C. We again quantified total CID^{CENP-A} in GSCs and their corresponding CB (Fig 3.11 C) and expressed total CID^{CENP-A} as a ratio of GSC:CB (Fig 3.11 D). In this case, HA-CENP-C overexpression opposed the CENP-C RNAi result, measuring a ratio trending towards 1.0 (*nanos-Gal4*$_{GSC/CB}$=1.22±0.06, n=47 cells; HA-CENP-C$_{GSC/CB}$=1.12±0.04, n=46 cells). Hence, HA-CENP-C expression promoted a CID^{CENP-A} ratio not significantly different to its respective *nanos-GAL4* control (Fig 3.11 D). To verify these results, we performed the same analysis in the HA-CENP-C; CENP-C RNAi rescue line. Indeed, quantitation of rescue versus *nanos-GAL4* controls returned the CID^{CENP-A} ratio to 1.2 as one would expect in control GSC/CBs (*nanos-Gal4*$_{GSC/CB}$=1.23±0.07, n=43 cells; HA-CENP-C; CENP-C RNAi$_{GSC/CB}$=1.20±0.06, n=42 cells).

Lastly, we quantitated CID^{CENP-A} asymmetry in the transheterozygote *cenp-C^{IR35}/cal1^{2K32}* mutant females. Given that CID^{CENP-A} appears to assemble at the normal rate in G_2/prophase in these GSCs, we wondered whether asymmetry would be affected. We again quantified total CID in GSCs and CBs, and expressed total CID^{CENP-A} as a ratio between GSC:CBs. In this case, CID^{CENP-A} asymmetry was slightly higher than the expected value of 1.2 in favour of the GSC side (*cenp-C^{IR35}/cal1^{2K32}*$_{GSC/CB}$=1.33±0.08, n=41 cells). Given that CID^{CENP-A} assembly is still present as normal in these transheterozygote GSCs, it is probable that the CID^{CENP-A} asymmetry being observed is established during S-phase, rather than during the assembly phase in G_2/prophase. Combining the asymmetry data of CENP-C RNAi (increased asymmetry), HA-CENP-C overexpression (less asymmetry), rescue (normal) and mutant (increased asymmetry), it appears CENP-C is imperative to coordinating an asymmetric CID^{CENP-A} distribution in GSCs and CBs.

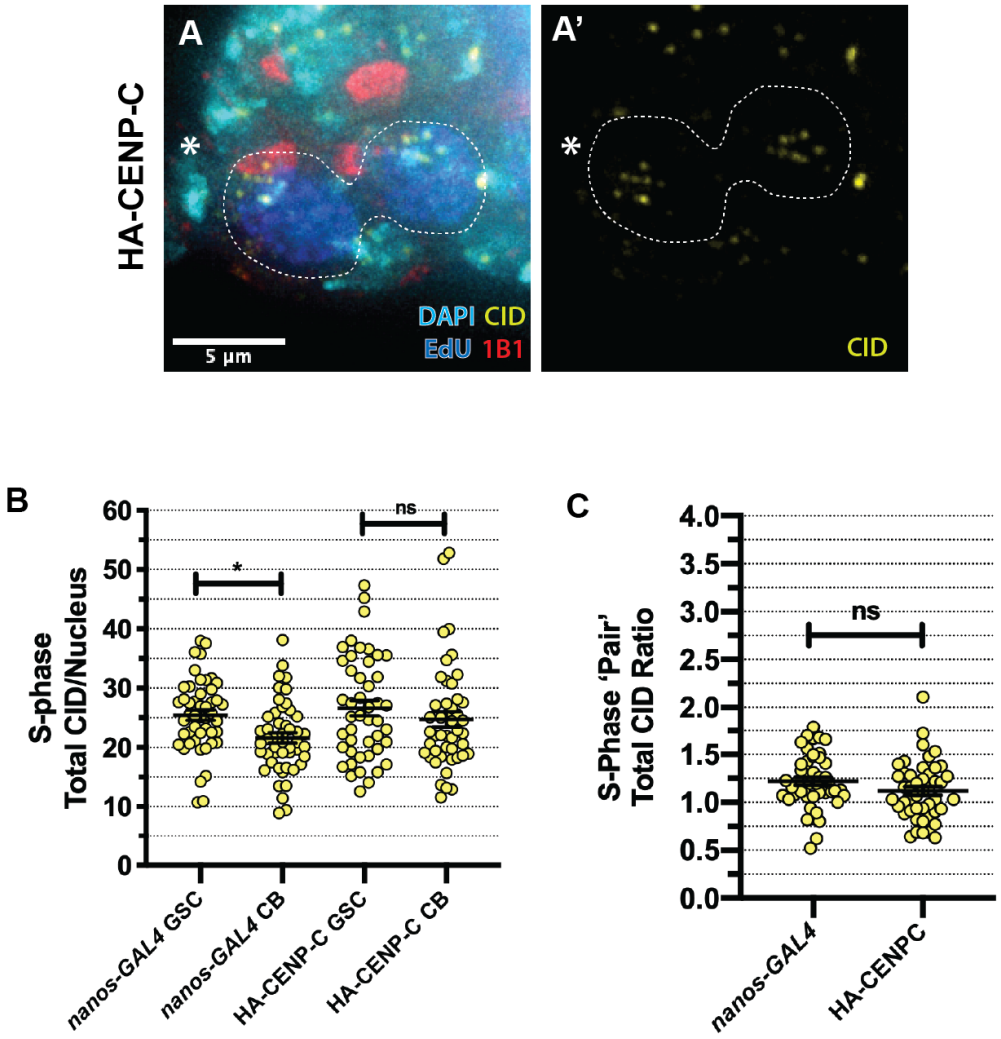

Figure 3.11: Quantitation of CID^{CENP-A} asymmetry between GSC and CB S-phase pairs in HA-CENP-C. (A) Immunostaining of HA-CENP-C GSC and CB, stained with DAPI (cyan), EdU (blue), 1B1 (red) and CID^{CENP-A} (yellow, A'). S-phase GSCs and CBs are positive for EdU, contain a bridge spectrosome and clustered centromeres. GSC/CB pairs are highlighted. * denotes cap cells. Scale bar = 5 µm. (B) Quantitation of total CID^{CENP-A} integrated density per GSC and CB for *nanos-GAL4* and HA-CENP-C. (C) Quantitation of the ratio of total CID^{CENP-A} fluorescent intensity (integrated density) between GSC/CB S-phase pairs in *nanos-GAL4* versus HA-CENP-C. Each point represents the ratio of total CID^{CENP-A} between GSC versus its corresponding CB. *$p<0.05$, ns = non-significant. Error bars = SEM.

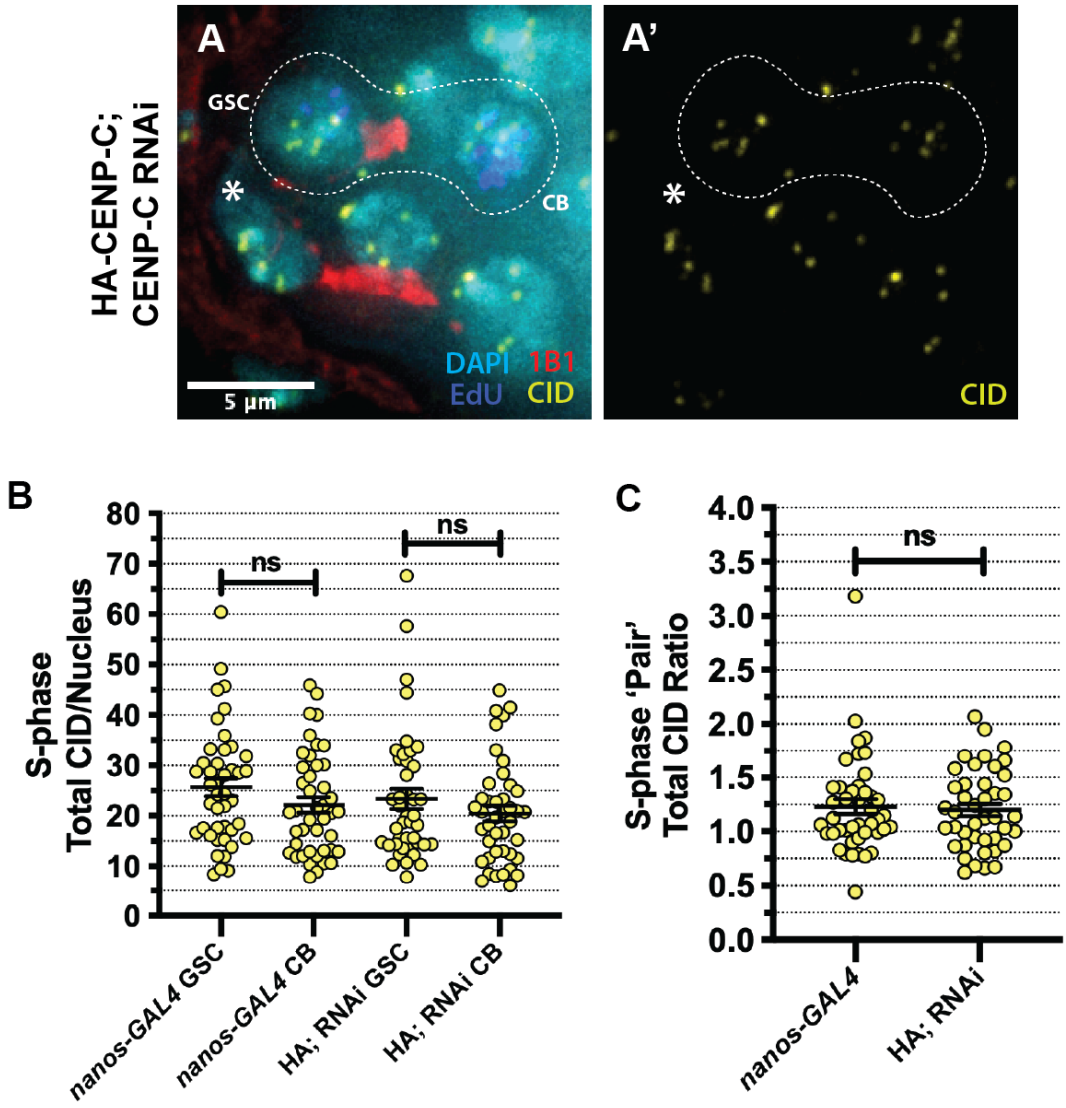

Figure 3.12: Quantitation of CID^{CENP-A} asymmetry between GSC and CB S-phase pairs in HA-CENP-C; CENP-C RNAi rescue. (A) Immunostaining of HA-CENP-C; CENP-C RNAi GSC and CB, stained with DAPI (cyan), EdU (blue), 1B1 (red) and CID^{CENP-A} (yellow, A'). S-phase GSCs and CBs are positive for EdU, contain a bridge spectrosome and clustered centromeres. GSC/CB pairs are highlighted. * denotes cap cells. Scale bar = 5 µm. (B) Quantitation of total CID^{CENP-A} integrated density per S-phase GSCs and CBs for *nanos-GAL4* and HA-CENP-C; CENP-C RNAi. (C) Quantitation of the ratio of total CID^{CENP-A} fluorescent intensity (integrated density) between GSC/CB S-phase pairs in *nanos-GAL4* versus HA-CENP-C; CENP-C RNAi. Each point represents the ratio of total CID^{CENP-A} between GSC versus its corresponding CB. ns = non-significant. Error bars = SEM.

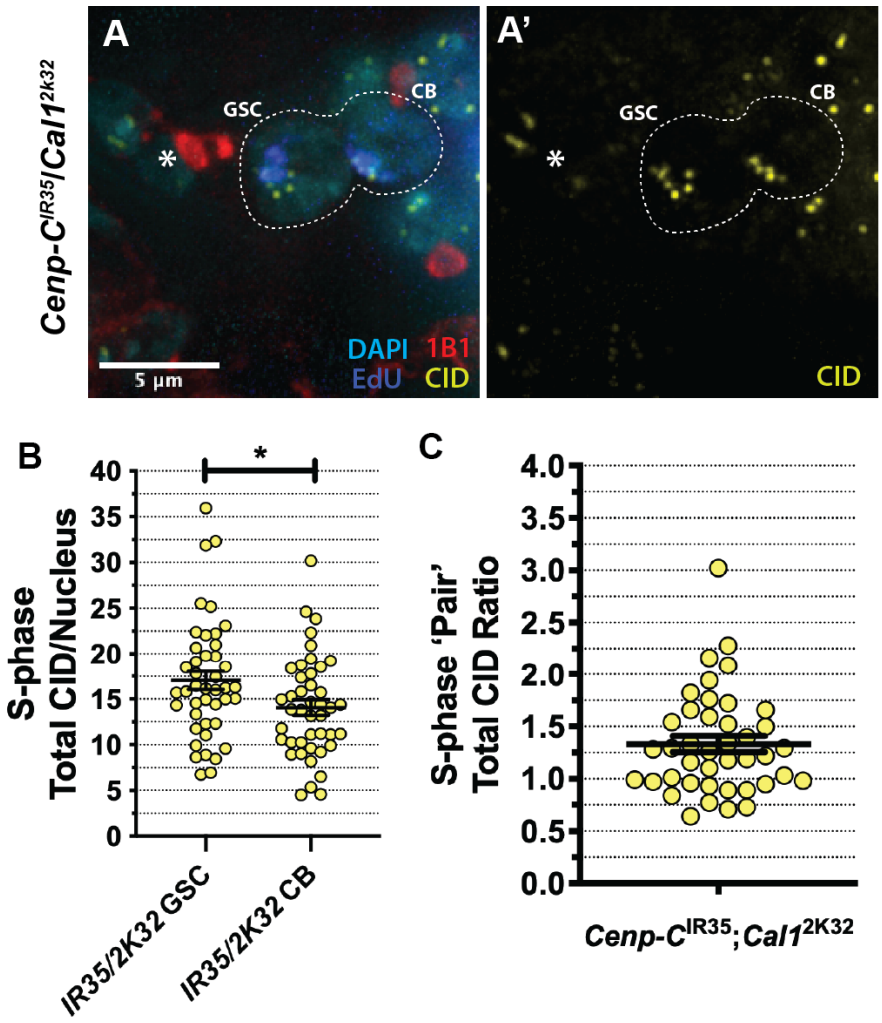

Figure 3.13: Quantitation of CID^{CENP-A} asymmetry in transheterozygous *cenp-C/cal1* mutant. (A) Immunostaining of *cenp-C*^{IR35}/*cal1*^{2k32} transheterozygous mutant GSC and CB, stained with DAPI (cyan), EdU (blue), 1B1 (red) and CID^{CENP-A} (yellow, A'). Scale bar = 5 µm. (B) Quantitation of CID fluorescent intensity (integrated density) between S-phase GSCs and CBs in the transheterozygous *cenp-C/cal1* mutant. Each point represents the total CID^{CENP-A} integrated density per GSC/CB nucleus. (D) Quantitation of the ratio of total CID^{CENP-A} fluorescent intensity (integrated density) between GSC/CB S-phase pairs in *cenp-C*^{IR35}/*cal1*^{2k32}. Each point represents the ratio of total CID^{CENP-A} between GSC versus its corresponding CB. *p<0.01. Error bars = SEM.

3.6 Chapter Summary and Discussion

A summary of the major findings presented in chapter 3:

1. CENP-C is assembled between the end of DNA replication and G_2 phase up until prophase in female *Drosophila* GSCs, in a similar manner to CID^{CENP-A}.

2. CENP-C is required for the assembly of new CID^{CENP-A} in G_2/prophase.

3. Overexpression of HA-CENP-C and *cenp-C^{IR35}/cal1^{2K32}* C-terminal mutants are not sufficient to disrupt CID^{CENP-A} assembly in GSCs.

4. CENP-C is asymmetrically distributed between GSC and CB at a similar ratio to CID^{CENP-A}.

5. CID asymmetry inherited between GSCs and CBs can be disrupted through (i) depletion of CENP-C (increase CID^{CENP-A} asymmetry), (ii) expression of HA-CENP-C (decrease CID^{CENP-A} asymmetry), and (iii) *cenp-C^{IR35}/cal1^{2K32}* transheterozygous mutants (increase CID^{CENP-A} asymmetry).

3.6.1 CENP-C assembles in G_2/prophase and is required for CID^{CENP-A} assembly at the same cell cycle time.

In symmetrical models of cell division, it is well-known that CENP-C plays a key role in centromere assembly (Carroll et al., 2010; Roure et al., 2019). Depletion of CENP-C leads to a strong reduction in CENP-A level, measured by the loss of CENP-A/CID (Carroll et al., 2010; Erhardt et al., 2008; Falk et al., 2015). Thus, it can be argued that CENP-C indeed plays two essential functions: 1) to build a sound kinetochore platform, and 2) to maintain and propagate a centromere across the cell cycle. Disruption to either function is detrimental to long-term cellular viability. In this chapter, we show that (1) CENP-C assembles in G_2/prophase in a

similar timing and amount to CID^{CENP-A}. (2) We provide strong evidence that depleting CENP-C by approximately 60% in GSCs disrupts the CID^{CENP-A} assembly in GSCs, maintaining a CID^{CENP-A} level no higher than their S-phase levels. In CENP-C-depleted GSCs, CID^{CENP-A} assembly factor CAL1 is also depleted at the centromere. A stronger depletion of CENP-C results in an agametic phenotype (loss of germ cells). Here, as with all cell division, it is probable that a critical support level of CID^{CENP-A} is required for cell division to occur. In contrast, expression of HA-CENP-C alone did not disrupt CID^{CENP-A} assembly. Rather, CID^{CENP-A} appeared at levels comparable to the *nanos-GAL4* control in this case. This suggests that expression of CENP-C alone is not sufficient to drive more CID^{CENP-A} to the centromere. Although centromeric CENP-C levels do increase in the HA-CENP-C GSCs, residual CENP-C also appeared to accumulate pan-nuclear (data not shown). This suggests a limit in the amount of CENP-C that could be recruited to the centromere, possibly due to saturation of CID^{CENP-A} assembly by other factors (e.g. Cyclins, HASPIN). Given the interdependence of CID^{CENP-A}, CAL1 and CENP-C, a full overpowering of the centromere may well rely on a co-expression of CENP-C with the assembly factor CAL1, or even also with CID^{CENP-A}. In the transheterozygote *cenp-*C^{IR35}*/cal1*^{2K32}, CID assembled at a normal rate. However, this may well be due to the presence of one *wild type* copy of CENP-C and CAL1 also being present, compromising the result. Importantly though, CENP-C depletion alone is sufficient to disrupt assembly of CID^{CENP-A}. Therefore, we sought to understand the impact this would have on how the centromere is maintained, focussing on CID^{CENP-A} asymmetry as a readout.

3.6.2 CENP-C maintains an asymmetric distribution of CID between stem and daughter cells

Given CENP-C impacts CID assembly, we wished to determine the effect CENP-C was having on the maintenance of CID^{CENP-A} across the cell division cycle. To do this we looked at GSC-CB S-phase 'pairs', measuring total CID^{CENP-A} intensity in each GSC and CB nucleus and expressing as a ratio. Here we showed that upon depletion of CENP-C, the GSC/CB CID^{CENP-A} distribution ratio increases significantly from 1.2 to 1.45. Thus, GSCs retain more CID^{CENP-A} compared to

their respective daughter cells when CENP-C is depleted. This suggests a role for CENP-C in maintaining sister CID^{CENP-A} asymmetry across the GSC division. Specifically, given that CID^{CENP-A} assembly is largely absent, these GSCs are entering mitosis with primarily parental CID^{CENP-A}. In male GSCs and ISCs, we know that parental CID^{CENP-A} is retained by the stem cell whereas newly synthesised CID^{CENP-A} is distributed to the daughter cell (García del Arco et al., 2018; Ranjan et al., 2019). Moreover in the *Drosophila* midgut epithelium, CENP-C is present only in ISCs and not their endocycling daughter cells (García del Arco et al., 2018). Together, our data suggests that parental CID^{CENP-A} is strongly maintained by GSCs, even despite CENP-C depletion.

In addition, upon HA-CENP-C expression (50% increase), CID^{CENP-A} asymmetry trends towards a symmetrical 1:1 distribution of CID^{CENP-A}, albeit non-significant compared to the control (1.12). Here, a larger frequency of data points can be seen below or around 1.0. Therefore, we are seeing the opposite effect on CID^{CENP-A} asymmetry when we deplete or increase CENP-C. Analysing transheterozygote *cenp-C^{IR35}/cal1^{2K32}* GSCs (which we know complete CID^{CENP-A} assembly), we observed a smaller increase in CID^{CENP-A} asymmetry (1.33 versus a normal ratio of 1.2). Again, this smaller increase in asymmetry compared to the CENP-C RNAi could be explained by one *wild type* copy of *Cenp-C* and *cal1* also being present. Nevertheless, we can interpret here that CENP-C and CAL1 interaction effects asymmetry. Given homozygotes of *cenp-C^{IR35}* and *cal1^{2K32}* are female sterile (not shown), their interaction at their respective C-termini probably play a much larger role in establishing and/or maintaining asymmetry than this transheterozygote can viably suggest. Given that CID^{CENP-A} assembly is present, yet asymmetry is still being affected, it is highly likely that centromere asymmetry is being established during S-phase rather than during the assembly phase itself. This would parallel with findings in the male germline that a high frequency of unidirectional fork movements exist during S-phase (Wooten et al., 2019b), giving the cell a window of opportunity to establish histone asymmetry.

4. Understanding the role of the centromere in GSC maintenance and differentiation

4.1 Chapter Introduction

Understanding which genes influence stem cell fate is fundamental to basic stem cell biology. *Drosophila* stem cell niches (male/female germline, thoracic ventral nerve cord, midgut epithelium) represent powerful systems in which to genetically manipulate and study the requirement of such genes at a tissue level.

In 2014, a large scale RNAi screen was carried out in *Drosophila* female GSCs, covering approximately 25% of the genome (Yan et al., 2014). Here, a large array of gene hits (366 genes) were identified to be involved in the maintenance or differentiation of GSCs, or other processes of oogenesis. These hits, organised into networks, cover many aspects of cellular biology, including transcription and chromatin remodelling, ribosome biogenesis, splicing, DNA replication and significantly kinetochore and spindle assembly. To our interest, CENP-C proved to be the only centromeric hit in this screen (possibly due to the essential nature of CENP-A and its assembly chaperone CAL1). Moreover, the Hou and Knoblich labs also performed RNAi screens in male GSCs, as well as neuroblasts and intestinal stem cells in *Drosophila* (Liu et al., 2016; Neumüller et al., 2011; Zeng et al., 2015). It became apparent that CENP-C was a hit in both male, female and neural stem cells. Significantly, CENP-C was 1 of 42 hits common between these screens suggesting a possibly non-canonical role for CENP-C outside of its expected function in kinetochore assembly. Thus, given that epigenetic differences are proposed to direct ACD in adult stem cells (Lansdorp, 2007; Lansdorp et al., 2012), we reasoned CENP-C an important candidate to investigate in this context.

In this chapter, we elaborate on the impact CENP-C has on GSC maintenance and differentiation over time. Moreover, we characterise the inheritance of CID^{CENP-A} in the germline alone and in response to CENP-C depletion. We uncover the following findings:

1. CENP-C is required for long term GSC maintenance.
2. CID^{CENP-A} level decreases in GSCs with age; reduced CENP-C accelerates this reduction.
3. CID^{CENP-A} level and inheritance changes from GSC to germ cell cyst stages.

4.2 CENP-C regulates GSC proliferation and long term GSC maintenance.

In the female germline screen (Yan et al., 2014), CENP-C RNAi was characterised as being 'agametic/GSC loss/complex phenotype (differentiation defect and many empty ovaries)'. Hence, we sought to replicate and further characterise these phenotypes in more detail. To do this, we used the same respective transgenic responder and driver lines (*UAS-RNAi-CENP-C* (VALIUM22), *UAS-Dcr2;nanos-GAL4*). Given the temperature sensitive nature of the GAL4-UAS system, we firstly performed strong knockdowns of CENP-C (unquantifiable) at 29 ºC and then 25 ºC. Dissecting the progeny of these crosses at 3 days old, it became apparent that these knockdowns were too severe to induce a workable phenotype and were agametic. This result is unsurprising given that CENP-C is essential. Thus, we reduced the temperature of the knockdown to allow tissue development and phenotype analyses, settling on 22 ºC. Here, we dissected ovaries at 5 days old and observed an array of germ cell phenotypes resulting from a 63% knockdown of CENP-C (Fig 3.2 and 3.5). This gave us a system to fully characterise these phenotypes and understand the effects that aberrant centromere assembly and asymmetry has on GSC maintenance at a tissue level.

To probe the role of CENP-C in GSC proliferation or maintenance, control and knockdown ovaries were stained with 1B1 (to mark the spectrosome/fusome) and the germ cell marker VASA. Together, VASA and 1B1 staining of *nanos-GAL4* controls displayed that germaria contained the expected GSCs and germ cell content, in line with previous studies (Dattoli et al., 2020). In contrast, CENP-C-depleted germaria revealed a spectrum of GSC-related phenotypes (Fig 4.1 A-D). Quantitation of the frequency of these phenotypes (Fig 4.1 E) revealed that almost 1/3 of germaria (35%) displayed normal germarium development, comparable with the control. However, another approximately 1/3 of germaria (32%) displayed an accumulation of germs cells, combined with an increase in the number of round spectrosomes. This is indicative of a classical, so-called, GSC 'tumour' or GSC overproliferation phenotype (Casanueva and Ferguson, 2004) [Note: whether these cells are actually a transformed cancerous 'tumour' or just hyperplasia is untested].

The final third (29%) displayed an accumulation of GSCs and CBs in the niche, broken away/separated from 2-, 4- and 8 cell cysts (2cc, 4cc, 8cc). Here, these germ cell cysts were missing, indicating a failure of differentiation (Fig 4.1 C; differentiation defect). Lastly, a small proportion of germaria were lacking any GSCs (4%) (Fig 4.1 D; GSC loss). We proceeded to analyse these phenotypes after 10 days, to determine whether these phenotypes progressed further. Indeed, analysis at 10 days old revealed an augmentation of the GSC loss phenotype (21%) (Fig 4.1 E). These results suggest that CENP-C is required to regulate both GSC proliferation in the germarium, and that longer term depletion of CENP-C (10 days) leads to a loss of GSCs in the niche. Significantly, overexpression of HA-CENP-C alone did not result in differentiation defect or GSC loss phenotypes (not shown). Furthermore, HA-CENP-C overexpression rescued the differentiation defect and GSC loss phenotypes at 5 days old, when expressed in conjunction with the CENP-C shRNA (Normal Germaria = 71%; GSC Tumour = 28%; Differentiation Defect = 0%; GSC Loss = <1%) (Fig 4.1 E). Hence, CENP-C is required GSC proliferation, as well as the long term maintenance of the GSC population.

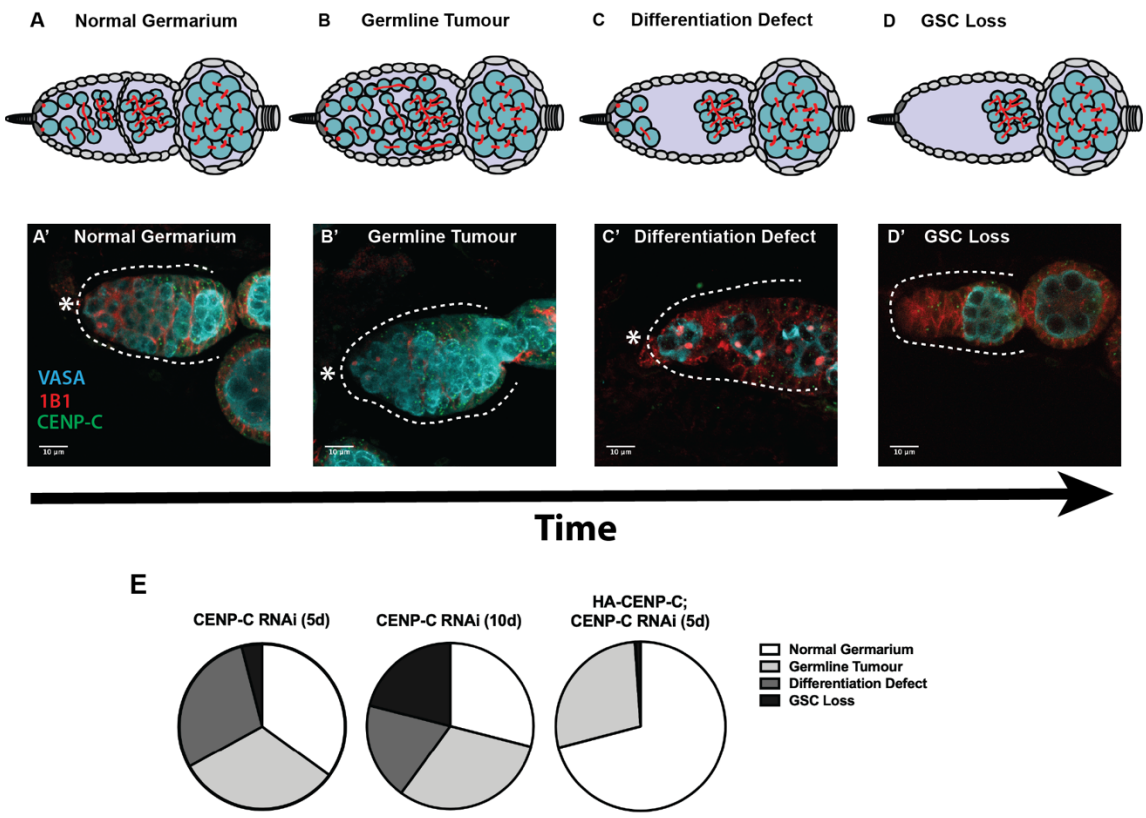

Figure 4.1: CENP-C depletion disrupts GSC maintenance and differentiation over time. (A-D) Characterisation of the phenotypes arising in CENP-C depleted germaria. (A, A') Normal germarium are healthy with a normal lineage of germ cysts and spectrosome/fusome development. (B, B') Germline tumours are characterised by an increased number of germ cells (GSCs, CBs, cysts) in the germaria, often displaced from their normal position with abnormal spectrosome/fusome morphology. (C, C') The differentiation defect is characterised by a pool of GSCs/CBs in the apical end of the germaria, separated from later stage developing cysts. (D, D') GSC loss is characterised by the absence of GSCs (and often CBs and early germ cysts) at the apical end of the germarium. *=cap cells. Scale bar=10 μm. (E) Quantitation of the frequency of the above phenotypes observed at 5 days and 10 days post-eclosion, and in rescue HA-CENP-C; CENP-C RNAi (5 day). Charts each represent 3 biological replicates (50 germaria analysed per replicate).

4.3 CID^{CENP-A} level reduces in GSCs with age, and CENP-C depletion accelerates its loss

Given that *wild type* GSCs retain 1.2-fold more CID^{CENP-A} in an asymmetric division, and that a small frequency of symmetric GSC divisions are known to occur over time, we hypothesised that CID^{CENP-A} and CENP-C levels would gradually be depleted in GSCs over time. We investigated this hypothesis in *wild type OregonR* GSCs at G_2/prophase. Here, we designed a long-term culture assay using *OregonR* females, dissecting ovaries at 5, 10 and 20 days post-eclosion. Here, we stained with DAPI and 1B1 to mark GSCs in G_2/prophase. To measure both CID^{CENP-A} and CENP-C levels, we split each timepoint into two batches, staining for CID^{CENP-A} and CENP-C separately. Doing this, all timepoints would be comparable and from the same replicates. Here, we saw a significant 45% decrease in CID^{CENP-A} levels between 5- and 20-day timepoints ($OregonR_{5\text{-}day}$=28.73±1.72, n=28 cells; $OregonR_{10\text{-}day}$=20.62±1.29, n=30 cells; $OregonR_{20\text{-}day}$=16.22±0.97, n=30 cells). Similarly, CENP-C reduced at a comparable rate at each timepoint ($OregonR_{5\text{-}day}$=28.22±1.35, n=28 cells; $OregonR_{10\text{-}day}$=19.46±1.23, n=29 cells; $OregonR_{20\text{-}day}$=15.44±1.11, n=29 cells). Hence, CID^{CENP-A} and CENP-C levels in GSCs reduce in correlation with GSC age. Thus, it is probable that this reduction in CID^{CENP-A} falls in line with a frequency of symmetric divisions (and in turn symmetric CID^{CENP-A} distribution), which reduce centromere levels over time.

We next wanted to determine whether CID^{CENP-A} levels correlated with GSC proliferative capacity over time, and if loss of CENP-C accelerated this loss of CID^{CENP-A}. Here, we quantified 5- and 10- day old germaria in both *nanos-GAL4* and CENP-C RNAi GSCs at G_2/prophase (indicated by a round spectrosome). In the CENP-C RNAi, we quantified normal/GSC tumour phenotypes at 5 days old (Fig 4.2 C). At 10 days, we specifically quantified germaria displaying the 'differentiation defect' phenotype, under the assumption CID^{CENP-A} level may be at its lowest, but still quantifiable, at this point (Fig 4.2 D). In our controls, we saw a reduction in total CID^{CENP-A} signal in the *nanos-GAL4* GSCs between 5- and 10-days old (*nanos-GAL4*$_{5\text{-}day}$=31.46±1.80, n=29 cells; *nanos-GAL4*$_{10\text{-}}$

$_{day}$=24.50±1.19, n=32 cells), comparable with *wild type* observations (Fig 4.3 A, B and E). Indeed, when we analysed CENP-C-depleted GSCs at 5- and 10- days old, we found that CID^{CENP-A} was reduced (CENP-C $RNAi_{5\text{-}day}$=20.21±1.40, n=33 cells; CENP-C $RNAi_{10\text{-}day}$=14.62±1.41, n=28 cells). Firstly, at 5 days old, we saw an expected ~30% decrease in CID^{CENP-A} level compared to G_2/prophase levels in the *nanos-GAL4* line (per results in Chapter 3, Fig 3.3). At 10 days old, CID^{CENP-A} level decreased further. Interestingly, the percentage decrease in CID between control 5- and 10- day old GSCs (19%) was amplified further upon knockdown of CENP-C, increasing to 28%. This further supports a role for CENP-C in CID^{CENP-A} maintenance as outlined in Chapter 3.

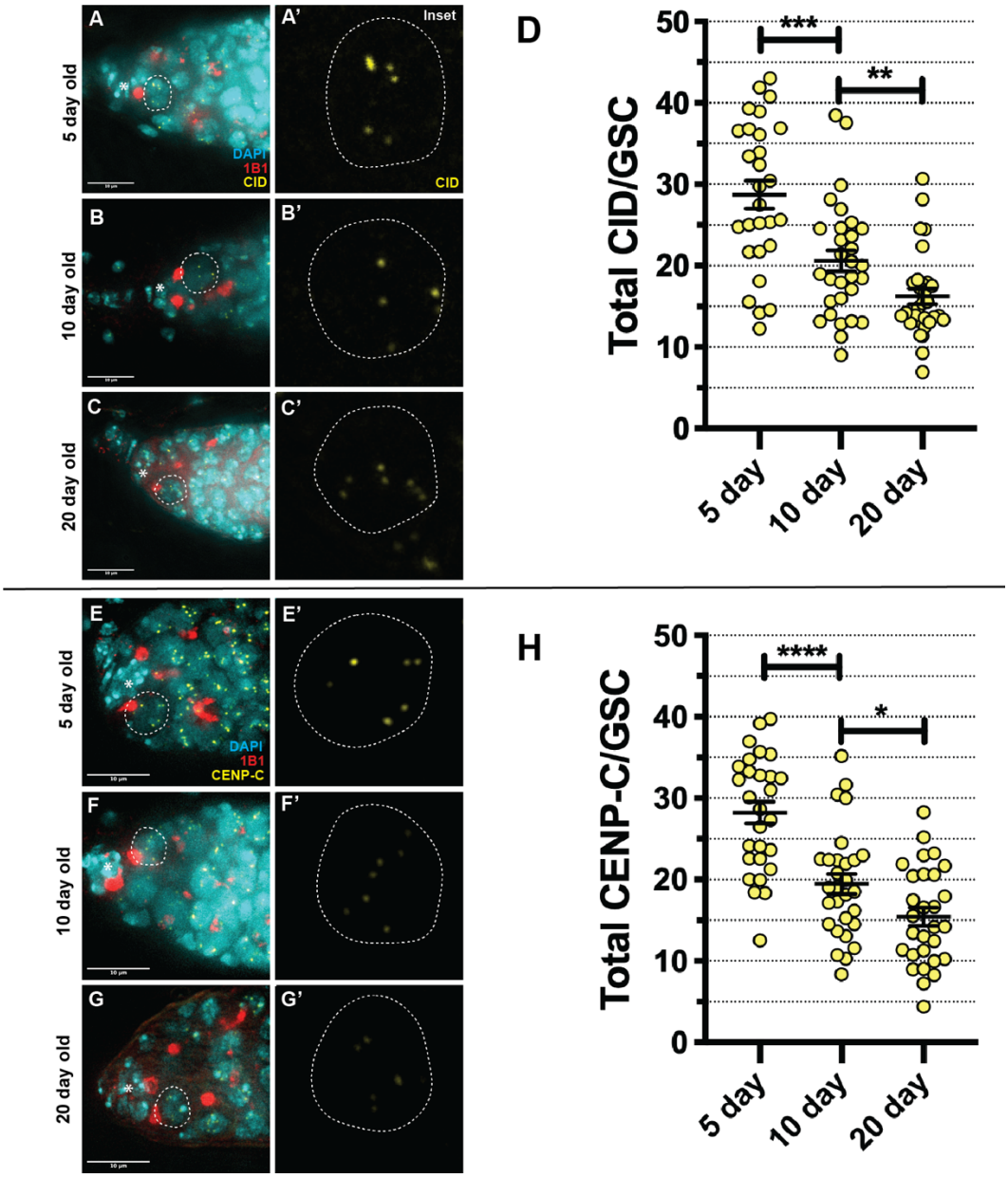

Figure 4.2: CID^{CENP-A} and CENP-C levels are depleted with GSC age. (A-C) Germaria of *wild type* (5-, 10- and 20-day old) stained with 1B1 (red), DAPI (cyan) and CID^{CENP-A} (yellow). GSCs are boxed and inset. * = cap cells. Scale bar = 10 μm. (D) Quantitation of total CID^{CENP-A} integrated density per GSC in *wild type* GSCs at 5, 10 and 20 days post eclosion. (E-G) Germaria of *wild type* (5-, 10- and 20-day old) stained with 1B1 (red), DAPI (cyan) and CENP-C (yellow). GSCs are boxed and inset. * = cap cells. Scale bar = 10 μm. (D) Quantitation of total CENP-C integrated density per GSC in *wild type* GSCs at 5, 10 and 20 days post eclosion. *p<0.05, **p<0.01, ***p<0.001, ****p<0.0001. Error bars = SEM.

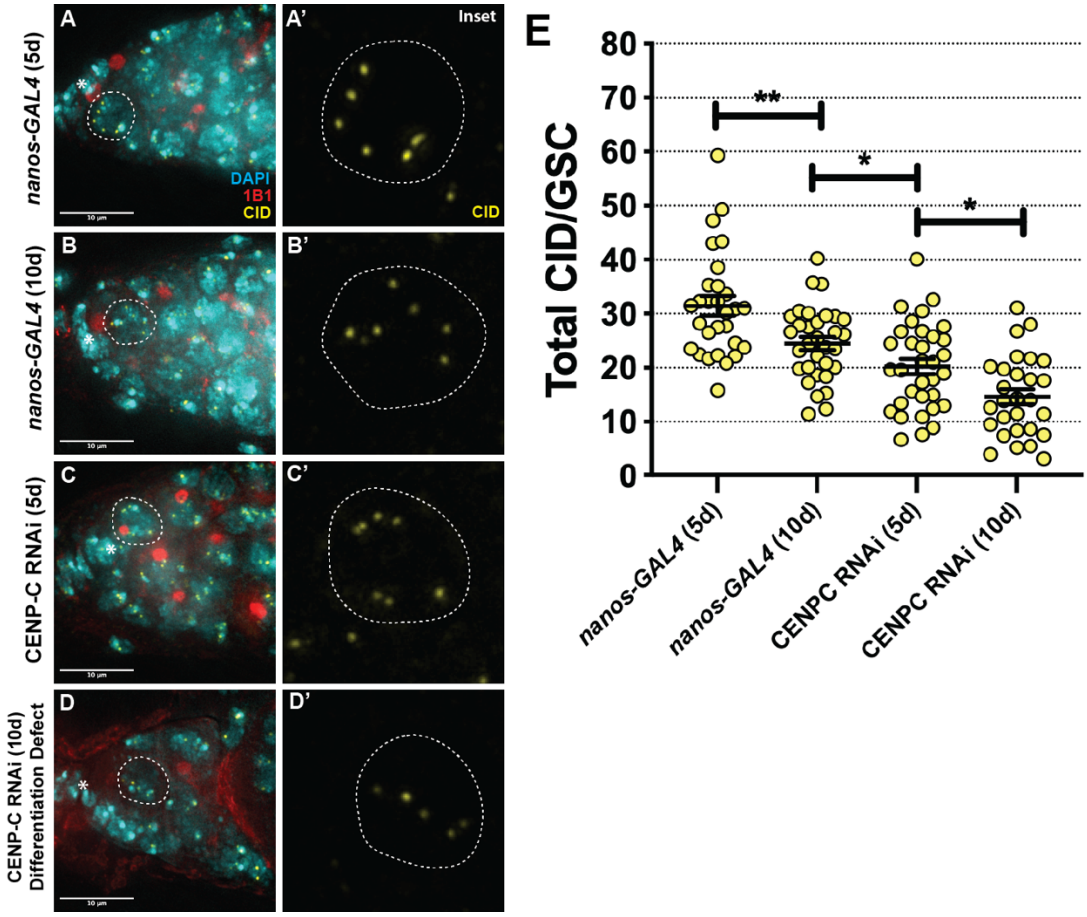

Figure 4.3: CID^{CENP-A} levels correlate with long-term disruption to GSC maintenance. (A-D) Germaria of *nanos-GAL4* (5d), *nanos-GAL4* (10d), CENP-C RNAi (5d) and CENP-C RNAi (10d, Differentiation Defect phenotype) stained with 1B1 (red), DAPI (cyan) and CID^{CENP-A} (yellow). GSCs are boxed and inset. * = cap cells. Scale bar = 10 μm. (E) Quantitation of total CID^{CENP-A} integrated density per GSC in *nanos-GAL4* (5d), *nanos-GAL4* (10d), CENP-C RNAi (5d) and CENP-C RNAi (10d, Differentiation Defect phenotype). *p<0.05, **p<0.01. Error bars = SEM.

4.4 CENP-C-depleted germ cells accumulate in S-phase, but not in mitosis.

Given CENP-C's essential role in kinetochore function in mitosis, we wished to determine whether CENP-C depleted GSCs were blocked in the cell cycle. We first assayed whether these germ cells were blocked in mitosis using an antibody against the well-known histone post-translational modification, phosphorylation at serine 10 of histone H3 (H3S10P), to mark cells in late G_2-phase to metaphase. Here, CENP-C depleted germaria displaying GSC tumour phenotypes were largely negative for H3S10P (Fig 4.4 A-H). H3S10P in combination with DAPI staining (marking DNA) allowed us to assess cells for chromosome segregation defects, which were also absent (data not shown). This suggests that the extent of CENP-C (63% reduction) does not result in mitotic arrest nor in chromosome segregation defects. Thus, this indicates that the canonical kinetochore function of CENP-C maintained sufficiently.

Mitotic delay or arrest would not necessarily explain the observed cell proliferation phenotype. To analyse interphase, we then used a 45 min incorporation of 5-ethynyl-2′-deoxyuridine (EdU), followed by fixation, to label cells with/without newly replicated DNA within this time period. Strikingly, we noticed that EdU cells were more abundant in CENP-C-depleted germaria (Fig 4.5 A-H). Given that all germ cells within each individual cyst replicate synchronously, we quantified this measuring the number of EdU-positive germ cysts (GSC/CB pairs, 2-, 4- and 8cc) present in the germarium (normal and GSC tumour phenotypes) at any one time. Quantitation showed that between 0-3 EdU positive cysts were present in *nanos-GAL4* germaria (median of 1), with this number increasing in the CENP-C RNAi (min/max 0-4, median of 2) (Fig 4.4 I). Hence, on average one extra germ cell cyst was in replication in each germarium upon CENP-C depletion. This suggests that cysts in the CENP-C RNAi progress slower through DNA replication in S-phase, perhaps contributing to the observed accumulation of germ cells in GSC tumours.

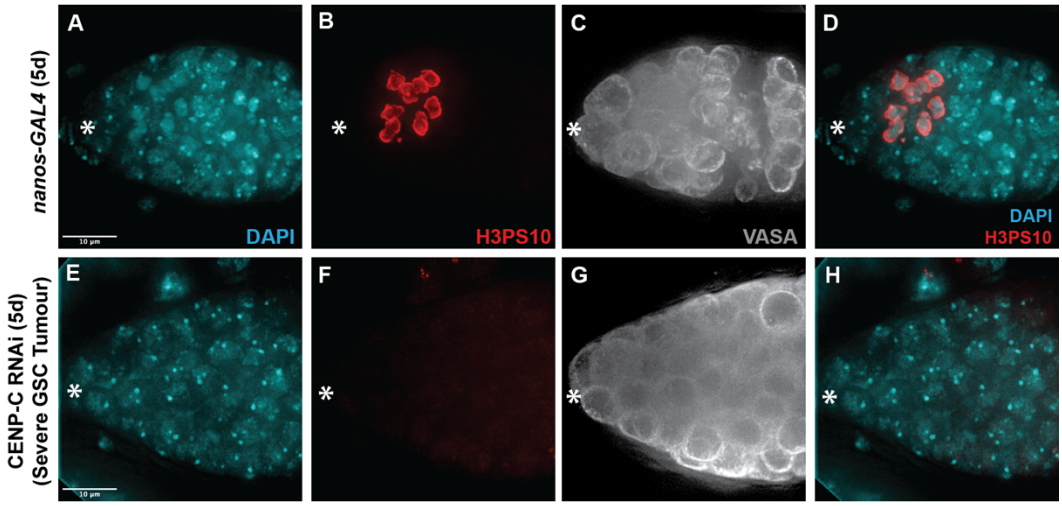

Figure 4.4: GSCs with reduced CENP-C continue to proliferate and are not arrested in mitosis. *nanos-GAL4* (A-D) versus CENP-C RNAi (E-H, germline tumour phenotype) stained with DAPI (cyan), VASA (grey) and H3S10P (red). * = cap cells. Scale bar = 10 µm.

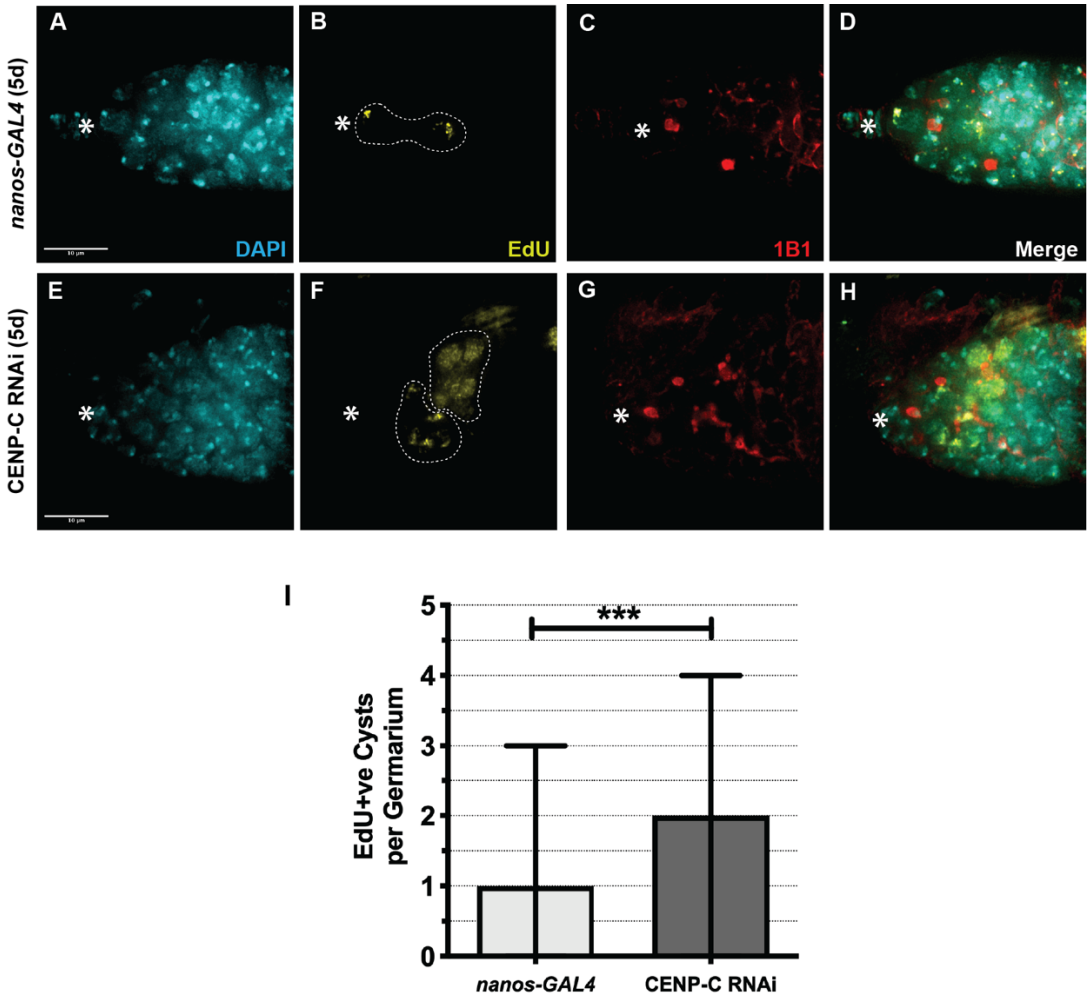

Figure 4.5: A higher frequency of S-phase cells are present in CENP-C-depleted germ cells. *nanos-GAL4* (A-D) versus CENP-C RNAi (E-H) stained with DAPI (cyan), EdU (yellow) and 1B1 (red). * = cap cells. Scale bar = 10 μm. (I) Quantitation of the number of EdU positive cysts per germarium. Graph represents the median ± Max/Min. One positive hit was quantified as a single EdU-positive GSC/CB, 2cc, 4cc or 8cc. ***p<0.0001.

4.5 CENP-C function in CID^{CENP-A} assembly/asymmetry in GSCs is distinct from its requirement outside of the niche.

Lastly, we wished to confirm the specificity of the role of CENP-C in GSCs versus its general function in (germ) cell division. To do this, we knocked down CENP-C using the germ cyst specific *bam-GAL4* driver, active in the 4-8 cell cysts. This allows us to separate the causality of the phenotypes we are seeing in the *nanos-GAL4* driven CENP-C knockdown versus general germ cell phenotypes. Indeed, when we incubated the cross at 29 ºC, we observed a strong CENP-C depletion in 4- and 8- cell cysts (Fig 4.6 B, B'). This result was reported in Dattoli *et al* as an internal control for *bam-GAL4* activity in conjunction with a CAL1 RNAi (Fig S5 S). However, we did not see any accumulation of germ cells or other phenotype associated with germ cell development/oogenesis when stained with DAPI and 1B1 (Fig 4.6 A-D'). This is distinct from the phenotypes we observed in the *nanos-GAL4* driven CENP-C RNAi (Fig 4.1 A-D) and suggests that CENP-C requirement in GSCs versus germ cells is unique.

Next, we wished to determine whether CID^{CENP-A} level is reduced in cyst cells (where *bam* is expressed) in response to depleted CENP-C. Surprisingly, CID^{CENP-A} level remained visibly normal in response to strong CENP-C depletion (Fig 4.7 B, B'). This stands in stark contrast to *nanos-GAL4*-driven RNAi, where we see a 37% reduction of CID^{CENP-A} and substantial phenotype penetrance. These findings are comparable with now published observations for CID^{CENP-A}, where *bam-GAL4*-driven CID^{CENP-A} RNAi remarkably did not diminish CID^{CENP-A} levels. Interestingly though, CAL1 knockdown at the BAM-stage did result in a minor decrease in CID^{CENP-A} level, yet no impact on germ cell division at this stage. This suggests that CID^{CENP-A} is very stable at this point in development, possibly due to impending meiosis I division. Taken together, these results support the idea that in addition to CAL1, CENP-C function in centromere assembly and maintenance in GSCs is critical and appears to be dispensable for later divisions occurring the germarium.

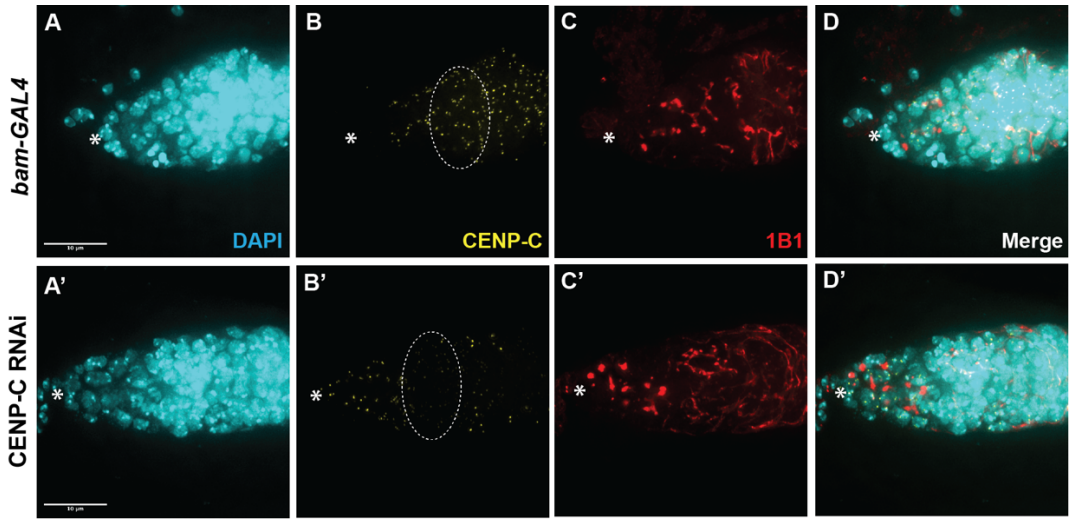

Figure 4.6: *bam-GAL4* driven CENP-C RNAi does not affect germline development. *bam-GAL4* (A-D) versus CENP-C RNAi (A'-D') stained with DAPI (cyan), CENP-C (yellow) and 1B1 (red). Circle marks region where *bam* is expressed and the knockdown begins. * = cap cells. Scale bar = 10 μm. This data is published in Fig S5 S of Dattoli *et al*, 2020.

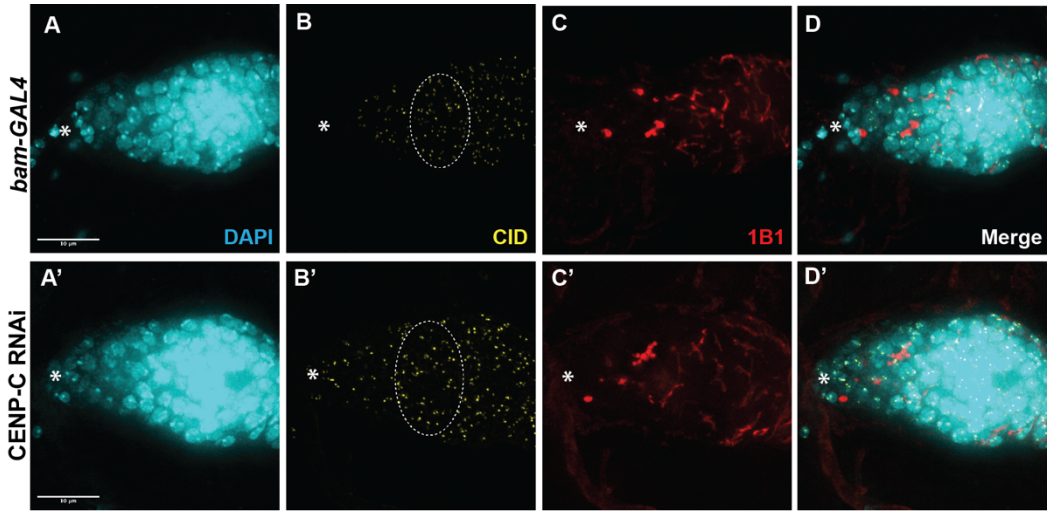

Figure 4.7: *bam-GAL4*-driven CENP-C RNAi does reduce CID levels in GSC cysts. *bam-GAL4* (A-D) versus CENP-C RNAi (A'-D') stained with DAPI (cyan), CID^{CENP-A} (yellow) and 1B1 (red). Circle marks region where *bam* is expressed and the knockdown begins. * = cap cells. Scale bar = 10 μm.

4.6 CID assembly dynamics differ between GSCs and cysts

Centromeres are known to have different assembly timings and amounts depending on cell function. In order to gain a better understanding on the dynamics of CID assembly in the germaria as a whole, we measured CID^{CENP-A} levels between GSCs and differentiated 8-cell cyst (8cc). To do this, we again used H3S10P as a marker of prophase in both GSCs and 8cc. Due to the synchronicity of these germ cyst cell cycles, 8ccs were identified as a cluster of 8 germ cells in the mid germarium which all contain H3S10P staining at prophase (Fig 4.8 A-F'). When staining with CID^{CENP-A} antibody, we noticed that although centromeric CID^{CENP-A} was labelled, there was also a nuclear non-centromeric localisation of the antibody. As we did not observe this localisation in CID^{CENP-A} -GFP transgenic flies, it is likely these localisation is a result of a cross reactivity between anti-H3S10P and anti- CID^{CENP-A} antibodies. Therefore, our quantitation focussed on centromeric CID^{CENP-A} only, and background was removed using FIJI software. When comparing GSC nuclei with that of 8cc nuclei, the 8cc nuclei are visibly smaller. Quantitation revealed a ~40% diminishment in centromeric CID^{CENP-A} per nucleus in 8cc (8cc = 323.4 ± 20.94, n = 26 cells) versus GSCs at a similar cell cycle stage (GSC = 547.2 ± 41.57, n = 24 cells) (Fig 4.8 G). Fig 4.8 below is taken from Dattoli *et al* and represents Fig 7 A-G of the manuscript. This result indicates that a change in CID^{CENP-A} assembly dynamics occurs somewhere between GSC and 8cc, probably in the transition from asymmetric to symmetric divisions.

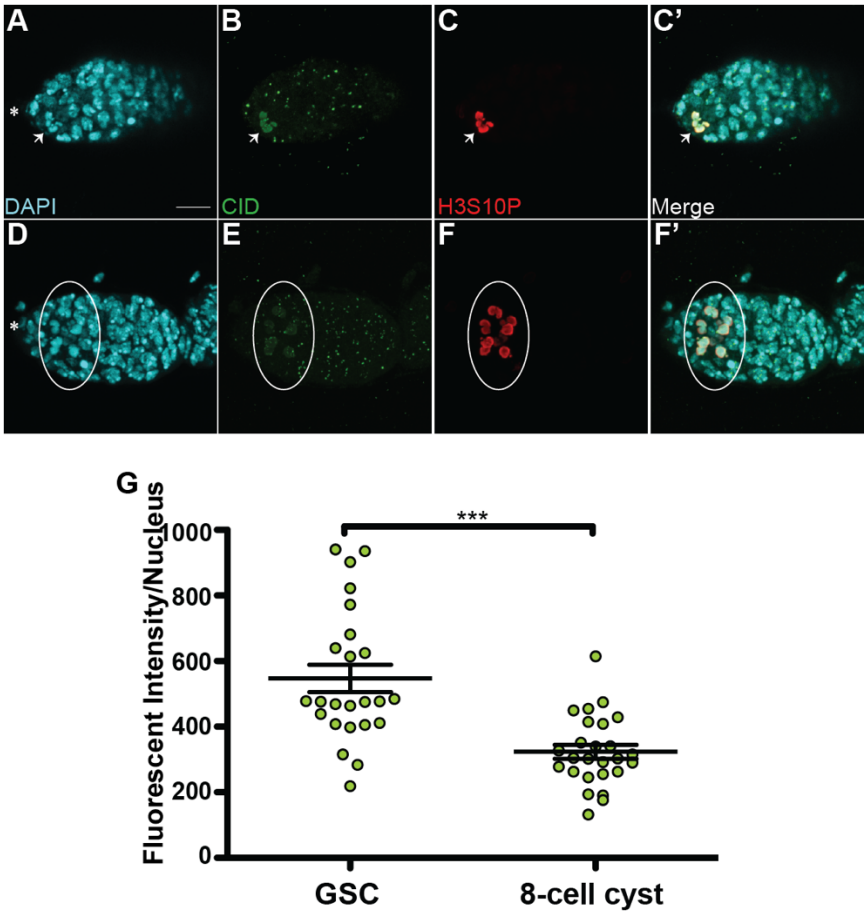

Figure 4.8: Cyst cells incorporate less CID^{CENP-A} compared with GSCs. (A–F′) Confocal z-stack projection of a *nanos-GAL4* germarium, stained for DAPI (cyan), anti- CID^{CENP-A} (green), and anti-H3S10P (red), to highlight a GSC (A–C′, arrow) and 8cc (D–F′, circle) in prophase. *=cap cells. Scale bar = 10 µm. (G) Quantification of CID fluorescence intensity (integrated density) at centromeres in GSCs and 8cc at prophase. Error bars = Standard Error of the Mean; ***p<0.001. This figure is published as Fig 7 A-G in Dattoli *et al*, 2020.

4.7 Chapter Summary and Discussion

A summary of the major findings presented in chapter 4:

1. CENP-C stimulates GSC proliferation and inhibits long term GSC maintenance.

2. Reduction in CENP-C leads to more germ cells in S-phase.

3. CID level in GSCs decreases with age, and CENP-C is required to regulate this reduction in CID^{CENP-A}.

4. CENP-C function in CID^{CENP-A} assembly and centromere asymmetry is possibly specific to GSCs and is not required at germ cell cyst stages.

5. CID^{CENP-A} assembly dynamics differ between GSCs and their downstream symmetrically dividing germ cell cysts.

4.7.1 CENP-C is required for long term GSC maintenance.

The data presented in Chapter 3 suggests that CENP-C is required for the asymmetric distribution of CID between sister centromeres. In CENP-C depleted GSCs, CID is maintained at an even high level in the stem cell, compared to the daughter cell. Here, GSCs retain ~1.45 fold more CID^{CENP-A} compared to their daughter cells. Given these cells also lack robust CID assembly (Fig 3.3), one can deduce that parental CID^{CENP-A} is strongly maintained in GSCs with reduced CENP-C. Therefore, we wished to determine how these implications would affect GSC maintenance or differentiation at a tissue level. Surprisingly, we see an array of phenotypes associated with decreased and dysfunctional centromere assembly in the germline. Firstly, strong CENP-C depletion did not allow germ cell development, in line with what we previously observed for CID^{CENP-A}. In a similar way, CAL1 depletion in female GSCs resulted in no centromere specification and subsequently an inability to divide, leaving 1 or 2 GSCs residing in adult germaria

(Dattoli et al., 2020). Moreover, CAL1 knockdown in male GSCs resulted in a substantial loss of GSCs at 10 days (Ranjan et al., 2019). Given this, contrary to what one might have thought, depletion of CENP-C by 63% (and in turn CID^{CENP-A} ; ~37% depletion) and CAL1 (~41% depletion) did not block cell division, but instead allowed for aberrant cell proliferation in the germarium. These GSC tumours are classically measured by increased GSC-like cells displaying round spectrosomes, and are often displaced from their normal GSC niche (Casanueva and Ferguson, 2004). Significantly, these cells appeared to have no mitotic defects or chromosome segregation errors at this point. This may not be surprising either as it has been previously shown that Hela cells can tolerate levels of CENP-A as low as 10% (Liu et al., 2006). However, it became apparent upon EdU incorporation that a larger proportion of cysts than normal were in S-phase, suggesting a delay in DNA replication. Indeed, CENP-C has been implicated in DNA replication previously, having been shown to be stable at S-phase centromeres (Hemmerich et al., 2008). Moreover, recent work from the Cleveland lab propose an error-correction mechanism for CENP-C in protecting centromeric CENP-A, while CENP-A on chromosome arms gets removed (Nechemia-Arbely et al., 2019). It is tempting to speculate how CENP-C may be acting across S-phase in an asymmetric system where CID^{CENP-A} has not yet been assembled.

Interestingly, we also observed a failure in differentiation at 5- and 10- days old. This suggests that there is a threshold of CID^{CENP-A} required in order to induce differentiation. This has been observed in iPSCs previously, where reduced CENP-A only allowed self-renewal (Ambartsumyan et al., 2010). Moreover, recent work from the Jansen lab have determined that inducing pluripotency results in a depletion of centromeric chromatin from iPSCs (Milagre et al., 2020), further emphasising the fact that CENP-A assembly is important for differentiation (and indeed proliferation in general). Lastly, we see GSC loss phenotypes that become more penetrant with age. This lines up with what has been observed for CAL1 RNAi in males (discussed above).

4.7.2 CID^{CENP-A} levels in GSCs decrease with age, and CENP-C accelerates this loss.

We determined that GSCs gradually deplete their centromere levels over time between 5-20 days old *wild type* germaria. Over a 15 day period, these levels reduce by approximately 45%. Assuming that symmetric GSC divisions harbour symmetric CID distribution between sister centromeres, this offers a good explanation for how and why CID^{CENP-A} /CENP-C levels would be gradually lost. Thus, this raises the possibility that adult stem cells display 'epigenetic age' at the level of the centromere, and this in turn may limit the proliferative lifespan of a stem cell. Indeed, epigenetic aging is a characteristic of adult stem cells, and has been previously characterised for numerous post-translational modifications (methylation, deacetylation) related to chromatin structure (Chen and Kerr, 2019; Ermolaeva et al., 2018), but never related to the centromere. To analyse the effect that CENP-C has on maintaining CID^{CENP-A} levels and proliferative capacity over time, we took 5 day old germaria displaying 'normal/germline tumours' and compared them to 10 day old 'differentiation defect' germaria. Indeed, we saw a significant reduction in CID^{CENP-A} level when compare to *nanos-GAL4* controls. Moreover, we saw a widening of this reduction in CENP-C RNAi 5 days versus 10 days. Thus, CENP-C loss accelerates this loss of CID^{CENP-A} between 5 and 10 days old. Over the life of the stem cell, CENP-C may well be directing how much CID^{CENP-A} gets inherited through mechanisms yet unknown.

4.7.3 CID inheritance changes from GSCs to germ cell cysts.

Centromeres adapt their centromeric levels and assembly timing for function in germ cells (Das et al., 2020; Dunleavy and Collins, 2017). We hypothesise that different cell states (e.g. quiescence, cycling) and cell divisions (mitosis, meiosis, ACD, SCD) all require differences in centromere mechanics in order function. CID is assembled in G_2/prophase in GSCs, and this GSC divides asymmetrically (Dattoli et al., 2020; Ranjan et al., 2019). Therefore, asymmetry in CID^{CENP-A} directs the inheritance of sister chromatids and in turn the polarity of the GSC

division (Carty and Dunleavy, 2020; Wooten et al., 2019a). We determine here that CID^{CENP-A}, but not CENP-C, is stable and can be removed from the centromere at germ cell cysts downstream from the GSC. Here, following the next cell division to the 16cc stage, the oocyte will then enter meiosis I. Given that the CID^{CENP-A} is stable and resistant to both direct RNAi (targeting CID^{CENP-A}) and indirect RNAi (targeting CENP-C) (Dattoli et al., 2020), it is probable that the centromere (upon differentiation at BAM-stage) is largely stable ahead of the pending meiotic division. This would explain the dispensability of CAL1 and CENP-C at these stages. To examine how CID^{CENP-A} is inherited from GSC through 8cc, we analysed prophase GSCs (fully assembled GSCs) versus prophase 8cc cells. Surprisingly, we see a 40% reduction in total CENP-A per nucleus. Thus, 16-cell cysts may well inherit centromere proteins originally synthesised in GSCs and CBs. This reduction in CID^{CENP-A} levels could be contributed to two possibilities: 1) The rate of new CID loading is reduced after asymmetric division, and/or 2) both GSCs and CBs have asymmetric CID^{CENP-A}/CENP-C levels in their respective asymmetric divisions. The latter would explain how CID^{CENP-A} levels reduced by ∼40% could be achieved. Likely, this suggests that GSCs and their daughter CBs could behave similarly in their divisions. Here, two consecutive asymmetric divisions (GSC-CB, CB-2cc) losing ∼20% of CID^{CENP-A} in each division may help explain a ∼40% drop in total CID^{CENP-A} levels from GSC to 8cc. In parallel with our observations in Dattoli *et al* and this thesis, we observed no significant reduction in CID^{CENP-A} after CID^{CENP-A}, CAL1 or CENP-C RNAi at 8cc stage (Dattoli *et al* Fig 6 and S5; this thesis Fig 4.6 and 4.7). Taken together, these results highlight that CID^{CENP-A} is inherited from the GSCs, with little to no new loading occurring in the 4-8ccs.

5. Investigating the role of the centromere in cell fate in an asymmetrically-dividing system

5.1 Chapter Introduction

By their nature, adult stem cells divide asymmetrically to produce a self-renewing stem cell (which maintains the stem cell population in its niche) and a differentiating daughter cell. Here, we infer that during an asymmetric division, the biased inheritance of sister chromatids is correlated with specific cell fates. In the previous chapter, we outlined supporting evidence that asymmetrically dividing stem cells inherit differing amounts of CENP-A, and that this asymmetry is dependent on CENP-C. In 2010, centromeres were first associated with stem cell fate in iPSCs, when depletion of CENP-A limited iPSCs differentiation capacity, allowing only stem cell self-renewal (Ambartsumyan et al., 2010). This suggested that a certain CENP-A threshold needs to be met in order to initiate differentiation. Recently, efforts have been made to establish and clarify the role of centromeres in stem cell fate, particularly in *Drosophila* stem cell niches. In *Drosophila* ISCs, CID^{CENP-A}, CAL1 and CENP-C depletions unsurprisingly result in loss of proliferation potential (García del Arco et al., 2018), indicated by loss of clonal size and consistent with the essential nature of centromeres. Similarly in male and female GSCs, CAL1 depletion reduced stem cell number (males) and blocked stem cell proliferation capacity (females) due to lack of centromere specification (Dattoli et al., 2020; Ranjan et al., 2019). Thus, centromere integrity in the stem cell is clearly required for long term tissue functionality.

Separating the canonical mitotic roles of the centromere, versus its effect on self-renewal/differentiation in these systems remained challenging. Moreover, an robust assay to measure GSC self-renewal versus differentiation was lacking in literature. This chapter overcomes these barriers to characterise and assay the balance of GSC/CBs in the female GSC niche (now published in Dattoli *et al,* 2020), providing insight into the impact of centromere perturbation (both assembly and asymmetry) on stem cell fate. Here, we uncover the following findings:

1. GSC/CB composition can be reliably assayed using a combination of germline markers.
2. Disrupting the centromeric core impacts GSC fate, promoting self-renewal.

5.2 Establishing an assay to measure female *Drosophila* GSC self-renewal

One of the major challenges of basic stem cell research is the ability to consistently and accurately identify stem cells from progenitor and surrounding cells within their microenvironment. This is especially difficult in mammalian tissues (e.g. blood, epithelium). where stem cells have been classically identified by BrdU labelling. This makes assaying self-renewal versus differentiation challenging *in vivo*. In contrast, the *Drosophila* germline represents a powerful system to study stem cells at a single cell level within their own microenvironment. Moreover, numerous markers exist to mark GSCs, as well as other cells within the GSC niche and beyond (discussed in 1.5). Despite this, no published method existed in either the male or female germline to effectively analyse GSC self-renewal versus differentiation. To connect asymmetric centromeres with stem cell fate (per the silent sister hypothesis), we required a method of assaying GSC self-renewal. Hence, we set about establishing a method to reliably assay GSC self-renewal versus differentiation in different genetic backgrounds in the germarium.

The major signalling pathway in the majority of *Drosophila* stem cells is the Dpp pathway (Section 1.5), homologous to the human BMP2 pathway. *Dpp* is transcriptionally regulated by Mothers against Dpp (Mad; human homolog SMAD3) and its binding partner Medea (Med; human homolog SMAD4), acting directly on the *bam* promotor to silence *bam* (Song et al., 2004). Activated Mad requires phosphorylation, and is thus marked with an antibody against phosphorylated Mad (pMad) – the classical GSC marker. On its own, counting stem cells using pMad as a marker can be powerful. However, it became apparent that different genetic backgrounds contain different niche sizes and in turn different numbers of GSCs in the niche. Thus, counting GSC numbers without any relative measurement for CB numbers, or control of niche/germarium size can compromise analysis. To control for this, we sought to use a second marker in combination with pMad to assay the number of GSCs and their relative number of CBs within a single GSC niche. For this, we used an antibody against Sex-lethal (Sxl). Briefly, *Sxl* is the master sex determination gene in *Drosophila*, which controls sexual

development through mRNA splicing (Malik et al., 2020). Here, SXL regulates dosage compensation of X-linked genes in females by suppressing those hyperactivated X-linked genes. In the germarium, Sxl is active in GSCs, CBs and 2cc (Salz et al., 2017), and downregulates *nanos* to induce differentiation. Using antibodies against pMad and SXL one can gauge the balance of GSCs to CBs by expressing the number of SXL positive cells as a ratio to the number of pMad cells. In other words, dividing the total number of SXL cells by the total number of pMad-positive GSCs.

We dissected an array of 5-day old germaria from various control genetic backgrounds and stained for pMad, SXL and DAPI (Fig 5.1 A-C). We then counted the number of pMad positive cells (GSCs) and SXL positive cells (GSCs/CBs/2cc) in each germarium (Fig 5.1 D). Next, we expressed these values in a ratio of SXL/pMad (Fig 5.1 E). This gives us a value for the balance of GSCs versus CBs/2ccs i.e. how many daughter cells per single stem cell. We quantified three control lines *OregonR* (*wild-type*, 5d), RNAi isogenic control (5d) and *nanos-GAL4* (5d). In *OregonR* germaria, the number of pMad positive cells was approximately 1 (1.23 ± 0.07) and the number of SXL positive cells was approximately 5 (4.98± 0.18). For the RNAi isogenic control (36303), the number of pMad positive cells was approximately 3 (3.18 ± 0.10) and the number of SXL positive cells was approximately 13 (13.38± 0.45). In *nanos-GAL4* (5d), the number of pMad positive cells was approximately 2 (1.69 ± 0.10) and the number of SXL positive cells was approximately 6 (6.39± 0.27). In each case, the number of positive pMad and SXL cells differ substantially. However, upon analysing the ratio of SXL/pMad in each germaria, the average ratio remained similar across each genetic background, with approximately 4 SXL-positive cells for every 1 pMad-positive cell (*Oregon R* 4.35± 0.18; RNAi isogenic control 4.33± 0.16; *nanos-GAL4* 4.15± 0.21). Indeed, a ratio of 4 would be expected, given each GSC should have a corresponding daughter CB and 2-cell cyst from that lineage (4 cells total). Therefore, we successfully established an assay to measure the balance of GSC and CBs, and in turn GSC self-renewal, regardless of genetic background.

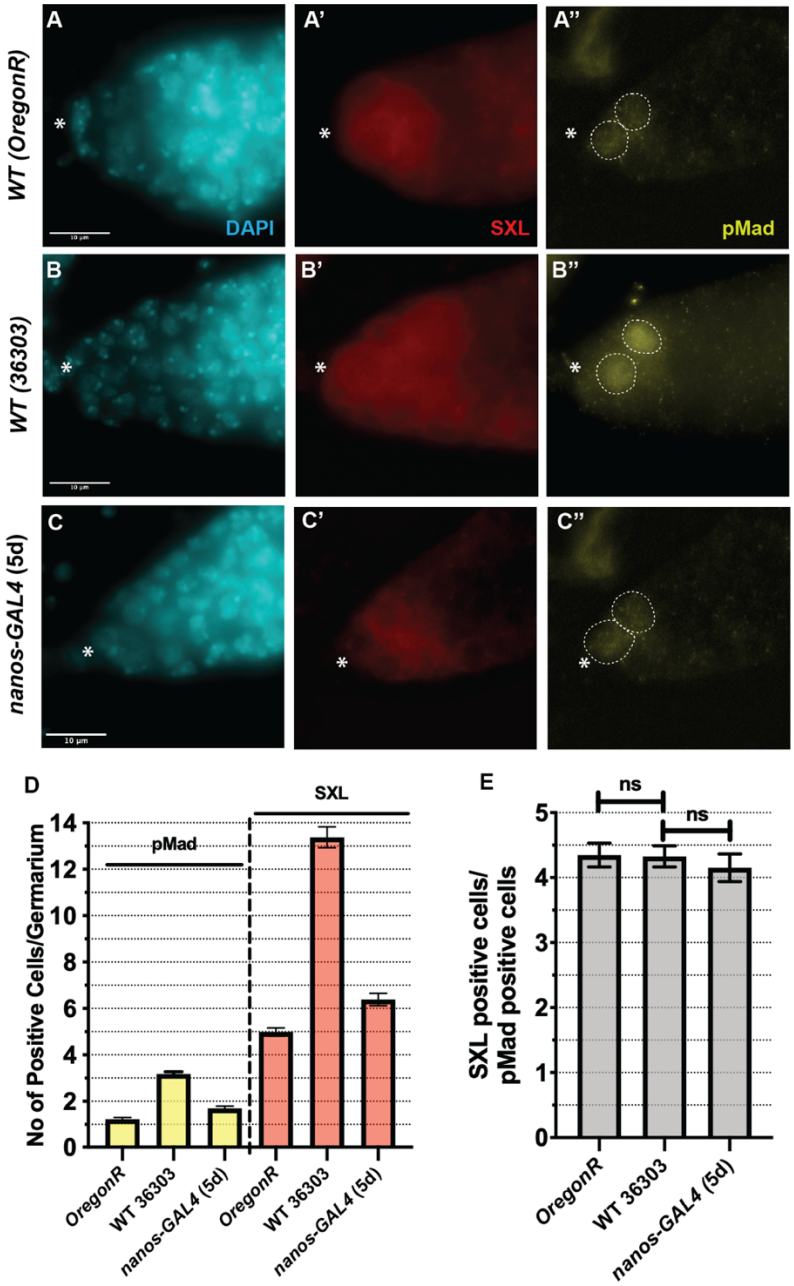

Figure 5.1: A method of characterising female GSC self-renewal versus differentiation. (A-C) Z-projections of *wild type* (*OregonR*), *wild type* (36303) and *nanos-GAL4* germaria stained with DAPI (cyan), Sex-Lethal (SXL, red) and pMad (yellow). To accurately count the number of positive cells, we scanned through all z-sections (0.5 µm z-depth) of each image. Scale bar = 10 µm. * = cap cells. Dashed line indicates pMad positive signal. (D) Quantitation of the number of pMad positive (left, yellow) and SXL positive (right, red) per germarium. (E) Quantitation expressed as a ratio of the number of SXL/pMad positive cells per germarium. ns = non-significant. Error bars = Standard error of the Mean (SEM).

5.3 Disruption to the centromeric core increases GSC self-renewal

Given we have now established a technique to assay GSC self-renewal, we next sought to understand whether disrupting the centromere by RNAi, overexpression or by mutant *Cenp-C/cal1* alleles affected GSC fate by promoting GSC self-renewal (reduction in SXL/pMad ratio) or differentiation (increase in SXL/pMad ratio). We first analysed CENP-C-depleted GSCs, already known to have defective CID assembly and increased CID^{CENP-A} asymmetry (Fig 5.2a/b). In control *nanos-GAL4* (5d) germaria, the number of pMad positive cells was approximately 2 (1.69 ± 0.10) and the number of SXL positive cells was approximately 5 (6.39 ± 0.27), with a SXL/pMad ratio of approximately 4 (4.15 ± 0.21). In CENP-C-depleted germaria (5d, normal and GSC tumour phenotypes), the number of pMad positive cells was approximately 3 (2.49 ± 0.13) and the number of SXL positive cells was approximately 5 (4.98± 0.18), with a ratio of 2.68 ± 0.17). Hence, the number of GSCs increased, yet the total number of daughter cells remained comparable. Thus, CENP-C depletion promotes GSC self-renewal. We then hypothesised that if the self-renewal rate was increased, over a number of cell divisions this ratio would reduce further. We therefore quantified CENP-C depleted germaria at 10 days post-eclosion (normal and GSC tumour phenotypes). Comparable with 5 days old, control *nanos-GAL4* at 10 days contained ~2 pMad positive cells (1.69 ± 0.10) and ~6 SXL cells (5.62 ± 0.24), with a slightly reduced, but non-significant, ratio of 3.69. However at 10 days old, in CENP-C depleted germaria the SXL/pMad ratio was reduced to ~2, primarily through a reduction in SXL positive cells (4.11 ± 0.32). Therefore, depletion of CENP-C does indeed promote continued GSC self-renewal over time.

In contrast to CENP-C depletion in germaria, expression of HA-tagged CENP-C displayed no effect on self-renewal. Here, HA-CENP-C-induced germaria dissected at 5 days old showed approximately 2 pMad positive cells on average (2.33 ± 0.11) but ~8 SXL positive cells (8.09 ± 0.24). Thus, the SXL/pMad ratio here remained normal at ~4 (3.78 ± 0.19). Indeed, HA-CENP-C overexpression was sufficient to almost partially rescue the self-renewal phenotype of the CENP-C RNAi (3.58 ± 0.12). This suggests that how much CID^{CENP-A} and which

CID^{CENP-A} pool (parental versus new) is inherited between sister centromeres could be critical to GSCs directing cell fate decisions.

Lastly, we analysed two transheterozygous *Cenp-C/cal1* mutant lines (Fig 5.3). To do this, we exploited both *cenp-*C^{IR35}*/cal1*^{2K32} (Chapter 3, defective in CID^{CENP-A} asymmetry), as well as *cenp-*$C^{Z3\text{-}4375}$*/cal1*^{2K32} germaria to determine whether these lines were defective in GSC self-renewal. Briefly, *cenp-*$C^{Z3\text{-}4375}$ is a viable allele that contains a missense C-terminal mutation that has been shown to destabilise CID protein levels in the female germline (Unhavaithaya and Orr-Weaver, 2013). It was apparent that indeed both these mutant lines could disrupt canonical GSC differentiation, promoting self-renewal. Here, in *cenp-*C^{IR35}*/cal1*^{2K32}, the number pMad positive cells approximated to 3 (2.63 ± 0.12), with 7 SXL cells (6.65 ± 0.27). In *cenp-*$C^{Z3\text{-}4375}$*/cal1*^{2K32} germaria, the number pMad positive cells approximated to 3 (2.86 ± 0.15), with 8 SXL cells (7.56 ± 0.24). The SXL/pMad ratios for these transheterozygotes were both reduced relative to the normal ratio of ~4 (2.66 ± 0.12 and 2.96 ± 0.19 respectively).

Taken together, our results show that disruption to the centromeric core tends to promote GSC self-renewal. This suggests that how CID^{CENP-A} is inherited (parental versus new), and/or the amount of CID^{CENP-A} is distributed between sister centromeres could be critical to GSCs directing cell fate decisions. Given that CID^{CENP-A} assembly is functioning in both HA-CENP-C over-expression and *cenp-*C^{IR35}*/cal1*^{2K32} lines, it appears that CID^{CENP-A} assembly is not the major determinant of cell fate. Rather, cell fate (self-renewal versus differentiation) appears to be reliant on CID^{CENP-A} asymmetry between sister centromeres. In conjunction with CID^{CENP-A} asymmetry, the absolute CID^{CENP-A} level per GSC nucleus is also likely to be playing a key role in allowing differentiation to occur.

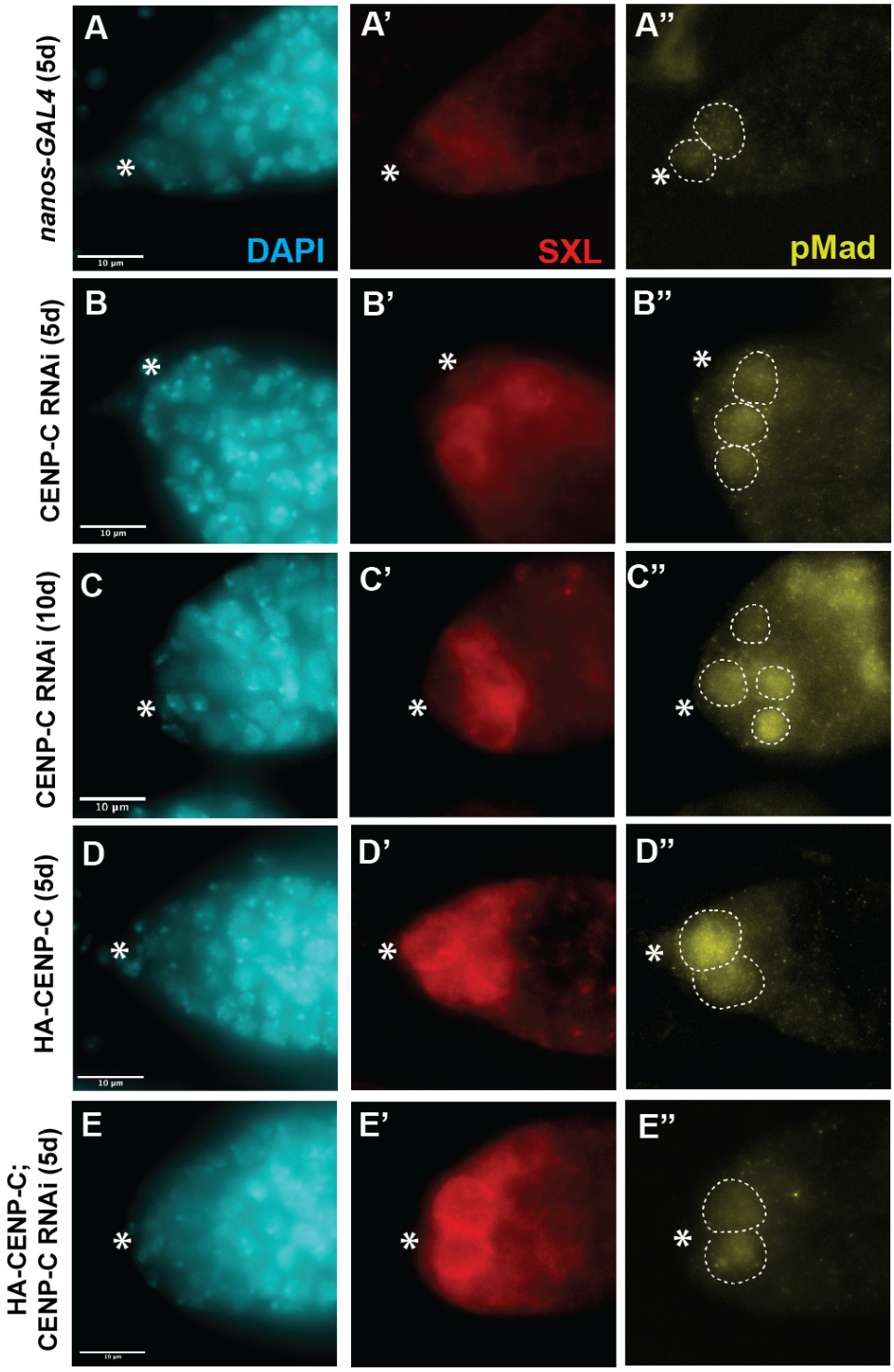

Figure 5.2a: Depletion of CENP-C in GSCs tends towards GSC self-renewal. (A-E) *nanos-GAL4*, CENPC RNAi (5 and 10d), HA-CENP-C, and HA-CENPC;CENPC RNAi (5d) rescue germaria stained with DAPI (cyan), Sex-Lethal (SXL, red) and pMad (yellow). Scale bar = 10 µm. * = cap cells. Dashed circle outlines pMad positive GSCs.

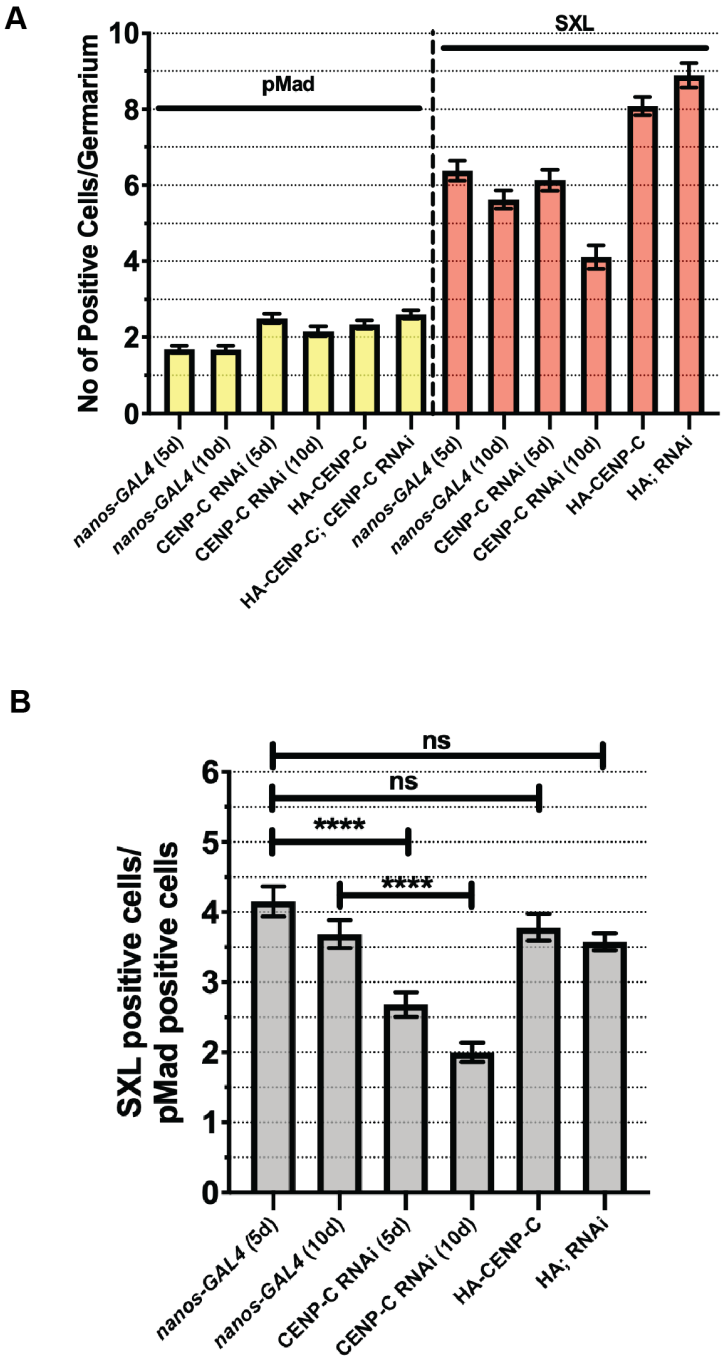

Figure 5.2b: Depletion of CENP-C in GSCs tends towards GSC self-renewal. (A) Quantitation of the number of pMad positive (left, yellow) and SXL positive (right, red) per germarium. (B) Quantitation expressed as a ratio of the number of SXL/pMad positive cells per germarium. **** $p<0.0001$. ns = non-significant. Error bars = Standard error of the Mean.

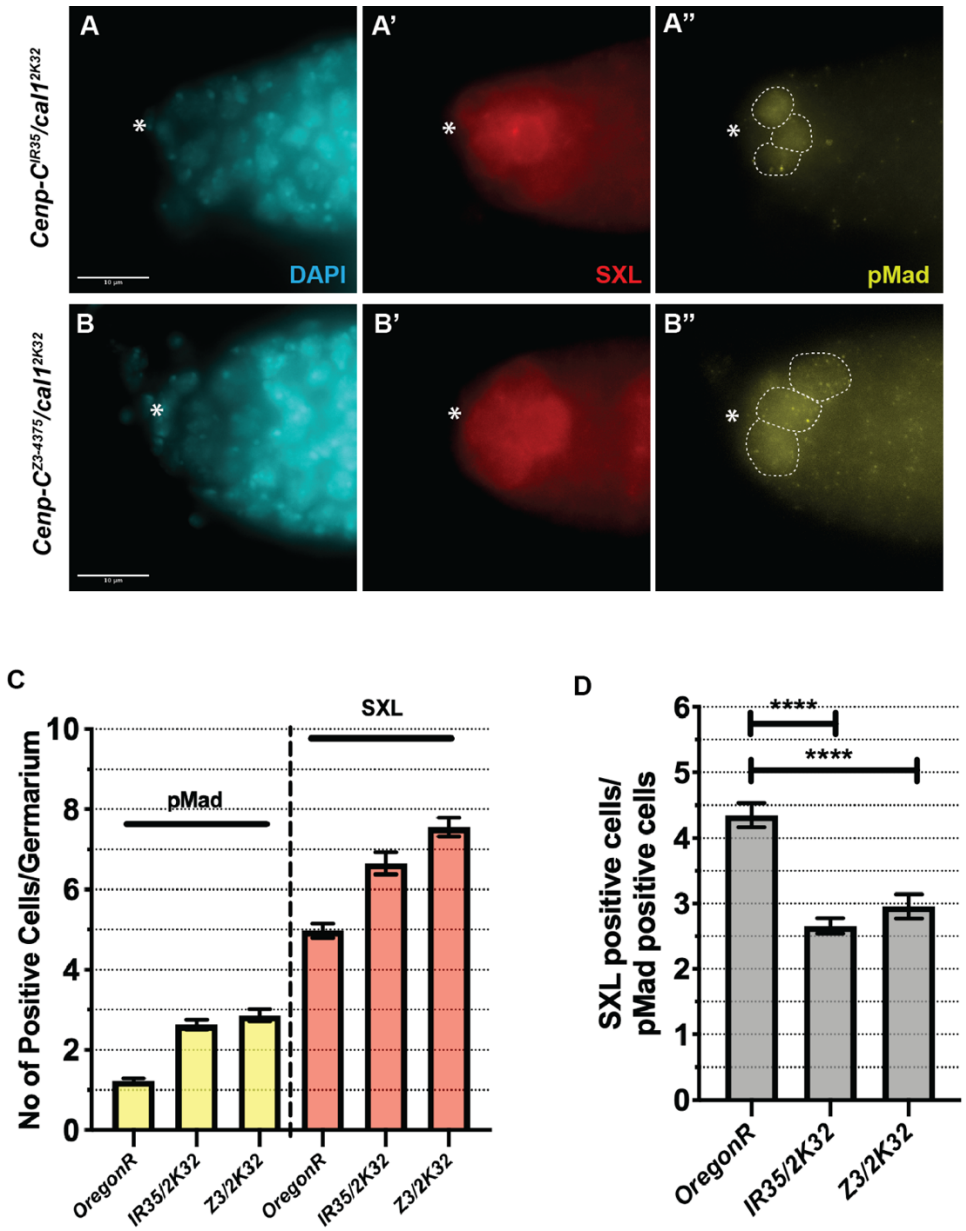

Figure 5.3: Transheterozygous *Cenp-C/cal1* germaria also disrupt the GSC/CB balance. (A and B) *cenp-C^{IR35}/cal1^{2K32}* (IR35/2K32) and *cenp-C$^{z3-4375}$/cal1^{2K32}* (Z3/2K32) germaria stained with DAPI (cyan), Sex-Lethal (SXL, red) and pMad (yellow). Scale bar = 10 µm. * = cap cells. (C) Quantitation of the number of pMad positive (left, yellow) and SXL positive (right, red) per germarium (D) Quantitation expressed as a ratio of the number of SXL/pMad positive cells per germarium. **** $p<0.0001$. Error bars = Standard error of the Mean.

5.4 Chapter Summary and Discussion

A summary of the major findings presented in chapter 4:

1) *Wild type* and RNAi control germaria contain different amounts of pMad positive (GSCs) and SXL positive (GSCs/CBs/2cc) cells. Using pMad alone therefore represents an invalid quantitation for assessing GSC self-renewal.

2) *Wild type* and control germaria can be reliably assayed for the balance of GSCs and CBs within their niche using a SXL/pMad ratio.

3) CENP-C depleted germaria (5d), as well as transheterozygous *cenp-C^{IR35}/cal1^{2K32} and cenp-C$^{z3-4375}$/cal1^{2K32}* germaria display reduced SXL/pMad ratios, implying a switch towards GSC self-renewal. CENP-C depleted germaria (10d) display an even further reduced SXL/pMad ratio.

4) HA-CENP-C overexpression has little to no effect on GSC self-renewal.

5.4.1 GSC self-renewal can be reliably assayed using a ratio of SXL/pMad.

Stem cells normally divide asymmetrically, producing a stem cell and differentiating daughter cell. To increase their population, stem cells can divide symmetrically to produce two daughter stem cells (SSC, self-renewal). Until now, no clear method of assaying self-renewal existed in *Drosophila*. The silent sister hypothesis proposes that epigenetic mechanisms might influence stem cell fate in an asymmetric division. Given we have disrupted the centromeric core in numerous ways (Chapter 3), we required a method to analyse the effect of these disruptions on GSC fate. Here, we present a reliable assay to measure the relative number of stem to daughter cells residing within the stem cell microenvironment.

In the literature, pMad is regularly used alone to measure the number of GSCs in both male and female GSC niches, as well as the midgut epithelium and neural stem cell niches. Surprisingly, we have found that in various common control genetic backgrounds, the number of GSCs (measured as pMad positive) can be different. Hence, this classical method of measuring possible GSC self-renewal has some reservations. To better analyse GSC self-renewal, there is a need for the relative measurement of stem to daughter cell number. We overcame this using a combination of pMad and SXL and calculating a ratio of the number of SXL/pMad. In the germarium, SXL marks the cytoplasm of GSCs, CBs and 2ccs (Salz et al., 2017). In each control genetic background analysed, we determined the relative number of pMad to SXL positive cells to be approximately 4. Hence, for every one stem cell, there is approximately 4 SXL cells (1 GSC, 1 CB and 1 2cc) or 3 daughter cells. This is regardless of the total number of stem and daughter cells in the germarium. Hence, we have characterised a reliable assay to measure the balance of GSCs to daughter cells within a germarium. Regrettably, this assay is specific to the female germline due to the female-specific nature of SXL expression. However, it represents a significant step forward to analysing stem cell fate over time.

We have since published this SXL/pMad assay in Dattoli *et al*. entitled 'Asymmetric assembly of centromeres epigenetically regulates stem cell fate', in the Journal of Cell Biology in 2020. Here, we were able to significantly increase the impact of the manuscript using this method. It allowed us to measure GSC self-renewal in three separate inducible germline overexpressions of $CID^{CENP\text{-}A}$-mCherry, CAL1-YFP;CID-mCherry and CAL1-YFP. Here, we determined that CID overexpression alone and CID/CAL1 double overexpression (but not CAL1 overexpression alone) resulted in a shift towards GSC self-renewal. Hence, we implicated the centromere (and $CID^{CENP\text{-}A}$ asymmetry) with stem cell fate (as per the manuscript title). This work is presented in Figures 5 A-L and N, and Fig 5S Q.

5.4.2 Disruption to the centromeric core promotes GSC self-renewal

We next sought to determine what effect disrupting the centromere (per Chapter 3) had on GSC fate. In Dattoli *et al*, we established that CID^{CENP-A} overexpression (both alone and in conjunction with CAL1) impacted GSC fate (trending SXL/pMad ratio towards ~2.5). Thus, we were interested in seeing what effect disruption to CENP-C would have on cell fate. In contrast to the CID^{CENP-A}/CAL1 overexpression, we found that HA-CENP-C overexpression at 25 °C does not affect cell fate. Although not studied here, it may be possible that cell fate would be impacted with a double overexpression with CID^{CENP-A} or CAL1. Nonetheless, we observed a trend towards self-renewal when we depleted CENP-C. Given that these GSCs are defective for CID^{CENP-A} assembly and contain an increased asymmetry in favour of the GSC centromeres, it is likely that increased retention of parental CID^{CENP-A} could be responsible for this self-renewal phenotype. Similarly, we investigated two transheterozygous lines containing mutant C-terminal alleles of *Cenp-C* and *cal1* (*cenp-C^{IR35}/cal1^{2K32}* and *cenp-C$^{\Delta 3\text{-}4375}$/cal1^{2K32}*). In both of these lines, the interaction of CENP-C and CAL1 is destabilised. In *cenp-C^{IR35}/cal1^{2K32}*, we know that CID assembly occurs as normal (possibly due to wild type CENP-C and CAL1 also being present), yet asymmetry is slightly increased in favour of the GSC (1.33 versus 1.20 expected). In both lines, GSC self-renewal is promoted, indicating that these GSCs favour self-renewal when the centromere is disrupted.

Overall, it is apparent that CENP-C could be required for organising the centromere in a manner that affects GSC fate. Particularly, the interaction between CENP-C and CAL1 is important for influencing cell fate. To further understand how this may occur, we would firstly need to understand when exactly in the cell cycle this asymmetry of CID^{CENP-A} gets established in the first place. How is parental CID inherited or maintained across S-phase? Is newly synthesised CID^{CENP-A} loaded asymmetrically across sister centromeres? At what timepoint in the cell cycle does CENP-C depletion impact sister centromere asymmetry? These questions require super resolution microscopy to resolve sister centromeres, as well as tools to distinguish old versus new CID^{CENP-A} pools e.g. CID^{CENP-A}-Dendra2 as utilised in (Ranjan et al., 2019). However, understanding these will unlock some

key epigenetic mechanisms as to how cell fate can be impacted in asymmetric systems.

6. Discussion

6.1 Stem cells epigenetically distinguish sister chromatids at the centromere

This thesis follows up some of the major findings published in Dattoli *et al* and Ranjan *et al*, bringing a mechanism to the epigenetic distinction of sister chromatids at the centromere in asymmetrically dividing stem cells. Centromeres are canonically symmetrical models of epigenetic inheritance. However, *Drosophila* stem cells have proven that certain cells are capable of intrinsically coordinating a quantitative asymmetric epigenetic inheritance pattern. Specifically, GSCs contain a 1.2 fold difference in $CID^{CENP\text{-}A}$ between sister centromeres at metaphase; and this difference is maintained up until centromere assembly in the following cell cycle (as measured in S-phase GSC/CB 'pairs') (Dattoli et al., 2020; Ranjan et al., 2019). Although epigenetic distinctions have been made previously in GSCs, i.e. the inheritance of parental versus newly synthesised histones H3-H4 (Tran et al., 2012; Wooten et al., 2019b); the centromere provides a most fundamental distinction, given its essential role in cell division. Indeed, it has been previously shown that parental $CID^{CENP\text{-}A}$ is also preferentially inherited, at least in male GSCs and ISCs (García del Arco et al., 2018; Ranjan et al., 2019). Yet, the centromere still maintains a quantitative difference between sister centromeres in these cells. This contributes towards the concept of 'mitotic drive' (Wooten et al., 2019a). A counterpart of meiotic drive (Lampson and Black, 2017), mitotic drive offers an explanation as to how the mitotic machinery coordinate in an asymmetrically-dividing stem cell. Ultimately, it is clear that understanding how the centromere coordinates itself in an asymmetric model provides an opportunity for centromere biologists to detail 'how' and 'what' drives the centromere machinery in a canonical cell division. Thus, this thesis seeks to understand the how and why centromeres can be distinguished in this manner.

6.2 CENP-C contributes towards mitotic drive by facilitating CID^{CENP-A} assembly, maintaining CID^{CENP-A} asymmetry and assembling a strong 'GSC-side' kinetochore.

Asymmetric division pertaining to adult stem cells requires directionality, dividing away from the stem cell microenvironment, or niche. This in turn requires the cell division to be coordinated by both cell polarity cues (e.g. centrosome asymmetry), and presumably asymmetry of the chromosomal mitotic machinery (e.g. the centromere/kinetochore and mitotic spindle?). Stem cells can use a strength differential between the two sister centromeres to retain particular sister chromatids, potentially relating to the expression of certain 'stem' genes (proposed by the silent sister hypothesis) (Lansdorp, 2007). The foundational strength at centromeric chromatin must be built upon to ultimately harbour this directionality through to the outer kinetochore and mitotic spindle. Indeed, we determined in chapter 3 that 1) CENP-C is assembled in G_2/prophase alongside the assembly of CID; and 2) CENP-C is asymmetrically distributed between GSCs and CBs, also at a similar ratio to CID^{CENP-A} (data published in Dattoli *et al*, 2020). Ultimately, the larger centromere/inner kinetochore results in more microtubules emanating from the stem pole (Dattoli et al., 2020; Ranjan et al., 2019). In males, Ranjan *et al* also showed this asymmetry for outer kinetochore protein, NDC80 (Ranjan et al., 2019). Together, these findings agree fully with the mitotic drive model since proposed by the Chen laboratory (Wooten et al., 2019a).

In addition to these findings, we determined that CENP-C plays a strong centromere maintenance role in these cells. Here, we show firstly that CENP-C is required for CID^{CENP-A} assembly in GSCs. Indeed, this is not a new result in the centromere field, having been previously characterised on numerous occasions (Carroll et al., 2010; Erhardt et al., 2008; Roure et al., 2019). However, few systems permit observation of the effects of defective centromere assembly at a tissue level. The *in vivo* consequences of aberrant CID^{CENP-A} assembly to the tissue development and maintenance of the germline that we observe are profound. In the absence of CENP-C (63% depletion) and in turn CID^{CENP-A} assembly, GSCs are ill-prepared for the next cell division. We can deduce that centromeres in these

GSCs contain largely parental CID^{CENP-A}, already known to be preferentially retained by *Drosophila* stem cells. Upon analysing S-phase GSC-CB 'pairs' in GSCs with reduced CENP-C, we observe GSCs retaining 1.45-fold more CID^{CENP-A} in comparison to their canonical 1.2-fold asymmetry. This observation suggests 1) Parental CID^{CENP-A} is strongly retained by the GSCs, even in the absence of new CID^{CENP-A} loading, and 2) CENP-C plays a strong maintenance role for CID^{CENP-A} asymmetry in GSCs.

In GSCs overexpressing HA-CENP-C, CID^{CENP-A} assembly is not disrupted and occurs at a level comparable to control cells. It is highly likely in this situation that overpowering the centromere with excess CID^{CENP-A} requires at least a double overexpression of CENP-C and CAL1 (and possibly CID^{CENP-A}), in line with the model for CENP-C as a recruiting factor of new CAL1-CID-H4 (Medina-Pritchard et al., 2020; Roure et al., 2019). Interestingly, concurrent overexpression of CID^{CENP-A} and CAL1 in GSCs reduces CID to a symmetric pattern (Dattoli et al., 2020). In addition, CID^{CENP-A} asymmetry remained non-significant with the control GSCs when CENP-C was overexpressed alone. It is still possible that increasing the HA-CENP-C overexpression through temperature (e.g. 29 °C) may reduce CID^{CENP-A} asymmetry to a symmetrical pattern. Lastly, the transheterozygous mutant $Cenp\text{-}C^{IR35}/cal1^{2k32}$ displays normal CID^{CENP-A} assembly, yet slightly increased CID^{CENP-A} asymmetry (1.33-fold) compared to what one would expect (1.2-fold). This implies a specific role for CAL1-CENP-C interaction to establish and/or maintain asymmetry. Combining the results of each genetic background (Table 6.1), these results also suggest that asymmetry is probably established during S-phase, as opposed to during the assembly phase (Figure 6.1 - Model). In many cases, we see effects on canonical asymmetry disrupted even in the presence of CID^{CENP-A} assembly.

Background	CID^{CENP-A} Level (Normalised to Control)	CID^{CENP-A} Assembly	GSC/CB CID^{CENP-A} Asymmetry (Ratio)	SXL/pMad
Control	100%	Yes	Normal (1.2)	Normal (4)
CENP-C RNAi	63%	No	Increased (1.45)	Decrease (2.5)
HA-CENP-C	100%	Yes	Normal/Small Decrease (1.12)	Normal (3.8)
Cenp-C^{IR35}/$cal1^{2k32}$	100%	Yes	Increase (1.33)	Decrease (2.3)
HA-CENP-C; CENP-C RNAi	80%	Yes	Normal (1.2)	Slight Decrease (3.5)

Table 6.1: Summary of CID^{CENP-A} assembly and CID^{CENP-A} asymmetry in each genetic background.

6.3 Making sense of parental histones: how might parental CID^{CENP-A} be maintained?

Drosophila stem cells are well-characterised to retain parental histones, specifically histones H3-H4 and CID^{CENP-A} (García del Arco et al., 2018; Ranjan et al., 2019; Tran et al., 2012; Wooten et al., 2019b). In *Drosophila* ISCs, the centromeres of ISCs and its endoreplicating daughter cell enterocyte (EB) offer some interesting insights into the workings of the parental CID^{CENP-A} pool. Here, CENP-C is present in the ISC but is absent from the EB (García del Arco et al., 2018). This suggests upon initial analysis that CENP-C could be maintaining the parental pool of CID^{CENP-A}. However, GSCs and ISCs display fundamental differences in future proliferative potential of their respective daughter cells. Whether CENP-C actually maintains the parental pool of CID^{CENP-A} remains debatable, with arguments to be made in support and against. Our data suggests

that this may not necessarily be the case. CENP-C depletion in GSCs result in the retention of more (parental) CID^{CENP-A} by the GSC, with less CID^{CENP-A} being distributed to the CB (most likely a consequence of no new CID^{CENP-A} assembly in G_2/prophase). This may better suggest a role for CENP-C in maintaining appropriate asymmetry (i.e. the amount and ratio between sister centromeres) rather than specifically maintaining the parental pool of CID^{CENP-A}, as suggested by observations in ISCs. Nonetheless, this is yet to be specifically proven in any system and requires the resolution sister centromeres in S-phase (using super resolution microscopy) to robustly answer this question.

Many questions still surround how parental and new CENP-A/ CID^{CENP-A} could be specifically recognised (or if they are specifically recognised at all). In the male germline, testes-derived DNA and chromatin fibres show a high frequency of unidirectional fork movement (Wooten et al., 2019b). This highlights a mechanism that could explain how parental and newly synthesised histones might be preferentially maintained on one strand versus another across the replication fork. Building upon this, an argument could be made that parental histones do not need to be specifically recognised and maintained asymmetrically. Here, asymmetric retention of old histones would, in theory, be intrinsic to the replication system of these cells. To prove this concept would require the culturing of adult stem cells (outside of their niche), followed by chromatin fibre extraction – a technically difficult task. Nonetheless, this hypothesis probably does not hold true for the centromere. Given the loading time for CID^{CENP-A} in *Drosophila* stem cells (G_2/prophase, after DNA replication and sister centromere establishment), it is highly probable that parental CID^{CENP-A} does require direct maintenance via CENP-C, CAL1 or other histone chaperones (e.g. Spt6, (Bobkov et al., 2020)). In this case, DNA replication in these adult stem cells would require the retention of parental CID^{CENP-A} across the replication fork before assembling newly-synthesized CID.

Interestingly, we see no evidence of chromosome mis-segregation or mitotic arrest when we deplete CENP-C by 63%. Instead, we observed a significant S-phase delay, whereby more germ cell cysts (from GSC/CB to 8cc) were undergoing DNA replication simultaneously, unlike in control germaria. This suggests CENP-C is

required also in DNA replication, outside of its role in an asymmetric mitosis. Here, CENP-C maybe required to maintain asymmetric CID^{CENP-A} establishment that might occur during S-phase. Indeed, CENP-C has been implicated in DNA replication previously, where FRAP/FCS studies show a large proportion of the CENP-C pool is stable at the centromere during S-phase (Hemmerich et al., 2008). This suggests that CENP-C is possibly maintaining or aiding in centromere reorganisation at the centromere. Furthermore, new insights emerged recently from ChIP-Seq studies in human cells, whereby CENP-C is required for an error-correction mechanism during S-phase, to compensate for CENP-A assembly on chromatin arms (Nechemia-Arbely et al., 2019). In these cells, CENP-A assembly (in G_1 phase, before DNA replication) occurs both at the centromere and in low amounts on chromatin arms. In S-phase, this CENP-A is removed on chromatin arms (where CENP-C is not present) but is maintained at the centromere locus, where it requires CENP-C to be maintained. It is tempting to speculate that such a mechanism may exist to maintain CID^{CENP-A} across the centromere in S-phase before assembling new CID^{CENP-A} in G_2/prophase. In any case, we have strong evidence that CENP-C's role extends beyond its general mitotic requirements of kinetochore assembly. Its role in stem cells is not merely its function in cell division, being instrumental to centromere 'strength' asymmetry, centromere assembly and ultimately cell fate (discussed in 6.6).

6.3 The centromere as a driver of asymmetric division in stem cells

Previous thinking in the stem cell field was that the centrosome was the primary driver of ACD, emanating from the discovery of an asymmetric retention of mother and daughter centrosomes in *Drosophila* (Yamashita et al., 2007). Although important to mitotic spindle formation, there appears to be a lack of consistency to mother/daughter centrosome directionality. Male GSCs preferentially retain the mother centrosome (Yamashita et al., 2007), yet female GSCs and neuroblasts retain daughter centrosomes (Januschke et al., 2011; Salzmann et al., 2014). Furthermore, mid-body segregation correlates with the inheritance of the daughter centrosome (i.e. it is opposite in male and female GSCs) (Salzmann et al., 2014). Hence, the retention of centrosomes appears quite disordered and inconsistent

amongst *Drosophila* stem cell populations. In contrast, both male and female GSCs retain stronger centromeres/kinetochores/mitotic spindles (Dattoli et al., 2020; Ranjan et al., 2019), independent of mother/daughter centrosome inheritance. Interestingly, in a *Drosophila Spindle Assembly Abormal-4* (*DSas-4*) mutant background, female GSCs are capable of forming mitotic spindle in the absence of centrioles (Stevens et al., 2007). Hence, it is possible that spindle assembly in asymmetrically-dividing GSCs is a chromatin- or centromere-driven process (as opposed to centrosome-driven), in a manner similar to oocyte spindle assembly in many systems (Radford et al., 2017). Moreover, spindle assembly reacts to centromere strength (Dattoli et al., 2020; Ranjan et al., 2019). Moving forward, understanding the molecular mechanisms behind the establishment and maintenance of asymmetric sister centromeres remains an important question. This thesis has shed some light on this mechanism, investigating the involvement of CENP-C in this process.

6.4 The Model of Centromere Assembly in Asymmetric Cell Division

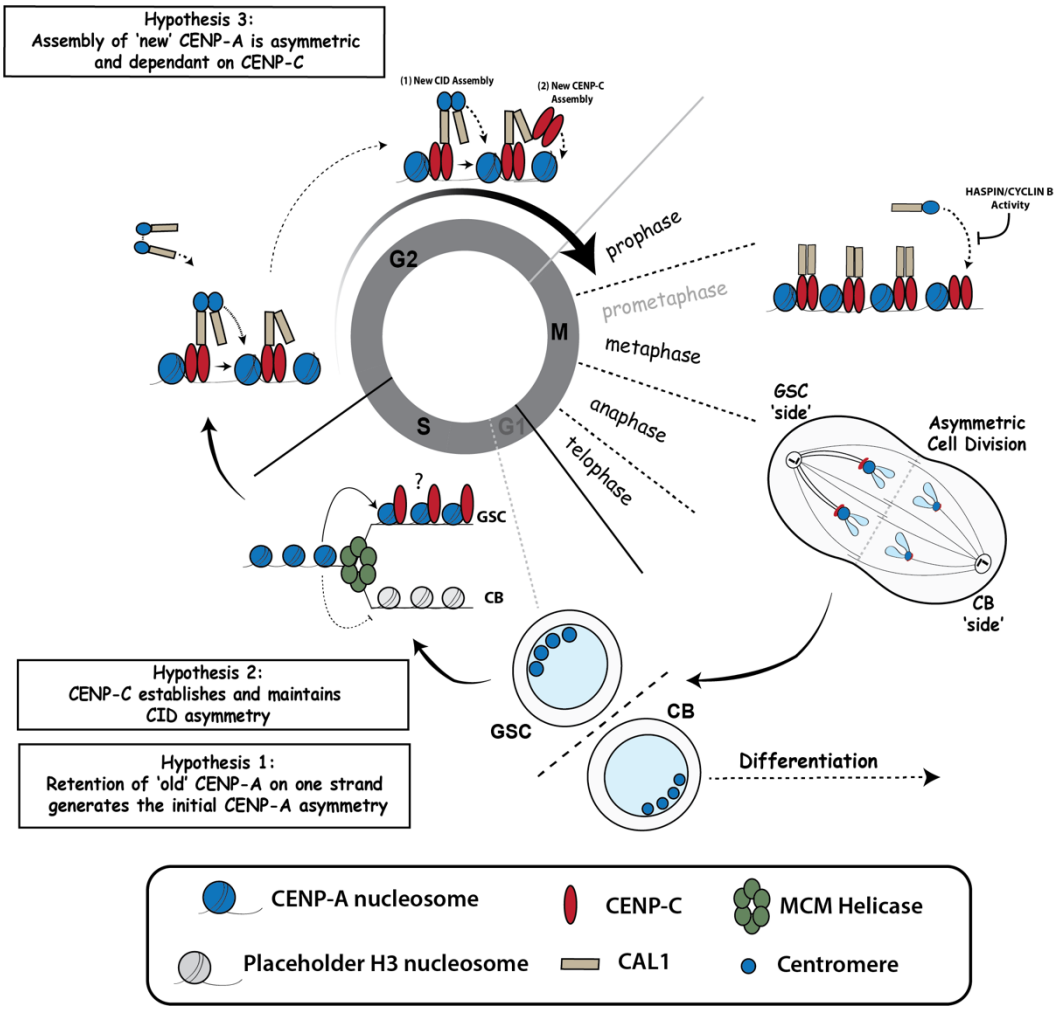

Figure 6.1: Model and outstanding questions regarding the propagation of the centromere in an asymmetrically-dividing system. After mitosis, the newly divided GSC has a very short G1-phase, entering immediately into S-phase. During replication, a unidirectional fork may allow parental 'old' CENP-A-H4 to be asymmetrically inherited between leading and lagging strands, in a manner similar to H3-H4 (Wooten et al., 2019b). The asymmetric inheritance of 'old' CENP-A may establish the initial asymmetry in the amount of CENP-A between sister centromeres (Hypothesis 1, bottom left). This asymmetry may be established by or maintained by CENP-C during S-phase (Hypothesis 2, middle left). Newly synthesised or 'new' CENP-A assembly occurs after DNA replication through to prophase. New CENP-A assembly might occur in an asymmetric manner and require CENP-C to be asymmetric between sister centromeres (Hypothesis 3, top left). By prophase, the centromere is fully assembled at centromere strength

between sister centromeres. Further assembly is limited by HASPIN and CYCLIN B activity (Dattoli et al., 2020).

6.5 Adult stem cell age epigenetically at the centromere

Aging is a multifactorial process involving a combination of many processes. Over the last decade, numerous studies have shown that the epigenome changes with age (known as 'epigenetic drift') (Pal and Tyler, 2016; Sen et al., 2016). In particular, age-associated epigenetic changes include DNA methylation, histone modifications and chromatin remodelling. Recent studies have shown that age-accompanied chromatin changes typically are associated with a gradual loss of constitutive heterochromatin – heterochromatin associated with highly repetitive DNA sequences, such as that observed at pericentric and telomeric regions (Allshire and Madhani, 2018; Trojer and Reinberg, 2007; Zhang et al., 2015). In fact, the centromere represents a specialised heterochromatin domain is characterised by CENP-A containing chromatin, flanked by pericentric heterochromatin (Bloom, 2014). In addition, CENP-A contains other specific histone modifications, particularly at its N-terminus (Srivastava and Foltz, 2018). Moreover, decreasing histone levels are also associated with normal aging, with restoration of these histone levels shown to extend lifespan in yeast (Feser et al., 2010). Ultimately, this epigenetic 'erosion' also pertains to stem cells and stem cell exhaustion (Chen and Kerr, 2019; Ermolaeva et al., 2018).

Stem cell exhaustion is protected by self-renewal of the stem cell, with rising evidence suggesting that self-renewal and differentiation are impaired by aging (Chen and Kerr, 2019; Ermolaeva et al., 2018). This leads to a functional decline in tissue integrity. Specific epigenetic regulators associated with epigenetic aging are critical to the maintenance of tissue-specific stem cells (e.g. haemopoietic stem cells), with the identification of true epigenetic regulators of stem cell age being key to any attempts to reverse stem cell aging (Chen and Kerr, 2019; Ermolaeva et al., 2018). A true epigenetic regulator of aging must decrease over time and directly influence cell fate. Indeed, in chapters 4 and 5 we present robust evidence that the centromere does both. In chapter 4, we firstly show that between 5-, 10- and 20-days that both CID^{CENP-A} and its recruiting factor CENP-C are gradually lost from

the centromere. Here, we quantified an approximate 45% drop in both CID^{CENP-A} and CENP-C from days 5 to 20. This strongly implies that that centromere is gradually lost with stem cell age. Moreover, when we deplete CENP-C, this loss of CID^{CENP-A} is accelerated, suggesting that this centromere 'erosion' involves loss of CENP-C as the recruiting and maintenance/stabilisation factor. This may well be a consequence of symmetric division of the stem cell, depleting the centromere pool over time. Secondly, in both chapter 4 and 5 we show that disruption to the centromere is linked to cell fate. In a CENP-C-depleted germline, we see an array of phenotypes from GSC-tumour, to differentiation defects, to GSC loss. In addition, when we disrupt the centromeric core by knockdown, overexpression (Dattoli et al., 2020) or mutant backgrounds, we see a shift in the balance of stem to daughter cell in the germarium (as determined by the SXL/pMad ratio). Furthermore, we also see an exacerbation of the SXL/pMad ratio when analysing CENP-C depleted GSCs at 10 days old. This reiterates the involvement of the centromere in aging.

This is the first time the centromere has been directly implicated in stem cell aging and lifespan. The investigation of the role of the centromere with age is largely underrepresented in literature. One study in 1984 observed centromere loss from chromosomes of aged women, as measured by positive or negative Cd-banding (a chromosome banding technique used to specifically recognise centromeric regions) on mitotic chromosomes (Nakagome et al., 1984). Another study measured a decline of CENP-A levels in pancreatic islet cells, but not exocrine cells (Lee et al., 2010). Reductions in CENP-A at the centromere have also been reported in p53-induced cellular senescence, proposed as a protective mechanism against chromosome mis-segregation and genome instability (Hédouin et al., 2017; Maehara et al., 2010). Other studies show that age-related aneuploidies could be explained by loss of cohesion at the centromere (Cheng and Liu, 2017). Therefore, centromere 'strength' may well play its role in aging. In an adult stem cell that displays differences in centromere strength between sister centromeres, possibly even more so.

But how might the centromere deplete with age? Elucidating this question is a fundamental question to centromere biology. Repetitive DNA can be lost with age.

It is well known that telomeric DNA shortens with age, modulating the cellular 'clock' and eventually results in cellular senescence (Maestroni et al., 2017). Given the repetitive nature of centromeric genomic regions, this may provide a clue to how the centromere ages. The centromere is also susceptible to instability but how this relates to age remains unsolved. One study in 2017 reported a high frequency of rearrangement and sister chromatid exchange at centromeric alpha-satellites (Giunta and Funabiki, 2017). Whether this loss of the centromere over time in stem cells is limited to the CCAN, or whether it is underpinned at a genetic level remains an open and valid question. It is conceivable that the centromeric DNA shortens also in stem cells over time, in a manner similar to telomere shortening. A better understanding of how centromeric DNA is replicated, and how the DNA repair machinery might deal with instability and replication stress at the centromere would be required to answer this question.

6.6 Centromeres epigenetically regulate stem cell fate

To probe the role of a disrupted centromere on stem cell fate, we were required to develop an assay that would be consistent in wild type germaria but respond to changes in the balance of GSC to daughter cells (CBs, 2ccs). Here, determining a ratio of SXL to pMad-positive cells proved consistent across control cells, from wild type *OregonR*, to RNAi isogenic control, to *nanos-GAL4* (ratio of approx 4:1). In other words, there is one GSC for every three daughter cells (1 GSC, 1 CB, 1 2cc). Interestingly, the composition of each germarium (i.e. total number of pMad and SXL positive cells) is different across each genetic background. However, the ratio remains the same. This method is much more robust in comparison to simply counting the number of stem cells present in each germaria, as this can change simply based on genetic background.

When we applied this assay to various backgrounds of disrupted centromere integrity, we saw the ratio of SXL/pMad changing in accordance. In CENP-C depleted germaria, this ratio was reduced to approximately 2.5 (for every stem cell, there are only 2.5 daughter cells on average), suggesting an alteration of the self-renewal pattern of the stem cell. When we expanded this assay to 10-day old

CENP-C-depleted flies, this ratio reduced further to 2. Moreover, we determined that CENP-C-depletion results in differentiation defects and GSC loss over time. Thus, it appears that CID^{CENP-A} levels (both though disrupted assembly and increased CID^{CENP-A} asymmetry) are playing a substantial role in long-term GSC maintenance and differentiation of early germ-cysts. Interestingly, when we analysed CID^{CENP-A}-mCherry; CAL1-YFP double overexpressed flies, the SXL/pMad ratio also reduces to 2.5 at 3 days old (published in Dattoli *et al*, 2020). The same is also true for *Cenp-C^{IR35};cal1^{2k32}* germaria. Yet, single overexpression of HA-CENP-C does not impact cell fate. However, we determined that HA-CENP-C overexpression alone does not impact CID^{CENP-A} level at centromeres. Ultimately, the impact on cell fate appears to reside with a disrupted centromeric core, whether that be decreased CID^{CENP-A}, increased CID^{CENP-A}, symmetric or increased asymmetric inheritances of CID^{CENP-A}. It is clear that the centromere can indeed epigenetically regulate adult stem cell fate in *Drosophila*.

How would the centromere react to a pluripotent state? Studies are emerging related to the role of centromeric chromatin on both the self-renewal and differentiation capabilities of these cells. It is still unclear whether embryonic or pluripotent stem cells (iPSCs), for example, display differences in centromere strength between sister centromeres. However, recent work from the Chen laboratory have shown that parental histones are maintained also by induced asymmetrically-dividing mouse embryonic stem cells (Ma et al., 2020). Here, old versus new histones H3 and H4 do not overlap, whereas histones H2A, H2B and H3.3 (the more dynamic histone) are inherited symmetrically. Significantly, when these stem cells are dividing symmetrically, old versus new histones H3 and H4 are inherited randomly (Ma et al., 2020). This gives plausibility to the same situation occurring for CENP-A in asymmetrically dividing stem cells beyond *Drosophila*.

In addition to centromere asymmetry, iPSCs appear to be heavily reliant on centromere ‘load’. In other words, there is a threshold of CENP-A required for them in order to differentiate. Otherwise, CENP-A-depleted iPSCs continuously self-renew (Ambartsumyan et al., 2010). This is in full agreement with our observations, that low levels of CID/CENP-A result in a tendency for GSCs to self-

renew and fail to differentiate. Additionally, new evidence from the Jansen lab shows that reprogramming differentiated iPSCs to pluripotency results in the removal of CENP-A, CENP-C and CENP-T from the centromere (Milagre et al., 2020). These results suggest that the reorganisation of the centromere is linked to stem cell state. Interestingly, centromere assembly requires exit from telophase into G_1, similar to differentiated human cells (Milagre et al., 2020). These differences compared to *Drosophila* GSCs perhaps reflect the requirements to remain pluripotent and an openness to differentiate to numerous cell types. On the other hand, adult *Drosophila* GSCs stem cells are largely unipotent and exhibit generally asymmetric patterns (and short G_1 phases). Overall, this shows that the centromere is highly active and responsive in a stem cell, as opposed to being a passive locus in the underlying mitotic machinery.

6.7 Concluding Remarks and Outstanding Questions

There are still many outstanding questions related to how the centromere is modulated by a stem cell:

1) When and how exactly is asymmetry established and maintained?
2) How are parental histones specifically maintained in an asymmetric system?
3) How is CENP-A lost at the centromere in an aging stem cell?
4) What role does centromeric DNA play in an asymmetrically-dividing system?
5) How does a pluripotent stem cell manage a centromere in an asymmetric division?
6) How does a disrupted centromere affect ‘stem’ versus ‘differentiation’ gene expression?

This thesis has progressed our understanding of the centromere in an asymmetrically-dividing adult stem cell population. It is evident that the centromere does indeed epigenetically distinguish sister centromeres in asymmetric cell division. Thus, these findings fully underpin the silent sister hypothesis, put forward by Lansdorp in 2007 (Lansdorp, 2007). Over time, the centromere integrity is also gradually lost in at the centromere. Moreover, a robust

centromeric core is essential to maintaining stem cell fate. Ultimately, it is clear that intrinsic stem cell homeostasis relies heavily on the centromere and its efficient maintenance throughout the cell cycle.

In conclusion, the centromere can drive stem cell identity.

7. Bibliography

Ables, E.T., Drummond-Barbosa, D., 2013. Cyclin E controls Drosophila female germline stem cell maintenance independently of its role in proliferation by modulating responsiveness to niche signals, in: Development. Company of Biologists, pp. 530–540. https://doi.org/10.1242/dev.088583

Ahmad, K., Henikoff, S., 2001. Centromeres are specialized replication domains in heterochromatin. J. Cell Biol. 153, 101–109. https://doi.org/10.1083/jcb.153.1.101

Akera, T., Chmátal, L., Trimm, E., Yang, K., Aonbangkhen, C., Chenoweth, D.M., Janke, C., Schultz, R.M., Lampson, M.A., 2017. Spindle asymmetry drives non-Mendelian chromosome segregation. Science. 358, 668–672. https://doi.org/10.1126/science.aan0092

Alberts, B., Johnson, A., Lewis, J., Raff, M., Roberts, K., Walter, P., 2014. Molecular Biology of the Cell. Garland Science.

Allshire, R.C., Karpen, G.H., 2008. Epigenetic regulation of centromeric chromatin: Old dogs, new tricks? Nat. Rev. Genet. https://doi.org/10.1038/nrg2466

Allshire, R.C., Madhani, H.D., 2018. Ten principles of heterochromatin formation and function. Nat. Rev. Mol. Cell Biol. https://doi.org/10.1038/nrm.2017.119

Ambartsumyan, G., Gill, R.K., Perez, S.D., Conway, D., Vincent, J., Dalal, Y., Clark, A.T., 2010. Centromere protein A dynamics in human pluripotent stem cell self-renewal, differentiation and DNA damage. Hum. Mol. Genet. 19, 3970–3982. https://doi.org/10.1093/hmg/ddq312

Amor, D.J., Andy Choo, K.H., 2002. Neocentromeres: Role in human disease, evolution, and centromere study. Am. J. Hum. Genet. https://doi.org/10.1086/342730

Baldi, S., Korber, P., Becker, P.B., 2020. Beads on a string—nucleosome array arrangements and folding of the chromatin fiber. Nat. Struct. Mol. Biol. https://doi.org/10.1038/s41594-019-0368-x

Barra, V., Fachinetti, D., 2018. The dark side of centromeres: types, causes and consequences of structural abnormalities implicating centromeric DNA. Nat. Commun. https://doi.org/10.1038/s41467-018-06545-y

Bassett, E.A., DeNizio, J., Barnhart-Dailey, M.C., Panchenko, T., Sekulic, N., Rogers, D.J., Foltz, D.R., Black, B.E., 2012. HJURP Uses Distinct CENP-A Surfaces to Recognize and to Stabilize CENP-A/Histone H4 for Centromere Assembly. Dev. Cell 22, 749–762. https://doi.org/10.1016/j.devcel.2012.02.001

Black, B.E. (Ed.), 2017. Centromeres and Kinetochores: Discovering the Molecular Mechanisms Underlying Chromosome Inheritance (Progress in Molecular and Subcellular Biology). Springer.

Black, B.E., Cleveland, D.W., 2011. Epigenetic centromere propagation and the nature of CENP-A nucleosomes. Cell. https://doi.org/10.1016/j.cell.2011.02.002

Black, B.E., Foltz, D.R., Chakravarthy, S., Luger, K., Woods, V.L., Cleveland, D.W., 2004. Structural determinants for generating centromeric chromatin. Nature 430, 578–582. https://doi.org/10.1038/nature02766

Black, B.E., Jansen, L.E.T., Maddox, P.S., Foltz, D.R., Desai, A.B., Shah, J. V., Cleveland, D.W., 2007. Centromere Identity Maintained by Nucleosomes Assembled with Histone H3

Containing the CENP-A Targeting Domain. Mol. Cell 25, 309–322. https://doi.org/10.1016/j.molcel.2006.12.018

Bloom, K.S., 2014. Centromeric heterochromatin: The primordial segregation machine. Annu. Rev. Genet. 48, 457–484. https://doi.org/10.1146/annurev-genet-120213-092033

Blower, M.D., Sullivan, B.A., Karpen, G.H., 2002. Conserved organization of centromeric chromatin in flies and humans. Dev. Cell 2, 319–330. https://doi.org/10.1016/S1534-5807(02)00135-1

Bobkov, G.O.M., Huang, A., van den Berg, S.J.W., Mitra, S., Anselm, E., Lazou, V., Schunter, S., Feederle, R., Imhof, A., Lusser, A., Jansen, L.E.T., Heun, P., 2020. Spt6 is a maintenance factor for centromeric CENP-A. Nat. Commun. 11, 1–14. https://doi.org/10.1038/s41467-020-16695-7

Bodor, D.L., Mata, J.F., Sergeev, M., David, A.F., Salimian, K.J., Panchenko, T., Cleveland, D.W., Black, B.E., Shah, J. V, Jansen, L.E., 2014. The quantitative architecture of centromeric chromatin. Elife e02137. https://doi.org/10.7554/eLife.02137

Brown, M.T., 1995. Sequence similarities between the yeast chromosome segregation protein Mif2 and the mammalian centromere protein CENP-C. Gene 160, 111–116. https://doi.org/10.1016/0378-1119(95)00163-Z

Brunet, S., Verlhac, M.H., 2011. Positioning to get out of meiosis: The asymmetry of division. Hum. Reprod. Update 17, 68–75. https://doi.org/10.1093/humupd/dmq044

Cairns, J., 1975. Mutation selection and the natural history of cancer. Nature 255, 197–200. https://doi.org/10.1038/255197a0

Carbone, L., Harris, R.A., Mootnick, A.R., Milosavljevic, A., Martin, D.I.K., Rocchi, M., Capozzi, O., Archidiacono, N., Konkel, M.K., Walker, J.A., Batzer, M.A., De Jong, P.J., 2012. Centromere remodeling in Hoolock leuconedys (Hylobatidae) by a new transposable element unique to the gibbons. Genome Biol. Evol. 4, 648–658. https://doi.org/10.1093/gbe/evs048

Carroll, C.W., Milks, K.J., Straight, A.F., 2010. Dual recognition of CENP-A nucleosomes is required for centromere assembly. J. Cell Biol. 189, 1143–1155. https://doi.org/10.1083/jcb.201001013

Carty, B.L., Dunleavy, E.M., 2020. Centromere assembly and non-random sister chromatid segregation in stem cells. Essays Biochem. https://doi.org/10.1042/ebc20190066

Casanueva, M.O., Ferguson, E.L., 2004. Germline stem cell number in the Drosophila ovary is regulated by redundant mechanisms that control Dpp signaling. Development 131, 1881–1890. https://doi.org/10.1242/dev.01076

Chang, C.H., Chavan, A., Palladino, J., Wei, X., Martins, N.M.C., Santinello, B., Chen, C.C., Erceg, J., Beliveau, B.J., Wu, C.T., Larracuente, A.M., Mellone, B.G., 2019. Islands of retroelements are major components of Drosophila centromeres. PLoS Biol. 17, e3000241. https://doi.org/10.1371/journal.pbio.3000241

Chen, C.C., Dechassa, M.L., Bettini, E., Ledoux, M.B., Belisario, C., Heun, P., Luger, K., Mellone, B.G., 2014. CAL1 is the Drosophila CENP-A assembly factor. J. Cell Biol. 204,

313–329. https://doi.org/10.1083/jcb.201305036

Chen, D., Kerr, C., 2019. The Epigenetics of Stem Cell Aging Comes of Age. Trends Cell Biol. https://doi.org/10.1016/j.tcb.2019.03.006

Chen, D., McKearin, D., 2003a. Dpp Signaling Silences bam Transcription Directly to Establish Asymmetric Divisions of Germline Stem Cells. Curr. Biol. 13, 1786–1791. https://doi.org/10.1016/j.cub.2003.09.033

Chen, D., McKearin, D.M., 2003b. A discrete transcriptional silencer in the bam gene determines asymmetric division of the Drosophila germline stem cell. Development. https://doi.org/10.1242/dev.00325

Cheng, J.M., Liu, Y.X., 2017. Age-related loss of cohesion: Causes and effects. Int. J. Mol. Sci. https://doi.org/10.3390/ijms18071578

Chmátal, L., Gabriel, S.I., Mitsainas, G.P., Martínez-Vargas, J., Ventura, J., Searle, J.B., Schultz, R.M., Lampson, M.A., 2014. Centromere strength provides the cell biological basis for meiotic drive and karyotype evolution in mice. Curr. Biol. 24, 2295–2300. https://doi.org/10.1016/j.cub.2014.08.017

Chueh, A.C., Northrop, E.L., Brettingham-Moore, K.H., Choo, K.H.A., Wong, L.H., 2009. LINE retrotransposon RNA is an essential structural and functional epigenetic component of a core neocentromeric chromatin. PLoS Genet. 5, e1000354. https://doi.org/10.1371/journal.pgen.1000354

Chueh, A.C., Wong, L.H., Wong, N., Choo, K.H.H.A., 2005. Variable and hierarchical size distribution of L1-retroelement-enriched CENP-A clusters within a functional human neocentromere. Hum. Mol. Genet. 14, 85–93. https://doi.org/10.1093/hmg/ddi008

Clevers, H., 2005. Stem cells, asymmetric division and cancer. Nat. Genet. https://doi.org/10.1038/ng1005-1027

Cohen, R.L., Espelin, C.W., De Wulf, P., Sorger, P.K., Harrison, S.C., Simons, K.T., 2008. Structural and functional dissection of Mif2p, a conserved DNA-binding kinetochore protein. Mol. Biol. Cell 19, 4480–4491. https://doi.org/10.1091/mbc.E08-03-0297

Conboy, M.J., Karasov, A.O., Rando, T.A., 2007. High incidence of non-random template strand segregation and asymmetric fate determination in dividing stem cells and their progeny. PLoS Biol. 5, 1120–1126. https://doi.org/10.1371/journal.pbio.0050102

Dansereau, D.A., Lasko, P., 2008. The development of germline stem cells in drosophila. Methods Mol. Biol. 450, 3–26. https://doi.org/10.1007/978-1-60327-214-8_1

Das, A., Black, B.E., Lampson, M.A., 2020. Maternal inheritance of centromeres through the germline, in: Current Topics in Developmental Biology. Academic Press Inc., pp. 35–54. https://doi.org/10.1016/bs.ctdb.2020.03.004

Dattoli, A.A., Carty, B.L., Kochendoerfer, A.M., Morgan, C., Walshe, A.E., Dunleavy, E.M., 2020. Asymmetric assembly of centromeres epigenetically regulates stem cell fate. J. Cell Biol. 219. https://doi.org/10.1083/JCB.201910084

de Sotero-Caio, C.G., Cabral-de-Mello, D.C., Calixto, M. da S., Valente, G.T., Martins, C., Loreto, V., de Souza, M.J., Santos, N., 2017. Centromeric enrichment of LINE-1

retrotransposons and its significance for the chromosome evolution of Phyllostomid bats. Chromosom. Res. 25, 313–325. https://doi.org/10.1007/s10577-017-9565-9

Duffy, J.B., 2002. GAL4 system indrosophila: A fly geneticist's swiss army knife. genesis 34, 1–15. https://doi.org/10.1002/gene.10150

Dunleavy, E.M., Beier, N.L., Gorgescu, W., Tang, J., Costes, S. V., Karpen, G.H., 2012. The Cell Cycle Timing of Centromeric Chromatin Assembly in Drosophila Meiosis Is Distinct from Mitosis Yet Requires CAL1 and CENP-C. PLoS Biol. 10, e1001460. https://doi.org/10.1371/journal.pbio.1001460

Dunleavy, E.M., Collins, C.M., 2017. Centromere Dynamics in Male and Female Germ Cells. Prog. Mol. Subcell. Biol. https://doi.org/10.1007/978-3-319-58592-5_15

Dunleavy, E.M., Roche, D., Tagami, H., Lacoste, N., Ray-Gallet, D., Nakamura, Y., Daigo, Y., Nakatani, Y., Almouzni-Pettinotti, G., 2009. HJURP Is a Cell-Cycle-Dependent Maintenance and Deposition Factor of CENP-A at Centromeres. Cell 137, 485–497. https://doi.org/10.1016/j.cell.2009.02.040

Earnshaw, W., Bordwell, B., Marino, C., Rothfield, N., 1986. Three human chromosomal autoantigens are recognized by sera from patients with anti-centromere antibodies. J. Clin. Invest. 77, 426–430. https://doi.org/10.1172/JCI112320

Earnshaw, W.C., Rothfield, N., 1985. Identification of a family of human centromere proteins using autoimmune sera from patients with scleroderma. Chromosoma 91, 313–321. https://doi.org/10.1007/BF00328227

Elabd, C., Cousin, W., Chen, R.Y., Chooljian, M.S., Pham, J.T., Conboy, I.M., Conboy, M.J., 2013. DNA methyltransferase-3-dependent nonrandom template segregation in differentiating embryonic stem cells. J. Cell Biol. 203, 73–85. https://doi.org/10.1083/jcb.201307110

Erhardt, S., Mellone, B.G., Betts, C.M., Zhang, W., Karpen, G.H., Straight, A.F., 2008. Genome-wide analysis reveals a cell cycle-dependent mechanism controlling centromere propagation. J. Cell Biol. 183, 805–818. https://doi.org/10.1083/jcb.200806038

Ermolaeva, M., Neri, F., Ori, A., Rudolph, K.L., 2018. Cellular and epigenetic drivers of stem cell ageing. Nat. Rev. Mol. Cell Biol. https://doi.org/10.1038/s41580-018-0020-3

Fabritius, A.S., Ellefson, M.L., McNally, F.J., 2011. Nuclear and spindle positioning during oocyte meiosis. Curr. Opin. Cell Biol. https://doi.org/10.1016/j.ceb.2010.07.008

Fachinetti, D., Diego Folco, H., Nechemia-Arbely, Y., Valente, L.P., Nguyen, K., Wong, A.J., Zhu, Q., Holland, A.J., Desai, A., Jansen, L.E.T., Cleveland, D.W., 2013. A two-step mechanism for epigenetic specification of centromere identity and function. Nat. Cell Biol. 15, 1056–1066. https://doi.org/10.1038/ncb2805

Falk, S.J., Guo, L.Y., Sekulic, N., Smoak, E.M., Mani, T., Logsdon, G.A., Gupta, K., Jansen, L.E.T., Van Duyne, G.D., Vinogradov, S.A., Lampson, M.A., Black, B.E., 2015. CENP-C reshapes and stabilizes CENP-A nucleosomes at the centromere. Science. 348, 699–703. https://doi.org/10.1126/science.1259308

Falk, S.J., Lee, J., Sekulic, N., Sennett, M.A., Lee, T.H., Black, B.E., 2016. CENP-C directs a

structural transition of CENP-A nucleosomes mainly through sliding of DNA gyres. Nat. Struct. Mol. Biol. 23, 204–208. https://doi.org/10.1038/nsmb.3175

Fang, J., Liu, Y., Wei, Y., Deng, W., Yu, Z., Huang, L., Teng, Y., Yao, T., You, Q., Ruan, H., Chen, P., Xu, R.M., Li, G., 2015. Structural transitions of centromeric chromatin regulate the cell cycle-dependent recruitment of CENP-N. Genes Dev. 29, 1058–1073. https://doi.org/10.1101/gad.259432.115

Fei, J.-F., Huttner, W.B., 2009. Nonselective Sister Chromatid Segregation in Mouse Embryonic Neocortical Precursor Cells. Cereb. Cortex 19, i49–i54. https://doi.org/10.1093/cercor/bhp043

Feser, J., Truong, D., Das, C., Carson, J.J., Kieft, J., Harkness, T., Tyler, J.K., 2010. Elevated Histone Expression Promotes Life Span Extension. Mol. Cell 39, 724–735. https://doi.org/10.1016/j.molcel.2010.08.015

Flemming, W., 1882. Zellsubstanz, Kern und Zelltheilung /, Zellsubstanz, Kern und Zelltheilung /. F.C.V Vogel, Leipzig. https://doi.org/10.5962/bhl.title.168645

Foltz, D.R., Jansen, L.E.T., Bailey, A.O., Yates, J.R., Bassett, E.A., Wood, S., Black, B.E., Cleveland, D.W., 2009. Centromere-Specific Assembly of CENP-A Nucleosomes Is Mediated by HJURP. Cell 137, 472–484. https://doi.org/10.1016/j.cell.2009.02.039

Foltz, D.R., Jansen, L.E.T., Black, B.E., Bailey, A.O., Yates, J.R., Cleveland, D.W., 2006. The human CENP-A centromeric nucleosome-associated complex. Nat. Cell Biol. 8, 458–469. https://doi.org/10.1038/ncb1397

Fox, P.M., Vought, V.E., Hanazawa, M., Lee, M.H., Maine, E.M., Sched, T., 2011. Cyclin e and CDK-2 regulate proliferative cell fate and cell cycle progression in the C. elegans germline. Development 138, 2223–2234. https://doi.org/10.1242/dev.059535

Fuchs, E., Segre, J.A., 2000. Stem cells: A new lease on life. Cell. https://doi.org/10.1016/S0092-8674(00)81691-8

Fuchs, E., Tumbar, T., Guasch, G., 2004. Socializing with the neighbors: Stem cells and their niche. Cell. https://doi.org/10.1016/S0092-8674(04)00255-7

Furuyama, S., Biggins, S., 2007. Centromere identity is specified by a single centromeric nucleosome in budding yeast. Proc. Natl. Acad. Sci. U. S. A. 104, 14706–14711. https://doi.org/10.1073/pnas.0706985104

García del Arco, A., Edgar, B.A., Erhardt, S., 2018. In Vivo Analysis of Centromeric Proteins Reveals a Stem Cell-Specific Asymmetry and an Essential Role in Differentiated, Non-proliferating Cells. Cell Rep. 22, 1982–1993. https://doi.org/10.1016/j.celrep.2018.01.079

Giunta, S., Funabiki, H., 2017. Integrity of the human centromere DNA repeats is protected by CENP-A, CENP-C, and CENP-T. Proc. Natl. Acad. Sci. U. S. A. 114, 1928–1933. https://doi.org/10.1073/pnas.1615133114

Glynn, M., Kaczmarczyk, A., Prendergast, L., Quinn, N., Sullivan, K.F., 2010. Centromeres: Assembling and propagating epigenetic function. Subcell. Biochem. 50, 223–249. https://doi.org/10.1007/978-90-481-3471-7_12

Gonzalez, M., He, H., Dong, Q., Sun, S., Li, F., 2014. Ectopic centromere nucleation by CENP-A

in fission yeast. Genetics 198, 1433–1446. https://doi.org/10.1534/genetics.114.171173

Goshima, G., Wollman, R., Goodwin, S.S., Zhang, N., Scholey, J.M., Vale, R.D., Stuurman, N., 2007. Genes required for mitotic spindle assembly in Drosophila S2 cells. Science. 316, 417–421. https://doi.org/10.1126/science.1141314

Greenbaum, M.P., Iwamori, T., Buchold, G.M., Matzuk, M.M., 2011. Germ cell intercellular bridges. Cold Spring Harb. Perspect. Biol. 3, 1–18. https://doi.org/10.1101/cshperspect.a005850

Guo, L.Y., Allu, P.K., Zandarashvili, L., McKinley, K.L., Sekulic, N., Dawicki-McKenna, J.M., Fachinetti, D., Logsdon, G.A., Jamiolkowski, R.M., Cleveland, D.W., Cheeseman, I.M., Black, B.E., 2017. Centromeres are maintained by fastening CENP-A to DNA and directing an arginine anchor-dependent nucleosome transition. Nat. Commun. 8, 15775. https://doi.org/10.1038/ncomms15775

Halanych, K.M., 2004. The new view of animal phylogeny. Annu. Rev. Ecol. Evol. Syst. https://doi.org/10.1146/annurev.ecolsys.35.112202.130124

Han, F., Lamb, J.C., Birchler, J.A., 2006. High frequency of centromere inactivation resulting in stable dicentric chromosomes of maize. Proc. Natl. Acad. Sci. U. S. A. 103, 3238–3243. https://doi.org/10.1073/pnas.0509650103

Harrington, J.J., Van Bokkelen, G., Mays, R.W., Gustashaw, K., Willard, H.F., 1997. Formation of de novo centromeres and construction of first-generation human artificial microchromosomes. Nat. Genet. 15, 345–355. https://doi.org/10.1038/ng0497-345

Hédouin, S., Grillo, G., Ivkovic, I., Velasco, G., Francastel, C., 2017. CENP-A chromatin disassembly in stressed and senescent murine cells. Sci. Rep. 7, 1–14. https://doi.org/10.1038/srep42520

Heeger, S., Leismann, O., Schittenhelm, R., Schraidt, O., Heidmann, S., Lehner, C.F., 2005. Genetic interactions of separase regulatory subunits reveal the diverged Drosophila Cenp-C homolog. Genes Dev. 19, 2041–2053. https://doi.org/10.1101/gad.347805

Hemmerich, P., Weidtkamp-Peters, S., Hoischen, C., Schmiedeberg, L., Erliandri, I., Diekmann, S., 2008. Dynamics of inner kinetochore assembly and maintenance in living cells. J. Cell Biol. 180, 1101–1114. https://doi.org/10.1083/jcb.200710052

Henikoff, S., Ahmad, K., Malik, H.S., 2001. The centromere paradox: Stable inheritance with rapidly evolving DNA. Science. https://doi.org/10.1126/science.1062939

Herrera, S.C., Bach, E.A., 2019. JAK/STAT signaling in stem cells and regeneration: from *Drosophila* to vertebrates. Development 146, dev167643. https://doi.org/10.1242/dev.167643

Heun, P., Erhardt, S., Blower, M.D., Weiss, S., Skora, A.D., Karpen, G.H., 2006. Mislocalization of the drosophila centromere-specific histone CID promotes formation of functional ectopic kinetochores. Dev. Cell 10, 303–315. https://doi.org/10.1016/j.devcel.2006.01.014

Horvitz, H.R., Herskowitz, I., 1992. Mechanisms of asymmetric cell division: Two Bs or not two Bs, that is the question. Cell. https://doi.org/10.1016/0092-8674(92)90468-R

Hsu, H.J., LaFever, L., Drummond-Barbosa, D., 2008. Diet controls normal and tumorous

germline stem cells via insulin-dependent and -independent mechanisms in Drosophila. Dev. Biol. 313, 700–712. https://doi.org/10.1016/j.ydbio.2007.11.006

Huynh, J.-R., 2007. Fusome as a Cell-Cell Communication Channel of Drosophila Ovarian Cyst, in: Cell-Cell Channels. Landes Bioscience, pp. 217–235. https://doi.org/10.1007/978-0-387-46957-7_16

Ikeno, M., Grimes, B., Okazaki, T., Nakano, M., Saitoh, K., Hoshino, H., McGill, N.I., Cooke, H., Masumoto, H., 1998. Construction of YAC-based mammalian artificial chromosomes. Nat. Biotechnol. 16, 431–439. https://doi.org/10.1038/nbt0598-431

Issigonis, M., Tulina, N., de Cuevas, M., Brawley, C., Sandler, L., Matunis, E., 2009. JAK-STAT Signal Inhibition Regulates Competition in the Drosophila Testis Stem Cell Niche. Science. 326, 153–156. https://doi.org/10.1126/science.1176817

Iwata-Otsubo, A., Dawicki-McKenna, J.M., Akera, T., Falk, S.J., Chmátal, L., Yang, K., Sullivan, B.A., Schultz, R.M., Lampson, M.A., Black, B.E., 2017. Expanded Satellite Repeats Amplify a Discrete CENP-A Nucleosome Assembly Site on Chromosomes that Drive in Female Meiosis. Curr. Biol. 27, 2365-2373.e8. https://doi.org/10.1016/j.cub.2017.06.069

Izuta, H., Ikeno, M., Suzuki, N., Tomonaga, T., Nozaki, N., Obuse, C., Kisu, Y., Goshima, N., Nomura, F., Nomura, N., Yoda, K., 2006. Comprehensive analysis of the ICEN (Interphase Centromere Complex) components enriched in the CENP-A chromatin of human cells. Genes to Cells 11, 673–684. https://doi.org/10.1111/j.1365-2443.2006.00969.x

Jain, M., Olsen, H.E., Turner, D.J., Stoddart, D., Bulazel, K. V, Paten, B., Haussler, D., Willard, H.F., Akeson, M., Miga, K.H., 2018. Linear assembly of a human centromere on the y chromosome. Nat. Biotechnol. 36, 321–323. https://doi.org/10.1038/nbt.4109

Jansen, L.E.T., Black, B.E., Foltz, D.R., Cleveland, D.W., 2007. Propagation of centromeric chromatin requires exit from mitosis. J. Cell Biol. 176, 795–805. https://doi.org/10.1083/jcb.200701066

Januschke, J., Llamazares, S., Reina, J., Gonzalez, C., 2011. Drosophila neuroblasts retain the daughter centrosome. Nat. Commun. 2, 243. https://doi.org/10.1038/ncomms1245

K. Subramaniam, G. Seydoux, 1999. nos-1 and nos-2, two genes related to Drosophila nanos, regulate primordial germ cell development and survival in Caenorhabditis elegans. Development 126, 4861–4871.

Kao, S.H., Tseng, C.Y., Wan, C.L., Su, Y.H., Hsieh, C.C., Pi, H., Hsu, H.J., 2015. Aging and insulin signaling differentially control normal and tumorous germline stem cells. Aging Cell 14, 25–34. https://doi.org/10.1111/acel.12288

Kato, H., Jiang, J., Zhou, B.R., Rozendaal, M., Feng, H., Ghirlando, R., Xiao, T.S., Straight, A.F., Bai, Y., 2013. A conserved mechanism for centromeric nucleosome recognition by centromere protein CENP-C. Science. 340, 1110–1113. https://doi.org/10.1126/science.1235532

Kirilly, D., Xie, T., 2007. The Drosophila ovary: An active stem cell community. Cell Res. https://doi.org/10.1038/sj.cr.7310123

Kixmoeller, K., Allu, P.K., Black, B.E., 2020. The centromere comes into focus: from CENP-A

nucleosomes to kinetochore connections with the spindle. Open Biol. 10, 1–21. https://doi.org/10.1098/rsob.200051

Klare, K., Weir, J.R., Basilico, F., Zimniak, T., Massimiliano, L., Ludwigs, N., Herzog, F., Musacchio, A., 2015. CENP-C is a blueprint for constitutive centromere-associated network assembly within human kinetochores. J. Cell Biol. 210, 11–22. https://doi.org/10.1083/jcb.201412028

Klein, S.J., O'Neill, R.J., 2018. Transposable elements: genome innovation, chromosome diversity, and centromere conflict. Chromosom. Res. https://doi.org/10.1007/s10577-017-9569-5

Kloc, M., Bilinski, S., Dougherty, M.T., Brey, E.M., Etkin, L.D., 2004. Formation, architecture and polarity of female germline cyst in Xenopus. Dev. Biol. 266, 43–61. https://doi.org/10.1016/j.ydbio.2003.10.002

Knoblich, J.A., 2010. Asymmetric cell division: Recent developments and their implications for tumour biology. Nat. Rev. Mol. Cell Biol. https://doi.org/10.1038/nrm3010

Knoblich, J.A., 2008. Mechanisms of Asymmetric Stem Cell Division. Cell. https://doi.org/10.1016/j.cell.2008.02.007

Köprunner, M., Thisse, C., Thisse, B., Raz, E., 2001. A zebrafish nanos-related gene is essential for the development of primordial germ cells. Genes Dev. 15, 2877–2885. https://doi.org/10.1101/gad.212401

Kunert, N., Marhold, J., Stanke, J., Stach, D., Lyko, F., 2003. Development. Development 118, 401–415. https://doi.org/8223268

Lam, A.L., Boivin, C.D., Bonney, C.F., Rudd, M.K., Sullivan, B.A., 2006. Human centromeric chromatin is a dynamic chromosomal domain that can spread over noncentromeric DNA. Proc. Natl. Acad. Sci. U. S. A. 103, 4186–4191. https://doi.org/10.1073/pnas.0507947103

Lampson, M.A., Black, B.E., 2017. Cellular and Molecular Mechanisms of Centromere Drive. Cold Spring Harb. Symp. Quant. Biol. 82, 249–257. https://doi.org/10.1101/sqb.2017.82.034298

Lange, C., Calegari, F., 2010. Cdks and cyclins link G1 length and differentiation of embryonic, neural and hematopoietic stem cells. Cell Cycle. https://doi.org/10.4161/cc.9.10.11598

Lanini, L., McKeon, F., 2017. Domains required for CENP-C assembly at the kinetochore. https://doi.org/10.1091/mbc.6.8.1049. https://doi.org/10.1091/MBC.6.8.1049

Lansdorp, P.M., 2007. Immortal Strands? Give Me a Break. Cell 129, 1244–1247. https://doi.org/10.1016/j.cell.2007.06.017

Lansdorp, P.M., Falconer, E., Tao, J., Brind'Amour, J., Naumann, U., 2012. Epigenetic differences between sister chromatids? Ann. N. Y. Acad. Sci. 1266, 1–6. https://doi.org/10.1111/j.1749-6632.2012.06505.x

Lee, S.H., Itkin-Ansari, P., Levine, F., 2010. CENP-A, a protein required for chromosome segregation in mitosis, declines with age in islet but not exocrine cells. Aging (Albany. NY). 2, 785–790. https://doi.org/10.18632/aging.100220

Lehmann, R., 2012. Germline stem cells: Origin and destiny. Cell Stem Cell.

https://doi.org/10.1016/j.stem.2012.05.016

Liu, S.T., Rattner, J.B., Jablonski, S.A., Yen, T.J., 2006. Mapping the assembly pathways that specify formation of the trilaminar kinetochore plates in human cells. J. Cell Biol. 175, 41–53. https://doi.org/10.1083/jcb.200606020

Liu, X., McLeod, I., Anderson, S., Yates, J.R., He, X., 2005. Molecular analysis of kinetochore architecture in fission yeast. EMBO J. 24, 2919–2930. https://doi.org/10.1038/sj.emboj.7600762

Liu, Y., Ge, Q., Chan, B., Liu, H., Singh, S.R., Manley, J., Lee, J., Weideman, A.M., Hou, G., Hou, S.X., 2016. Whole-animal genome-wide RNAi screen identifies networks regulating male germline stem cells in Drosophila. Nat. Commun. 7, 12149. https://doi.org/10.1038/ncomms12149

Losick, V.P., Morris, L.X., Fox, D.T., Spradling, A., 2011. Drosophila Stem Cell Niches: A Decade of Discovery Suggests a Unified View of Stem Cell Regulation. Dev. Cell 21, 159–171. https://doi.org/10.1016/J.DEVCEL.2011.06.018

Luger, K., Mäder, A.W., Richmond, R.K., Sargent, D.F., Richmond, T.J., 1997. Crystal structure of the nucleosome core particle at 2.8 Å resolution. Nature 389, 251–260. https://doi.org/10.1038/38444

Ma, B., Trieu, T.J., Cheng, J., Zhou, S., Tang, Q., Xie, J., Liu, J.L., Zhao, K., Habib, S.J., Chen, X., 2020. Differential Histone Distribution Patterns in Induced Asymmetrically Dividing Mouse Embryonic Stem Cells. Cell Rep. 32. https://doi.org/10.1016/j.celrep.2020.108003

Maehara, K., Takahashi, K., Saitoh, S., 2010. CENP-A Reduction Induces a p53-Dependent Cellular Senescence Response To Protect Cells from Executing Defective Mitoses. Mol. Cell. Biol. 30, 2090–2104. https://doi.org/10.1128/mcb.01318-09

Maestroni, L., Matmati, S., Coulon, S., 2017. Solving the telomere replication problem. Genes (Basel). https://doi.org/10.3390/genes8020055

Malik, H.S., 2009. The centromere-drive hypothesis: a simple basis for centromere complexity. Prog. Mol. Subcell. Biol. https://doi.org/10.1007/978-3-642-00182-6_2

Malik, H.S., Henikoff, S., 2009. Major Evolutionary Transitions in Centromere Complexity. Cell. https://doi.org/10.1016/j.cell.2009.08.036

Malik, S., Jang, W., Kim, J.Y., Kim, C., 2020. Mechanisms ensuring robust repression of the Drosophila female germline stem cell maintenance factor Nanos via posttranscriptional regulation. FASEB J. https://doi.org/10.1096/fj.202000656R

Manuelidis, L., 1978. Chromosomal localization of complex and simple repeated human DNAs. Chromosoma 66, 23–32. https://doi.org/10.1007/BF00285813

McKearin, D., Ohlstein, B., 1995. A role for the Drosophila Bag-of-marbles protein in the differentiation of cystoblasts from germline stem cells. Development 121, 2937–2947.

McKinley, K.L., Cheeseman, I.M., 2016. The molecular basis for centromere identity and function. Nat. Rev. Mol. Cell Biol. https://doi.org/10.1038/nrm.2015.5

Medina-Pritchard, B., Lazou, V., Zou, J., Byron, O., Abad, M.A., Rappsilber, J., Heun, P., Jeyaprakash, A.A., 2020. Structural basis for centromere maintenance by Drosophila CENP

-A chaperone CAL 1. EMBO J. 39, e103234. https://doi.org/10.15252/embj.2019103234

Mellone, B.G., Grive, K.J., Shteyn, V., Bowers, S.R., Oderberg, I., Karpen, G.H., 2011. Assembly of drosophila centromeric chromatin proteins during mitosis. PLoS Genet. 7, e1002068. https://doi.org/10.1371/journal.pgen.1002068

Meluh, P.B., Koshland, D., 2017. Evidence that the MIF2 gene of Saccharomyces cerevisiae encodes a centromere protein with homology to the mammalian centromere protein CENP-C. https://doi.org/10.1091/mbc.6.7.793. https://doi.org/10.1091/MBC.6.7.793

Mendiburo, M.J., Padeken, J., Fülöp, S., Schepers, A., Heun, P., 2011. Drosophila CENH3 is sufficient for centromere formation. Science. 334, 686–690. https://doi.org/10.1126/science.1206880

Meraldi, P., McAinsh, A.D., Rheinbay, E., Sorger, P.K., 2006. Phylogenetic and structural analysis of centromeric DNA and kinetochore proteins. Genome Biol. 7, R23. https://doi.org/10.1186/gb-2006-7-3-r23

Miga, K.H., Newton, Y., Jain, M., Altemose, N., Willard, H.F., Kent, E.J., 2014. Centromere reference models for human chromosomes X and y satellite arrays. Genome Res. 24, 697–707. https://doi.org/10.1101/gr.159624.113

Milagre, I., Pereira, C., Oliveira, R., Jansen, L., 2020. Reprogramming of Human Cells to Pluripotency Induces CENP-A Chromatin Depletion. Open Biol. 10, 200227. https://doi.org/10.1101/2020.02.21.960252

Morin, X., Bellaïche, Y., 2011. Mitotic Spindle Orientation in Asymmetric and Symmetric Cell Divisions during Animal Development. Dev. Cell. https://doi.org/10.1016/j.devcel.2011.06.012

Morrison, S.J., Kimble, J., 2006. Asymmetric and symmetric stem-cell divisions in development and cancer. Nature 441, 1068–1074. https://doi.org/10.1038/nature04956

Morrison, S.J., Spradling, A.C., 2008. Stem cells and niches: mechanisms that promote stem cell maintenance throughout life. Cell 132, 598–611. https://doi.org/10.1016/j.cell.2008.01.038

Musacchio, A., Desai, A., 2017. A molecular view of kinetochore assembly and function. Biology (Basel). https://doi.org/10.3390/biology6010005

Musich, P.R., Brown, F.L., Maio, J.J., 1980. Highly repetitive component α and related alphoid DNAs in man and monkeys. Chromosoma 80, 331–348. https://doi.org/10.1007/BF00292688

Nakagome, Y., Abe, T., Misawa, S., Takeshita, T., Iinuma, K., 1984. The “loss” of centromeres from chromosomes of aged women. Am. J. Hum. Genet. 36, 398–404.

Nechemia-Arbely, Y., Miga, K.H., Shoshani, O., Aslanian, A., McMahon, M.A., Lee, A.Y., Fachinetti, D., Yates, J.R., Ren, B., Cleveland, D.W., 2019. DNA replication acts as an error correction mechanism to maintain centromere identity by restricting CENP-A to centromeres. Nat. Cell Biol. 21, 743–754. https://doi.org/10.1038/s41556-019-0331-4

Nergadze, S.G., Piras, F.M., Gamba, R., Corbo, M., Cerutti, F., McCarter, J.G.W., Cappelletti, E., Gozzo, F., Harman, R.M., Antczak, D.F., Miller, D., Scharfe, M., Pavesi, G., Raimondi, E., Sullivan, K.F., Giulotto, E., 2018. Birth, evolution, and transmission of satellite-free

mammalian centromeric domains. Genome Res. 28, 789–799. https://doi.org/10.1101/gr.231159.117

Neumüller, R.A., Richter, C., Fischer, A., Novatchkova, M., Neumüller, K.G., Knoblich, J.A., 2011. Genome-wide analysis of self-renewal in Drosophila neural stem cells by transgenic RNAi. Cell Stem Cell 8, 580–593. https://doi.org/10.1016/j.stem.2011.02.022

Ohlstein, B., McKearin, D., 1997. Ectopic expression of the Drosophila Bam protein eliminates oogenic germline stem cells. Development 124, 3651–3662.

Okada, M., Cheeseman, I.M., Hori, T., Okawa, K., McLeod, I.X., Yates, J.R., Desai, A., Fukagawa, T., 2006. The cenp-H–I complex is required for the efficient incorporation of newly synthesized CENP-A into centromeres. Nat. Cell Biol. 8, 446–457. https://doi.org/10.1038/ncb1396

Orford, K.W., Scadden, D.T., 2008. Deconstructing stem cell self-renewal: Genetic insights into cell-cycle regulation. Nat. Rev. Genet. https://doi.org/10.1038/nrg2269

Orr, B., Sunkel, C.E., 2011. Drosophila CENP-C is essential for centromere identity. Chromosoma 120, 83–96. https://doi.org/10.1007/s00412-010-0293-6

Pal, S., Tyler, J.K., 2016. Epigenetics and aging. Sci. Adv. https://doi.org/10.1126/sciadv.1600584

Palladino, J., Chavan, A., Sposato, A., Mason, T.D., Mellone, B.G., 2020. Targeted De Novo Centromere Formation in Drosophila Reveals Plasticity and Maintenance Potential of CENP-A Chromatin. Dev. Cell 52, 379-394.e7. https://doi.org/10.1016/j.devcel.2020.01.005

Palmer, D.K., O'Day, K., Trong, H.L.E., Charbonneau, H., Margolis, R.L., 1991. Purification of the centromere-specific protein CENP-A and demonstration that it is a distinctive histone. Proc. Natl. Acad. Sci. U. S. A. 88, 3734–3738. https://doi.org/10.1073/pnas.88.9.3734

Palmer, D.K., O'Day, K., Wener, M.H., Andrews, B.S., Margolis, R.L., 1987. A 17-kD centromere protein (CENP-A) copurifies with nucleosome core particles and with histones. J. Cell Biol. 104, 805–815. https://doi.org/10.1083/jcb.104.4.805

Pidoux, A.L., Richardson, W., Allshire, R.C., 2003. Sim4: A novel fission yeast kinetochore protein required for centromeric silencing and chromosome segregation. J. Cell Biol. 161, 295–307. https://doi.org/10.1083/jcb.200212110

Politi, V., Perini, G., Trazzi, S., Pliss, A., Raska, I., Earnshaw, W.C., Della Valle, G., 2002. CENP-C binds the alpha-satellite DNA in vivo at specific centromere domains. J. Cell Sci. 115, 2317–2327.

Przewloka, M.R., Venkei, Z., Bolanos-Garcia, V.M., Debski, J., Dadlez, M., Glover, D.M., 2011. CENP-C is a structural platform for kinetochore assembly. Curr. Biol. 21, 399–405. https://doi.org/10.1016/j.cub.2011.02.005

Radford, S.J., Nguyen, A.L., Schindler, K., McKim, K.S., 2017. The chromosomal basis of meiotic acentrosomal spindle assembly and function in oocytes. Chromosoma. https://doi.org/10.1007/s00412-016-0618-1

Ranjan, R., Snedeker, J., Chen, X., 2019. Asymmetric Centromeres Differentially Coordinate

with Mitotic Machinery to Ensure Biased Sister Chromatid Segregation in Germline Stem Cells. Cell Stem Cell 25, 666-681.e5. https://doi.org/10.1016/j.stem.2019.08.014

Rathjen, J., Rathjen, P., 2013. Embryonic Stem Cells, in: Brenner's Encyclopedia of Genetics: Second Edition. Academic Press, pp. 479–481. https://doi.org/10.1016/B978-0-12-374984-0.00490-3

Raychaudhuri, N., Dubruille, R., Orsi, G.A., Bagheri, H.C., Loppin, B., Lehner, C.F., 2012. Transgenerational Propagation and Quantitative Maintenance of Paternal Centromeres Depends on Cid/Cenp-A Presence in Drosophila Sperm. PLoS Biol. 10, e1001434. https://doi.org/10.1371/journal.pbio.1001434

Rebecca Sheng, X., Matunis, E., 2011. Live imaging of the Drosophila spermatogonial stem cell niche reveals novel mechanisms regulating germline stem cell output. Development 138, 3367–3376. https://doi.org/10.1242/dev.065797

Resende, L.P.F., Jones, D.L., 2012. Local signaling within stem cell niches: insights from Drosophila. Curr. Opin. Cell Biol. 24, 225–231. https://doi.org/10.1016/j.ceb.2012.01.004

Rivera, H., Zuffardi, O., Araschio, P.M., Caiulo, A., Anichini, C., Scarinci, R., Vivarelli, R., 1989. Alternate centromere inactivation in a pseudodicentric (15;20)(pter;pter) associated with a progressive neurological disorder. J. Med. Genet. 26, 626–630. https://doi.org/10.1136/jmg.26.10.626

Rivera, T., Haggblom, C., Cosconati, S., Karlseder, J., 2017. A balance between elongation and trimming regulates telomere stability in stem cells. Nat. Struct. Mol. Biol. 24, 30–39. https://doi.org/10.1038/nsmb.3335

Rocchi, M., Archidiacono, N., Schempp, W., Capozzi, O., Stanyon, R., 2012. Centromere repositioning in mammals. Heredity (Edinb). https://doi.org/10.1038/hdy.2011.101

Rocheteau, P., Gayraud-Morel, B., Siegl-Cachedenier, I., Blasco, M.A., Tajbakhsh, S., 2012. A Subpopulation of Adult Skeletal Muscle Stem Cells Retains All Template DNA Strands after Cell Division. Cell 148, 112–125. https://doi.org/10.1016/J.CELL.2011.11.049

Rosin, L., Mellone, B.G., 2016. Co-evolving CENP-A and CAL1 Domains Mediate Centromeric CENP-A Deposition across Drosophila Species. Dev. Cell 37, 136–147. https://doi.org/10.1016/j.devcel.2016.03.021

Roure, V., Medina-Pritchard, B., Lazou, V., Rago, L., Anselm, E., Venegas, D., Jeyaprakash, A.A., Heun, P., 2019. Reconstituting Drosophila Centromere Identity in Human Cells. Cell Rep. 29, 464-479.e5. https://doi.org/10.1016/j.celrep.2019.08.067

Ryder, P. V., Lerit, D.A., 2018. RNA localization regulates diverse and dynamic cellular processes. Traffic. https://doi.org/10.1111/tra.12571

Saitoh, H., Tomkiel, J., Cooke, C.A., Ratrie, H., Maurer, M., Rothfield, N.F., Earnshaw, W.C., 1992. CENP-C, an autoantigen in scleroderma, is a component of the human inner kinetochore plate. Cell 70, 115–125. https://doi.org/10.1016/0092-8674(92)90538-N

Salz, H.K., Dawson, E.P., Heaney, J.D., 2017. Germ cell tumors: Insights from the Drosophila ovary and the mouse testis. Mol. Reprod. Dev. https://doi.org/10.1002/mrd.22779

Salzmann, V., Chen, C., Chiang, C.Y.A., Tiyaboonchai, A., Mayer, M., Yamashita, Y.M., 2014.

Centrosome-dependent asymmetric inheritance of the midbody ring in Drosophila germline stem cell division. Mol. Biol. Cell 25, 267–275. https://doi.org/10.1091/mbc.E13-09-0541

Salzmann, V., Inaba, M., Cheng, J., Yamashita, Y.M., 2013. Lineage tracing quantification reveals symmetric stem cell division in drosophila male germline stem cells. Cell. Mol. Bioeng. 6, 441–448. https://doi.org/10.1007/s12195-013-0295-6

Schittenhelm, R.B., Althoff, F., Heidmann, S., Lehner, C.F., 2010. Detrimental incorporation of excess Cenp-A/Cid and Cenp-C into Drosophila centromeres is prevented by limiting amounts of the bridging factor Cal1. J. Cell Sci. 123, 3768–79. https://doi.org/10.1242/jcs.067934

Schuh, M., Lehner, C.F., Heidmann, S., 2007. Incorporation of Drosophila CID/CENP-A and CENP-C into Centromeres during Early Embryonic Anaphase. Curr. Biol. 17, 237–243. https://doi.org/10.1016/j.cub.2006.11.051

Sekulic, N., Bassett, E.A., Rogers, D.J., Black, B.E., 2010. The structure of (CENP-A-H4) 2 reveals physical features that mark centromeres. Nature 467, 347–351. https://doi.org/10.1038/nature09323

Sen, P., Shah, P.P., Nativio, R., Berger, S.L., 2016. Epigenetic Mechanisms of Longevity and Aging. Cell. https://doi.org/10.1016/j.cell.2016.07.050

Shamblott, M.J., Axelman, J., Wang, S., Bugg, E.M., Littlefield, J.W., Donovan, P.J., Blumenthal, P.D., Huggins, G.R., Gearhart, J.D., 1998. Derivation of pluripotent stem cells from cultured human primordial germ cells. Proc. Natl. Acad. Sci. U. S. A. 95, 13726–13731. https://doi.org/10.1073/pnas.95.23.13726

Sherley, J.L., 2011. Overlooked areas need attention for sound evaluation of DNA strand inheritance patterns in Drosophila male germline stem cells. J. Cell Sci. https://doi.org/10.1242/jcs.096925

Shlyakhtina, Y., Moran, K.L., Portal, M.M., 2019. Asymmetric inheritance of cell fate determinants: Focus on RNA. Non-coding RNA. https://doi.org/10.3390/NCRNA5020038

Shono, N., Ohzeki, J.I., Otake, K., Martins, N.M.C., Nagase, T., Kimura, H., Larionov, V., Earnshaw, W.C., Masumoto, H., 2015. CENP-C and CENP-I are key connecting factors for kinetochore and CENP-A assembly. J. Cell Sci. 128, 4572–4587. https://doi.org/10.1242/jcs.180786

Singh, A.M., Dalton, S., 2009. The Cell Cycle and Myc Intersect with Mechanisms that Regulate Pluripotency and Reprogramming. Cell Stem Cell. https://doi.org/10.1016/j.stem.2009.07.003

Song, X., Wong, M.D., Kawase, E., Xi, R., Ding, B.C., McCarthy, J.J., Xie, T., 2004. Bmp signals from niche cells directly repress transcription of a differentiation-promoting gene, bag of marbles, in germline stem cells in the Drosophila ovary. Development. https://doi.org/10.1242/dev.01026

Spradling, A., Fuller, M.T., Braun, R.E., Yoshida, S., 2011. Germline stem cells. Cold Spring Harb. Perspect. Biol. 3, a002642. https://doi.org/10.1101/cshperspect.a002642

Srivastava, S., Foltz, D.R., 2018. Posttranslational modifications of CENP-A: marks of

distinction. Chromosoma. https://doi.org/10.1007/s00412-018-0665-x

Stellfox, M.E., Bailey, A.O., Foltz, D.R., 2013. Putting CENP-A in its place. Cell. Mol. Life Sci. https://doi.org/10.1007/s00018-012-1048-8

Stevens, N.R., Raposo, A.A.S.F., Basto, R., St Johnston, D., Raff, J.W.W., 2007. From Stem Cell to Embryo without Centrioles. Curr. Biol. 17, 1498–1503. https://doi.org/10.1016/j.cub.2007.07.060

Stine, R.R., Matunis, E.L., 2013. JAK-STAT Signaling in Stem Cells, in: Advances in Experimental Medicine and Biology. pp. 247–267. https://doi.org/10.1007/978-94-007-6621-1_14

Sugimoto, K., Yata, H., Muro, Y., Himeno, M., 1994. Human centromere protein C (cenp-c) is a DNA-binding protein which possesses a novel DNA-binding motif. J. Biochem. 116, 877–881. https://doi.org/10.1093/oxfordjournals.jbchem.a124610

Sullivan, B.A., Karpen, G.H., 2004. Centromeric chromatin exhibits a histone modification pattern that is distinct from both euchromatin and heterochromatin. Nat. Struct. Mol. Biol. 11, 1076–1083. https://doi.org/10.1038/nsmb845

Sullivan, K.F., Hechenberger, M., Masri, K., 1994. Human CENP-A contains a histone H3 related histone fold domain that is required for targeting to the centromere. J. Cell Biol. 127, 581–592. https://doi.org/10.1083/jcb.127.3.581

Swartz, S.Z., McKay, L.S., Su, K.C., Bury, L., Padeganeh, A., Maddox, P.S., Knouse, K.A., Cheeseman, I.M., 2019. Quiescent Cells Actively Replenish CENP-A Nucleosomes to Maintain Centromere Identity and Proliferative Potential. Dev. Cell 51, 35-48.e7. https://doi.org/10.1016/j.devcel.2019.07.016

Tachiwana, H., Kagawa, W., Shiga, T., Osakabe, A., Miya, Y., Saito, K., Hayashi-Takanaka, Y., Oda, T., Sato, M., Park, S.Y., Kimura, H., Kurumizaka, H., 2011. Crystal structure of the human centromeric nucleosome containing CENP-A. Nature. https://doi.org/10.1038/nature10258

Takahashi, K., Yamanaka, S., 2006. Induction of Pluripotent Stem Cells from Mouse Embryonic and Adult Fibroblast Cultures by Defined Factors. Cell 126, 663–676. https://doi.org/10.1016/j.cell.2006.07.024

Takayama, S., Dhahbi, J., Roberts, A., Mao, G., Heo, S.-J., Pachter, L., Martin, D.I.K., Boffelli, D., 2014. Genome methylation in D. melanogaster is found at specific short motifs and is independent of DNMT2 activity. Genome Res. 24, 821. https://doi.org/10.1101/GR.162412.113

Thomson, J.A., 1998. Embryonic stem cell lines derived from human blastocysts. Science. 282, 1145–1147. https://doi.org/10.1126/science.282.5391.1145

Thorpe, P.H., Bruno, J., Rothstein, R., 2009. Kinetochore asymmetry defines a single yeast lineage. Proc. Natl. Acad. Sci. U. S. A. 106, 6673–6678. https://doi.org/10.1073/pnas.0811248106

Tran, V., Feng, L., Chen, X., 2013. Asymmetric distribution of histones during Drosophila male germline stem cell asymmetric divisions. Chromosom. Res. 21, 255–269.

https://doi.org/10.1007/s10577-013-9356-x

Tran, V., Lim, C., Xie, J., Chen, X., 2012. Asymmetric division of Drosophila male germline stem cell shows asymmetric histone distribution. Science. 338, 679–682. https://doi.org/10.1126/science.1226028

Trazzi, S., Perini, G., Bernardoni, R., Zoli, M., Reese, J.C., Musacchio, A., Della Valle, G., 2009. The C-terminal domain of CENP-C displays multiple and critical functions for mammalian centromere formation. PLoS One 4, e5832. https://doi.org/10.1371/journal.pone.0005832

Trojer, P., Reinberg, D., 2007. Facultative Heterochromatin: Is There a Distinctive Molecular Signature? Mol. Cell. https://doi.org/10.1016/j.molcel.2007.09.011

Tsuda, M., Sasaoka, Y., Kiso, M., Abe, K., Haraguchi, S., Kobayashi, S., Saga, Y., 2003. Conserved role of nanos proteins in germ cell development. Science. 301, 1239–1241. https://doi.org/10.1126/science.1085222

Unhavaithaya, Y., Orr-Weaver, T.L., 2013. Centromere proteins CENP-C and CAL1 functionally interact in meiosis for centromere clustering, pairing, and chromosome segregation. Proc. Natl. Acad. Sci. 110, 19878–19883. https://doi.org/10.1073/pnas.1320074110

Valdivia, M.M., Brinkley, B.R., 1985. Fractionation and initial characterization of the kinetochore from mammalian metaphase chromosomes. J. Cell Biol. 101, 1124–1134. https://doi.org/10.1083/jcb.101.3.1124

Venkei, Z.G., Yamashita, Y.M., 2018. Emerging mechanisms of asymmetric stem cell division. J. Cell Biol. https://doi.org/10.1083/jcb.201807037

Verdaasdonk, J.S., Bloom, K., 2011. Centromeres: Unique chromatin structures that drive chromosome segregation. Nat. Rev. Mol. Cell Biol. https://doi.org/10.1038/nrm3107

Vermaak, D., Hayden, H.S., Henikoff, S., 2002. Centromere Targeting Element within the Histone Fold Domain of Cid. Mol. Cell. Biol. 22, 7553–7561. https://doi.org/10.1128/mcb.22.21.7553-7561.2002

Voullaire, L., Saffery, R., Earle, E., Irvine, D. V., Slater, H., Dale, S., Sart, D. Du, Fleming, T., Andy Choo, K.H., 2001. Mosaic inv dup(8p) marker chromosome with stable neocentromere suggests neocentromerization is a post-zygotic event. Am. J. Med. Genet. 102, 86–94. https://doi.org/10.1002/1096-8628(20010722)102:1<86::AID-AJMG1390>3.0.CO;2-T

Wang, Z., Lin, H., 2004. Nanos Maintains Germline Stem Cell Self-Renewal by Preventing Differentiation. Science. 303, 2016–2019. https://doi.org/10.1126/science.1093983

Warburton, P.E., Cooke, C.A., Bourassa, S., Vafa, O., Sullivan, B.A., Stetten, G., Gimelli, G., Warburton, D., Tyler-Smith, C., Sullivan, K.F., Poirier, G.G., Earnshaw, W.C., 1997. Immunolocalization of CENP-A suggests a distinct nucleosome structure at the inner kinetochore plate of active centromeres. Curr. Biol. 7, 901–904. https://doi.org/10.1016/S0960-9822(06)00382-4

Waugh O'Neill, R.J., O'Neill, M.J., Marshall Graves, J.A., 1998. Undermethylation associated with retroelement activation and chromosome remodelling in an interspecific mammalian hybrid. Nature 393, 68–72. https://doi.org/10.1038/29985

Westhorpe, F.G., Straight, A.F., 2013. Functions of the centromere and kinetochore in chromosome segregation. Curr. Opin. Cell Biol. https://doi.org/10.1016/j.ceb.2013.02.001

Whole genome - Homo sapiens - Ensembl genome browser 99 [WWW Document], 2019. URL http://jan2020.archive.ensembl.org/Homo_sapiens/Location/Genome?r=1:1-1000000 (accessed 5.17.20).

Wiegmann, B.M., Trautwein, M.D., Winkler, I.S., Barr, N.B., Kim, J.W., Lambkin, C., Bertone, M.A., Cassel, B.K., Bayless, K.M., Heimberg, A.M., Wheeler, B.M., Peterson, K.J., Pape, T., Sinclair, B.J., Skevington, J.H., Blagoderov, V., Caravas, J., Kutty, S.N., Schmidt-Ott, U., Kampmeier, G.E., Thompson, F.C., Grimaldi, D.A., Beckenbach, A.T., Courtney, G.W., Friedrich, M., Meier, R., Yeates, D.K., 2011. Episodic radiations in the fly tree of life. Proc. Natl. Acad. Sci. U. S. A. 108, 5690–5695. https://doi.org/10.1073/pnas.1012675108

Wooten, M., Ranjan, R., Chen, X., 2019a. Asymmetric Histone Inheritance in Asymmetrically Dividing Stem Cells. Trends Genet. 36, 30–43. https://doi.org/10.1016/j.tig.2019.10.004

Wooten, M., Snedeker, J., Nizami, Z.F., Yang, X., Ranjan, R., Urban, E., Kim, J.M., Gall, J., Xiao, J., Chen, X., 2019b. Asymmetric histone inheritance via strand-specific incorporation and biased replication fork movement. Nat. Struct. Mol. Biol. 26, 732–743. https://doi.org/10.1038/s41594-019-0269-z

Xiao, H., Wang, F., Wisniewski, J., Shaytan, A.K., Ghirlando, R., Fitzgerald, P.C., Huang, Y., Wei, D., Li, S., Landsman, D., Panchenko, A.R., Wu, C., 2017. Molecular basis of CENP-C association with the CENP-A nucleosome at yeast centromeres. Genes Dev. 31, 1958–1972. https://doi.org/10.1101/gad.304782.117

Xie, J., Wooten, M., Tran, V., Chen, B.C., Pozmanter, C., Simbolon, C., Betzig, E., Chen, X., 2015. Histone H3 Threonine Phosphorylation Regulates Asymmetric Histone Inheritance in the Drosophila Male Germline. Cell 163, 920–933. https://doi.org/10.1016/j.cell.2015.10.002

Yadav, V., Sun, S., Billmyre, R.B., Thimmappa, B.C., Shea, T., Lintner, R., Bakkeren, G., Cuomo, C.A., Heitman, J., Sanyal, K., 2018. RNAi is a critical determinant of centromere evolution in closely related fungi. Proc. Natl. Acad. Sci. U. S. A. 115, 3108–3113. https://doi.org/10.1073/pnas.1713725115

Yadlapalli, S., Cheng, J., Yamashita, Y.M., 2011a. Drosophila male germline stem cells do not asymmetrically segregate chromosome strands. J. Cell Sci. 124, 933–939. https://doi.org/10.1242/jcs.079798

Yadlapalli, S., Cheng, J., Yamashita, Y.M., 2011b. Reply to: Overlooked areas need attention for sound evaluation of DNA strand inheritance patterns in Drosophila male germline stem cells. J. Cell Sci. https://doi.org/10.1242/jcs.097949

Yadlapalli, S., Yamashita, Y.M., 2013. Chromosome-specific nonrandom sister chromatid segregation during stem-cell division. Nature 498, 251–254. https://doi.org/10.1038/nature12106

Yamashita, Y.M., Mahowald, A.P., Perlin, J.R., Fuller, M.T., 2007. Asymmetric inheritance of mother versus daughter centrosome in stem cell division. Science. 315, 518–521.

https://doi.org/10.1126/science.1134910

Yan, D., Neumüller, R.A., Buckner, M., Ayers, K., Li, H., Hu, Y., Yang-Zhou, D., Pan, L., Wang, X., Kelley, C., Vinayagam, A., Binari, R., Randklev, S., Perkins, L.A., Xie, T., Cooley, L., Perrimon, N., 2014. A regulatory network of Drosophila germline stem cell self-renewal. Dev. Cell 28, 459–473. https://doi.org/10.1016/j.devcel.2014.01.020

Yoda, K., Ando, S., Morishita, S., Houmura, K., Hashimoto, K., Takeyasu, K., Okazaki, T., 2000. Human centromere protein A (CENP-A) can replace histone H3 in nucleosome reconstitution in vitro. Proc. Natl. Acad. Sci. U. S. A. 97, 7266–7271. https://doi.org/10.1073/pnas.130189697

Zemach, A., McDaniel, I.E., Silva, P., Zilberman, D., 2010. Genome-Wide Evolutionary Analysis of Eukaryotic DNA Methylation. Science. 328, 916–919. https://doi.org/10.1126/SCIENCE.1186366

Zeng, X., Han, L., Singh, S.R., Liu, H., Neumüller, R.A., Yan, D., Hu, Y., Liu, Y., Liu, W., Lin, X., Hou, S.X., 2015. Genome-wide RNAi screen identifies networks involved in intestinal stem cell regulation in Drosophila. Cell Rep. 10, 1226–38. https://doi.org/10.1016/j.celrep.2015.01.051

Zhang, J., Li, L., 2005. BMP signaling and stem cell regulation. Dev. Biol. 284, 1–11. https://doi.org/10.1016/J.YDBIO.2005.05.009

Zhang, W., Friebe, B., Gill, B.S., Jiang, J., 2010. Centromere inactivation and epigenetic modifications of a plant chromosome with three functional centromeres. Chromosoma 119, 553–563. https://doi.org/10.1007/s00412-010-0278-5

Zhang, W., Li, J., Suzuki, K., Qu, J., Wang, P., Zhou, J., Liu, X., Ren, R., Xu, X., Ocampo, A., Yuan, T., Yang, J., Li, Y., Shi, L., Guan, D., Pan, H., Duan, S., Ding, Z., Li, M., Yi, F., Bai, R., Wang, Y., Chen, C., Yang, F., Li, X., Wang, Z., Aizawa, E., Goebl, A., Soligalla, R.D., Reddy, P., Esteban, C.R., Tang, F., Liu, G.H., Belmonte, J.C.I., 2015. A Werner syndrome stem cell model unveils heterochromatin alterations as a driver of human aging. Science. 348, 1160–1163. https://doi.org/10.1126/science.aaa1356

Zhao, X., Moore, D.L., 2018. Neural stem cells: developmental mechanisms and disease modeling. Cell Tissue Res. https://doi.org/10.1007/s00441-017-2738-1

8. Appendices

8.1 Chemical Reagents and Common Buffers

Reagent	Composition	Note
Immunostaining		
1X PBS	1X Phosphate-Buffered Saline (157 mM Na+, 140mM Cl−, 4.45mM K+, 10.1 mM HPO42−, 1.76 mM H2PO4−)	
4% Paraformaldehyde (Fixation)	4 % (v/v) paraformaldehyde in 1X PBS	Fixation timing is highly antibody dependant. Anti-SMAD3 requires 5 mins fixation. Anti-CAL1 requires 30 mins. Standard fixation timing is 15 mins.
IF Wash Buffer (0.4 % PBST)	1X PBS with 0.4 % (v/v) Triton-X	
Blocking Buffer (1-5% Bovine Serum Albumin)	1-5% (w/v) Bovine Serum Albumin (BSA) in 0.4 % PBST	Make fresh every 2 days
DAPI Staining Buffer	1X PBS with 1µg/ml DAPI	10 mins incubation followed by 20 min wash with 0.4 % PBST
Mounting Media	30 µl per slide	Invitrogen SlowFade™ Gold Antifade Mountant
Click Chemistry		
5-Ethynyl-2´-deoxyuridine (EdU) (0.01 mM)	1 µl 10 mM EdU in 1 mL 1X PBS	Incubate samples for 45 mins before fixation
Copper (II) Sulphate	0.1 M $CuSO_4$	
(+)-Sodium L-ascorbate	1 M Sodium L-ascorbate	Make fresh every few months. Ascorbic acid turns yellow when oxidised with air.
6-Carboxyfluorescein-TEG azide (Berry and Associates)	Dissolved 1 mg/mL in DMSO	
Cyanine 3 TEG azide (Berry and Associates)	Dissolved 1 mg/mL in DMSO	

Single Fly DNA Preparation		
Squishing Buffer	10 mM Tris-HCl, 1 mM EDTA, 25 mM NaCl, 0.2 mg/ml Proteinase K in dH_20	Add Proteinase K right before use

8.2 Fly Stocks used during this study

Genotype	**Gene**	**Source**	**Balancer**	**Construct Type/Function**	**Target Regions**	**Reference**
Oregon-R-modENCODE	*(wild type)*	BDSC_25211	n/a	n/a	n/a	
y[1] v[1]; P{y[+t7.7]=CaryP}attP2	(RNAi isogenic control)	BDSC_36303	n/a	n/a	n/a	
P{w[+mC]=UAS-Dcr-2.D}1, w[1118]; P{w[+mC]=GAL4-nos.NGT}40	*nanos*	BDSC_25751	n/a	GAL4	n/a	
bam-GAL4:VP16}1	*bam*	M. Fuller	n/a	GAL4	n/a	
y[1] sc[*] v[1] sev[21]; P{y[+t7.7] v[+t1.8]=TRiP.GL00689}attP2	*Cenp-C*			dsRNA, 2nd Generation, Valium22. TRiP Germline	Cenp-$C^{GL00689}$ (5'UTR)	
UASp-HA-CENP-C	*Cenp-C*	K. McKim	SM6, Cy	UASp	n/a	
Cenp-C^{IR35}	*Cenp-C*	T. Orr-Weaver	TM3, Sb	n/a	n/a	(Unhavaithaya and Orr-Weaver, 2013)

UASp-HA-CENP-C; P{y[+t7.7] v[+t1.8]=TRiP.GL00689}attP2	*Cenp-C*	This Study	CyO; Dr	dsRNA, 2nd Generation, Valium22. TRiP Germline; UASp	Cenp-C^{GL00689} (5'UTR)	
cal1^{2K32}	*cal1*	T. Orr-Weaver	TM3, Sb	n/a		(Unhavaithaya and Orr-Weaver, 2013)
y[1] w[*]; wg[Sp-1]/CyO; Dr[1]/TM3, Sb[1]	-	BDSC_59967	*wg[Sp-1]/CyO; Dr/TM3, Sb*	Double Balancer	n/a	

8.3 List of Primary Antibodies

Target	Antibody Description	Product Identifier	Concentration
CENP-A (CID)	Rabbit pAb (Active Motif)	#39719	1/1000
CENP-C	Sheep pAb (Dunleavy Lab)	n/a	1/2000
hu-li tai shao (Hts)	Mouse mAb (Developmental Studies Hybridoma Bank)	1B1	1/500
VASA	Rabbit mAb (Santa Cruz Biotechnologies)		1/500
VASA	Rat mAb (Developmental Studies Hybridoma Bank)	Vas	1/500
Histone H3 (phospho S10)	Mouse pAb	ab14955	1/1000
HA	Mouse mAb (Lowndes Lab)	n/a	1/500
CAL1	Rabbit mAb (Erhardt Lab; (Erhardt et al., 2008))	n/a	1/1000
Anti-Smad3 (phospho S423 + S425) (pMad)	Rabbit mAb (Abcam)	ab52903	1/1000
SEX-LETHAL	Mouse mAb (Developmental Studies Hybridoma Bank)	M114	1/500
4′,6-diamidino-2-phenylindole (DAPI)	n/a	D1306	1 mg/mL stock

8.4 List of Secondary Antibodies

Target	Antibody Description	Product Identifier	Concentration
Mouse IgG	Goat Anti-Mouse Alexa Fluor 488 (Life Technologies)	A-11029	1/500
Mouse IgG	Goat Anti-Mouse Alexa Fluor 546 (Life Technologies)	A-11030	1/500
Mouse IgG	Goat Anti-Mouse Alexa Fluor 647 (Life Technologies)	A-21236	1/500
Rabbit IgG	Goat Anti-Rabbit Alexa Fluor 488 (Life Technologies)	A-11034	1/500
Rabbit IgG	Goat Anti-Rabbit Alexa Fluor 546 (Life Technologies)	A-11035	1/500
Rabbit IgG	Goat Anti-Rabbit Cyanine 5 (Invitrogen)	A-10523	1/500
Rat IgG	Goat Anti-Rat Alexa Fluor 546 (Life Technologies)	A-11081	1/500
Sheep IgG	Donkey Anti-Sheep Alexa Fluor 546 (Life Technologies)	A-21098	1/500
Sheep IgG	Donkey Anti-Sheep Alexa Fluor 647 (Life Technologies)	A-21448	1/500
Mouse IgG	Donkey Anti-Mouse Alexa Fluor 488 (Life Technologies)	A-21202	1/500
Mouse IgG	Donkey Anti-Mouse Alexa Fluor 546 (Life Technologies)	A-10036	1/500
Rabbit IgG	Donkey Anti-Rabbit Alexa Fluor 488 (Life Technologies)	A-21206	1/500
Rabbit IgG	Donkey Anti-Rabbit Alexa Fluor 546 (Life Technologies)	A-10040	1/500

8.5 Ben L. Carty and Elaine M. Dunleavy, 2020

Ben L. Carty, Elaine M. Dunleavy; Centromere assembly and non-random sister chromatid segregation in stem cells. *Essays Biochem* 4 September 2020; 64 (2): 223–232. doi: https://doi.org/10.1042/EBC20190066

Essays in Biochemistry (2020) **00** 1–10
https://doi.org/10.1042/EBC20190066

Review Article

Centromere assembly and non-random sister chromatid segregation in stem cells

Ben L. Carty and Elaine M. Dunleavy

Centre for Chromosome Biology, Biomedical Sciences, National University of Ireland Galway, Galway H91 W2TY, Ireland

Correspondence: Elaine M. Dunleavy (elaine.dunleavy@nuigalway.ie)

Asymmetric cell division (ACD) produces daughter cells with separate distinct cell fates and is critical for the development and regulation of multicellular organisms. Epigenetic mechanisms are key players in cell fate determination. Centromeres, epigenetically specified loci defined by the presence of the histone H3-variant, centromere protein A (CENP-A), are essential for chromosome segregation at cell division. ACDs in stem cells and in oocyte meiosis have been proposed to be reliant on centromere integrity for the regulation of the non-random segregation of chromosomes. It has recently been shown that CENP-A is asymmetrically distributed between the centromeres of sister chromatids in male and female *Drosophila* germline stem cells (GSCs), with more CENP-A on sister chromatids to be segregated to the GSC. This imbalance in centromere strength correlates with the temporal and asymmetric assembly of the mitotic spindle and potentially orientates the cell to allow for biased sister chromatid retention in stem cells. In this essay, we discuss the recent evidence for asymmetric sister centromeres in stem cells. Thereafter, we discuss mechanistic avenues to establish this sister centromere asymmetry and how it ultimately might influence cell fate.

Introduction

Asymmetric cell division in stem cells

The asymmetric nature of a stem cell is fundamental to the development of diverse multicellular organisms and stem cell maintenance throughout adult life. In this sense, asymmetric cell division (ACD) allows for organism complexity by generating and maintaining diverse and specialised cell types. Examples of such include haematopoietic stem cells facilitating haematopoiesis of blood cells [1], and gametogenesis made possible by germline stem cells (GSCs) that divide asymmetrically in the gonads [2,3]. Moreover, ACD is not limited to stem cells, as meiosis is also an inherently asymmetric process [4,5]. ACD generates two distinct cell fates in these cell types. Stem cells divide asymmetrically to produce a daughter cell that self-renews as well as a differentiating daughter cell. Similarly, female meiosis produces the oocyte and polar bodies. These ACDs ultimately present unique biological challenges. Disruption to this balance of self-renewal versus differentiation, and/or gametogenesis, is detrimental to normal tissue homoeostasis and contributes towards the aetiology of diseases such as cancer and potentially infertility [6–8].

Stem cells regulate these distinct cell fate decisions both intrinsically and extrinsically. The stem cell microenvironment, or niche, plays a powerful role in regulating the extrinsic signalling factors that allow the stem cell to make cell fate decisions [9–11]. Signalling ligands, through, e.g. bone morphogenic protein (BMP) and Janus kinase signal transducers and activators of transcription (JAK/STAT) pathways, are well characterised and heavily influence stem cell division from the niche [12–15].

Received: 18 March 2020
Revised: 21 April 2020
Accepted: 30 April 2020

Version of Record published:
00 xx 00

Essays in Biochemistry (2020) **00** 1–10
https://doi.org/10.1042/EBC20190066

Intrinsic processes have also been extensively studied, mostly pertaining to asymmetric protein/ribonucleic acid (RNA) localisation and cell polarity, differences which ultimately impact gene expression [16–18]. Epigenetics encompasses the heritable changes in gene expression that do not alter the original genetic code. Epigenetic mechanisms inform the transcriptional status of daughter cells, providing additional methods to alter cell fate. To carry this so-called 'epigenetic memory' from one cell division to the next, the parental chromatin needs to be inherited along with the duplicated deoxyribonucleic acid (DNA) sequence. The centromere is the primary constriction site of the chromosome and is essential for faithful chromosome segregation at cell division. The centromere itself is epigenetically specified by the histone H3 variant, centromere protein A (CENP-A), providing a structural framework for the efficient inheritance of chromosomes at cell division. In the case of a stem cell, it is postulated that the epigenetic landscape between sister chromatids differ, and in particular at centromeres [19,20]. The incorporation of a histone variant such as CENP-A or the post-translational modification of histones might potentially serve as epigenetic marks that distinguish sister centromeres and chromatids [19–21]. In this mini-review, we discuss the assembly of the centromere as a paradigm of epigenetic inheritance in ACD in stem cells, mechanisms of how sister centromere asymmetry may arise, and possible impacts on cell fate.

Non-random chromosome segregation

Non-random chromosome segregation is a phenomenon in which two supposedly identical sister chromatids can be distinguished and one sister chromatid is selectively segregated towards a specific daughter cell. The non-random segregation of sister chromatids has previously been observed in certain stem cell subpopulations [22–24]. In 1975, Cairns [25] originally proposed the immortal strand hypothesis as a method of explaining this phenomenon. The hypothesis assumes that adult stem cells retain the parental, older, template DNA as a protective measure to limit the accumulation of aberrant mutations arising from erroneous DNA replication [25]. Although not widely accepted, this hypothesis proved quite resistant to challenge due to limitations in methods available to robustly test it. However, reconciling this hypothesis with our current understanding of DNA repair, stem cell turnover and the overall organisation of the genome it now appears an unlikely prospect [26]. Moreover, studies in the well-established *Drosophila* GSC system further oppose this hypothesis, concluding that immortal stands are not exhibited by these cells [27–30].

The silent sister chromatid hypothesis, proposed by Lansdorp [26] in 2007, may help better explain non-random chromosome segregation. This hypothesis states that ACD and cell fate decisions are orchestrated by epigenetic differences between sister chromatids. Indeed, evidence for epigenetically distinct sister chromatids is now emerging, again in *Drosophila*. In male GSCs, pre-existing (parental) histones H3 and H4 are selectively retained, whereas newly synthesised H3 and H4 are segregated to the daughter cell [31,32]. Furthermore, there is evidence for the selective retention of post-translationally modified histone H3 at threonine 3 (H3T3P) in GSCs [33].

It has also been reported that pre-existing (parental) CENP-A, the histone H3-variant that defines the centromere [34], is similarly retained by GSCs and intestinal stem cells (ISCs) [35,36]. Recent studies from the Chen and Dunleavy laboratories have implicated the centromere in the control of non-random sister chromatid segregation in both male and female Drosophila GSCs [35,37]. Both studies show that more CENP-A is present on sister chromatids of the future GSC. Furthermore, the asymmetric distribution of CENP-A correlates with an asymmetric distribution of kinetochore proteins and microtubules. Both studies propose that these asymmetries might ultimately bias sister chromatid segregation (Figure 1). In addition, Dattoli et al. [37] showed that disruption of sister centromere asymmetry changes the balance of stem versus daughter cell. Here, disruption to the centromeric core possibly regulates cell fate decisions by maintaining stem cells in a self-renewing state [37].

Sister centromere asymmetry in non-random chromosome segregation

Centromeres constitute the primary constriction site of a chromosome and form the chromatin landscape to which the kinetochore assembles and microtubules subsequently attach [38]. Hence, the centromere is the foundation for faithful chromosome segregation in a dividing cell. Stem cell divisions are asymmetrically orientated by means of both cell and spindle polarity [39–42]. Similarly, oocytes display asymmetric cell and spindle polarities [43], as well as centromere asymmetries [44,45], proposed to bias chromosome segregation in meiosis [44,46,47]. Hence, it is conceivable that differences in centromere strength between individual sister chromatids might drive stem cell identity by directing non-random sister chromatid segregation.

Asymmetric distribution of kinetochore proteins was first observed in budding yeast post-meiotic lineages [48]. Studies by Ranjan et al. [35] and Dattoli et al. [37] have now shown that in both male and female Drosophila GSCs, future stem cell centromeres are 'stronger'. Specifically, sister chromatids retained in the stem cell contain 1.2–1.4-fold more CENP-A and harbour stronger kinetochores, measured for centromere protein C (CENP-C) and NDC80 [35,37]. Stronger centromeres and kinetochores correlate with the emanation of more microtubules on the

Essays in Biochemistry (2020) **00** 1–10
https://doi.org/10.1042/EBC20190066

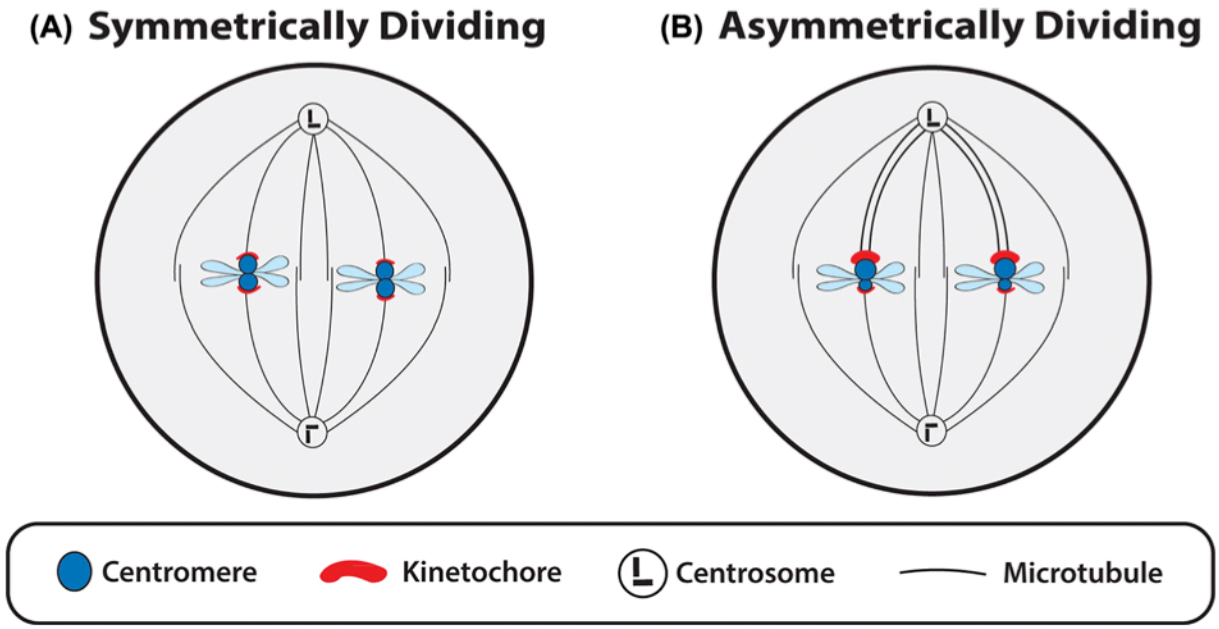

Figure 1. Centromere and spindle configurations in a symmetrically versus asymmetrically dividing mitotic cell

(**A**) Metaphase of a canonical symmetrically dividing mitotic cell (e.g. HeLa cell). The centromere proteins (blue) are assembled equally between sister chromatids. The kinetochores (red) capture the mitotic spindle equally. (**B**) Metaphase of an asymmetrically dividing mitotic cell (e.g. *Drosophila* GSC). The centromere and kinetochore proteins are assembled in an asymmetric manner between sister chromatids. Stronger centromeres capture more spindle fibres, leading to non-random sister chromatid segregation.

stem side [35,37]. In males, the timing of nuclear envelope breakdown facilitates differential microtubule activities, with the GSC-side nuclear envelope breaking down earlier in G_2-phase [35]. Conceptually, these stem cell populations display a 'mitotic drive' [49].

Previous studies in *Drosophila* have shown directionality in the retention of additional cellular components, for example mother and daughter centrosomes. Male GSCs retain the mother centrosome [50], whereas female GSCs retain the daughter centrosome [51]. Moreover, midbody segregation in male and female GSCs correlates with daughter centrosome inheritance [51], which is opposite in either sex. Recent observations of centromere and microtubule bias towards the GSC side in males and females do not appear to correlate with mother centrosome inheritance [35,37]. In both cases, GSC centromeres are stronger, independently of mother or daughter centrosome retention. Therefore, we hypothesise that centromere strength might be a driver of asymmetric spindle assembly in these stem cells. Surprisingly, female GSCs are capable of forming a mitotic spindle in the absence of centrioles, in a *Drosophila Spindle Assembly Abnormal-4* (*DSas-4)* mutant background [52]. This raises the possibility that spindle assembly in GSCs could be a more chromatin- or even centromere-driven process, similar to meiotic spindle assembly observed in oocytes of many different systems [53]. It would be interesting to know whether the microtubule strength asymmetry is maintained in acentrosomal *DSas-4* mutant GSCs [52]. Nonetheless, now that epigenetically distinct sister centromeres have been identified, questions moving forward should aim to elucidate how the stem cell might mechanistically distinguish such centromeres.

Can CENP-A assembly drive sister centromere asymmetry?

Upon symmetric cell division, total CENP-A is distributed equally between both daughter cells such that each receives 50%. In order to ensure centromere function, newly synthesised CENP-A must be replenished in each cell cycle to 100%, classically measured by an increase/recovery in CENP-A level [54,55]. The majority of symmetrically dividing cells assemble centromeres after mitosis, at early G_1-phase [56]. Differing cell cycle timings for centromere assembly have been reported for some organisms and cell types [57–61]. Most interesting are those with an assembly timing before, as opposed to after, chromosome segregation. Of particular interest, gametes display a unique timing for the assembly of CENP-A. Such examples include that of *Drosophila* spermatocytes and starfish oocytes, which load CENP-A in meiotic prophase I [57,60,61].

Essays in Biochemistry (2020) **00** 1–10
https://doi.org/10.1042/EBC20190066

In addition to unique centromere assembly timings, exceptions exist also in the amount of CENP-A loaded at centromeres. The centromeric locus comprises interspersed H3 and CENP-A containing chromatin [62], which allows flexibility in terms of being able to accommodate varying amounts of CENP-A nucleosomes. Strikingly, *Drosophila* spermatocytes assemble CENP-A to an unexpected level (more than two-fold increase) [57] – easily enough to compensate for CENP-A dilution by half at premeiotic S-phase. This allows for two consecutive meiotic divisions in the absence of new CENP-A loading. Thus, it is possible that CENP-A assembly is a fluid epigenetic process unbound to the status quo of equal and complete replenishment to 100% CENP-A capacity at each cell division. Rather, centromeres can adapt both CENP-A assembly timing and abundance depending on the requirement of the cell type. This appears again to be the case for asymmetrically dividing stem cells. Ranjan et al. [35] and Dattoli et al. [37] have both established the CENP-A assembly timing for male and female GSCs, as well as neural stem cells, with assembly of CENP-A occurring after DNA replication, during G_2-phase up to prophase. Significantly, this assembly timing differs from canonical centromere assembly occurring after chromosome segregation in G_1-phase.

Unique centromere assembly dynamics in *Drosophila* stem cells raise two important points. First, centromere assembly in *Drosophila* GSCs is gradual, occurring from G_2-phase up to prophase, the longest cell cycle phase in GSCs [63]. This gradual loading draws some similarity to the long duration of CENP-A assembly observed in spermatocytes at meiotic prophase I, in starfish oocytes and quiescent human cultured cells [57,60,61]. Active CENP-A assembly in quiescent cells epigenetically marks and maintains future proliferative potential. Second, CENP-A levels increase by approximately 30% on an average in female GSCs [37]. Here, CENP-A assembly is potentially asymmetric relative to the complete and equal CENP-A assembly observed in a symmetrically dividing cell [64]. Ultimately, asymmetry in the distribution of CENP-A between sister chromatids might occur in two ways: (i) through the selective retention of 'old' CENP-A nucleosomes on one daughter strand at DNA replication and (ii) through the asymmetric assembly of 'new' CENP-A nucleosomes after DNA replication up to prophase (Figure 2). However, whether this sister centromere asymmetry pre-exists centromere assembly, or is actively established through the centromere assembly machinery is yet to be clarified.

Shortened G_1-phases have been observed in numerous stem cell populations [63,65–68], perhaps making G_2/M a more favourable option for the assembly of the centromere. It has been proposed that a short G_1 phase limits the sensitivity of stem cells to differentiation cues [65–67]. Another possibility is that centromere assembly after DNA replication allows the cell to first generate asymmetry before loading the mitotic components. This is also supported by recent work from the Chen lab. Using a sequential nucleoside analogue incorporation assay, Wooten et al. [32] have elucidated a biased unidirectional replication fork movement in testes-derived DNA and chromatin fibres. These results suggest that replication mechanisms might generate histone asymmetry in asymmetrically dividing cells [32,49]. To this point, the DNA replication marker 5-Ethynyl-2′-deoxyuridine (EdU) is first incorporated at GSC centromeres and pericentromeres [37]. A favourable explanation for this would be the need to establish asymmetric CENP-A (and histone H3/H4) patterning as early as possible in the cell cycle. However, whether this centromere assembly timing is conserved in pluripotent lineages is yet to be elucidated. Indeed, how the epigenetic memory at centromeres reacts and adapts to a pluripotent state remains an important question.

Molecular control of CENP-A asymmetry

Previous studies showed that CENP-A assembly is strongly linked to cell cycle regulation [58,69–72]. In addition, recent findings by Dattoli et al. [37] proposed the involvement of the cell cycle machinery in establishing sister centromere asymmetry. Specifically, the authors demonstrated that CENP-A assembly is promoted by CYCLIN A during G_2, while excessive loading is inhibited by CYCLIN B through the HASPIN kinase, between late prophase and metaphase [37]. Significantly, HASPIN phosphorylates H3 on the threonine 3, a well-known pericentric mark that has been already implicated in regulating ACD in *Drosophila* male GSCs [33]. In this study, Xie et al. [33] showed that H3T3P distinguishes pre-existing H3, which is enriched in the stem cell, from newly synthesised H3, which is enriched in the cell that differentiates. Importantly, it provided a key proof of principle that post-translational modifications to histones can epigenetically distinguish sister chromatids. It is possible that the timing of H3T3 phosphorylation, and it asymmetric distribution at pericentromeres, might limit (asymmetric) CENP-A assembly. It would be interesting to examine non-phosphorylatable (H3T3A) and phosphomimetic (H3T3D) mutant lines to determine any effect on CENP-A assembly or asymmetry in this background [33]. However, the point at which sister centromere asymmetry is established in the cell cycle is currently unknown; this might occur in S-phase when the centromere is replicated and parental CENP-A is inherited (Figure 2, Hypothesis 1), or during the time of new CENP-A assembly between DNA replication and prophase (Figure 2, Hypothesis 2).

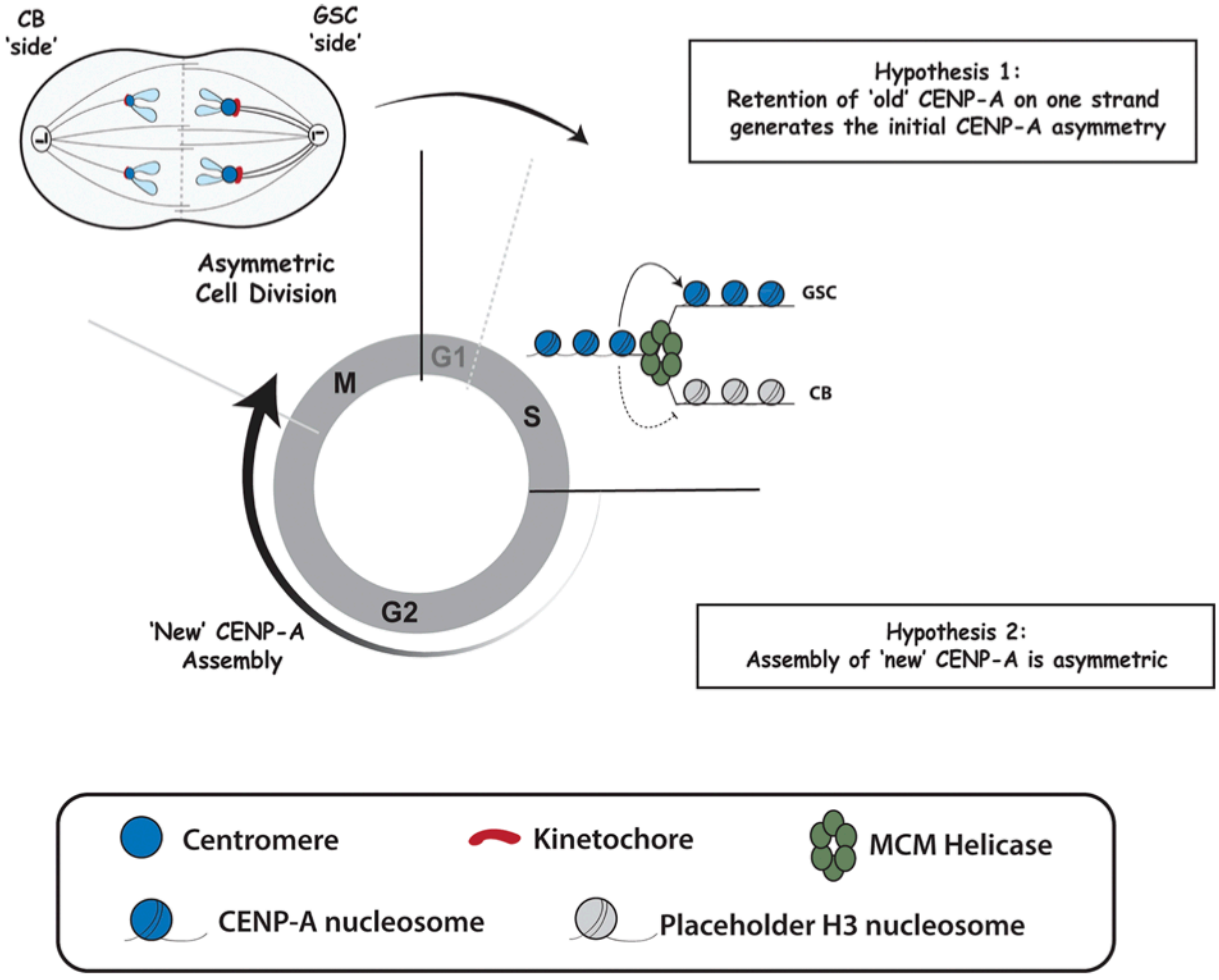

Figure 2. Current model and outstanding questions regarding the establishment of asymmetric sister centromeres in *Drosophila* GSCs

After mitosis, the newly divided GSC has a very short G_1-phase, entering immediately into S-phase. During replication, a unidirectional fork may allow parental 'old' CENP-A-H4 to be asymmetrically inherited between leading and lagging strands, in a manner similar to H3-H4 [32]. In the absence of new CENP-A assembly in S-phase, histone H3 is deposited at centromeres acting as a 'placeholder' [88]. The asymmetric inheritance of 'old' CENP-A may establish the initial asymmetry in the amount of CENP-A between sister centromeres (Hypothesis 1, top right). Newly synthesised or 'new' CENP-A assembly occurs after DNA replication through to prophase. New CENP-A assembly might occur in an asymmetric manner (Hypothesis 2, bottom right). Abbreviation: CB, cystoblast daughter cell.

For a fuller picture of this centromere assembly mechanism and to deduce some key mechanistic targets, consideration from what we already know about canonical (symmetrical) centromere assembly is necessary. Furthermore, more in-depth knowledge about the inherent self-propagation of centromeres is required. Recently, the Heun lab has reconstituted the *Drosophila* CENP-A assembly cycle in human cells [73]. Here, ectopic targeting of *Drosophila* proteins, CENP-A, the core centromere component CENP-C and the CENP-A assembly factor, chromosome alignment defect 1 (CAL1) [74] to human cell LacO arrays reveals an epigenetic loop of assembly and self-propagation. In this model, pre-existing CENP-C provides the recognition site for CAL1 to assemble new CENP-A-H4. Interestingly, CENP-C was identified as a positive hit in a number of stem cell maintenance/differentiation RNA interference (RNAi) screens carried out in *Drosophila* [75–77]. CENP-C is also asymmetrically distributed in GSCs and ISCs [36,37], and is known to play direct roles in CENP-A assembly and maintenance [69,78,79]. However, there are important differences between GSCs and ISCs in this context. In GSCs, there is a quantitative difference in the amount of CENP-C, with GSCs retaining approximately 1.2-fold more CENP-C compared with the cystoblast (CB) daughter cell (which retains mitotic capacity) [37]. On the other hand, CENP-C can only be detected in ISCs and not in the

Essays in Biochemistry (2020) **00** 1–10
https://doi.org/10.1042/EBC20190066

enteroblast (EB) [36]. The EB can further differentiate into an enterocyte (EC) or enteroendocrine (EE) cell without dividing [80]. The absence of CENP-C here could be explained by the non-dividing and endoreplicating nature of the immature EB. Nonetheless, CENP-C's asymmetry in favour of the stem cell in both systems suggest a potential role for CENP-C in parental CENP-A maintenance. Clearly, it stands as an interesting candidate to investigate in the context of marking an asymmetric assembly and maintenance of centromeres.

Centromere structure and the dynamics of associated proteins during S-phase may warrant additional investigation in ACD. In Drosophila GSCs, DNA replication begins around the centromere almost immediately after mitosis [37] – an unusual timing relative to many symmetrically dividing cells. Although the mechanisms of centromere replication remain unclear, the Cleveland lab has recently uncovered a role for an error-correction mechanism to maintain the centromere integrity throughout replication involving CENP-C and the moving replication fork [81]. Chromatin Immunoprecipitation-Sequencing (ChIP-Seq) analysis in human cells revealed that CENP-A is loaded primarily at the centromeric site, but also at a lower level throughout the entire chromosome during G_1-phase. Subsequently, the replication fork removes this ectopic CENP-A on chromosome arms, with CENP-C being key to maintaining the integrity of the centromere locus at the replication fork [81]. This may help explain why CENP-C is largely stable at centromeres during mid-late S-phase in human cells [82] – to protect the integrity of the centromere. However, whether such a mechanism exists in asymmetrically dividing cells is unknown. Interactions between CENP-A and the DNA replication machinery might also generate asymmetry. Recent studies in human cells may indicate a starting point for investigating the handling of CENP-A during replication in ACD. Indeed, the human CENP-A assembly factor, Holliday Junction Recognition Protein (HJURP) (functional homologue of Drosophila CAL1) [83,84] binds pre-existing 'old' CENP-A in S-phase, and auxin-induced degradation of HJURP resulted in subsequent loss of CENP-A through S-phase [85]. Furthermore, human CENP-A interacts with the minichromosome maintenance complex component (MCM) helicase component MCM2, and disruption of this interaction decreases CENP-A intensity through S-phase [85,86]. In *Drosophila* ACD, it is tempting to speculate that modifications to the handling of CENP-A at the replication fork may exist in order to bias the inheritance of 'old' CENP-A on one strand. Perhaps CENP-A, CAL1 or CENP-C contain post-translational modifications that allow the replication machinery to preferentially distinguish 'old' versus 'new' CENP-A in preparation for ACD.

Centromeres epigenetically regulate stem cell fate

ACD is a highly regulated process and errors can lead to cancer and infertility. Given the widespread implications in stem cell biology, understanding the molecular control of self-renewal versus differentiation is a primary motivation of all stem cell biologists. How the epigenetic state of stem cells changes depending on potency, environment and age are all key areas to be fully addressed.

CENP-A was first linked to stem cell self-renewal by Ambartsumyan et al. in 2010 [87]. Surprisingly, *CENP-A* depletion in induced pluripotent stem cells (iPSCs) still allowed self-renewal. However, when induced to differentiate, *CENP-A*-depleted cells could then no longer support lineage commitment, undergoing significant p53-dependent apoptosis. Again, we see an example of the fluidity of centromere assembly in response to cellular requirement. In this case, a higher CENP-A threshold needs to be met for differentiation to initiate. However, whether centromere specification can truly be an epigenetic mechanism to direct cell fate, or whether it is simply a marker of proliferation capacity of the stem cell had remained unclear.

First indications of a role for the centromere assembly machinery in stem cell division capacity in a multicellular organism appeared in *Drosophila* ISCs. Depletion of CENP-A, CAL1 and CENP-C in the midgut epithelium resulted in the loss of ISCs proliferation capacity, as measured by the vast decrease in clonal size [36]. Furthermore, long-term depletion of CAL1 resulted in ISCs loss [36]. In GSCs, CAL1 depletion in males led to reduced numbers of stem cells in the niche, indicating a possible self-renewal failure [35], while CAL1 knockdown in females blocked GSCs proliferation presumably due to a failure in centromere specification [37]. However, depleting CAL1 in each case does not allow full distinction between a stem-specific role in the germline, versus an inability to divide due to the lack of essential centromere proteins (CENP-A, CENP-C). Hence, overexpression of centromere proteins proved an effective approach to disrupt stem cell self-renewal in this system. Specifically, co-overexpression of CENP-A and CAL1 in female GSCs shifted the distribution of CENP-A between GSCs and CBs from asymmetric (1.2:1) to symmetric (1:1), shifting stem cells towards self-renewal [37]. Similarly, knockdown of HASPIN also disrupted CENP-A asymmetry [37]. In line with these findings, CENP-A asymmetry is lost upon CAL1 depletion in males GSCs [35]. Taken together, accumulating evidence suggests that GSCs require asymmetric sister centromeres to direct non-random sister chromatid segregation and subsequent stem cell fate.

Future perspectives

Moving forward, there are many avenues which warrant significant investigation. What relationship does centromere asymmetry have with stem cell polarity cues? Moreover, the extent to which sister centromere asymmetry is observed outside of metazoans should be determined in order to understand how well this phenomenon is conserved. The influence of the centromere as an epigenetic determinant of cell fate also warrants further investigation. How this epigenetically biased segregation ultimately affects cell fate remains elusive. Whether this creates a mechanical asymmetry in multicellular organisms, or indeed whether the gene expression status of stem cells is affected by disrupting centromere asymmetry, are all unanswered questions. Due to the potency of these adult *Drosophila* stem cell lineages, reservations must be made, as they largely display tissue-specific unipotency. Expansion of these studies into pluripotent lineages in other multicellular organisms is also required.

Summary

- The silent sister chromatid hypothesis proposes that epigenetic mechanisms regulate stem cell fate.
- In a *Drosophila* model stem cell system, centromeres of sister chromatid pairs show an asymmetric distribution of the centromeric histone CENP-A. Disruption of this sister centromere asymmetry in stem cells perturbs the balance of stem and daughter cells.
- The unique timing of centromere assembly in stem cells (between DNA replication and prophase) might serve as a mechanism for asymmetric CENP-A distribution and the epigenetic regulation of stem cell identity.

Competing Interests

The authors declare that there are no competing interests associated with the manuscript.

Funding

This work was supported by the Science Foundation Ireland-PIYRA [grant number 13/YI/2187 (to E.M.D.)]; the Government of Ireland Postgraduate Fellowship [grant number 2018/1208 (to B.L.C.)]; and the Thomas Crawford Hayes Travel Fund 2019 from the National University of Ireland Galway [grant number XXXX].

Author Contribution

B.L.C. and E.M.D. wrote the manuscript.

Acknowledgements

We thank Prof Kevin Sullivan, Drs Anna Ada Dattoli and Caitríona Collins for their insights and critical reading of the manuscript.

Abbreviations

ACD, asymmetric cell division; CAL1, chromosome alignment defect 1; CB, cystoblast; CENP-A, centromere protein A; CENP-C, centromere protein C; ChIP-Seq, chromatin immunoprecipitation-sequencing; DNA, deoxyribonucleic acid; DSas-4, *Drosophila* spindle assembly abnormal-4; EB, enteroblast; EC, Enterocyte; EE, enteroendocrine; GSC, germline stem cell; H3T3P, phosphorylated histone H3 at threonine 3; HJURP, Holliday junction recognition protein; iPSC, induced pluripotent stem cell; ISC, intestinal stem cell; RNA, ribonucleic acid; RNA, RNA interference.

References

1 Crane, G.M., Jeffery, E. and Morrison, S.J. (2017) Adult haematopoietic stem cell niches. *Nat. Rev. Immunol.* **17**, 573–590, https://doi.org/10.1038/nri.2017.53
2 Spradling, A., Fuller, M.T., Braun, R.E. and Yoshida, S. (2011) Germline stem cells. *Cold Spring Harb. Perspect. Biol.* **3**, a002642, https://doi.org/10.1101/cshperspect.a002642
3 Lehmann, R. (2012) Germline stem cells: origin and destiny. *Cell Stem Cell* **10**, 729–739, https://doi.org/10.1016/j.stem.2012.05.016

4 Fabritius, A.S., Ellefson, M.L. and McNally, F.J. (2011) Nuclear and spindle positioning during oocyte meiosis. *Curr. Opin. Cell Biol.* **23**, 78–84, https://doi.org/10.1016/j.ceb.2010.07.008
5 Brunet, S. and Verlhac, M.H. (2011) Positioning to get out of meiosis: the asymmetry of division. *Hum. Reprod. Update* **17**, 68–75, https://doi.org/10.1093/humupd/dmq044
6 Morrison, S.J. and Kimble, J. (2006) Asymmetric and symmetric stem-cell divisions in development and cancer. *Nature* **441**, 1068–1074, https://doi.org/10.1038/nature04956
7 Clevers, H. (2005) Stem cells, asymmetric division and cancer. *Nat. Genet.* **37**, 1027–1028, https://doi.org/10.1038/ng1005-1027
8 Knoblich, J.A. (2010) Asymmetric cell division: recent developments and their implications for tumour biology. *Nat. Rev. Mol. Cell Biol.* **11**, 849–860, https://doi.org/10.1038/nrm3010
9 Losick, V.P., Morris, L.X., Fox, D.T. and Spradling, A. (2011) Drosophila stem cell niches: a decade of discovery suggests a unified view of stem cell regulation. *Dev. Cell* **21**, 159–171, https://doi.org/10.1016/j.devcel.2011.06.018
10 Resende, L.P.F. and Jones, D.L. (2012) Local signaling within stem cell niches: insights from *Drosophila*. *Curr. Opin. Cell Biol.* **24**, 225–231, https://doi.org/10.1016/j.ceb.2012.01.004
11 Morrison, S.J. and Spradling, A.C. (2008) Stem cells and niches: mechanisms that promote stem cell maintenance throughout life. *Cell* **132**, 598–611, https://doi.org/10.1016/j.cell.2008.01.038
12 Issigonis, M., Tulina, N., de Cuevas, M., Brawley, C., Sandler, L. and Matunis, E. (2009) JAK-STAT signal inhibition regulates competition in the Drosophila testis stem cell niche. *Science* **326**, 153–156, https://doi.org/10.1126/science.1176817
13 Zhang, J. and Li, L. (2005) BMP signaling and stem cell regulation. *Dev. Biol.* **284**, 1–11, https://doi.org/10.1016/j.ydbio.2005.05.009
14 Herrera, S.C. and Bach, E.A. (2019) JAK/STAT signaling in stem cells and regeneration: from *Drosophila* to vertebrates. *Development* **146**, dev167643, https://doi.org/10.1242/dev.167643
15 Stine, R.R. and Matunis, E.L. (2013) JAK-STAT signaling in stem cells. *Adv. Exp. Med. Biol.* 247–267
16 Venkei, Z.G. and Yamashita, Y.M. (2018) Emerging mechanisms of asymmetric stem cell division. *J. Cell Biol.* **217**, 3785–3795, https://doi.org/10.1083/jcb.201807037
17 Shlyakhtina, Y., Moran, K.L. and Portal, M.M. (2019) Asymmetric inheritance of cell fate determinants: focus on RNA. *Noncoding RNA* **5**, 38, https://doi.org/10.3390/ncrna5020038
18 Ryder, P.V. and Lerit, D.A. (2018) RNA localization regulates diverse and dynamic cellular processes. *Traffic* **19**, 496–502
19 Tran, V., Feng, L. and Chen, X. (2013) Asymmetric distribution of histones during *Drosophila* male germline stem cell asymmetric divisions. *Chromosome Res.* **21**, 255–269, https://doi.org/10.1007/s10577-013-9356-x
20 Lansdorp, P.M., Falconer, E., Tao, J., Brind'Amour, J. and Naumann, U. (2012) Epigenetic differences between sister chromatids? *Ann N.Y. Acad. Sci.* **1266**, 1–6, https://doi.org/10.1111/j.1749-6632.2012.06505.x
21 Xie, J., Wooten, M., Tran, V. and Chen, X. (2017) Breaking symmetry – asymmetric histone inheritance in stem cells. *Trends Cell Biol.* **27**, 527–540, https://doi.org/10.1016/j.tcb.2017.02.001
22 Conboy, M.J., Karasov, A.O. and Rando, T.A. (2007) High incidence of non-random template strand segregation and asymmetric fate determination in dividing stem cells and their progeny. *PLoS Biol.* e102, https://doi.org/10.1371/journal.pbio.0050102
23 Rocheteau, P., Gayraud-Morel, B., Siegl-Cachedenier, I., Blasco, M.A. and Tajbakhsh, S. (2012) A subpopulation of adult skeletal muscle stem cells retains all template DNA strands after cell division. *Cell* **148**, 112–125, https://doi.org/10.1016/j.cell.2011.11.049
24 Fei, J.-F. and Huttner, W.B. (2009) Nonselective sister chromatid segregation in mouse embryonic neocortical precursor cells. *Cereb. Cortex* **19**, i49–i54, https://doi.org/10.1093/cercor/bhp043
25 Cairns, J. (1975) Mutation selection and the natural history of cancer. *Nature* **255**, 197–200, https://doi.org/10.1038/255197a0
26 Lansdorp, P.M. (2007) Immortal strands? Give me a break. *Cell* **129**, 1244–1247, https://doi.org/10.1016/j.cell.2007.06.017
27 Yadlapalli, S., Cheng, J. and Yamashita, Y.M. (2011) Drosophila male germline stem cells do not asymmetrically segregate chromosome strands. *J. Cell Sci.* **124**, 933–939, https://doi.org/10.1242/jcs.079798
28 Yadlapalli, S., Cheng, J. and Yamashita, Y.M. (2011) Reply to: Overlooked areas need attention for sound evaluation of DNA strand inheritance patterns in Drosophila male germline stem cells. *J. Cell Sci.* **124**, 4138–4139
29 Sherley, J.L. (2011) Overlooked areas need attention for sound evaluation of DNA strand inheritance patterns in *Drosophila* male germline stem cells. *J. Cell Sci.* **124**, 4137
30 Yadlapalli, S. and Yamashita, Y.M. (2013) Chromosome-specific nonrandom sister chromatid segregation during stem-cell division. *Nature* **498**, 251–254, https://doi.org/10.1038/nature12106
31 Tran, V., Lim, C., Xie, J. and Chen, X. (2012) Asymmetric division of *Drosophila* male germline stem cell shows asymmetric histone distribution. *Science* **338**, 679–682, https://doi.org/10.1126/science.1226028
32 Wooten, M., Snedeker, J., Nizami, Z.F., Yang, X., Ranjan, R., Urban, E. et al. (2019) Asymmetric histone inheritance via strand-specific incorporation and biased replication fork movement. *Nat. Struct. Mol. Biol.* **26**, 732–743, https://doi.org/10.1038/s41594-019-0269-z
33 Xie, J., Wooten, M., Tran, V., Chen, B.C., Pozmanter, C., Simbolon, C. et al. (2015) Histone H3 threonine phosphorylation regulates asymmetric histone inheritance in the *Drosophila* male germline. *Cell* **163**, 920–933, https://doi.org/10.1016/j.cell.2015.10.002
34 Mendiburo, M.J., Padeken, J., Fülöp, S., Schepers, A. and Heun, P. (2011) Drosophila CENH3 is sufficient for centromere formation. *Science* **334**, 686–690, https://doi.org/10.1126/science.1206880
35 Ranjan, R., Snedeker, J. and Chen, X. (2019) Asymmetric centromeres differentially coordinate with mitotic machinery to ensure biased sister chromatid segregation in germline stem cells. *Cell Stem Cell* **25**, 666–681.e5, https://doi.org/10.1016/j.stem.2019.08.014
36 García del Arco, A., Edgar, B.A. and Erhardt, S. (2018) *In vivo* analysis of centromeric proteins reveals a stem cell-specific asymmetry and an essential role in differentiated, non-proliferating cells. *Cell Rep.* **22**, 1982–1993, https://doi.org/10.1016/j.celrep.2018.01.079

37 Dattoli, A.A., Carty, B.L., Kochendoerfer, A.M., Morgan, C., Walshe, A.E. and Dunleavy, E.M. (2020) Asymmetric assembly of centromeres epigenetically regulates stem cell fate. *J. Cell Biol.* **219**
38 Westhorpe, F.G. and Straight, A.F. (2013) Functions of the centromere and kinetochore in chromosome segregation. *Curr. Opin. Cell Biol.* **25**, 334–340, https://doi.org/10.1016/j.ceb.2013.02.001
39 Deng, W. and Lin, H. (1997) Spectrosomes and fusomes anchor mitotic spindles during asymmetric germ cell divisions and facilitate the formation of a polarized microtubule array for oocyte specification in Drosophila. *Dev. Biol.* **189**, 79–94, https://doi.org/10.1006/dbio.1997.8669
40 Lin, H. and Spradling, A.C. (1995) Fusome asymmetry and oocyte determination in Drosophila. *Dev. Genet.* **16**, 6–12, https://doi.org/10.1002/dvg.1020160104
41 Yamashita, Y.M., Jones, D.L. and Fuller, M.T. (2003) Orientation of asymmetric stem cell division by the APC tumor suppressor and centrosome. *Science* **301**, 1547–1550, https://doi.org/10.1126/science.1087795
42 Bang, C. and Cheng, J. (2015) Dynamic interplay of spectrosome and centrosome organelles in asymmetric stem cell divisions. *PLoS ONE* **10**, e0123294, https://doi.org/10.1371/journal.pone.0123294
43 Akera, T., Chmátal, L., Trimm, E., Yang, K., Aonbangkhen, C., Chenoweth, D.M. et al. (2017) Spindle asymmetry drives non-Mendelian chromosome segregation. *Science* **358**, 668–672, https://doi.org/10.1126/science.aan0092
44 Chmátal, L., Gabriel, S.I., Mitsainas, G.P., Martínez-Vargas, J., Ventura, J., Searle, J.B. et al. (2014) Centromere strength provides the cell biological basis for meiotic drive and karyotype evolution in mice. *Curr. Biol.* **24**, 2295–2300, https://doi.org/10.1016/j.cub.2014.08.017
45 Iwata-Otsubo, A., Dawicki-McKenna, J.M., Akera, T., Falk, S.J., Chmátal, L., Yang, K. et al. (2017) Expanded satellite repeats amplify a discrete CENP-a nucleosome assembly site on chromosomes that drive in female meiosis. *Curr. Biol.* **27**, 2365–2373.e8, https://doi.org/10.1016/j.cub.2017.06.069
46 Malik, H.S. (2009) The centromere-drive hypothesis: a simple basis for centromere complexity. *Prog. Mol. Subcell. Biol.* **48**, 33–52, https://doi.org/10.1007/978-3-642-00182-6˙2
47 Lampson, M.A. and Black, B.E. (2017) Cellular and molecular mechanisms of centromere drive. *Cold Spring Harb. Symp. Quant. Biol.* **82**, 249–257, https://doi.org/10.1101/sqb.2017.82.034298
48 Thorpe, P.H., Bruno, J. and Rothstein, R. (2009) Kinetochore asymmetry defines a single yeast lineage. *Proc. Natl. Acad. Sci. U.S.A.* **106**, 6673–6678, https://doi.org/10.1073/pnas.0811248106
49 Wooten, M., Ranjan, R. and Chen, X. (2019) Asymmetric histone inheritance in asymmetrically dividing stem cells. *Trends Genet.* **36**, 30–43, https://doi.org/10.1016/j.tig.2019.10.004
50 Yamashita, Y.M., Mahowald, A.P., Perlin, J.R. and Fuller, M.T. (2007) Asymmetric inheritance of mother versus daughter centrosome in stem cell division. *Science* **315**, 518–521, https://doi.org/10.1126/science.1134910
51 Salzmann, V., Chen, C., Chiang, C.Y.A., Tiyaboonchai, A., Mayer, M. and Yamashita, Y.M. (2014) Centrosome-dependent asymmetric inheritance of the midbody ring in Drosophila germline stem cell division. *Mol. Biol. Cell* **25**, 267–275, https://doi.org/10.1091/mbc.e13-09-0541
52 Stevens, N.R., Raposo, A.A.S.F., Basto, R., St Johnston, D. and Raff, J.W.W. (2007) From stem cell to embryo without centrioles. *Curr. Biol.* **17**, 1498–1503, https://doi.org/10.1016/j.cub.2007.07.060
53 Radford, S.J., Nguyen, A.L., Schindler, K. and McKim, K.S. (2017) The chromosomal basis of meiotic acentrosomal spindle assembly and function in oocytes. *Chromosoma* **126**, 351–364, https://doi.org/10.1007/s00412-016-0618-1
54 Jansen, L.E.T., Black, B.E., Foltz, D.R. and Cleveland, D.W. (2007) Propagation of centromeric chromatin requires exit from mitosis. *J. Cell Biol.* **176**, 795–805, https://doi.org/10.1083/jcb.200701066
55 Schuh, M., Lehner, C.F. and Heidmann, S. (2007) Incorporation of *Drosophila* CID/CENP-A and CENP-C into centromeres during early embryonic anaphase. *Curr. Biol.* **17**, 237–243, https://doi.org/10.1016/j.cub.2006.11.051
56 Glynn, M., Kaczmarczyk, A., Prendergast, L., Quinn, N. and Sullivan, K.F. (2010) Centromeres: assembling and propagating epigenetic function. *Subcell. Biochem.* **50**, 223–249, https://doi.org/10.1007/978-90-481-3471-7˙12
57 Dunleavy, E.M., Beier, N.L., Gorgescu, W., Tang, J., Costes, S.V. and Karpen, G.H. (2012) The cell cycle timing of centromeric chromatin assembly in *Drosophila* meiosis is distinct from mitosis yet requires CAL1 and CENP-C. *PLoS Biol.* e1001460, https://doi.org/10.1371/journal.pbio.1001460
58 Mellone, B.G., Grive, K.J., Shteyn, V., Bowers, S.R., Oderberg, I. and Karpen, G.H. (2011) Assembly of drosophila centromeric chromatin proteins during mitosis. *PLoS Genet.* **7**, e1002068, https://doi.org/10.1371/journal.pgen.1002068
59 Ahmad, K. and Henikoff, S. (2001) Centromeres are specialized replication domains in heterochromatin. *J. Cell Biol.* **153**, 101–109, https://doi.org/10.1083/jcb.153.1.101
60 Swartz, S.Z., McKay, L.S., Su, K.C., Bury, L., Padeganeh, A., Maddox, P.S. et al. (2019) Quiescent cells actively replenish CENP-A nucleosomes to maintain centromere identity and proliferative potential. *Dev. Cell* **51**, 35–48.e7, https://doi.org/10.1016/j.devcel.2019.07.016
61 Raychaudhuri, N., Dubruille, R., Orsi, G.A., Bagheri, H.C., Loppin, B. and Lehner, C.F. (2012) Transgenerational propagation and quantitative maintenance of paternal centromeres depends on Cid/Cenp-A presence in Drosophila sperm. *PLoS Biol.* e1001434, https://doi.org/10.1371/journal.pbio.1001434
62 Sullivan, B.A. and Karpen, G.H. (2004) Centromeric chromatin exhibits a histone modification pattern that is distinct from both euchromatin and heterochromatin. *Nat. Struct. Mol. Biol.* **11**, 1076–1083, https://doi.org/10.1038/nsmb845
63 Hsu, H.J., LaFever, L. and Drummond-Barbosa, D. (2008) Diet controls normal and tumorous germline stem cells via insulin-dependent and -independent mechanisms in Drosophila. *Dev. Biol.* **313**, 700–712, https://doi.org/10.1016/j.ydbio.2007.11.006
64 Bodor, D.L., Mata, J.F., Sergeev, M., David, A.F., Salimian, K.J., Panchenko, T. et al. (2014) The quantitative architecture of centromeric chromatin. *Elife* e02137, https://doi.org/10.7554/eLife.02137
65 Singh, A.M. and Dalton, S. (2009) The cell cycle and myc intersect with mechanisms that regulate pluripotency and reprogramming. *Cell Stem Cell* **5**, 141–149, https://doi.org/10.1016/j.stem.2009.07.003

66 Lange, C. and Calegari, F. (2010) Cdks and cyclins link G1 length and differentiation of embryonic, neural and hematopoietic stem cells. *Cell Cycle* **9**, 1893–1900
67 Orford, K.W. and Scadden, D.T. (2008) Deconstructing stem cell self-renewal: genetic insights into cell-cycle regulation. *Nat. Rev. Genet.* **9**, 115–128, https://doi.org/10.1038/nrg2269
68 Fox, P.M., Vought, V.E., Hanazawa, M., Lee, M.H., Maine, E.M. and Sched, T. (2011) Cyclin e and CDK-2 regulate proliferative cell fate and cell cycle progression in the *C. elegans* germline. *Development* **138**, 2223–2234
69 Erhardt, S., Mellone, B.G., Betts, C.M., Zhang, W., Karpen, G.H. and Straight, A.F. (2008) Genome-wide analysis reveals a cell cycle-dependent mechanism controlling centromere propagation. *J. Cell Biol.* **183**, 805–818, https://doi.org/10.1083/jcb.200806038
70 Stankovic, A., Guo, L.Y., Mata, J.F., Bodor, D.L., Cao, X.J., Bailey, A.O. et al. (2017) A dual inhibitory mechanism sufficient to maintain cell-cycle-restricted CENP-A assembly. *Mol. Cell* **65**, 231–246, https://doi.org/10.1016/j.molcel.2016.11.021
71 Silva, M.C.C., Bodor, D.L., Stellfox, M.E., Martins, N.M.C., Hochegger, H., Foltz, D.R. et al. (2012) Cdk activity couples epigenetic centromere inheritance to cell cycle progression. *Dev. Cell* **22**, 52–63, https://doi.org/10.1016/j.devcel.2011.10.014
72 McKinley, K.L. and Cheeseman, I.M. (2014) Polo-like kinase 1 licenses CENP-a deposition at centromeres. *Cell* **158**, 397–411, https://doi.org/10.1016/j.cell.2014.06.016
73 Roure, V., Medina-Pritchard, B., Lazou, V., Rago, L., Anselm, E., Venegas, D. et al. (2019) Reconstituting Drosophila centromere identity in human cells. *Cell Rep.* **29**, 464–479.e5, https://doi.org/10.1016/j.celrep.2019.08.067
74 Chen, C.C., Dechassa, M.L., Bettini, E., Ledoux, M.B., Belisario, C., Heun, P. et al. (2014) CAL1 is the Drosophila CENP-A assembly factor. *J. Cell Biol.* **204**, 313–329, https://doi.org/10.1083/jcb.201305036
75 Yan, D., Neumüller, R.A., Buckner, M., Ayers, K., Li, H., Hu, Y. et al. (2014) A regulatory network of *Drosophila* germline stem cell self-renewal. *Dev. Cell* **28**, 459–473, https://doi.org/10.1016/j.devcel.2014.01.020
76 Liu, Y., Ge, Q., Chan, B., Liu, H., Singh, S.R., Manley, J. et al. (2016) Whole-animal genome-wide RNAi screen identifies networks regulating male germline stem cells in Drosophila. *Nat. Commun.* **7**, 12149, https://doi.org/10.1038/ncomms12149
77 Neumüller, R.A., Richter, C., Fischer, A., Novatchkova, M., Neumüller, K.G. and Knoblich, J.A. (2011) Genome-wide analysis of self-renewal in Drosophila neural stem cells by transgenic RNAi. *Cell Stem Cell* **8**, 580–593, https://doi.org/10.1016/j.stem.2011.02.022
78 Falk, S.J., Guo, L.Y., Sekulic, N., Smoak, E.M., Mani, T., Logsdon, G.A. et al. (2015) CENP-C reshapes and stabilizes CENP-A nucleosomes at the centromere. *Science* **348**, 699–703, https://doi.org/10.1126/science.1259308
79 Falk, S.J., Lee, J., Sekulic, N., Sennett, M.A., Lee, T.H. and Black, B.E. (2016) CENP-C directs a structural transition of CENP-A nucleosomes mainly through sliding of DNA gyres. *Nat. Struct. Mol. Biol.* **23**, 204–208, https://doi.org/10.1038/nsmb.3175
80 Ohlstein, B. and Spradling, A. (2007) Multipotent Drosophila intestinal stem cells specify daughter cell fates by differential notch signaling. *Science* **315**, 988–992, https://doi.org/10.1126/science.1136606
81 Nechemia-Arbely, Y., Miga, K.H., Shoshani, O., Aslanian, A., McMahon, M.A., Lee, A.Y. et al. (2019) DNA replication acts as an error correction mechanism to maintain centromere identity by restricting CENP-A to centromeres. *Nat. Cell Biol.* **21**, 743–754, https://doi.org/10.1038/s41556-019-0331-4
82 Hemmerich, P., Weidtkamp-Peters, S., Hoischen, C., Schmiedeberg, L., Erliandri, I. and Diekmann, S. (2008) Dynamics of inner kinetochore assembly and maintenance in living cells. *J. Cell Biol.* **180**, 1101–1114, https://doi.org/10.1083/jcb.200710052
83 Dunleavy, E.M., Roche, D., Tagami, H., Lacoste, N., Ray-Gallet, D., Nakamura, Y. et al. (2009) HJURP is a cell-cycle-dependent maintenance and deposition factor of CENP-A at centromeres. *Cell* **137**, 485–497, https://doi.org/10.1016/j.cell.2009.02.040
84 Foltz, D.R., Jansen, L.E.T., Bailey, A.O., Yates, J.R., Bassett, E.A., Wood, S. et al. (2009) Centromere-specific assembly of CENP-A nucleosomes is mediated by HJURP. *Cell* **137**, 472–484, https://doi.org/10.1016/j.cell.2009.02.039
85 Zasadzińska, E., Huang, J., Bailey, A.O., Guo, L.Y., Lee, N.S., Srivastava, S. et al. (2018) Inheritance of CENP-A nucleosomes during DNA replication requires HJURP. *Dev. Cell* **47**, 348–362.e7, https://doi.org/10.1016/j.devcel.2018.09.003
86 Huang, H., Strømme, C.B., Saredi, G., Hödl, M., Strandsby, A., González-Aguilera, C. et al. (2015) A unique binding mode enables MCM2 to chaperone histones H3-H4 at replication forks. *Nat. Struct. Mol. Biol.* **22**, 618–626, https://doi.org/10.1038/nsmb.3055
87 Ambartsumyan, G., Gill, R.K., Perez, S.D., Conway, D., Vincent, J., Dalal, Y. et al. (2010) Centromere protein A dynamics in human pluripotent stem cell self-renewal, differentiation and DNA damage. *Hum. Mol. Genet.* **19**, 3970–3982, https://doi.org/10.1093/hmg/ddq312
88 Dunleavy, E.M., Almouzni, G. and Karpen, G.H. (2011) H3.3 is deposited at centromeres in S phase as a placeholder for newly assembled CENP-A in G phase. *Nucleus* **2**, 146–157, https://doi.org/10.4161/nucl.2.2.15211

8.6 Anna Ada Dattoli, Ben L. Carty, Antje M. Kochendoerfer, Conall Morgan, Annie E. Walshe, Elaine M. Dunleavy, 2020.

Anna Ada Dattoli, Ben L. Carty, Antje M. Kochendoerfer, Conall Morgan, Annie E. Walshe, Elaine M. Dunleavy; Asymmetric assembly of centromeres epigenetically regulates stem cell fate. *J Cell Biol* 6 April 2020; 219 (4): e201910084.
doi: https://doi.org/10.1083/jcb.201910084

JCB Journal of Cell Biology

ARTICLE

Asymmetric assembly of centromeres epigenetically regulates stem cell fate

Anna Ada Dattoli, Ben L. Carty, Antje M. Kochendoerfer, Conall Morgan, Annie E. Walshe, and Elaine M. Dunleavy

Centromeres are epigenetically defined by CENP-A–containing chromatin and are essential for cell division. Previous studies suggest asymmetric inheritance of centromeric proteins upon stem cell division; however, the mechanism and implications of selective chromosome segregation remain unexplored. We show that *Drosophila* female germline stem cells (GSCs) and neuroblasts assemble centromeres after replication and before segregation. Specifically, CENP-A deposition is promoted by CYCLIN A, while excessive CENP-A deposition is prevented by CYCLIN B, through the HASPIN kinase. Furthermore, chromosomes inherited by GSCs incorporate more CENP-A, making stronger kinetochores that capture more spindle microtubules and bias segregation. Importantly, symmetric incorporation of CENP-A on sister chromatids via HASPIN knockdown or overexpression of CENP-A, either alone or together with its assembly factor CAL1, drives stem cell self-renewal. Finally, continued CENP-A assembly in differentiated cells is nonessential for egg development. Our work shows that centromere assembly epigenetically drives GSC maintenance and occurs before oocyte meiosis.

Introduction

Stem cells are fundamental for the generation of all tissues during embryogenesis and replace lost or damaged cells throughout the life of an organism. At division, stem cells generate two cells with distinct fates: (1) a cell that is an exact copy of its precursor, maintaining the "stemness," and (2) a daughter cell that will subsequently differentiate (Betschinger and Knoblich, 2004; Inaba and Yamashita, 2012). Epigenetic mechanisms, heritable chemical modifications of the DNA/nucleosome that do not alter the primary genomic nucleotide sequence, regulate the process of self-renewal and differentiation of stem cells (Christophersen and Helin, 2010; Eun et al., 2010). In *Drosophila* male germline stem cells (GSCs), before division, phosphorylation at threonine 3 of histone H3 (H3T3P) preferentially associates with chromosomes that are inherited by the future stem cell (Xie et al., 2015). Furthermore, centromeric proteins seem to be asymmetrically distributed between stem and daughter cells in the *Drosophila* intestine and germline (García Del Arco et al., 2018; Ranjan et al., 2019). These findings support the "silent sister hypothesis" (Lansdorp, 2007), according to which epigenetic variations differentially mark sister chromatids driving selective chromosome segregation during stem cell mitosis (Dai et al., 2005; Lansdorp, 2007; Caperta et al., 2008; Tran et al., 2013; Xie et al., 2015). Centromeres, the primary constriction of chromosomes, are crucial for cell division, providing the chromatin surface where the kinetochore assembles (McKinley and Cheeseman, 2016). In turn, the kinetochore ensures the correct attachment of spindle microtubules and faithful chromosome partition into the two daughter cells upon division (Musacchio and Desai, 2017). Centromeric chromatin contains different kinds of DNA repeats (satellite and centromeric retrotransposons; Fukagawa and Earnshaw, 2014; Chang et al., 2019) wrapped around nucleosomes containing the histone H3 variant centromere protein A (CENP-A). Centromeres are not specified by a particular DNA sequence. Rather, they are specified epigenetically by CENP-A (Black and Cleveland, 2011; Allshire and Karpen, 2008; Fukagawa and Earnshaw, 2014; Karpen and Allshire, 1997). Centromere assembly, classically measured as CENP-A deposition to generate centromeric nucleosomes, occurs at the end of mitosis (between telophase and G1) in humans (Jansen et al., 2007; Hemmerich et al., 2008). Additional cell cycle timings for centromere assembly have been reported in flies (Mellone et al., 2011; Ahmad and Henikoff, 2001; Schuh et al., 2007). Interestingly, *Drosophila* spermatocytes and starfish oocytes are the only cells known to date to assemble centromeres before chromosome segregation, during prophase of meiosis I (Dunleavy et al., 2012; Swartz et al., 2019; Raychaudhuri et al., 2012). These examples show that centromere assembly dynamics can differ among metazoans and also among different cell types in the same organism.

Centre for Chromosome Biology, Biomedical Sciences, National University of Ireland Galway, Galway, Ireland, UK.

Correspondence to Elaine M. Dunleavy: elaine.dunleavy@nuigalway.ie.

A key player in centromere assembly in vertebrates is HJURP (holliday junction recognition protein), which localizes at centromeres during the cell cycle window of CENP-A deposition (Dunleavy et al., 2009; Foltz et al., 2009). Furthermore, centromere assembly is regulated by the cell cycle machinery. In flies, deposition of CID (the homologue of CENP-A) requires activation of the anaphase promoting complex/cyclosome (APC/C) and degradation of CYCLIN A (CYCA; Mellone et al., 2011; Erhardt et al., 2008). In humans, centromere assembly is antagonized by Cdk1 activity, while the kinase Plk1 promotes assembly (Silva et al., 2012; Stankovic et al., 2017; McKinley and Cheeseman, 2014). Additionally, the CYCLIN B (CYCB)/Cdk1 complex inhibits the binding of CENP-A to HJURP, preventing CENP-A loading at centromeres (Yu et al., 2015). To date, little is known about centromere assembly dynamics and functions in stem cell asymmetric divisions. *Drosophila melanogaster* ovaries provide an excellent model to study stem cells in their native niche (Yan et al., 2014). In this tissue, germline stem cells (GSCs) are easily accessible and can be manipulated genetically. Moreover, centromere assembly mechanisms in GSCs and their differentiated cells, cystoblasts (CBs), could be used to epigenetically discriminate between these two cell types. In *Drosophila,* CID binds to CAL1 (fly functional homologue of HJURP; Chen et al., 2014; Barnhart et al., 2011) in a prenucleosomal complex, and its localization to centromeres requires CAL1 and CENP-C (Erhardt et al., 2008; Mellone et al., 2011).

Here we investigated the dynamics of CENP-A deposition in *Drosophila* GSCs. We show that GSC centromeres are assembled after replication, but before chromosome segregation, with neural stem cells following the same trend. Centromere assembly in GSCs is tightly linked to the G2/M transition. Indeed, CYCA localizes at centromeres, and its knockdown is responsible for a marked reduction of centromeric CID and CENP-C, but not CAL1. Surprisingly, excessive CID deposition is prevented by CYCB, through the kinase HASPIN. Our superresolution microscopy analysis of GSCs at prometaphase and metaphase shows that CID incorporation on sister chromatids occurs asymmetrically, and chromosomes that will be inherited by the stem cell are loaded with more CID. Moreover, GSC chromosomes make stronger kinetochores, which anchor more spindle fibers. This asymmetric distribution of CID between GSC and CB is maintained also at later stages of the cell cycle, while it is not observed in differentiated cells outside of the niche. We also find that the depletion of CAL1 at centromeres blocks GSC proliferation and differentiation. Notably, overexpression of both CID and CAL1, as well as HASPIN knockdown, promotes stem cell self-renewal and disrupts the asymmetric inheritance of CID. Conversely, overexpression of CAL1 causes GSC-like tumors. Finally, CAL1 and CID knockdown at later stages of egg development have no obvious effect on cell division, suggesting that these cells inherit CID from GSCs. Taken together, our findings establish centromere assembly as a new epigenetic pathway that regulates stem cell fate.

Results

Nuclear distribution of centromeres in GSCs changes through the cell cycle

The cell cycle assembly time of centromeres in female GSCs is currently unknown. To elucidate this, we observed the distribution of centromeres throughout the cell cycle. The *Drosophila* female GSC niche is found at the apical end of the germarium, the anterior tip of the adult ovariole (Fig. 1 A, region 1). The niche comprises the terminal filament and the cap cells. A cytoplasmic roundish structure called the spectrosome connects two to three GSCs to the cap cells (Fig. 1 A). The spectrosome is present in both GSCs and CBs, and its shape can be used to define the cell cycle stage (Kao et al., 2015; Ables and Drummond-Barbosa, 2013). Upon asymmetric division, the daughter cell closer to the niche retains the stemness, while the other, the CB, differentiates and is detached from the niche together with its spectrosome. Each CB undergoes four rounds of mitosis with incomplete cytokinesis, giving rise to 16-cell cysts of cystocytes (CCs) interconnected to each other through the fusome, a branched spectrosome. After completion of S phase, 16-cell cysts start meiosis and form a synaptonemal complex. The oocyte originates from either of the two CCs with four fusome-bridges (Fig. 1 A, region 2a–b, brown cells; Rangan et al., 2011; Christophorou et al., 2013). In region 3, the 16-cell cysts mature to an egg chamber containing 15 nurse cells that provide for the oocyte (Fig. 1 A, region 3), which completes meiosis (McLaughlin and Bratu 2015; Hughes et al., 2018).

To achieve our aim, we used transgenic flies expressing CID coupled to GFP to follow centromeres and H2Av coupled to RFP (Schuh et al., 2007) to follow chromatin condensation. To identify each phase of mitosis in GSCs, we used the phosphorylation at serine 10 of histone H3 (H3S10P; Matias et al., 2015; Hendzel et al., 1997). At interphase, chromatin is not condensed (Fig. 1 BI), centromeres are spread throughout the nucleus (Fig. 1, BII and BV), and H3S10P signal is absent (Fig. 1 BV and Fig. 3 BV). At prophase, H3S10P signal is present, chromosomes begin to condense, and centromeres start to align (Fig. 1, C and D). At this stage, we observed on average 5.7 centromere foci per cell. At metaphase, chromosomes and centromeres are completely aligned on the metaphase plate, and we observed an average of 6.9 centromere foci (Fig. 1, EI and EII). At this stage, it is possible to clearly distinguish the centromeres of each set of sister chromatids that will be inherited respectively by the new GSC and CB (Fig. 1, EII and EV). At anaphase, chromosomes and centromeres migrate to the opposite pole of each new daughter cell (Fig. 1, FI, FII, and FV), and an average of 3.1 centromere foci (despite the high level of clustering) are visible per cell. At telophase, the H3S10P signal is reduced, the chromatin starts to decondense, and centromeres remain located at the opposite side of each new nucleus (not depicted).

To identify cells in S phase, we used 5-ethynyl-2′-deoxyuridine (EdU) to label nuclei with or without newly replicated DNA (Salic and Mitchison, 2008). After EdU incorporation, ovaries were antibody-stained to study centromere positioning in GSCs and CBs during replication (Fig. 1, G and H). In EdU-negative cells, the spectrosome is round, the DNA is not condensed, and on average 5.2 centromeres are scattered throughout the nucleus (Fig. 1, GI–GV), indicating that the cells are likely to be in G2 phase or early prophase. Interestingly, 100% of cells analyzed (50/50) show that GSCs and CBs were simultaneously positive for EdU staining (Fig. 1, HI–HV). In these cells, centromeres assumed a similar localization to that observed during anaphase

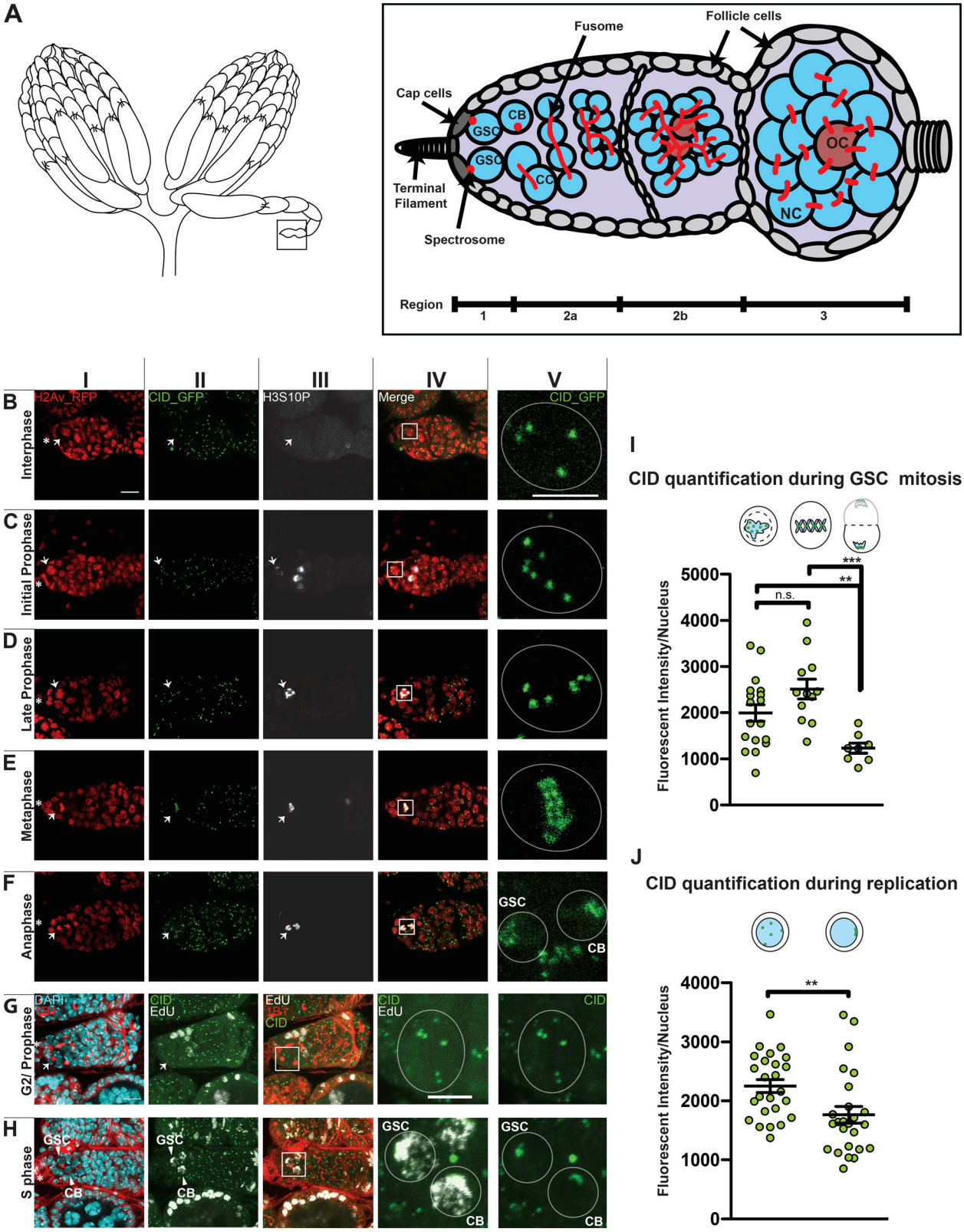

Figure 1. **Centromere assembly in GSCs occurs after replication but before chromosome segregation. (A)** Diagram of *Drosophila* ovary (left) and germarium containing the germline stem cell (GSC) niche (right). NC, nurse cell; OC, oocyte; CB, cystoblast; CC, cystocyte. The spectrosome (red) connects GSCs to the cap cells (dark gray). **(B–F)** Confocal z-stack projection of a germarium expressing H2Av-RFP (red; I) and CID-GFP (green; II) and stained for H3S10P (white; III) showing centromere localization in GSC nuclei throughout the cell cycle; inset (V) marked by box in merged image (IV). Interphase (B), initial and late prophase (C and D), metaphase (E), anaphase (F). **(G and H)** Wild type germarium stained for DAPI (cyan), EdU (white), anti-CID (green), and anti-1B1 (red); G2/ prophase GSCs (G) and EdU-positive (S phase) GSC and CB (H). **(I and J)** Quantification of CID-GFP fluorescence intensity observed at centromeres at prophase,

metaphase, and anaphase (I) or antibody staining at replication and G2/prophase (J). Star indicates the terminal filament; arrows indicate GSCs; arrowheads indicate GSC and CB; <1-d-old heterozygous CID-GFP/H2Av-RFP and wild-type females; scale bar 10 µm (I–IV) or 5 µm (V). Cartoons indicate the cell cycle phase. Fluorescence Intensity is expressed as integrated density after background subtraction (see Materials and methods); data are represented as the mean ± SEM; **, P < 0.005; ***, P < 0.0005, n.s., not significant; calculated with unpaired *t* test with Welch's correction.

and telophase, localizing to the opposite poles of the GSC and CB nuclei, with mostly four centromere foci (the exact number could not be detected due to clustering; Fig. 1, FV and HV). With the aid of several cell cycle markers (FUCCI, DACAPO) we did not succeed to isolate the G1 stage (not depicted), suggesting that it is very short in GSCs, as previously proposed (Ables and Drummond-Barbosa, 2013). In summary, our cell cycle analysis of centromere localization in M and interphase shows that centromeres are localized at the opposite poles of the new GSC and CB nuclei at anaphase, and that during DNA replication, centromeres retain this localization.

Centromeric recruitment of CID occurs after replication and before chromosome segregation in *Drosophila* GSCs and neuroblasts (NBs)

To assess the cell cycle timing of centromere assembly in GSCs, we quantified the CID fluorescent intensity (integrated density, Fig. S1, A–E; see Materials and methods) in mitosis and interphase. We first quantified the total amount of CID-GFP per nucleus at each phase of mitosis using the H3S10P marker (Fig. 1 I). No significant difference in CID level was detected between prophase (GSC_p = 1,993 ± 180, *n* = 18 cells) and metaphase (GSC_m = 2,512 ± 213, *n* = 12 cells). At anaphase, the CID level drops to about half the metaphase level (GSC_a = 1,230 ± 109.4, *n* = 8 cells). Using antibody staining, we quantified CID in S phase and G2 phase/prophase cells (Fig. 1 J). The total amount of CID detected per nucleus in S phase cells was significantly lower than the value obtained for G2 phase/prophase: GSC_{+EdU} = 1,764 ± 104.9 (*n* = 25 cells); $GSC_{G2/prophase}$ = 2,252 ± 108.6 (*n* = 25 cells). These results show that low levels of CID are observed at anaphase and replication, while considerably higher levels of CID are measured during G2 phase and prophase, suggesting that CID assembly in GSCs occurs after replication and before chromosome segregation. Furthermore, gradual deposition of CID might continue up to metaphase.

To exclude the possibility that these dynamics were a specific feature of GSCs, we investigated CID deposition in neural stem cells of the thoracic ventral nerve chord (tVNC; Fig. S1 F) in larval brains. To isolate reactivated NBs in G2/prophase, we antibody stained with the NB marker Deadpan (Boone and Doe, 2008) and the G2 regulator CYCA that is degraded at metaphase (Lilly et al., 2000). Deadpan-positive NBs display different sizes, between 4 and 8 µm (Fig. 2 G; Chell and Brand, 2010). We quantified the total amount of CID per nucleus in these cells through antibody staining (Fig. 2 H). In the CYCA-negative NBs, the DNA is not condensed, indicating that they are neither in mitosis nor in G2/prophase. We therefore labeled them as G1/S phase NBs. Our quantification shows that CYCA-positive NBs have 65% and 90% more CID compared with the G1/S phase NBs (G2/prophase = 4,190 ± 364, *n* = 30 cells; G1/S phase (4 µm) = 2,191 ± 151, *n* = 31 cells; G1/S phase (5–8 µm) = 2,552 ± 155, *n* = 30 cells; 9 tVNC analyzed). Our results confirm that, similar to GSCs, neural stem cells likely also assemble centromeres during the G2/M transition.

Correct CID deposition at GSC centromeres requires both CYCA and CYCB

Previous work showed that CENP-A assembly into centromeric chromatin is tightly linked to key cell cycle regulators (Stankovic et al., 2017). For instance, in *Drosophila*, CYCA accumulation and degradation in G2 phase is crucial for CID assembly (Erhardt et al., 2008; Mellone et al., 2011). Our work shows that in GSCs, centromeric recruitment of CID initiates in early G2 phase and continues until at least prophase (Fig. 1), coinciding with CYCA and CYCB activities. Therefore, we characterized the localization pattern of CYCA and B in GSCs with respect to centromeres. CYCA was previously shown to have both cytoplasmic and nuclear localization, specifically co-localizing with CID at the centromeres in Kc167 cells (Erhardt et al., 2008). We confirm using antibody staining that this is the case also for GSCs (Fig. 2, A–D′). This is different from the CYCB localization pattern, as it shows both cytoplasmic and nuclear localization but fails to localize at centromeres (Fig. 2, E–H′). Next, we used the GAL4 upstream activating sequence (GAL4: UAS) system (Duffy, 2002) to induce the RNAi-mediated depletion of CYCA and B specifically in GSCs using the germline-specific driver *nanos-Gal4* (Mathieu et al., 2013). To confirm both knockdowns, control *nanos-Gal4* and CYCA/B RNAi ovaries were antibody stained against CYCA or CYCB (Fig. S1, I–N′). VASA staining (Yan et al., 2014) of ovaries showed that control germaria chambers are filled with germ cells (Fig. 2, I–J′), while CYCA depletion leads to a loss of germ cells (Fig. 2, K–L′). Furthermore, the few germ cells left appear to be as twice as big as the germ cells in the control (focus on inset in Fig. 2, J′ and L′). Similar to what has been previously described (Mathieu et al., 2013), we observed that CYCB-depleted germaria have more cells compared with the control, by counting the number of VASA-positive cells from a similar number of z-stack projections (*nanos-Gal4* = 34.8 ± 2.3 cells, *n* = 21 germaria; CYCB RNAi = 50.6 ± 2.3, *n* = 23 germaria, not depicted; Fig. 2, M–N′). We did not observe these phenotypes in a nontarget mCherry RNAi control (Fig. S1, O–Q′). Given that CYCA knockdown can induce endoreduplication (Rotelli et al., 2019), we performed EdU staining on control and CYCA RNAi germaria. GSCs with a round spectrosome and decondensed DNA are EdU negative and can therefore be considered in G2/prophase (Fig. S1, R–T′). We next quantified total centromeric CID in GSCs nuclei in G2/prophase (Fig. 2, J′, J″, L′, L″, N′, N″, and O). We first observed that *nanos-Gal4* GSCs contain an average of 5.4 centromere foci detected with CID antibody, while GSCs depleted for CYCA show only 4. We found that in CYCA-knockdown GSCs, these levels are reduced by 40% compared with the control (Fig. 2 O, *nanos-Gal4* =

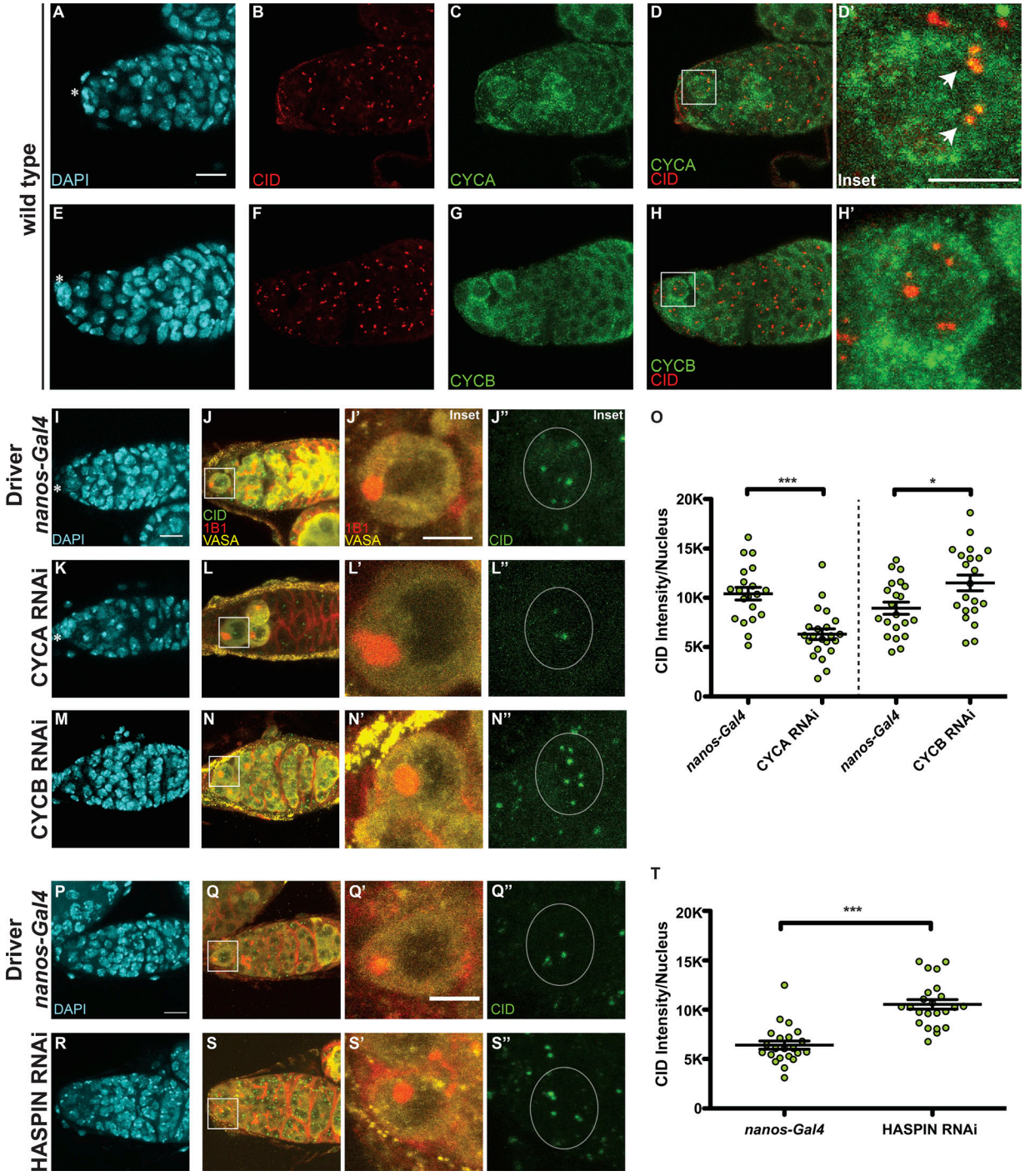

Figure 2. **CID deposition in GSCs requires CYCA, CYCB, and HASPIN. (A–H)** Wild-type germaria stained for DAPI (cyan), anti-CID (red), and anti-CYCA or anti-CYCB (green). **(I–N″)** Confocal z-stack projection of *nanos-Gal4* (I–J″), CYCA RNAi (K–L″), CYCB RNAi (M–N″) germaria, stained for DAPI (cyan), anti-VASA (yellow), anti-CID (green), and anti-1B1 (spectrosome, red). **(O)** Quantification of CID fluorescence intensity at centromeres per nucleus (L). **(P–S″)** Confocal z-stack projection of *nanos-Gal4* (P–Q″) and HASPIN RNAi germaria (R–S″), stained for DAPI (cyan), anti-VASA (yellow), anti-CID (green), and anti-1B1 (spectrosome, red). **(T)** Quantification of CID fluorescence intensity (MGVs) at centromeres per nucleus. Data are represented as the mean ± SEM; ***, $P < 0.0005$; *, $P < 0.05$, calculated with unpaired *t* test with Welch's correction. Star indicates the terminal filament and arrows indicate centromeres; 3-d-old female flies; scale bar, 10 µm; inset, 5 µm.

10,411 ± 642, $n = 20$ cells; CYCA RNAi = 6,303 ± 538.5, $n = 22$ cells, reported as mean gray value [MGV] to not take into account differences measured in single centromere foci size [not depicted]). In the case of CYCB RNAi, quantitation of CID revealed that GSCs show a 28% increase in CID compared with the control (Fig. 2 O, *nanos-Gal4* = 8,941 ± 610.8, 5.4 centromere foci, $n = 21$ cells; CYCB RNAi = 11,512 ± 801.8, 5.6 centromere foci, $n = 21$ cells, again reported as MGV). Taken together, our data show that

CYCA and CYCB have opposite effects on CID intensity. Specifically, CYCA depletion is responsible for a 40% loss of centromeric CID, while CYCB RNAi causes a 28% increase in CID level.

Centromeric CAL1 level is not affected by CYCA deficiency, while CID incorporation is inhibited by the HASPIN kinase

To test whether the loss of CID observed in CYCA-deficient GSCs was due to a loss of CAL1 and/or CENP-C, we antibody stained control and knockdown germaria for both CAL1 and CENP-C (Fig. S2, A–F″). CAL1 is detectable not only at centromeres but also in nucleoli (Unhavaithaya and Orr-Weaver, 2013; Schittenhelm et al., 2010; Erhardt et al., 2008). In this case, we specifically quantified the centromeric CAL1 in GSCs at G2/prophase and found no significant difference between the *nanos-Gal4* and CYCA RNAi samples (Fig. S2 R, *nanos-Gal4* = 3,921 ± 546.4, n = 15 cells; CYCA RNAi = 2,865 ± 457.8, n = 14 cells). In contrast, CENP-C levels are reduced (Fig. S2 S, *nanos-Gal4* = 7,060 ± 730.1, n = 15 cells; CYCA RNAi = 4,269 ± 525.6, n = 14 cells). These results suggest that the diminishment of CENP-C and CID observed in GSCs with reduced CYCA might be independent of CAL1. Because we found that CYCB has a role in CID deposition, we tested whether this occurs through its canonical pathway, which involves the activation of the kinase HASPIN that phosphorylates H3T3P (Moutinho-Santos and Maiato, 2014). Therefore, we performed HASPIN knockdown using the *nanos-Gal4* driver (Fig. 2, O–R″). We first confirmed this knockdown by immunofluorescence (Fig. S2 H–K′) and real-time quantitative PCR (qPCR; Fig. S2 L). Next, we again measured the amount of CID in G2/prophase GSCs (Fig. 2 S). Interestingly, we found that GSCs in the HASPIN RNAi showed a 65% increase in CID level compared with the control (Fig. 2 S, *nanos-Gal4*, 6,408 ± 418, 4.1 centromere foci, n = 22 cells; HASPIN RNAi, 10,542 ± 479, 5.1 centromere foci, n = 22 cells, reported as MGV). This result indicates that regular CID deposition at centromeres involves HASPIN.

Superresolution imaging reveals that GSC chromosomes are loaded with more CID, make stronger kinetochores, and capture more spindle fibers

To explore whether the timing of CID assembly might be linked to an asymmetric distribution of CID on chromosomes, we investigated CID distribution on sister chromatids in GSCs before division. Specifically, we used superresolution microscopy to examine CID intensity at sister centromeres at prometaphase and metaphase. To capture GSCs in this specific time window, we used the H3T3P marker (Xie et al., 2015). As expected, this marker first appears in GSCs at late prophase, while at anaphase the signal is lost (Fig. S2, M–Q). Importantly, superresolution microscopy allowed us to resolve eight individual sister chromatid pairs at these stages (16 centromere foci; Fig. 3). Using the position and orientation of the spectrosome, which has a round shape during mitosis (Ables and Drummond-Barbosa, 2013), we specifically identified centromeres that will be inherited by the GSCs (spectrosome proximal) and centromeres that will belong to the CBs (spectrosome distal, Fig. 3, A–D′; and Fig. S3, A–N′). Next, we measured the total amount of CID present on one set of chromosomes versus the other. For comparison, we conducted the same analysis on differentiated CCs of neighboring four-cell cysts that divide symmetrically (Figs. 3 E and S3, O–T). The ratio obtained shows that centromeres present on the GSC side incorporate ∼20% more CID, compared with centromeres of the CB side (ratio GSC_{side}/CB_{side} = 1.192 ± 0.072, n = 9 GSCs in prometaphase/metaphase; Fig. 3 E, values shown in Fig. S3 T). Importantly, this CID asymmetry is not observed in CCs at the same time window (ratio CCA_{side}/CCB_{side} = 1.016 ± 0.027, n = 9 CC in prometaphase/metaphase; Fig. 3 E, values shown in Fig. S3 T). To check whether bigger centromeres dock more spindle fibers, as already proposed (Drpic et al., 2018), we antibody stained GSCs in prometaphase and metaphase for tubulin (Fig. 3, F–I′; and Fig. S3 U–Y′). We observed more spindle fibers nucleated from the daughter centrosome, inherited by the GSC (Salzmann et al., 2014), compared with those nucleated from the mother centrosome on the CB side. This is detectable on bioriented spindles at both prometaphase and metaphase (Fig. 3, F–I′; and Fig. S3, U–Y′). To quantify this signal, we measured fluorescent intensity of the spindle on the GSC side versus the CB side (expressed as integrated density). The ratio of the two areas per cell analyzed show that GSC chromosomes display ∼48% more spindle microtubules compared with the CB chromosomes (ratio GSC_{side}/CB_{side} = 1.48 ± 0.2, n = 10 GSCs in prometaphase/metaphase). We also confirmed by performing costaining for both tubulin and CID that the microtubules nucleated from the centrosome were captured by centromeres (Fig. 3, J–K′). Next, we investigated whether the asymmetric distribution of CID is maintained later in the cell cycle. Specifically, we analyzed anaphase GSCs in transgenic flies expressing H2Av-RFP/CID-GFP and replicating GSC-CB couples (Fig. 3, L–O) in wild-type EdU-stained flies. As shown (Fig. 3, L–M″), both anaphase and S phase GSCs appear to retain the higher amount of CID. Quantitation revealed that at S phase, GSCs retain 14% more CID compared with CBs (Fig. 3 N; ratio GSC/CB = 1.14 ± 0.04, n = 27 couples GSC-CB analyzed; anaphase data not depicted because of the low number of cells analyzed). Furthermore, this value is not significantly different from the values found at prometaphase for GSC chromosomes (Fig. 3 N). Finally, we assessed whether centromeres that harbor more CID make bigger kinetochores, which could bias segregation (Drpic et al., 2018). For this, we quantified the amount of CENP-C in replicating GSC-CB couples (Fig. 3, O–O″), detecting a higher amount in GSCs (Fig. 3 P, ratio GSC/CB = 1.27 ± 0.05, n = 36 GSC-CB couples analyzed). These results suggest that chromosomes are labeled with a differential amount of CID upon centromere assembly. Moreover, chromosomes inherited by the GSCs harbor more CID and make bigger kinetochores that capture more spindle fibers compared with CB chromosomes.

In GSCs, CAL1 is crucial for division and differentiation, as well as CID and CENP-C recruitment to centromeres

To test the role of centromeres in stem cell asymmetric division, we performed functional analyses knocking down CID and CAL1 in GSCs (Dietzl et al., 2007). Controls stained for VASA and the spectrosome (1B1) showed germaria filled with germ cells (Fig. S4 A) and GSCs having a round spectrosome attached to the cap

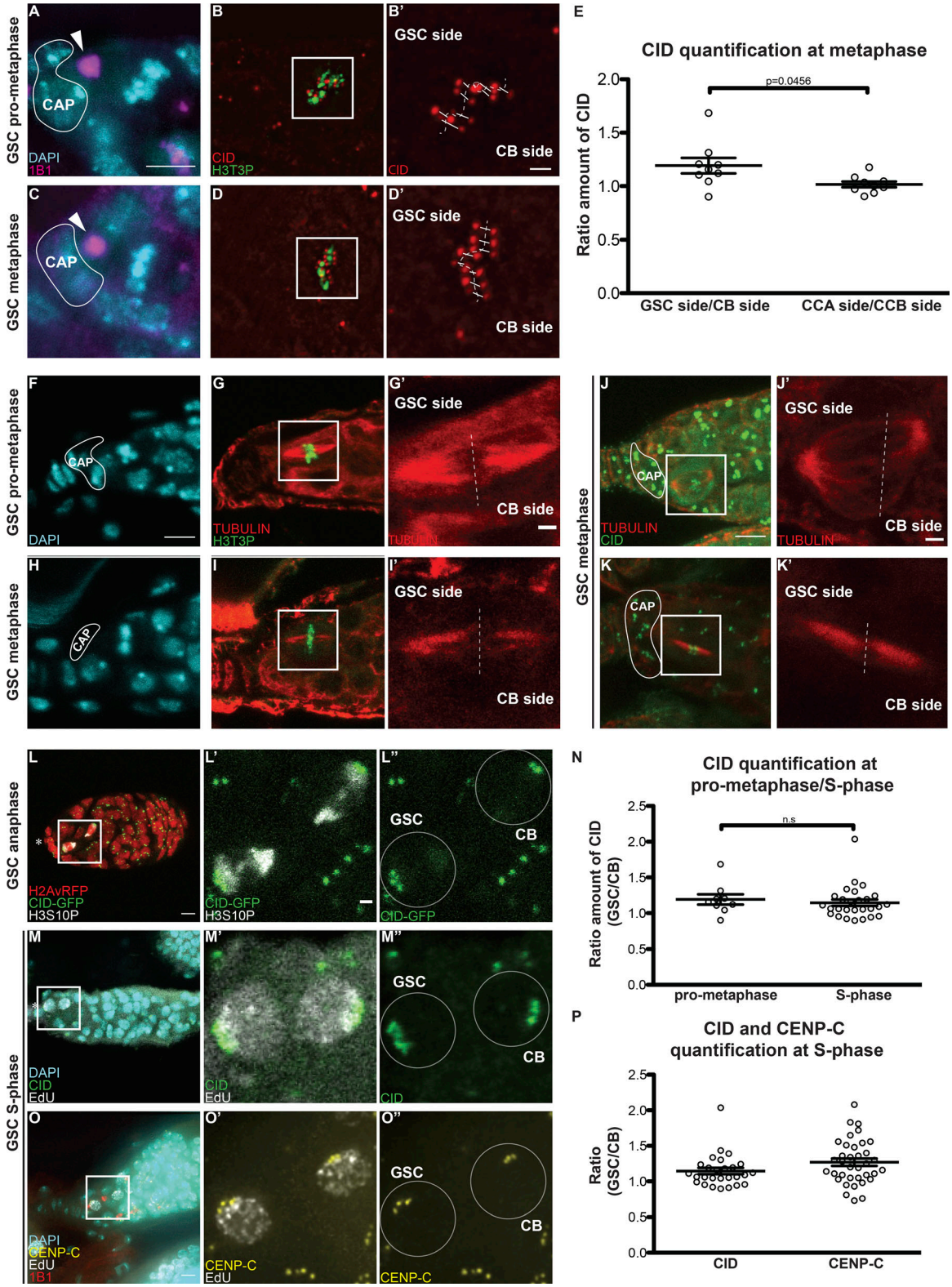

Figure 3. **Sister chromatids of GSCs and CBs retain differential amounts of CID and CENP-C. (A–D′)** Superresolution (N-SIM) z-stack projection of a GSC at prometaphase (A–B′) and metaphase (C–D′) stained for DAPI (cyan), anti-1B1 (spectrosome, magenta), anti-CID (red), and anti-H3T3P (green). **(E)** Ratio of the total amount of CID detected on the chromosomes of the GSC side and the total amount of CID detected on the chromosomes of the CB side, and similarly for the control CCA and CCB sides of cyst cells (CC). **(F–I′)** Confocal z-stack projection of a GSC at prometaphase (F–G′) and metaphase (H–I′) stained for DAPI (cyan), anti-TUBULIN (red), and anti-H3T3P (green). **(J–K′)** Confocal z-stack projection of a GSC at metaphase stained for anti-TUBULIN (red), anti-CID (green). **(L–L″)** Confocal z-stack projection of a H2Av-RFP/CID-GFP germarium, capturing a GSC and CB at anaphase. **(M–M″)** Confocal z-stack projection capturing a GSC and CB at S phase stained for DAPI (cyan), EdU (white), and anti-CID (green). **(N)** Comparison of the ratio of the total amount of CID detected on the

chromosomes of the GSC side and the total amount of CID detected on the chromosomes of the CB side at prometaphase, and the amount of CID detected between GSCs and CBs at S phase. **(O–O″)** Confocal z-stack projection of a GSC and CB at S phase stained for DAPI (cyan), EdU (white), and anti-CENP-C (yellow). **(P)** Comparison of the ratio of CID and CENP-C between GSCs and CBs at S phase. White line, cap cells; arrowheads, spectrosome. Data are represented as the mean ± SEM; P value in E calculated through the use of different tests: unpaired *t* test with Welch's correction (plotted); Mann–Whitney *U* test P value = 0.0244; Wilcoxon matched-pairs signed rank test P value = 0.0195; n.s., not significant. In A–L″, 30-min-old female flies; in N–O″, <1-d-old female flies; scale bar, 5 µm; inset, 1 µm.

cells (Fig. S4 A, arrows). As expected for an essential gene, CID knockdown resulted in empty ovaries with no VASA-positive cells, and therefore no germ cells (Fig. S4 A). For the CAL1 knockdown, we confirmed a >10-fold depletion of CAL1 expression through real-time qPCR (Fig. 4 A, see Materials and methods). Phenotypic analysis of CAL1-depleted ovaries showed they were largely empty (Fig. S4 A). However, 18% of germaria (3 of 16) showed the presence of a few cells (1–3) that were VASA positive with a round spectrosome and located 90% of the time at the apical end of germaria (Fig. S4 A). Older flies (7 d after eclosion) showed a higher frequency of this phenotype (~30%, 5 of 16 germaria; not depicted). The 1–3 cells left show all the features of GSCs (Fig. 4, BI–BIV). They are VASA positive (Fig. S4 A) and located at the apical end of the germarium close to the terminal filament in the niche; have a round spectrosome (Fig. S4 A, compare Fig. 4, BII and CII); stain positive for phosphorylation of mothers against Dpp (pMAD), a BMP signaling indicator present in GSCs (Song et al., 2004; compare Fig. 4, BIII and CIII); and do not express the differentiation marker bag of marbles (BAM; Fig. S4 B). This analysis confirms that also in stem cells, CAL1 is crucial for cell division and therefore also for differentiation.

Given that CAL1 is located at both centromeres and nucleoli, we investigated the depletion of both CAL1 pools in GSCs. In *nanos-Gal4* flies (Fig. S4 C), CAL1 colocalizes with both CENP-C and the nucleolar marker FIBRILLARIN (Fig. S4 C). In the CAL1 knockdown samples, CAL1 is still present in the nucleolus of GSCs, colocalizing with FIBRILLARIN (Fig. S4 C); however, it is missing from the centromeres, as we could not distinguish any CAL1 signal outside of the nucleolus overlapping with CENP-C (Fig. S4 C). Indeed, neither CENP-C nor CID is detectable at centromeres in the knockdown GSCs (Fig. 4, D and E). From our observations, we conclude that (a) knockdown depletes the pool of CAL1 at centromeres, but not the one at the nucleolus; and (b) knockdown of centromeric CAL1 is responsible for the loss of functional centromeres in GSCs.

Overexpression of CAL1 and CID, as well as HASPIN knockdown, promotes stem cell self-renewal

To further explore centromere function in GSCs, we performed overexpression of CID, CAL1, or CAL1 together with CID. For this purpose, we crossed flies carrying CID-mCherry (CID_OE), CAL1-YFP (CAL1_OE), or both CAL1-YFP and CID-mCherry (CAL1-CID_OE) transgenes to a *nanos-Gal4* driver line. Ovaries from F1 progeny were screened for correct localization of the fusion proteins, confirmed using antibody staining against CID and FIBRILLARIN (Fig. S5, A–O′). As expected, the *nanos-Gal4* control does not show any YFP or RFP fluorescence (Fig. S5, A–E′). In the CAL1-CID_OE, CAL1-YFP colocalizes with CID-mCherry and with CID antibody (Fig. S5, F–I [arrow] and Fig. S5 J), but we could not detect any colocalization with FIBRILLARIN in nucleoli (Fig. S5, F′–I′ [arrow] and Fig. S5 J′). In the CAL1_OE, CAL1 localizes as expected at centromeres (Fig. S5, K–N, arrows, and Fig. S5 O) and at nucleoli (Fig. S5, K–N′ [arrowheads] and Fig. S5 O′). We also show that CID_OE colocalizes with CID antibody (Fig. S5 P). We next quantified the number of round spectrosomes, using antibody staining against 1B1, indicative of GSC and CB cells (Fig. 5, A–D and M). In *nanos-Gal4*, we found an average of two spectrosomes/germarium (Fig. 5 A [arrows] and Fig. 5 M; *nanos-Gal4*$_{1B1}$ = 1.84 ± 0.16, *n* = 30 germaria). In the CID_OE and CAL1-CID_OE, this number increases ~1.4-fold (Fig. 5, B and C [arrows] and Fig. 5 M, CID_OE$_{1B1}$ = 2.70 ± 0.24; CAL1-CID_OE$_{1B1}$ = 2.61 ± 0.17, *n* = 30 germaria), while in the CAL1_OE, the number almost doubles (Fig. 5 D [arrows] and Fig. 5 M; CAL1_OE$_{1B1}$ = 3.51 ± 0.31, *n* = 30 germaria). To measure the GSC/CB balance, we used the stem cell marker pMAD (Song et al., 2004) and SEX-LETHAL (SXL; Fig. 5, E–L and N), a marker that labels the GSC–CB transition. SXL is present from GSCs up to the two-cell cyst stage and can therefore be used to define the size of the germarium compartment containing GSCs and early differentiated cells (Chau et al., 2009). Our quantification shows that *nanos-Gal4* germaria have approximately one pMAD-positive cell (*nanos-Gal4*$_{pMAD}$ = 1.36 ± 0.10, *n* = 30 germaria; Fig. 5, E and N), while this number doubles in all the overexpression lines (Fig. 5, F–H and N; CAL1-CID_OE$_{pMAD}$ = 2.10 ± 0.13; CAL1_OE$_{pMAD}$ = 2.20 ± 0.13 and CID_OE = 2.46 ± 0.15). SXL staining revealed that there is no difference in the number of SXL-positive cells between the *nanos-Gal4* control, CID_OE, or CAL1-CID_OE (*nanos-Gal4*$_{SXL}$ = 4.80 ± 0.33, *n* = 30 germaria; CAL1-CID_OE$_{SXL}$ = 4.86 ± 0.25; CID_OE = 4.93 ± 0.30; Fig. 5, I–K and N), while overexpression of CAL1 alone is responsible for an increase in the number of SXL-positive cells compared with the control (CAL1_OE$_{SXL}$ = 6.86 ± 0.27, *n* = 30 germaria; Fig. 5, L and N). This analysis shows that CID, CAL1-CID, and CAL1 overexpression leads to an increase in the number of GSCs compared with the control. We next calculated the SXL/pMAD ratio as a measure for the number of GSCs, CBs, and two-cell cysts in the germarium. In control germaria, there are 3.5 SXL-positive cells for each pMAD-positive cell (*nanos-Gal4*$_{SXL/pMAD}$ = 3.53 ± 0.29). This ratio does not change in the CAL1_OE (CAL1_OE$_{SXL/pMAD}$ = 3.38 ± 0.22), which indicates that differentiation occurs at an expected rate compared with the control. However, in the CAL1-CID_OE and CID_OE, ~2 SXL-positive cells are present for each pMAD-positive cell (CAL1-CID_OE$_{SXL/pMAD}$ = 2.47 ± 0.23; CID_OE$_{SXL/pMAD}$ = 2.23 ± 0.19; Fig. S5 Q). This means that GSCs overexpressing CAL1-CID and/or CID self-renew rather than differentiate. To exclude the possibility that phenotypes were due to the genetic background of the responder flies, we conducted the

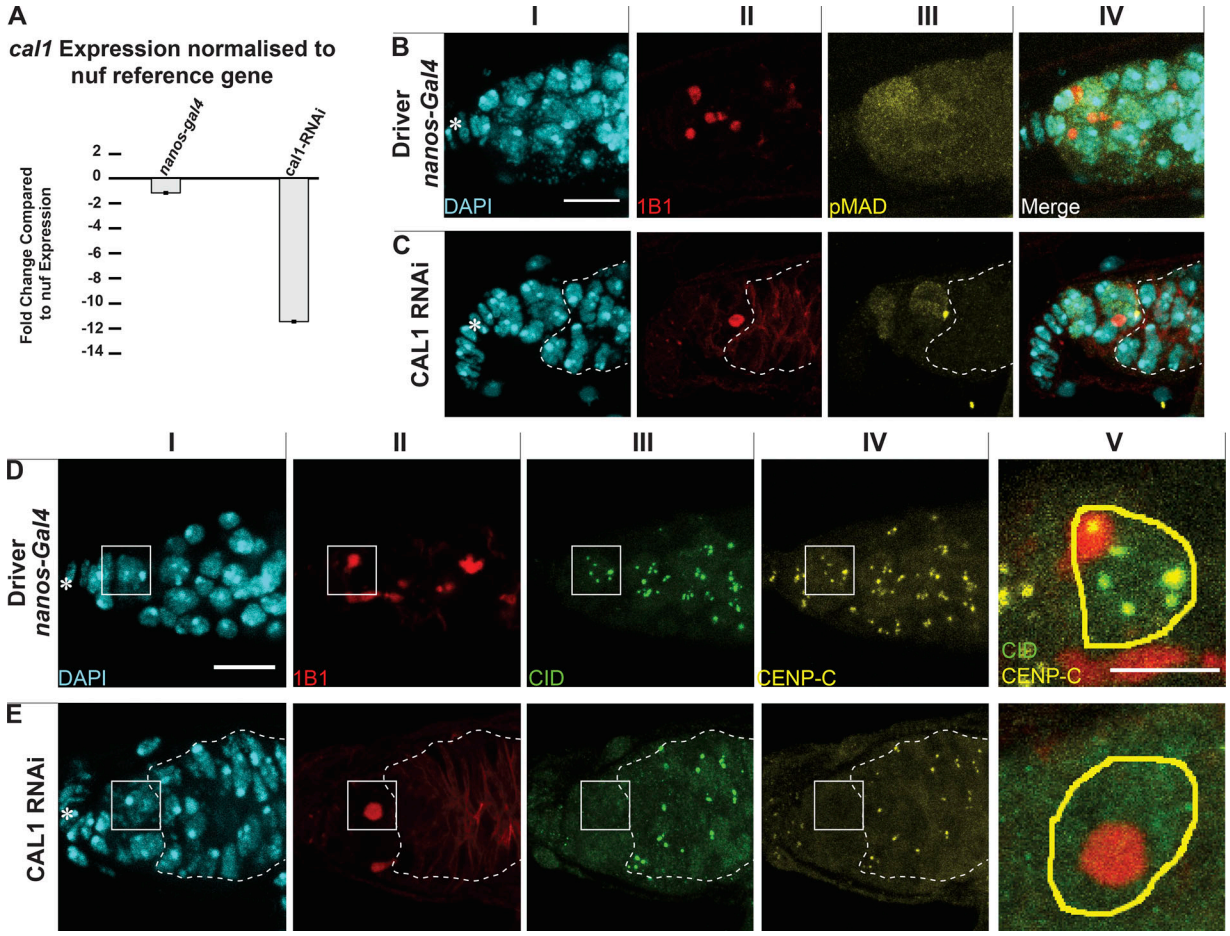

Figure 4. **CAL1 knockdown blocks cell proliferation. (A)** CAL1 knockdown confirmation by real time qPCR. **(B and C)** Confocal z-stack projection of *nanos-Gal4* (B) and CAL1 RNAi (C) germaria, stained for DAPI (cyan), anti-1B1 (spectrosome, red), and anti-pMAD (labels GSCs, yellow). **(D and E)** Confocal z-stack projection of *nanos-Gal4* (D) and CAL1 RNAi germaria (E), stained for DAPI (cyan), anti-1B1 (spectrosome, red), anti-CID (green), and anti-CENP-C (yellow). Star indicates the terminal filament; dotted lines represent follicle cells; 3-d-old female flies; scale bar, 10 µm; DV and EV, 5 µm.

same analysis on lines in which the overexpression is not induced and found similar values to the *nanos-Gal4* control (not depicted). Altogether, our results suggest that the overexpression of CAL1 and CID together, as well as CID alone, promotes self-renewal, while CAL1 overexpression stimulates proliferation.

Because we found that HASPIN has a role in CID assembly, and given its proposed role in GSC asymmetric division in male flies (Xie et al., 2015), we tested whether HASPIN knockdown disrupts the GSC/CB balance in the germarium. We found that HASPIN knockdown germaria have a higher number of round spectrosomes, as well as a higher number of pMAD-positive cells, compared with the control (*nanos-Gal4*$_{1B1}$ = 2.6 ± 0.19, n = 60 germaria analyzed; *nanos-Gal4*$_{pMAD}$ = 1.72 ± 0.10, n = 54 germaria analyzed; HASPIN_RNAi$_{1B1}$ = 3.80 ± 0.19, n = 60 germaria analyzed; HASPIN_RNAi$_{pMAD}$ = 3.01 ± 0.13, n = 54 germaria analyzed; Fig. 5, O–S). These results confirm that also HASPIN regulates GSC/CB content in *Drosophila* germaria.

GSC self-renewal disrupts asymmetric inheritance of CID

To investigate whether the asymmetric inheritance of CID between GSC and CB has a role in regulating the stem cell asymmetric division (Fig. 5), we quantified the amount of CID in replicating GSC-CB couples in controls, CAL1-CID_OE, and HASPIN knockdown germaria (Fig. 6, A–D). We again observed CID asymmetry in control couples (Fig. 6, A, A′, and D; ratio GSC/CB = 1.18 ± 0.04, n = 22 GSC-CB couples analyzed). Notably, CID asymmetry is lost in both CAL1-CID_OE or HASPIN knockdown couples (Fig. 6, B–D, ratio GSC/CB: CAL1-CID_OE = 1.02 ± 0.06, n = 24 GSC-CB couples analyzed; HASPIN$_{RNAi}$ = 1.00 ± 0.03, n = 20 GSC-CB couples analyzed). This result indicates that in germaria enriched with GSCs at the expense of CBs, there is also a loss of asymmetric CID inheritance.

To examine CAL1 and CID requirements at later stages of egg development, we performed knockdown experiments for CENPs using the *bam-Gal4* driver (active in 4–8-cell cysts). Ovaries were stained for VASA and BAM to mark 4–8-cell cysts. Surprisingly, we noticed that cell division past this stage is not impaired by depletion of either CID or CAL1 (Fig. 6, E–G). Remarkably, in the CID RNAi, we did not observe a significant diminishment of CID compared with the control (Fig. 6, E and F). In the CAL1 RNAi, CID levels appear to be reduced, but cell division proceeds normally (Fig. 6, E and G). In 16-cell cysts, after the BAM region, we confirmed a reduction of CAL1 in the CAL1 knockdown samples compared with the *bam-Gal4* driver (Fig.

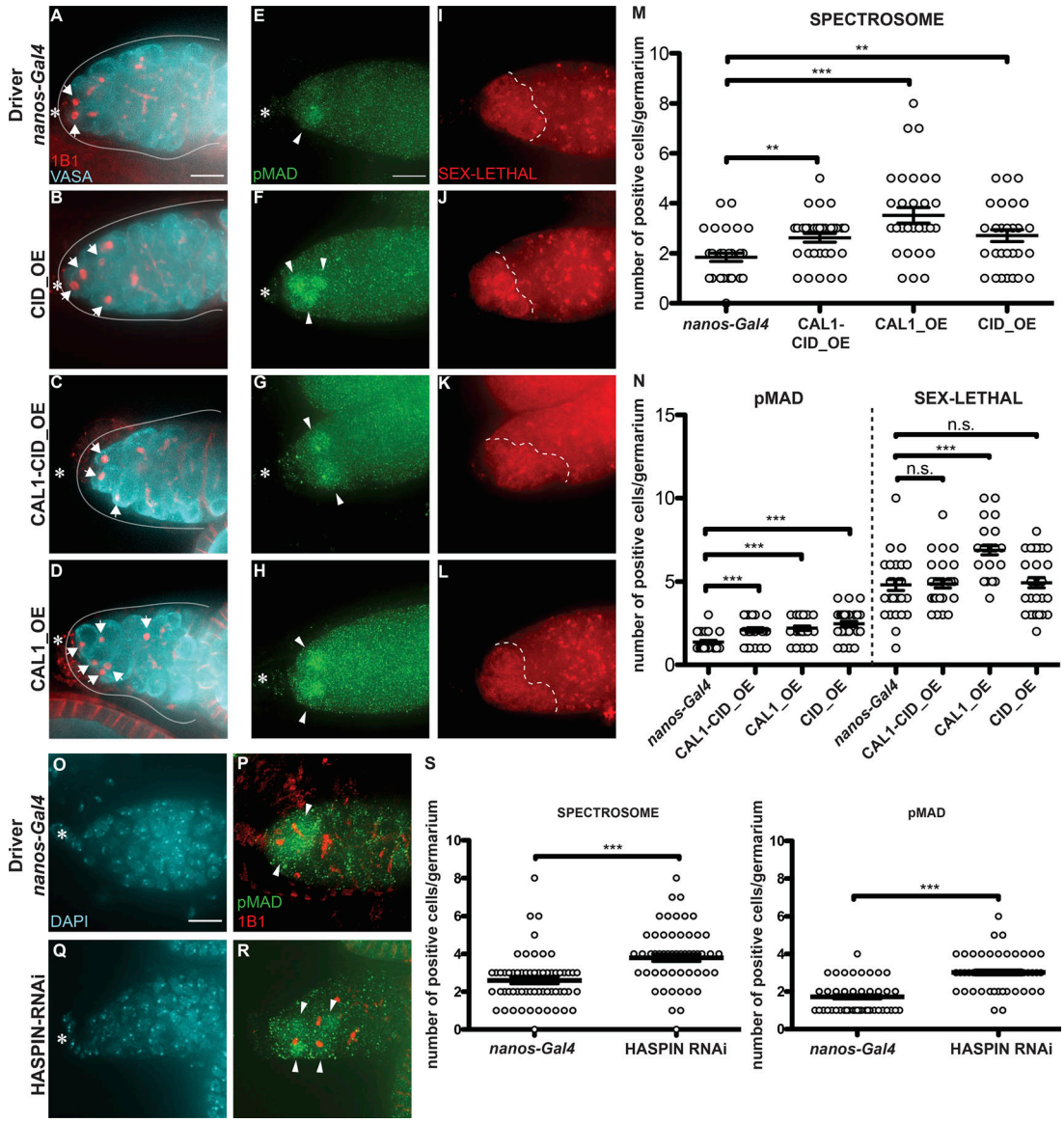

Figure 5. **CID and CAL1 overexpression and HASPIN knockdown promote stem cell self-renewal. (A–D)** Wide-field z-stack projection of *nanos-Gal4* (A), UAS_ CID-mCherry (CID_OE; B) UAS_CAL1-YFP_UAS_CID-mCherry (CAL1-CID_OE; C), and UAS_CAL1-YFP (CAL1_OE; D) germaria, stained for VASA (cyan) and anti-1B1 (spectrosome, red). **(E–L)** Confocal z-stack projection of *nanos-Gal4* (E and I), CID_OE (F and J), CAL1-CID_OE (G and K), and CAL1_OE (H and L) germaria, stained for anti-pMAD (green) and anti-SXL (red). **(M)** Spectrosome quantification. **(N)** pMAD and SXL quantification. **(O–R)** Wide-field z-stack projection of *nanos-Gal4* (O and P) and HASPIN RNAi (Q and R) germaria stained for DAPI (cyan), anti-pMAD (green), and anti-1B1 (spectrosome red). **(S)** Spectrosome (left) and pMAD (right) quantitation in *nanos-Gal4* and HASPIN RNAi. Data are represented as the mean ± SEM; ***, P < 0.0005; **, P < 0.005, n.s., not significant; calculated with unpaired *t* test with Welch's correction. Star, terminal filament; arrows, spectrosome; arrowheads, pMAD-positive cells; dotted line, SXL regions; solid line, germarium; 3-d-old female flies; scale bar, 10 µm.

S5 R). To check the impact of CAL1 reduction on centromere assembly, we antibody-stained samples against CENP-C. In the control cysts, identified through the fusome morphology (Fig. 6, H′–K′, arrows in Fig. 6 I′), two to four centromere foci closely opposed to the nucleolus are normally visible (Unhavaithaya and Orr-Weaver, 2013; Fig. 6, J′–K′). In the CAL1 knockdown sample (Fig. 6, L′–O′), we did not observe any change in the amount of CENP-C (Fig. 6, N′–O′). Since CID/CENP-C levels were not decreased after expression of CID/CAL1 RNAi using the *bam-Gal4* driver, we sought to confirm this knockdown approach in germaria. Therefore, we tested the functionality of the driver on another centromere protein (CENP-C). Our results (Fig. S5 S) confirm effective CENP-C knockdown at this stage. In addition, since other drivers successfully knocked down CAL1 and CID, this observation supports the idea that at this stage CID and CENP-C are already assembled at centromeres and that CAL1 function is dispensable, at least for the cell division occurring after the eight-cell stage.

CID assembly dynamics differ between GSCs and cysts

To better understand the dynamics of CID assembly in GSCs and differentiated CCs, we measured the amount of CID per nucleus

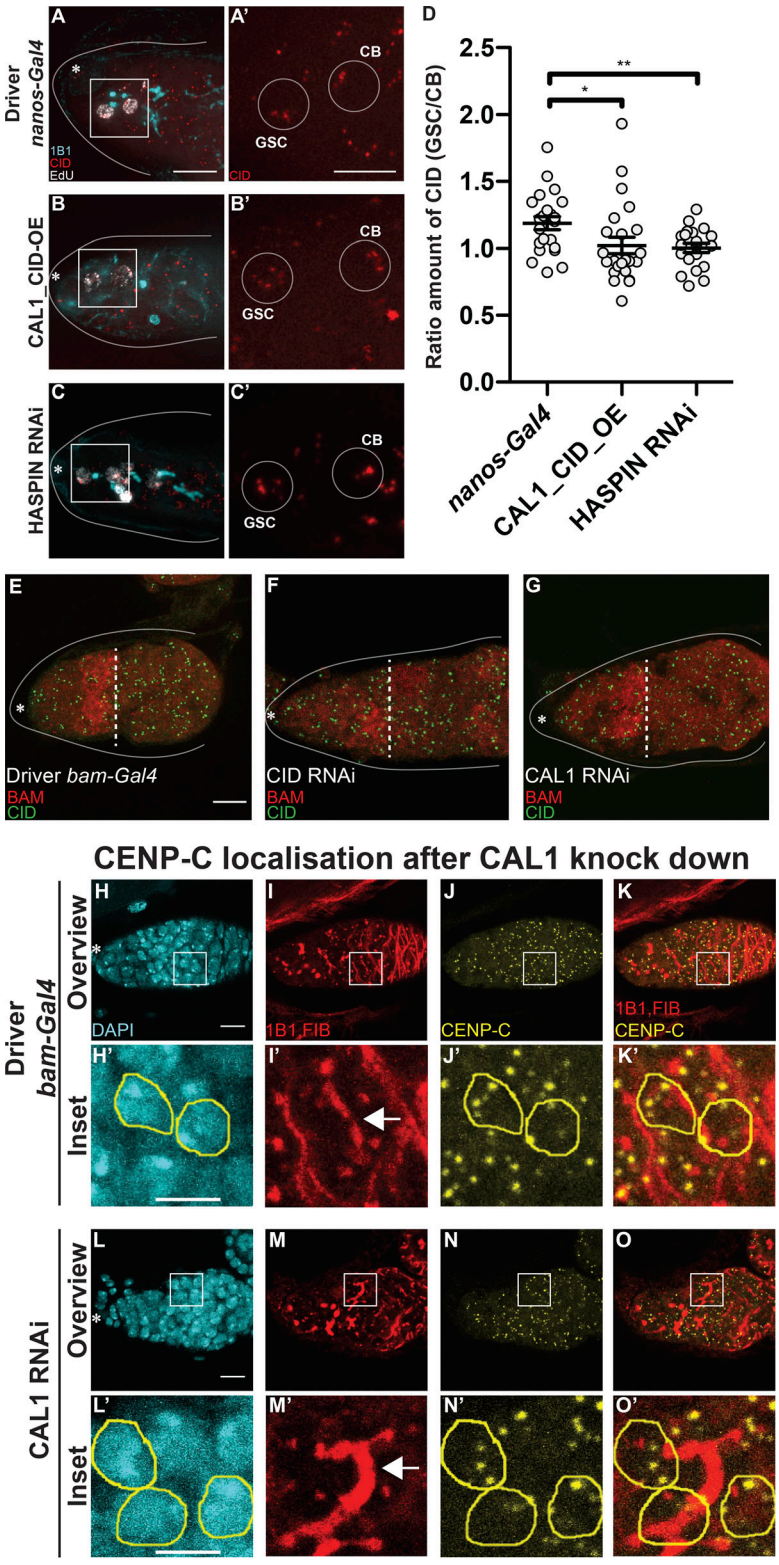

Figure 6. **GSC self-renewal disrupts CID asymmetric inheritance. (A–C′)** Wide-field z-stack projection of *nanos-Gal4* (A and A′), CAL1-CID_OE (B and B′), and HASPIN RNAi (C and C′) germaria stained for 1B1 (spectrosome, cyan), EdU (white), anti-CID (red). **(D)** Ratio of the total amount of CID detected in the GSC and the total amount of CID detected in the CB at S phase. **(E–G)** Confocal z-stack projection of *bam-Gal4* (E), CID RNAi (F), and CAL1 RNAi (G) germaria, stained for anti-BAM (red) and anti-CID (green). **(H–O′)** Confocal z-stack projection of *bam-Gal4* (H–K′) and CAL1 RNAi (L–O′) germaria, stained for DAPI (blue), anti-1B1 (red), anti-FIBRILLARIN (red), and anti-CENP-C (yellow). 16-cell cysts were selected based on the fusome morphology (arrow) in the control (H′–K′) and in the CAL1 RNAi (L′–O′). Data are represented as the mean ± SEM; *, $P < 0.05$; **, $P < 0.005$, calculated with unpaired *t* test with Welch's correction. Star, terminal filament; dotted line, end of the BAM-positive region; arrow, fusome; solid line, germarium; 3-d-old female flies; scale bar, 10 µm; inset, 5 µm.

in both cell types to detect possible differences. We used H3S10P to mark GSCs and synchronously dividing eight-cell cysts at prophase (Fig. 7, A–F′). We noted that anti-CID staining at prophase labels centromeric CID but also shows a nuclear non-centromeric localization. As we did not observe this localization with CID-GFP, it is possible that it results from this specific antibody combination. Therefore, we focused our quantification on centromeric CID signals only. Compared with prophase GSCs, CC nuclei are smaller, yet centromeric foci are present in a similar number. From our quantification, we detected an ∼40% diminishment in the total amount of CID in CCs at the eight-cell stage (CC = 323.4 ± 20.94, *n* = 26 cell analyzed; Fig. 7 I), compared

with GSCs (GSC = 547.2 ± 41.57, n = 24 cell analyzed; Fig. 7 I). This indicates a dramatic change in CID assembly dynamics, such that it is not replenished to 100% each cell division. Taken together with our observation of no significant reduction in CID after CID or CAL1 RNAi at this stage (Figs. 6 and S5), these data suggest that CID is inherited from the GSCs with little new CID loading occurring in cysts.

Discussion

In this study, we performed a detailed characterization of centromere dynamics throughout the cell cycle in *Drosophila* female GSCs. Our analysis reveals that GSCs initiate CID incorporation after replication and that its deposition continues until at least prophase (Fig. 7 H). *Drosophila* neural stem cells follow the same trend. Notably, this timing is different from existing studies in other metazoans. We also found that CYCA, CYCB, and HASPIN are critically involved in CID (and CENP-C) loading at centromeres. According to our model (Fig. 7 H), CYCA promotes centromere assembly, while CYCB prevents excessive deposition of CID, through the HASPIN kinase. Moreover, chromosomes that will be inherited by GSCs are labeled with a higher amount of CID and capture more spindle microtubules (Fig. 7 J). Importantly, we show that overexpression of CAL1 and CID together, as well as HASPIN knockdown, promotes stem cell self-renewal, disrupting the asymmetric inheritance of CID. Depletion of CAL1 in stem cells blocks cell division, while CAL1 overexpression causes GSC-like tumors, highlighting its crucial role in cell proliferation. We raise three main points of discussion: (1) the biological significance of centromere assembly in G2-M phase; (2) CAL1 is a cell proliferation marker; and (3) CID incorporation into centromeric chromatin occurs before meiosis.

Biological significance of centromere assembly in G2-M phase

Cell cycle time

According to our data, CID deposition occupies a wide window of time from after replication and early G2 phase to prophase. The assembly of GSC centromeres during the G2/M transition could be due to the contraction of the G1 phase, a characteristic of stem cells (Pauklin and Vallier, 2013; White and Dalton, 2005; Becker et al., 2006). Yet, in fly embryonic divisions, G1 phase is missing, and instead CID loading occurs at anaphase (Schuh et al., 2007). Therefore, G2/M assembly might be a unique property of stem cells. This timing is also similar to the one found for *Drosophila* spermatocytes, which assemble centromeres in prophase of meiosis I (Dunleavy et al., 2012; Raychaudhuri et al., 2012). These spermatocytes undergo an arrest in prophase I for days, indicating a gradual loading of CID over a long period of time. Intriguingly, a similar phenomenon has been recently observed in G0-arrested human tissue culture cells and starfish oocytes (Swartz et al., 2019). Given that GSCs are mostly in G2 phase (Yamashita et al., 2003), *Drosophila* stem cells might show similar properties to quiescent cells. According to the most recent models, there is a dual mechanism for CENP-A deposition: (a) a rapid pulse during G1 in mitotically dividing cells; and (b) a slow but constant CENP-A deposition in nondividing cells to actively maintain centromeres (Swartz et al., 2019). Indeed, while previous studies in *Drosophila* NBs show a rapid pulse of CENP-A incorporation at telophase/G1 (Dunleavy et al., 2012), the majority of the loading could occur between G2 and prophase. Our new results also support this model.

Cell cycle regulation

Incorporation of CID before chromosome segregation might reflect a different CYCLIN-CDK activity in these cells. For instance, it has been already shown that in *Drosophila* GSCs CYCLIN E, a canonical G1/S cyclin, exists in its active form (in combination with Cdk2) throughout the cell cycle, indicating that some of the biological process commonly occurring in G1 phase might actually take place in G2 phase (Ables and Drummond-Barbosa, 2013). This is in line with our functional findings, where depletion of CYCA causes a decreased efficiency in CID and CENP-C assembly. We also found that this loss might be independent from CAL1. Surprisingly, correct CID deposition in GSCs also requires CYCB and HASPIN. Indeed, an inhibitory mechanism for CID deposition through CYCB has already been proposed in mammals (Stankovic et al., 2017). Interestingly, in *Drosophila* male GSCs, centromeric CAL1 is reduced between G2 and prometaphase (Ranjan et al., 2019), further suggesting a role for additional regulators of CID assembly, such as CYCA/B or HASPIN, at this time.

Epigenetic mechanism to drive cell fate during stem cell asymmetric division

According to our results, asymmetric cell division of GSCs is epigenetically regulated by differential amounts of centromeric proteins deposited at sister chromatids, which in turn can influence the attachment of spindle microtubules and can ultimately bias chromosome segregation. It is interesting to speculate on the temporal sequence of these events. Two scenarios can be proposed: (a) the nucleation of microtubules from the GSC centrosome requires bigger kinetochores; or (b) bigger kinetochores require a higher amount of spindle fibers to attach. Our results together with recent studies support the latter scenario. In fact, in *Drosophila* male GSCs, asymmetric distribution of centromeric proteins is established before microtubule attachment. Furthermore, microtubule disruption leaves asymmetric loading of CID intact, while it disrupts the asymmetric segregation of sister chromatids (Ranjan et al., 2019). Our data confirm this model, as we observe symmetric segregation of CID upon HASPIN knockdown. Indeed, in vertebrates HASPIN knockdown causes spindle defects (Wang et al., 2012; Yamagishi et al., 2010; Kelly et al., 2010). Specifically, we observed that a 1.2-fold difference in CID and CENP-C levels between GSC and CB chromosomes can bias segregation. While this difference is small, it fits with the observation that small changes in CENP-A level (on the order of 2–10% per day) impact on centromere functionality in the long run (Swartz et al., 2019). In *Drosophila* male GSCs, an asymmetric distribution of CID on sister chromatids >1.4-fold was reported (Ranjan et al., 2019). This higher value might reflect distinct systems in males and females or the quantitation methods used. Importantly, CID asymmetry in males is established in G2/prophase, in line with the time window we define for CID assembly. Further support for

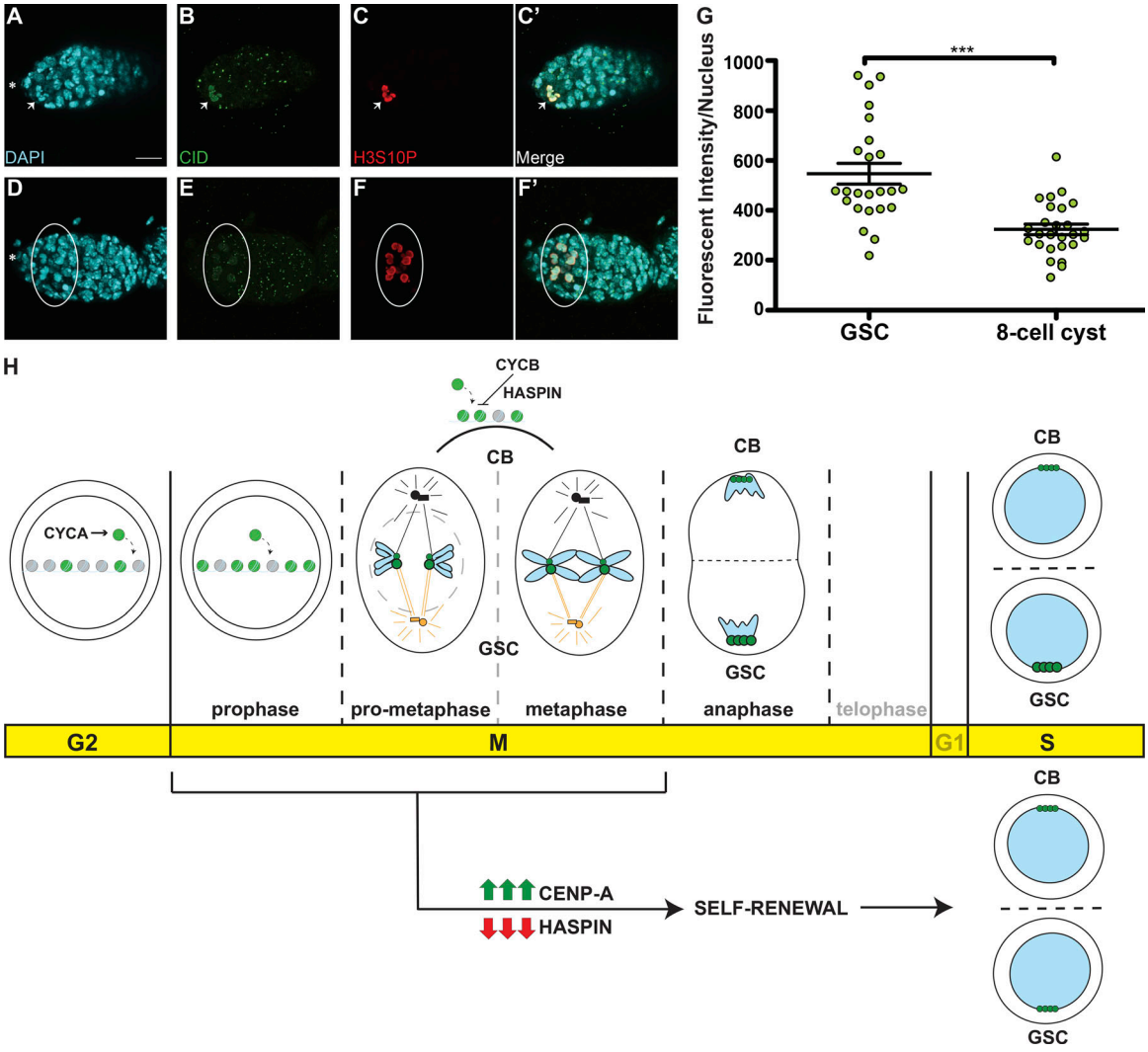

Figure 7. **Cyst cells incorporate less CID compared with GSCs. (A–F′)** Confocal z-stack projection of a *nanos-Gal4* germarium, stained for DAPI (cyan), anti-CID (green), and anti-H3S10P (red), to highlight a GSC (A–C′, arrow) and eight-cell cysts (D–F′, circle) in prophase. **(G)** Quantification of CID fluorescence intensity (integrated density) at centromeres in GSCs and eight-cell cysts at prophase obtained using wide-field microscopy. Data are represented as the mean ± SEM; ***, P < 0.0001. Star, terminal filament; 3-d-old female flies; scale bar, 10 µm. **(H)** Model for centromere assembly during the cell cycle. After replication, at early G2 phase, centromere assembly starts, promoted by CYCA, and centromeric nucleosomes (green) replace canonical nucleosomes (gray). This process continues until at least prophase. Excessive CID deposition is prevented by CYCB through HASPIN. At prometaphase, microtubules from centrosomes attach to centromeres through the kinetochore. At this point, sister chromatid pairs are loaded with differential amounts of CID (green) and CENP-C (not depicted) at centromeres. Chromosomes that retain more CID (bigger centromeres, figurative), make bigger kinetochores and attract more microtubules nucleating from the daughter centrosome (orange) and will be inherited by the GSC. At anaphase, and at replication, centromeres are clustered at the opposite sides of the two daughter nuclei. CID and CENP-C asymmetry is detected also at S phase. Telophase and G1 are shown as transparent because of the lack of data for these two phases. CID overexpression or HASPIN knockdown promotes GSC self-renewal and disrupts CID asymmetric inheritance.

unexpected CID loading dynamics comes from our finding that GSCs in G2/prophase contain ∼30% more CID on average compared with S phase, indicating that CID is not replenished to 100% each cell cycle. Interestingly, the time course of H3T3P appearance during the GSC cell cycle closely follows the timing of CID incorporation, suggesting that the asymmetric deposition of CID might drive the differential phosphorylation of the histone H3 on sister chromatids. Finally, our results are in line with findings that the long-term retention of CENP-A in mouse oocytes has a role in establishing asymmetric centromere inheritance in meiosis (Smoak et al., 2016).

CAL1 is a cell proliferation marker

Our functional studies support a role for CAL1 in cell proliferation, with no apparent role in asymmetric cell division (Figs. 4 and 5). Indeed, centromeric proteins have been already proposed as biomarkers for cell proliferation (Swartz et al., 2019). Specifically, our functional analysis of centromeric proteins, as well as the HASPIN kinase, allowed us to discriminate between the classic role of centromeres in cell division and a role in asymmetric cell division. In our favorite scenario, CAL1 is needed to make functional centromeres crucial for cell division, while the asymmetric distribution of CID sister chromatids regulates asymmetric cell division and might depend on other

factors, such as HASPIN. However, we cannot rule out that the effects on cell fate observed with our functional analysis might reflect alternative CAL1 functions outside of the centromere, for example due to changes in chromosome structure or gene expression.

CID incorporation into centromeric chromatin occurs before meiosis

Centromeres are crucially assembled in GSCs and therefore before meiosis of the oocyte takes place. Thus, it is possible that the 16-cell cysts inherit centromeric proteins synthesized and deposited in the GSCs, and the rate of new CID loading is reduced. This would explain why CAL1 function at centromeres is dispensable at this developmental stage.

Ultimately, our results provide the first functional evidence that centromeres have a role in the epigenetic pathway that specifies stem cell identity. Furthermore, our data support the silent sister hypothesis (Lansdorp, 2007), according to which centromeres can drive asymmetric division in stem cells.

Materials and methods

Generation of transgenic flies

Transgenic lines expressing either C-terminal tagged CAL1-YFP, or CID with the mCherry tag inserted between the N-terminus and the histone fold domain (CID-mCherry), or both (CAL1-YFP-CID-mCherry) under control of UASp sequences were generated by transposable (P) element transformation of pUASp vector (kind gift from X. Chen, Johns Hopkins University, Baltimore, MD) in w^{1118}embryos (injection, selection, and balancing by BestGene). Specifically, CAL1-YFP and CID-mCherry constructs were placed in tandem following UASp sequences in the same plasmid. *cid* and *cal1* cDNA were amplified from wild type (Oregon R). mCherry containing three codons for glycine residues at both sides was inserted in between *cid N-terminal* and *cid C-terminal* as described (Schuh et al., 2007). Cloning of pUASp_CID-mCherry and pUASp CAL1-YFP was performed through Gibson Assembly (NEB), combining multiple fragments including the gene of interest and the FP tag. Primer sequences used are as follows. (1) pUASp-CID-mCherry, pUASp-CID-Nt_Fw: 5′-AGGCCACTAGTGGATCTGGATCCTATGCCACGACACAGCAGAGCCAAGC-3′; CID-Nt_Rv-mCherry: 5′-ATCCTCCTCGCCCTTGCTCACCATACCACCACCGGTCTGGTTTTGCGCA-3′; mCherry_Fw-CID-Nt: 5′-TGCGCAAAACCAGACCGGTGGTGGTATGGTGAGCAAGGGCGAGGAGGAT-3′; CID-Ct_Fw: 5′-GCATGGACGAGCTGTACAAGGGTGGTGGTAGGCGGCGCAAAGCGGCCAA-3′; mCherry-Rv: 5′-TTGGCCGCTTTGCGCCGCCTACCACCACCCTTGTACAGCTCGTCCATGC-3′; CID-Ct-pUASp_Rv: 5′-TTAACGTTAACGTTCGAGGTCGACTCTAAAATTGCCGACCCCGGTCGCA-3′; (2) pUASp-CAL1-YFP, pUASp-CAL1_Fw: 5′-ATAGGCCACTAGTGGATCTGGATCCTATGGCGAATGCGGTGGTGGACGA-3′; CAL1-YFP_Rv: 5′-TCCTCGCCCTTGCTCACCATCTTGTCACCGGAATTATTCTCGAGTATGC-3′; CAL1-YFP_Fw: 5′-CAGCATACTCGAGAATAATTCCGGTGACAAGATGGTGAGCAAGGGCGAGGA-3′; pUASp-YFP_Rv: 5′-GTTAACGTTAACGTTCGAGGTCGACTTTACTTGTACAGCTCGTCCATGC-3′. pUASp-CAL1-YFP_UAS_CID-mCherry was performed through restriction cloning of the fragment CAL1 YFP and UASp sequence into the pUASp-CID-mCherry plasmid in front of CID-mCherry. Primers of the UASp sequence used are as follows. EcoRI-UASp_Fw: 5′-CCGAATTCTTACATACATACTAGAATTGGC-3′; UASp-NotI_Rv: 5′-CCGCGGCCGCTGCACTGAATTTAAGTGTATACTTC-3′.

Fly stocks and husbandry

Stocks were cultured on standard cornmeal medium (NUTRI-fly) preserved with 0.5% propionic acid and 0.1% Tegosept at 20°C under a 12-h light-dark cycle. UAS-RNAi lines were obtained from the Bloomington Stock Center (CYCA 35694; CYCB 38981; HASPIN 57787) and Vienna Drosophila RNAi Center (CAL1 45248; CENP-A/CID 102090). The germline-specific promoters *nanos* and *bam* were used to drive GAL4 expression (P{w[+mC] = UAS-Dcr-2.D}1, w[1118]; P{w[+mC] = GAL4-nos.NGT}40, provided by Bloomington Stock Center, #25751; *bam-Gal4* was a kind gift from M.T. Fuller, Stanford University, Stanford, CA).

Crosses were performed at 20°C, 25°C, and 29°C, specifically: CAL1 and CID knockdown using the *nanos-Gal4* driver were performed both at 25°C and 20°C, while CAL1 and CID knockdown using the *bam-Gal4* driver were both conducted at 29°C. CYCA knockdown with *nanos-Gal4* driver was performed at 25°C. CYCB knockdown using the *nanos-Gal4* was performed at 25°C, HASPIN knockdown using the *nanos-Gal4* driver was performed at 20°C, and then larvae were moved at 29°C for 8 d. Crosses for overexpression were performed using *nanos-Gal4* driver at 25°C. Transgenic lines expressing GFP-tagged CENP-A/CID and RFP-tagged H2Av (heterozygotes; Schuh et al., 2007) under respective endogenous promoters were a kind gift from C. Lehner (University of Zurich, Zurich, Switzerland). Results obtained from each experiment rely on three biological replicates, unless otherwise specified.

Immunofluorescence

GSCs usually undergo mitotic division at very low frequency (Yamashita et al., 2003); therefore, to increase our chance to catch multiple cell cycle phases during cell division at once, we used young female flies (<1 d old) for centromere assembly quantifications and measurements of the asymmetry in the replication couples. To quantify metaphase GSCs in Fig. 3, we used young female flies 30 min old. For all the other experiments, we used 3-d-old female flies. Ovaries from young adult females were dissected in 1× PBS and fixed in 4% PFA. For quantification of CID in NBs, brains from third-instar larvae were dissected and fixed as described above. To carry out the tubulin staining, ovaries were fixed in ice-cold methanol for 20 min at 4°C, followed by acetone at −20°C for an additional 2 min. After fixation, samples were immediately washed in 1× PBS, 0.4% Triton X-100 (0.4PBT). Samples were then blocked in 0.4PBT with 1% BSA for 3–4 h at room temperature and incubated with primary antibodies (in blocking buffer) overnight at 4°C and with secondary antibodies (in blocking buffer) for 1 h at room temperature.

EdU assays

Ovaries from young female flies were dissected and incubated for 30 min with EdU (0.01 mM) in 1× PBS and then fixed as

described. After washing in 0.4PBT, ovaries were incubated for 30 min in the dark with 2 mM CuSO4, 300 uM fluorescent azide and 10 mM ascorbic acid. Samples were then washed with 0.4PBT for 10 min and then blocked and stained as described above.

Antibodies

For immunostaining, the following antibodies were used: rabbit anti-CENP-A (CID) antibody (Active Motif 39719; 1:500), rat anti-CID (Active Motif 61735; 1:500), guinea pig anti-CENP-C (Erhardt et al., 2008; 1:1,000), sheep anti-CENP-C aa 1-732 (this study, 1:2,000), rabbit anti-H3S10P (Abcam ab5176, 1:1,000), mouse anti-H3S10P (Abcam ab14955; 1:1,000), rabbit anti-H3T3P (MERK 05-746R; 1:1,000), rabbit anti-VASA (Santa Cruz sc-30210; 1:250), goat anti-VASA (Santa Cruz sc-26877; 1:100), mouse anti-Fibrillarin (Abcam ab4566; 1:500), mouse anti-BAM (Developmental Studies Hybridoma Bank ab10570327; 1:10), mouse anti-CYCA (Developmental Studies Hybridoma Bank, A12 ab528188; 1:250 of the concentrated version), mouse anti-CYCB (Developmental Studies Hybridoma Bank, F2F4 ab2245815; 1:250 of the concentrated version), rabbit anti-pMAD (Abcam ab52903; 1:250), mouse anti-SPECTROSOME/1B1 (Developmental Studies Hybridoma Bank ab528070; 1:50), rat anti-DEADPAN (Abcam 195173; 1:100), mouse anti-tubulin (Abcam ab44928; 1:100), and rabbit anti-CAL1 (Bade et al., 2014; 1:1,000).

Confocal microscopy

Images of immunostained ovaries mounted in SlowFade Gold antifade reagent (Invitrogen S36936) were taken using an inverted Fluoview 1000 laser scanning microscope (Olympus) equipped with a 60× oil-immersion UPlanS-Apo objective (NA 1.2). The samples were excited at 404, 473, 559, and 635 nm, respectively, for DAPI and Alexa Fluor 488, 546, and 647. Light was guided to the sample via D405/473/559/635 dichroic mirror (Chroma). The emission light was guided via a size-adjustable pinhole, set at 115 µm. Fluorescence passed through a 430–455-, 490–540-, 575–620-, 655–755-nm bandpass filter for detection of DAPI and Alexa Fluor 488, 546, and 647, respectively, in sequential mode. Images were acquired as z-stacks with a step size of 0.5 µm.

Superresolution microscopy

Superresolution images of immunostained ovaries mounted in SlowFade Gold antifade reagent (Invitrogen S36936) were acquired using structured illumination microscopy (SIM). Samples were prepared on high precision cover glass (Zeiss). 3D SIM images were acquired on an N-SIM (Nikon Instruments) using a 100× 1.49-NA lens and refractive index–matched immersion oil (Nikon Instruments). Samples were imaged using a Nikon Plan Apo TIRF objective (NA 1.49, oil immersion) and an Andor DU-897X-5254 camera using 405-, 488-, 561-, and 640-nm laser lines. Z-step size for Z stacks was set to 0.120 µm as required by manufacturer software. For each focal plane, 15 images (five phases, three angles) were captured with the NIS-Elements software. SIM image processing, reconstruction, and analysis were performed using the N-SIM module of the NIS-Element Advanced Research software. Images were checked for artifacts using the SIM check software (http://www.micron.ox.ac.uk/software/SIMCheck.php). Images were reconstructed using NiS Elements software v4.6 (Nikon Instruments) from a z-stack comprising ≥1 µm of optical sections. In all SIM image reconstructions, the Wiener and Apodization filter parameters were kept constant.

Wide-field microscopy

Images of immunostained ovaries mounted in SlowFade Gold antifade reagent (Invitrogen S36936) were acquired using a DeltaVision Elite microscope system (Applied Precision) equipped with a 100× oil-immersion UPlanS-Apo objective (NA 1.4). Images were acquired as z-stacks with a step size of 0.2 µm. Fluorescence passed through a 435/48, 525/48, 597/45, 632/34 nm bandpass filter for detection of DAPI, Alexa Fluor 488, mCherry, and Alexa Fluor 647, respectively, in sequential mode.

Quantification

For each quantification, one cell/germarium was considered, unless specified otherwise. Images from a single cell (nucleus) were projected (maximum intensity) to capture all the centromeres present in the cell at a specific cell cycle phase. ImageJ software (National Institutes of Health; Schneider et al., 2012) was used to measure fluorescent intensity of CID in the following way (Fig. S1). The background was subtracted from the projected image. The threshold was adjusted, and the image was converted to binary. Overlapping centromeres were separated using the command "watershed." Next, the command "analyze particles" was used to select centromeres. Size was adjusted to eliminate unwanted objects. Finally, integrated density (MGV*area) or MGVs from each centromere focus were extracted and used as fluorescent intensity to measure the total amount of fluorescence per nucleus. In Figs. 1, 2, 3, 6, and S1, we used the integrated density, because for stages such as replication, metaphase, and anaphase, centromeres are highly clustered and single centromere foci cannot be separated. In the quantification of CID in GSCs and cysts, we used the integrated density, because of the strong clustering observed after projection of the cysts. In the remaining quantifications of CID (Figs. 2 and S2), we used MGV. Quantification of pMAD- and SXL-positive cells was obtained by counting the positive cells for each signal through the z-stack of each image. Statistical analysis was performed using Prism software. Data distribution was assumed to be normal, but this was not formally tested. The P value in each graph shown was calculated with unpaired *t* test with Welch's correction. In addition, for the graph shown in Fig. 3 E, we used Mann–Whitney *U* test and the Wilcoxon matched-pairs signed rank test.

RNA isolation and qPCR

Drivers (*nanos-Gal4*) and CAL1 knockdown flies were collected 7 d after hatching at 20°C and then dissected to extract ovaries. Drivers (*nanos-Gal4*) and HASPIN knockdown flies were collected after crossing was performed as described above. Total RNA from each sample was stored in TRIzol (Ambion, Life Technologies, 1559-6026) at −80°C until processing. RNA extraction and purification was performed with RNeasy MinElute

clean up kit (Qiagen 74204). All the isolated RNAs were then standardized to the same concentration, and cDNA was synthesized (High Capacity RNA to cDNA, Thermo Fisher Biosciences, 4387406). qPCR was performed using the Applied Biosystem StepOnePlus Instrument and Power Up Sybr Green Master mix (Applied Biosystems A25780). The following genes, from *Drosophila* genome, were considered for this experiment: *Glyceraldehyde 3-phosphate dehydrogenase* (*gapdh*); *Ribosomal Protein L32* (*rpl32/rp49*); *nuclear-fall-out* (*nuf*); and *cal1*. Primers for all the considered genes were designed using MacVector to amplify 75–150-bp fragments of the desired gene (Fig. S2 A). Before the qPCR experiment, these primers were tested with a mixture of cDNA from *Drosophila* ovaries to make sure they would amplify only a single region from the genome. Next, we checked primer efficiencies with a dilution curve (10^{-1} to 10^{-5}) to make sure their range was within the negligible value of 1.9–2.0. Among the reference genes considered (*gapdh*; *rpl32/rp49*; *nuf*), *nuf* is highly stable at 20°C, between both control and the knockdown sample. Therefore, qPCR samples were standardized with *nuf*, and relative fold change values were calculated in Microsoft Excel and standardized against our reference gene based on published formulas (Livak and Schmittgen, 2001). Each qPCR experiment consisted of two biological replicates, and each sample was analyzed using three technical replicates per qPCR experiment. According to the Minimum Information for Publication of Quantitative Real-Time PCR Experiments (MIQE) guidelines (Bustin et al., 2009), primer sequences used, relative efficiency, and amplification factor used in the calculation are as follows: *gapdh*, Fw 5′-GCTGGTGCCGAATACATCGTGG-3′; Rv 5′-CCAAGTTGACGCCGCAAACG-3′; efficiency, 90.7%, amplification factor, 1.91; *rpl32/rpl49*, Fw 5′-CCGCTTCAAGGGACAGTATCTGATGC-3′; Rv 5′-TTCTGCATGAGCAGGACCTCCAGC-3′; efficiency, 88.1%; amplification factor, 1.89; *nuf*, Fw 5′-TGGCGAAAATGAGTATCCCACCC-3′; Rv 5′-GGTTGTGTCCACTGTTGTTACCCACG-3′; efficiency, 105.8%; amplification factor, 2.06; *cal1*, Fw 5′-GTGAACGACAAGAGATTCCAGCGAC-3′; Rv 5′-AGTCCCTGCTCGGTCAGTGTGAAG-3′; efficiency, 102.9%; amplification factor: 2.03; *haspin*, Fw 5′-ACGTCGAAGCTCAATATGCCA-3′; Rv 5′-ACGGAAGTGGTGTACACTGATG-3′; efficiency, 109.2%; amplification factor, 2.09.

Online supplemental material

Fig. S1 illustrates the quantification strategy used in this study and shows the dynamics of CID assembly observed in *Drosophila* NBs as well as CYCA and CYCB knockdown confirmation. Fig. S2 shows the disrupted assembly dynamics of CENP-C and CAL1 on *Drosophila* GSC chromosomes upon CYCA knockdown. It also shows HASPIN knockdown confirmation and the temporal course of the H3T3P marker during *Drosophila* GSC mitosis. Fig. S3 shows the images used to determine asymmetric distribution of CID and spindle microtubules on GSC sister chromatids before chromosome segregation. Fig. S4 shows the consequences of CID and CAL1 knockdown using *nanos-Gal4* driver on *Drosophila* germaria and centromere assembly. Fig. S5 shows the localization of overexpressed CAL1-YFP, CAL1-YFP_CID-mCherry, and CID-mCherry in the transgenic flies generated for this study. It also shows the ratio of SXL/pMAD-positive cells obtained for each transgenic line compared with the control and the CAL1 and CENP-C knockdown confirmation using *bam-Gal4* driver.

Acknowledgments

We thank Gary Karpen and Sylvia Erhardt for antibodies. Antibodies obtained from the Developmental Studies Hybridoma Bank, created by the National Institute of Child Health and Human Development of the National Institutes of Health, are maintained at the University of Iowa, Department of Biology, Iowa City, IA.

E.M. Dunleavy, A.M. Kochendoerfer, C. Morgan, and A.E. Walsh are funded by Science Foundation Ireland PIYRA 13/YI/2187. A.A. Dattoli is funded by Government of Ireland Postdoctoral Fellowship 2017/1324 and Science Foundation Ireland PIYRA 13/YI/2187. B.L. Carty is funded by Government of Ireland Postgraduate Fellowship 2018/1208. The authors acknowledge the facilities and technical assistance of the National Centre for Bioengineering Science qPCR Facility, funded by National University of Ireland, Galway, and the Government of Ireland's Program for Research in Third Level Institutions, Cycles 4 and 5, National Development Plan 2007-2013, the Centre for Microscopy & Imaging at the National University of Ireland, Galway (www.imaging.nuigalway.ie), and the Edinburgh Super-Resolution Imaging Consortium at the Institute of Genetics and Molecular Medicine at the University of Edinburgh (https://www.esric.org/). Stocks were obtained from the Bloomington Drosophila Stock Center (National Institutes of Health P40OD018537).

The authors declare no competing interests.

Author contributions: A.A. Dattoli and E.M. Dunleavy conceived and designed the study. A.A. Dattoli performed the molecular biological experiments, fluorescence microscopy imaging, and data analysis in the experiments presented in Figs. 1, 2 (A–O), 3, 4, and 6. B.L. Carty devised the GSC self-renewal assay (SXL/pMAD) in Fig. 5 and performed the molecular biological experiments, fluorescence microscopy imaging, and data analysis in the experiment presented in Figs. 3 (O and P) and 7 (A–I). A.A. Dattoli and A.M. Kochendoerfer performed the molecular biological experiments, fluorescence microscopy imaging, and data analysis in the experiments presented in Fig. 5 (A–N). A.A. Dattoli and C. Morgan performed the molecular biological experiments, fluorescence microscopy imaging, and data analysis in the experiments presented in Figs. 2 (P–T) and 5 (O–S). A.A. Dattoli and A.E. Walsh generated the transgenic fly lines. A.A. Dattoli and E.M. Dunleavy wrote the manuscript.

Submitted: 16 October 2019
Revised: 10 December 2019
Accepted: 10 February 2020

References

Ables, E.T., and D. Drummond-Barbosa. 2013. Cyclin E controls Drosophila female germline stem cell maintenance independently of its role in proliferation by modulating responsiveness to niche signals. *Development.* 140:530–540. https://doi.org/10.1242/dev.088583

Ahmad, K., and S. Henikoff. 2001. Centromeres are specialized replication domains in heterochromatin. *J. Cell Biol.* 153:101–110. https://doi.org/10.1083/jcb.153.1.101

Allshire, R.C., and G.H. Karpen. 2008. Epigenetic regulation of centromeric chromatin: old dogs, new tricks? *Nat. Rev. Genet.* 9:923–937. https://doi.org/10.1038/nrg2466

Bade, D., A.L. Pauleau, A. Wendler, and S. Erhardt. 2014. The E3 ligase CUL3/RDX controls centromere maintenance by ubiquitylating and stabilizing CENP-A in a CAL1-dependent manner. *Dev. Cell.* 28:508–519. https://doi.org/10.1016/j.devcel.2014.01.031

Barnhart, M.C., P. Henning, J.L. Kuich, M.E. Stellfox, J.A. Ward, E.A. Bassett, B.E. Black, and D.R. Foltz. 2011. HJURP Is a CENP-A Chromatin Assembly Factor Sufficient to Form a Functional de Novo Kinetochore. *J. Cell Biol.* 194:229–243. https://doi.org/10.1083/jcb.201012017

Becker, K.A., P.N. Ghule, J.A. Therrien, J.B. Lian, J.L. Stein, A.J. van Wijnen, and G.S. Stein. 2006. Self-renewal of human embryonic stem cells is supported by a shortened G1 cell cycle phase. *J. Cell. Physiol.* 209:883–893. https://doi.org/10.1002/jcp.20776

Betschinger, J., and J.A. Knoblich. 2004. Dare to be different: asymmetric cell division in Drosophila, C. elegans and vertebrates. *Curr. Biol.* 14:R674–R685. https://doi.org/10.1016/j.cub.2004.08.017

Black, B.E., and D.W. Cleveland. 2011. Epigenetic centromere propagation and the nature of CENP-a nucleosomes. *Cell.* 144:471–479. https://doi.org/10.1016/j.cell.2011.02.002

Boone, J.Q., and C.Q. Doe. 2008. Identification of Drosophila Type II Neuroblast Lineages Containing Transit Amplifying Ganglion Mother Cells. *Dev. Neurobiol.* 68:1185–1195.

Bustin, S.A., V. Benes, J.A. Garson, J. Hellemans, J. Huggett, M. Kubista, R. Mueller, T. Nolan, M.W. Pfaffl, G.L. Shipley, et al. 2009. The MIQE guidelines: minimum information for publication of quantitative real-time PCR experiments. *Clin. Chem.* 55:611–622. https://doi.org/10.1373/clinchem.2008.112797

Caperta, A.D., M. Rosa, M. Delgado, R. Karimi, D. Demidov, W. Viegas, and A. Houben. 2008. Distribution patterns of phosphorylated Thr 3 and Thr 32 of histone H3 in plant mitosis and meiosis. *Cytogenet. Genome Res.* 122:73–79. https://doi.org/10.1159/000151319

Chang, C.H., A. Chavan, J. Palladino, X. Wei, N.M.C. Martins, B. Santinello, C.C. Chen, J. Erceg, B.J. Belivea, C.T. Wu, et al. 2019. Islands of Retroelements Are Major Components of Drosophila Centromeres. *PLoS.* 17:e3000241. https://doi.org/10.5061/dryad.rb1bt3j

Chau, J., L.S. Kulnane, and H.K. Salz. 2009. Sex-lethal facilitates the transition from germline stem cell to committed daughter cell in the Drosophila ovary. *Genetics.* 182:121–132. https://doi.org/10.1534/genetics.109.100693

Chell, J.M., and A.H. Brand. 2010. Nutrition-responsive glia control exit of neural stem cells from quiescence. *Cell.* 143:1161–1173. https://doi.org/10.1016/j.cell.2010.12.007

Chen, C.C., M.L. Dechassa, E. Bettini, M.B. Ledoux, C. Belisario, P. Heun, K. Luger, and B.G. Mellone. 2014. CAL1 is the Drosophila CENP-A assembly factor. *J. Cell Biol.* 204:313–329. https://doi.org/10.1083/jcb.201305036

Christophersen, N.S., and K. Helin. 2010. Epigenetic control of embryonic stem cell fate. *J. Exp. Med.* 207:2287–2295. https://doi.org/10.1084/jem.20101438

Christophorou, N., T. Rubin, and J.R. Huynh. 2013. Synaptonemal complex components promote centromere pairing in pre-meiotic germ cells. *PLoS Genet.* 9:e1004012. https://doi.org/10.1371/journal.pgen.1004012

Dai, J., S. Sultan, S.S. Taylor, and J.M.G. Higgins. 2005. The kinase haspin is required for mitotic histone H3 Thr 3 phosphorylation and normal metaphase chromosome alignment. *Genes Dev.* 19:472–488. https://doi.org/10.1101/gad.1267105

Dietzl, G., D. Chen, F. Schnorrer, K.C. Su, Y. Barinova, M. Fellner, B. Gasser, K. Kinsey, S. Oppel, S. Scheiblauer, et al. 2007. A genome-wide transgenic RNAi library for conditional gene inactivation in Drosophila. *Nature.* 448:151–156. https://doi.org/10.1038/nature05954

Drpic, D., A.C. Almeida, P. Aguiar, F. Renda, J. Damas, H.A. Lewin, D.M. Larkin, A. Khodjakov, and H. Maiato. 2018. Chromosome Segregation Is Biased by Kinetochore Size. *Curr. Biol.* 28:1344–1356.e5. https://doi.org/10.1016/j.cub.2018.03.023

Duffy, J.B. 2002. GAL4 system in Drosophila: a fly geneticist's Swiss army knife. *Genesis.* 34:1–15. https://doi.org/10.1002/gene.10150

Dunleavy, E.M., N.L. Beier, W. Gorgescu, J. Tang, S.V. Costes, and G.H. Karpen. 2012. The cell cycle timing of centromeric chromatin assembly in Drosophila meiosis is distinct from mitosis yet requires CAL1 and CENP-C. *PLoS Biol.* 10:e1001460. https://doi.org/10.1371/journal.pbio.1001460

Dunleavy, E.M., D. Roche, H. Tagami, N. Lacoste, D. Ray-Gallet, Y. Nakamura, Y. Daigo, Y. Nakatani, and G. Almouzni-Pettinotti. 2009. HJURP is a cell-cycle-dependent maintenance and deposition factor of CENP-A at centromeres. *Cell.* 137:485–497. https://doi.org/10.1016/j.cell.2009.02.040

Erhardt, S., B.G. Mellone, C.M. Betts, W. Zhang, G.H. Karpen, and A.F. Straight. 2008. Genome-wide analysis reveals a cell cycle-dependent mechanism controlling centromere propagation. *J. Cell Biol.* 183:805–818. https://doi.org/10.1083/jcb.200806038

Eun, S.H., Q. Gan, and X. Chen. 2010. Epigenetic regulation of germ cell differentiation. *Curr. Opin. Cell Biol.* 22:737–743. https://doi.org/10.1016/j.ceb.2010.09.004

Foltz, D.R., L.E.T. Jansen, A.O. Bailey, J.R. Yates III, E.A. Bassett, S. Wood, B.E. Black, and D.W. Cleveland. 2009. Centromere-specific assembly of CENP-a nucleosomes is mediated by HJURP. *Cell.* 137:472–484. https://doi.org/10.1016/j.cell.2009.02.039

Fukagawa, T., and W.C. Earnshaw. 2014. The centromere: chromatin foundation for the kinetochore machinery. *Dev. Cell.* 30:496–508. https://doi.org/10.1016/j.devcel.2014.08.016

García Del Arco, A., B.A. Edgar, and S. Erhardt. 2018. In Vivo Analysis of Centromeric Proteins Reveals a Stem Cell-Specific Asymmetry and an Essential Role in Differentiated, Non-proliferating Cells. *Cell Reports.* 22:1982–1993. https://doi.org/10.1016/j.celrep.2018.01.079

Hemmerich, P., S. Weidtkamp-Peters, C. Hoischen, L. Schmiedeberg, I. Erliandri, and S. Diekmann. 2008. Dynamics of inner kinetochore assembly and maintenance in living cells. *J. Cell Biol.* 180:1101–1114. https://doi.org/10.1083/jcb.200710052

Hendzel, M.J., Y. Wei, M.A. Mancini, A. Van Hooser, T. Ranalli, B.R. Brinkley, D.P. Bazett-Jones, and C.D. Allis. 1997. Mitosis-Specific Phosphorylation of Histone H3 Initiates Primarily within Pericentromeric Heterochromatin during G2 and Spreads in an Ordered Fashion Coincident with Mitotic Chromosome Condensation. *Chromosoma.* 106:348–360.

Hughes, S.E., D.E. Miller, A.L. Miller, and R.S. Hawley. 2018. Female Meiosis: Synapsis, Recombination, and Segregation in Drosophila Melanogaster. Genetics. 208:875–908.

Inaba, M., and Y.M. Yamashita. 2012. Asymmetric stem cell division: precision for robustness. *Cell Stem Cell.* 11:461–469. https://doi.org/10.1016/j.stem.2012.09.003

Jansen, L.E.T., B.E. Black, D.R. Foltz, and D.W. Cleveland. 2007. Propagation of centromeric chromatin requires exit from mitosis. *J. Cell Biol.* 176:795–805. https://doi.org/10.1083/jcb.200701066

Kao, S.H., C.Y. Tseng, C.L. Wan, Y.H. Su, C.C. Hsieh, H. Pi, and H.J. Hsu. 2015. Aging and insulin signaling differentially control normal and tumorous germline stem cells. *Aging Cell.* 14:25–34. https://doi.org/10.1111/acel.12288

Karpen, G., and R. Allshire. 1997. The Case for Epigenetic Effects on Centromere Identity and Function. *Trends Genet.* 13:489–496.

Kelly, A.E., C. Ghenoiu, J.Z. Xue, C. Zierhut, H. Kimura, and H. Funabiki. 2010. Survivin reads phosphorylated histone H3 threonine 3 to activate the mitotic kinase Aurora B. *Science.* 330:235–239. https://doi.org/10.1126/science.1189505

Lansdorp, P.M. 2007. Immortal strands? Give me a break. *Cell.* 129:1244–1247. https://doi.org/10.1016/j.cell.2007.06.017

Lilly, M.A., M. de Cuevas, and A.C. Spradling. 2000. Cyclin A associates with the fusome during germline cyst formation in the Drosophila ovary. *Dev. Biol.* 218:53–63. https://doi.org/10.1006/dbio.1999.9570

Livak, K.J., and T.D. Schmittgen. 2001. Analysis of relative gene expression data using real-time quantitative PCR and the 2(-Delta Delta C(T)) Method. *Methods.* 25:402–408. https://doi.org/10.1006/meth.2001.1262

Mathieu, J., C. Cauvin, C. Moch, S.J. Radford, P. Sampaio, C.N. Perdigoto, F. Schweisguth, A.J. Bardin, C.E. Sunkel, K. McKim, et al. 2013. Aurora B and cyclin B have opposite effects on the timing of cytokinesis abscission in Drosophila germ cells and in vertebrate somatic cells. *Dev. Cell.* 26:250–265. https://doi.org/10.1016/j.devcel.2013.07.005

Matias, N.R., J. Mathieu, and J.R. Huynh. 2015. Abscission is regulated by the ESCRT-III protein shrub in Drosophila germline stem cells. *PLoS Genet.* 11:e1004653. https://doi.org/10.1371/journal.pgen.1004653

McKinley, K.L., and I.M. Cheeseman. 2014. Polo-like kinase 1 licenses CENP-A deposition at centromeres. *Cell.* 158:397–411. https://doi.org/10.1016/j.cell.2014.06.016

McKinley, K.L., and I.M. Cheeseman. 2016. The molecular basis for centromere identity and function. *Nat. Rev. Mol. Cell Biol.* 17:16–29. https://doi.org/10.1038/nrm.2015.5

McLaughlin, J.M., and D.P. Bratu. 2015. Drosophila Melanogaster Oogenesis: An Overview. *In* Drosophila Oogenesis: Methods in Molecular Biology. Vol. 1328. Bratu D and G McNeil, editors. Humana Press, New York, NY. pp. 1–20.

Mellone, B.G., K.J. Grive, V. Shteyn, S.R. Bowers, I. Oderberg, and G.H. Karpen. 2011. Assembly of Drosophila centromeric chromatin proteins during mitosis. *PLoS Genet.* 7:e1002068. https://doi.org/10.1371/journal.pgen.1002068

Moutinho-Santos, T., and H. Maiato. 2014. Plk1 puts a (Has)pin on the mitotic histone code. *EMBO Rep.* 15:203–204. https://doi.org/10.1002/embr.201438472

Musacchio, A., and A. Desai. 2017. A Molecular View of Kinetochore Assembly and Function. *Biology (Basel).* 6:E5. https://doi.org/. https://doi.org/10.3390/biology6010005

Pauklin, S., and L. Vallier. 2013. The cell-cycle state of stem cells determines cell fate propensity. *Cell.* 155:135–147. https://doi.org/10.1016/j.cell.2013.08.031

Rangan, P., C.D. Malone, C. Navarro, S.P. Newbold, P.S. Hayes, R. Sachidanandam, G.J. Hannon, and R. Lehmann. 2011. piRNA production requires heterochromatin formation in Drosophila. *Curr. Biol.* 21:1373–1379. https://doi.org/10.1016/j.cub.2011.06.057

Ranjan, R., J. Snedeker, and X. Chen. 2019. Asymmetric Centromeres Differentially Coordinate with Mitotic Machinery to Ensure Biased Sister Chromatid Segregation in Germline Stem Cells. *Cell Stem Cell.* 25:666–681.e5. https://doi.org/10.1016/j.stem.2019.08.014

Raychaudhuri, N., R. Dubruille, G.A. Orsi, H.C. Bagheri, B. Loppin, and C.F. Lehner. 2012. Transgenerational propagation and quantitative maintenance of paternal centromeres depends on Cid/Cenp-A presence in Drosophila sperm. *PLoS Biol.* 10:e1001434. https://doi.org/10.1371/journal.pbio.1001434

Rotelli, M.D., R.A. Policastro, A.M. Bolling, A.W. Killion, A.J. Weinberg, M.J. Dixon, G.E. Zentner, E. Walczak, M.A. Lilly, and B.R. Calvi. 2019. A Cyclin A-Myb-MuvB-Aurora B Network Regulates the Choice between Mitotic Cycles and Polyploid Endoreplication Cycles. *PLoS Genet.* 15:e1008253.

Salic, A., and T.J. Mitchison. 2008. A chemical method for fast and sensitive detection of DNA synthesis in vivo. *Proc. Natl. Acad. Sci. USA.* 105:2415–2420. https://doi.org/10.1073/pnas.0712168105

Salzmann, V., C. Chen, C.-Y.A. Chiang, A. Tiyaboonchai, M. Mayer, and Y.M. Yamashita. 2014. Centrosome-dependent asymmetric inheritance of the midbody ring in Drosophila germline stem cell division. *Mol. Biol. Cell.* 25:267–275. https://doi.org/10.1091/mbc.e13-09-0541

Schittenhelm, R.B., F. Althoff, S. Heidmann, and C.F. Lehner. 2010. Detrimental incorporation of excess Cenp-A/Cid and Cenp-C into Drosophila centromeres is prevented by limiting amounts of the bridging factor Cal1. *J. Cell Sci.* 123:3768–3779. https://doi.org/10.1242/jcs.067934

Schneider, C.A., W.S. Rasband, and K.W. Eliceiri. 2012. NIH Image to ImageJ: 25 years of image analysis. *Nat. Methods.* 9:671–675. https://doi.org/10.1038/nmeth.2089

Schuh, M., C.F. Lehner, and S. Heidmann. 2007. Incorporation of Drosophila CID/CENP-A and CENP-C into centromeres during early embryonic anaphase. *Curr. Biol.* 17:237–243. https://doi.org/10.1016/j.cub.2006.11.051

Silva, M.C.C., D.L. Bodor, M.E. Stellfox, N.M.C. Martins, H. Hochegger, D.R. Foltz, and L.E.T. Jansen. 2012. Cdk activity couples epigenetic centromere inheritance to cell cycle progression. *Dev. Cell.* 22:52–63. https://doi.org/10.1016/j.devcel.2011.10.014

Smoak, E.M., P. Stein, R.M. Schultz, M.A. Lampson, and B.E. Black. 2016. Long-Term Retention of CENP-A Nucleosomes in Mammalian Oocytes Underpins Transgenerational Inheritance of Centromere Identity. *Curr. Biol.* 26:1110–1116. https://doi.org/10.1016/j.cub.2016.02.061

Song, X., M.D. Wong, E. Kawase, R. Xi, B.C. Ding, J.J. McCarthy, and T. Xie. 2004. Bmp signals from niche cells directly repress transcription of a differentiation-promoting gene, bag of marbles, in germline stem cells in the Drosophila ovary. *Development.* 131:1353–1364. https://doi.org/10.1242/dev.01026

Stankovic, A., L.Y. Guo, J.F. Mata, D.L. Bodor, X.J. Cao, A.O. Bailey, J. Shabanowitz, D.F. Hunt, B.A. Garcia, B.E. Black, and L.E.T. Jansen. 2017. A Dual Inhibitory Mechanism Sufficient to Maintain Cell-Cycle-Restricted CENP-A Assembly. *Mol. Cell.* 65:231–246. https://doi.org/10.1016/j.molcel.2016.11.021

Swartz, S.Z., L.S. McKay, K.C. Su, L. Bury, A. Padeganeh, P.S. Maddox, K.A. Knouse, and I.M. Cheeseman. 2019. Quiescent Cells Actively Replenish CENP-A Nucleosomes to Maintain Centromere Identity and Proliferative Potential. *Dev. Cell.* 51:35–48.e7. https://doi.org/10.1016/j.devcel.2019.07.016

Tran, V., L. Feng, and X. Chen. 2013. Asymmetric distribution of histones during Drosophila male germline stem cell asymmetric divisions. *Chromosome Res.* 21:255–269. https://doi.org/10.1007/s10577-013-9356-x

Unhavaithaya, Y., and T.L. Orr-Weaver. 2013. Centromere proteins CENP-C and CAL1 functionally interact in meiosis for centromere clustering, pairing, and chromosome segregation. *Proc. Natl. Acad. Sci. USA.* 110:19878–19883. https://doi.org/10.1073/pnas.1320074110

Wang, F., N.P. Ulyanova, J.R. Daum, D. Patnaik, A.V. Kateneva, G.J. Gorbsky, and J.M. Higgins. 2012. Haspin inhibitors reveal centromeric functions of Aurora B in chromosome segregation. *J. Cell Biol.* 199:251–268. https://doi.org/10.1083/jcb.201205106

White, J., and S. Dalton. 2005. Cell Cycle Control of Embryonic Stem Cells. *Stem Cell Rev.* 1:131–138. https://doi.org/SCR:1:2:131 [pii]\r. https://doi.org/10.1385/SCR:1:2:131

Xie, J., M. Wooten, V. Tran, B.C. Chen, C. Pozmanter, C. Simbolon, E. Betzig, and X. Chen. 2015. Histone H3 Threonine Phosphorylation Regulates Asymmetric Histone Inheritance in the Drosophila Male Germline. *Cell.* 163:920–933. https://doi.org/10.1016/j.cell.2015.10.002

Yamagishi, Y., T. Honda, Y. Tanno, and Y. Watanabe. 2010. Two histone marks establish the inner centromere and chromosome bi-orientation. *Science.* 330:239–243. https://doi.org/10.1126/science.1194498

Yamashita, Y.M., D.L. Jones, and M.T. Fuller. 2003. Orientation of asymmetric stem cell division by the APC tumor suppressor and centrosome. *Science.* 301:1547–1550. https://doi.org/10.1126/science.1087795

Yan, D., R.A. Neumüller, M. Buckner, K. Ayers, H. Li, Y. Hu, D. Yang-Zhou, L. Pan, X. Wang, C. Kelley, et al. 2014. A regulatory network of Drosophila germline stem cell self-renewal. *Dev. Cell.* 28:459–473. https://doi.org/10.1016/j.devcel.2014.01.020

Yu, Z., X. Zhou, W. Wang, W. Deng, J. Fang, H. Hu, Z. Wang, S. Li, L. Cui, J. Shen, et al. 2015. Dynamic phosphorylation of CENP-A at Ser68 orchestrates its cell-cycle-dependent deposition at centromeres. *Dev. Cell.* 32:68–81. https://doi.org/10.1016/j.devcel.2014.11.030

JCB

Supplemental material

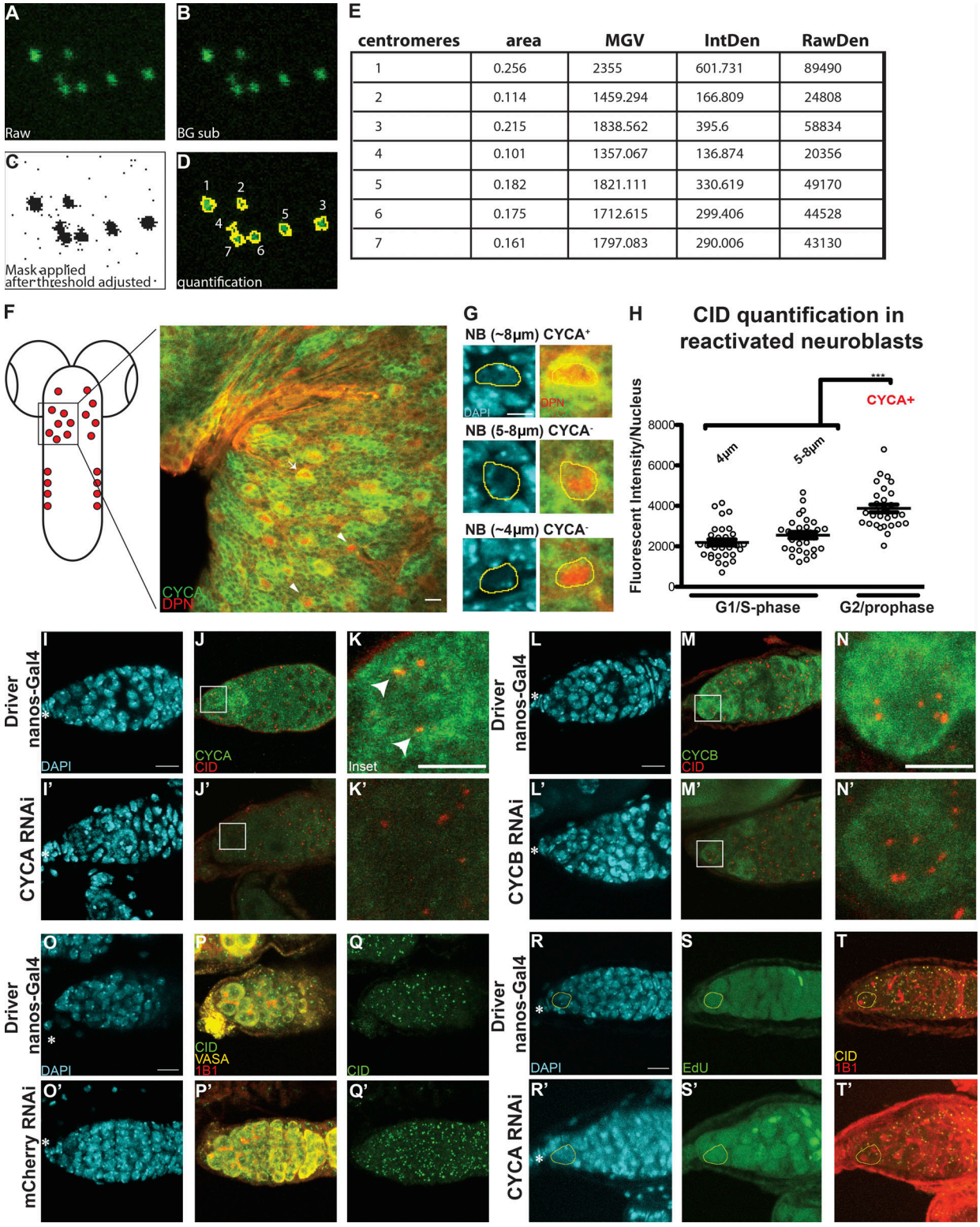

centromeres	area	MGV	IntDen	RawDen
1	0.256	2355	601.731	89490
2	0.114	1459.294	166.809	24808
3	0.215	1838.562	395.6	58834
4	0.101	1357.067	136.874	20356
5	0.182	1821.111	330.619	49170
6	0.175	1712.615	299.406	44528
7	0.161	1797.083	290.006	43130

Figure S1. **Centromere assembly occurs after replication but before chromosome segregation. (A–E)** Example image used for quantification (from Fig. 1 C, not oriented; see Materials and methods). **(F)** Diagram of *Drosophila* larval brain containing NBs (red) and confocal z-stack projection of a section of the tVNC stained with for DAPI (cyan), anti-CYCA (green), anti-DPN (red), and anti-CID (not depicted). **(G)** NBs in the tVNC are present in different sizes. **(H)** Quantification of fluorescence intensity of CID at centromeres in CYCA-negative and -positive NBs. Fluorescence intensity is expressed as integrated density after background subtraction (see Materials and methods); ***, $P < 0.0005$. **(I–N′)** Confocal z-stack projection of a *nanos-Gal4* (I–N), CYCA RNAi (I′–K′), and CYCB RNAi (L–N′) germarium at 25°C, stained for DAPI (blue), anti-CID (red), and anti-CYCA and or CYC B (green). **(O–Q′)** Confocal z-stack projection of a *nanos-Gal4* (O–Q), mCherry RNAi (O′–Q′) germarium. **(R–T′)** Confocal z-stack projection of a *nanos-Gal4* (R–T), CYCA RNAi (R′–T′) germarium stained for DAPI (cyan), EdU (green), anti-CID (yellow), and anti-1B1 (spectrosome, red). Scale bar, 10 µm; inset, 5 µm.

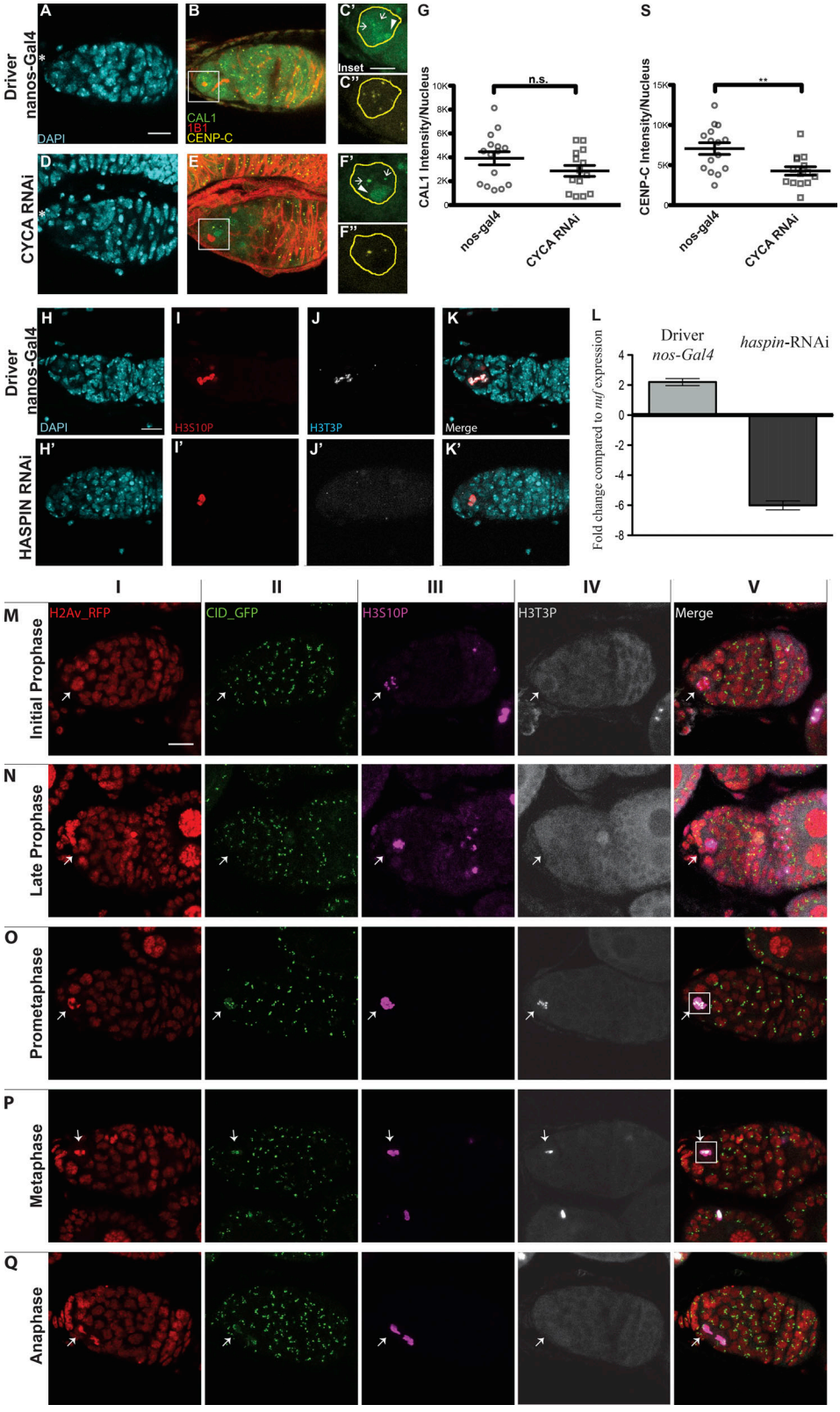

Figure S2. **CID deposition requires CYCA, CYCB, and HASPIN in *Drosophila* female GSCs. (A–F″)** Confocal z-stack projection of *nanos-Gal4* (A–C″), CYCA RNAi (D–F″) germaria stained for DAPI (blue), anti-CAL1 (green), anti-CENP-C (yellow), and anti-1B1 (spectrosome, red). **(G)** Quantification of fluorescence intensity of centromeric CAL1 per nucleus, using CENP-C as a centromeric marker based on two biological replicates. n.s., not significant. **(S)** Quantification of fluorescence intensity of CENP-C per nucleus, based on two biological replicates; **, P < 0.005. **(H–K′)** Confocal z-stack projection of *nanos-Gal4* (H–K), HASPIN RNAi (H′–K′) germaria, stained for DAPI (blue), anti-H3S10P (red), and anti-H3T3P (gray). **(L)** HASPIN knockdown confirmation by real-time qPCR. **(M–Q)** Time course of the H3T3P (white) and H3S10P (magenta) signal appearance. Scale bar, 10 µm; inset, 5 µm.

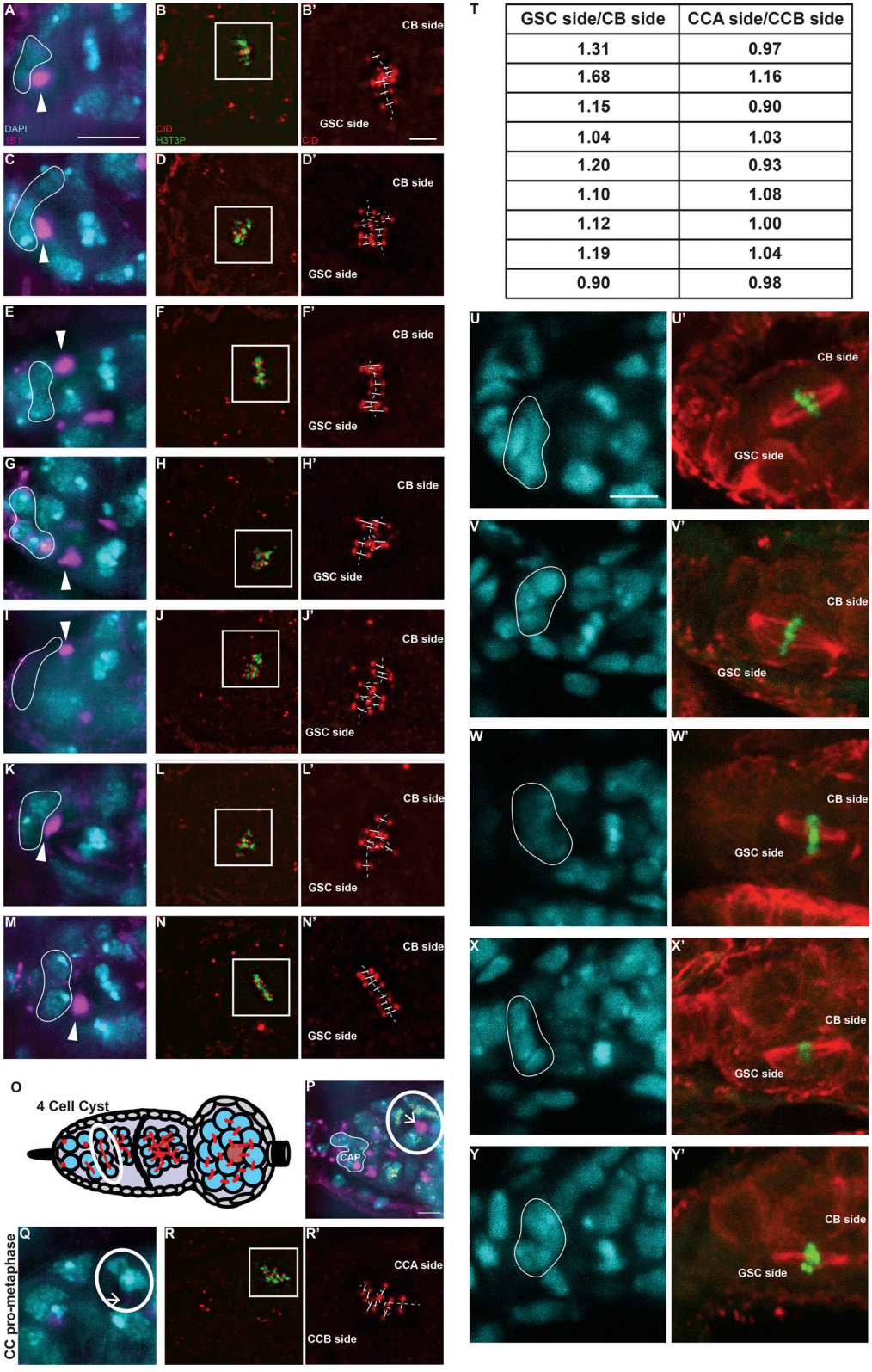

T

GSC side/CB side	CCA side/CCB side
1.31	0.97
1.68	1.16
1.15	0.90
1.04	1.03
1.20	0.93
1.10	1.08
1.12	1.00
1.19	1.04
0.90	0.98

Figure S3. **Chromosomes retain differential amounts of CID and CENP-C upon centromere assembly in *Drosophila* female GSCs. (A–N′)** Super-resolution SIM z-stack projection of a *Drosophila* GSC of a wild-type germarium in prometaphase and metaphase, stained for DAPI (blue), anti-CID (red), anti-H3T3P (green), and anti-SPECTROSOME (magenta). **(O)** Diagram of *Drosophila* germarium, highlighting the four-cell cyst stage containing four CCs. **(P)** Superresolution SIM z-stack projection of a germarium capturing four CCs in prometaphase/metaphase, which divide synchronously. **(Q–R′)** Super-resolution SIM z-stack projection of a CC at prometaphase. **(T)** Table of the ratio values obtained for each cell analyzed. **(U–Y′)** Confocal z-stack projection of a GSC of a wild-type germarium in prometaphase and metaphase, stained for DAPI (cyan), anti-TUBULIN (red), and anti-H3T3P (green). White line highlights the cap cells; arrowheads, spectrosome; arrows, fusome (not yet visible in the z-stacks projected); scale bar, 5 µm; inset, 1 µm.

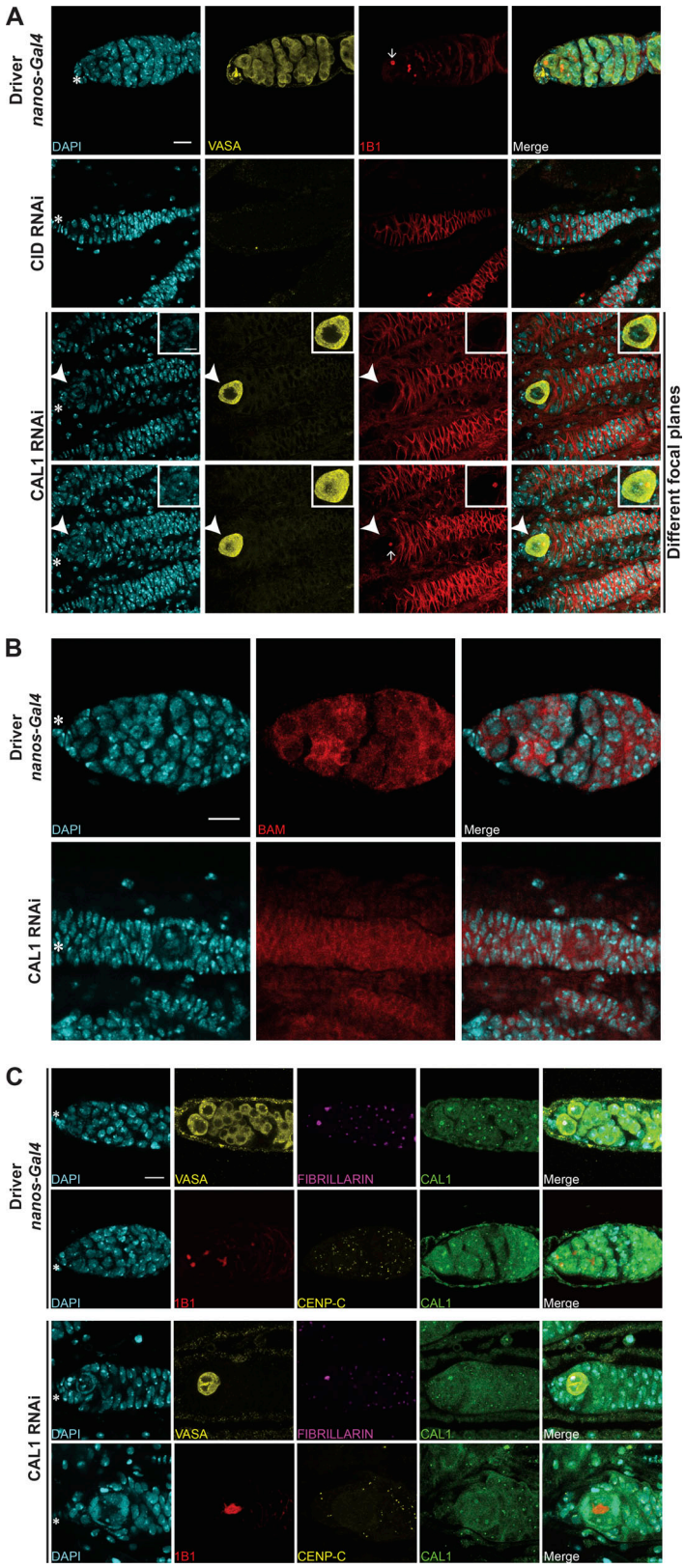

Figure S4. **CAL1 knockdown blocks cell proliferation**. **(A)** Confocal z-stack projection of *nanos-Gal4,* CID RNAi, and CAL1 RNAi germaria, stained for DAPI (blue), anti-VASA (yellow), and anti-1B1 (spectrosome, red). **(B)** Confocal z-stack projection of *bam-Gal4,* CID RNAi, and CAL1 RNAi germaria, stained for DAPI (blue) and anti-BAM (red). **(C)** Confocal z-stack projection of a *nanos-Gal4* (20°C) germarium stained for DAPI (blue) and anti-VASA (yellow), anti-FIBRILLARIN (magenta), and anti-CAL1 (green) and stained for DAPI (blue), anti-1B1 (red), anti-CENP-C (yellow), and anti-CAL1 (green). Confocal z-stack projection of a CAL1 RNAi (20°C) stained for DAPI (blue), anti-VASA (yellow), anti-FIBRILLARIN (magenta), and anti-CAL1 (green) and stained for DAPI (blue), anti-1B1 (red), anti-CENP-C (yellow), and anti-CAL1 (green). Star indicates the position of the terminal filament; 3-d-old female flies; scale bar, 10 µm.

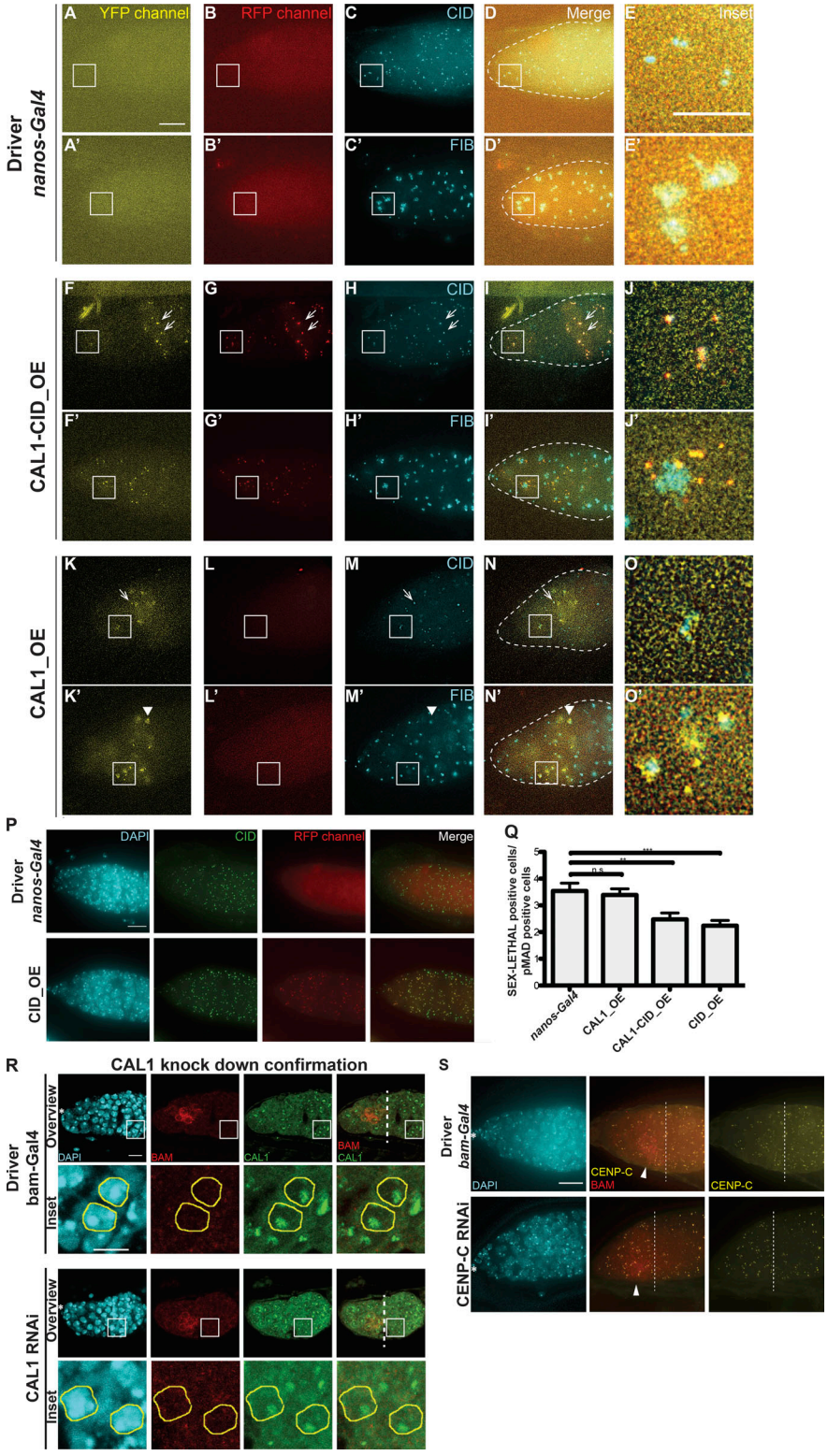

Figure S5. **CID and CAL1 overexpression and HASPIN knockdown promote stem cell self-renewal. (A–O')** Wide-field z-stack projection of *nanos-Gal4*, UAS_CAL1-YFP_UAS_CID-mCherry (CID-CAL1_OE), and UAS-CAL1-YFP (CAL1_OE) germaria, stained for anti-CID and or anti-FIB (cyan). Star, terminal filament; arrows, centromeres; arrowheads, nucleolus; 3-d-old female flies. **(P)** Wide-field z-stack projection of *nanos-Gal4* and UAS_CID-mCherry germaria stained for DAPI (cyan) and anti-CID (green). **(Q)** Ratio of the number of SXL-positive cells to the number of pMAD-positive cells. n.s., not significant; **, P < 0.005; ***, P < 0.0005. **(R)** Confocal z-stack projection *bam-Gal4* and CAL1 RNAi germaria stained for DAPI (blue), anti-BAM (red) and anti-CAL1 (green). Germ cells belonging to the 16-cell cyst chamber were selected based on the VASA marker (not depicted) and the lack of BAM signal in the control and in the CAL1 RNAi. **(S)** Confocal z-stack projection of *bam-Gal4* and CENP-C RNAi germaria, stained for DAPI (blue), anti-BAM (red), and anti-CENP-C (yellow). Star, terminal filament; white dotted line in R and S, the end of the BAM-positive region; arrowheads, BAM-positive cells. Scale bar, 10 µm; inset, 5 µm.